Higher-Order Analysis of the Superfluid-Mott Transition at Finite Temperature

Untersuchung des Suprafluid-Mott Isolator Übergangs in höherer Ordnung bei endlicher Temperatur

Bachelorarbeit
in
Theoretischer Physik

von
Sven Stawinski

durchgeführt am
Fachbereich Physik
der Technischen Universität Kaiserslautern

unter Anleitung von
Prof. Dr. Sebastian Eggert

14.07.2021

Zusammenfassung

In dieser Arbeit wird ein neuer Ansatz zur Behandlung des Bose-Hubbard Modells, insbesondere der Thermodynamik des Suprafluid-Mott Isolator Phasenübergangs, untersucht. Dieser Ansatz ist von einem hybriden Typ, in dem Sinne, dass die Molekularfeldtheorie numerisch exakt behandelt wird und anschließend eine störungstheoretische Entwicklung um diese numerisch bekannten Eigenfunktionen und Eigenwerte analytisch durchgeführt wird. Das erhaltene Resultat für die Spitze der Mott-Phase mit einem Teilchen pro Gitterplatz am Temperaturnullpunkt weicht nur um 5% von dem Ergebnis von Quanten Monte-Carlo Simulationen ab. Dies verbessert bereits merkbar die Molekularfeldtheorie, deren Vorhersage um 17% von dem Quanten Monte-Carlo Resultat abweicht. Die Rechnungen liefern in bestimmten Regionen des Phasendiagramms unphysikalische Resultate, da dort die Störungsreihe nicht konvergiert, was diskutiert wird. Das korrigierte Resultat für das großkanonische Potential ermöglicht es, thermodynamische Größen auf verschiedenen Linien in verschiedenen Phasendiagrammen bei fester Temperatur zu analysieren, wobei je einer der Parameter des Bose-Hubbard Modells konstant gehalten wird. Sowohl der Ordnungsparameter als auch die Teilchenzahl und die Entropie werden auf horizontalen und vertikalen Linien analysiert. Des Weiteren werden der Ordnungsparameter und die Entropie auf Linien konstanter Teilchenzahl untersucht und diskutiert, was die für das Experiment realistischere Situation ist. Im letzten Kapitel wird dann die Temperatur bei konstanter Entropie und Teilchenzahl betrachtet. Das erlaubt eine Diskussion der Temperaturänderung bei einem adiabatischen Anschalten eines optischen Gitters. Dies wird quantifiziert, indem ein dreidimensionales einfach kubisches Gitter betrachtet wird, wofür die Parameter des Bose-Hubbard Modells in Abhängigkeit der Gittertiefe berechnet werden können. Dadurch ist es möglich, die Temperatur eines stark wechselwirkenden Bose-Gases vorherzusagen, nachdem ein optisches Gitter adiabatisch eingeschaltet wurde, solange die Teilchenzahl und die initiale Entropie bekannt sind. Dies ist für Experimente von großem Interesse, wo es nur schwer möglich ist, die Temperatur eines stark wechselwirkenden Systems zu bestimmen.

Abstract

In this thesis a new approach to the Bose-Hubbard model, in particular to the thermodynamics of the superfluid-Mott insulator transition, is pursued. This approach is of a hybrid type, meaning that the mean-field Hamiltonian is treated exactly using numerical methods and then a perturbative expansion around these numerically known eigenfunctions and eigenenergies is carried out analytically. The obtained result for the tip of the unity filling Mott lobe at zero temperature only deviates by 5% from quantum Monte-Carlo data. This already notably improves mean-field theory which produces a deviation of 17%. These calculations yield non-physical results in certain regions of the phase diagram, as the perturbative expansion is not converging there, which will be discussed. The corrected result for the grand-canonical potential makes it possible to analyze thermodynamic quantities on different lines in different fixed-temperature phase diagrams where either one of the parameters of the Bose-Hubbard model is fixed. The order parameter, the particle number and the entropy will be analyzed on horizontal and vertical lines. Further the order parameter and the entropy will be analyzed and physically discussed on lines of constant particle number, which is more realistic in the experiment. In the final chapter, the temperature for constant entropy and particle number will be considered. This enables a discussion of the change in temperature when an optical lattice is adiabatically turned on. This will be made quantitative, by considering a three-dimensional simple cubic lattice structure for which the parameters of the Bose-Hubbard model can be calculated in terms of the lattice depth. By this, it is then possible to predict the temperature of a strongly correlated Bose gas after an optical lattice is adiabatically turned on, as long as the particle number and the initial entropy are known. This is of great interest for the experiment, where it is rather difficult to measure the temperature of a strongly correlated system.

Contents

Chapter 1

Introduction

1.1 Motivation

Nowadays, the field of ultracold atoms is at the frontier of modern quantum physics. One of the reasons for this are the great advances in cooling techniques starting in the 1970s, which were honoured with the Nobel prize in 1997 [1–3]. On the one hand this led to the great success of the experimental realization of Bose-Einstein condensation, which was honoured with the Nobel prize in 2001 [4, 5]. On the other hand it also led to the possibility of loading ultracold atoms into optical lattices, i.e. periodic potentials created by laser light, see section 1.3 [6].
These systems make it possible to realize and test a great variety of condensed matter systems, including those not that easily accessible with ordinary matter, like systems with strong correlations [7]. A great advantage of these systems is the unprecedented control over the system parameters which allow for a lot of interesting possibilities to observe novel physical phenomena and test theoretical models.
Because of these great advances in controllability and the remarkable unification of quantum optics, atomic and condensed matter physics these advances were even called the third quantum revolution in Ref. [8] after the first one at the beginning of the 20th century and the second one connected to the gain in experimental control over single particles and the investigation of the non-locality of quantum mechanics [9].
One example for the great success of the field of ultracold atoms in optical lattices is the experimental realization of the superfluid to Mott insulator transition [7], see sections 1.4 and 2.4, which is a prime example for the effect of strong correlations. Also topological systems could be realized [10–13] and many people believe that this newly formed field will also find applications in quantum computing [14, 15], quantum simulation [16–18] as well as quantum metrology [19]. Besides also providing fundamental insights into quantum theory [20] and quantum field theories [21], ultracold atoms can also provide tests for research fields that seem totally unrelated like quantum gravity [22].
The superfluid-Mott insulator transition in particular is believed to find a lot of applications itself, which makes the transition of interest in general [19, 23, 24]. A reason why the thermodynamics of the transition is of particular interest is the following: Nowadays a lot of experiments are done with ultracold atoms in optical lattices. To this end particles are trapped [25] and then an optical lattice is adiabatically turned on. In the case of bosonic atoms, on which this thesis will focus,

the system then undergoes a transition from a superfluid to a Mott insulator phase [7, 26]. Unfortunately there is no viable possibility known to determine the temperature of a strongly correlated system [27]. But because initial temperature and entropy can be determined from the theory of weakly interacting Bose gases [28], we can infer the temperature of the system after the lattice is turned on by entropy matching. This can be provided by a good thermodynamic understanding of the transition, which is why it is of great practical interest.

1.2 Historical overview

In 1937 deBoer and Verwey found a class of materials, including for example NiO, that should be conducting following ordinary band theory but experimentally turned out to be of bad conductivity or even insulating [29]. In the same year Mott and Peierls proposed that these findings could be explained by strong electrostatic interactions preventing the electrons from moving and thus from conducting [30]. This was further investigated and understood by Mott approximately 10 years after [31]. Today these materials that should be conducting following band theory but actually are insulating due to strong correlations are called Mott insulators.
In 1963 Hubbard proposed a simple model describing electrons in solids [32]. The second quantized Hamiltonian of the model in the canonical ensemble is given by

$$\hat{H}_{\mathrm{H}} = \sum_{i,j\in\Lambda}\sum_{\sigma=\pm1} T_{ij}\hat{c}^{\dagger}_{i,\sigma}\hat{c}_{j,\sigma} + \frac{1}{2}I\sum_{i\in\Lambda}\sum_{\sigma=\pm1}\hat{n}_{i,\sigma}\hat{n}_{i,-\sigma}, \tag{1.1}$$

see section 2.2 for a brief overview of second quantization. Here, $\hat{c}^{\dagger}_{i,\sigma}$ and $\hat{c}_{i,\sigma}$ are the creation and annihilation operators creating/annihilating an electron in the Wannier state of atom i with magnetic spin quantum number $\sigma/2$, Λ denotes the "lattice" of atoms, $\hat{n}_{i,\sigma} = \hat{c}^{\dagger}_{i,\sigma}\hat{c}_{i,\sigma}$ is the occupation number operator and $T_{ij}, I \in \mathbb{R}$ are real numbers in order for the Hamiltonian to be Hermitian, whose precise definitions are unimportant here.
This model uses a simple dynamical picture to describe electrons in one energy band. They can tunnel from an atom i to an atom j with amplitude T_{ij} and they feel an interaction with strength I when both a spin up as well as a spin down electron are at the same atom. This model actually describes a transition from a conducting metal to a Mott insulator phase and thus captures the surprising effects found in the 1930s. Since then there has been a lot of interest in metal-insulator transitions. In 1989 Fisher *et al.* investigated a model analogous to the Hubbard model describing spinless bosons, the Bose-Hubbard model [33]. Originally they thought that this model could describe ^{4}He in porous media, granular superconductors or Josephson junctions. The Hamiltonian of the model without disorder is given by

$$\hat{H}_{\mathrm{BH}} = -\sum_{i,j\in\Lambda} J_{ij}\hat{a}^{\dagger}_{i}\hat{a}_{j} + \frac{V}{2}\sum_{i\in\Lambda}\hat{n}_i(\hat{n}_i - 1) - (\mu - J_0)\sum_{i\in\Lambda}\hat{n}_i, \tag{1.2}$$

where now $\hat{a}^{\dagger}_{i}$ and $\hat{a}_i$ create/annihilate bosons in the respective Wannier states. Again the occupation number operator is denoted by $\hat{n}_i = \hat{a}^{\dagger}_{i}\hat{a}_i$. The first term again describes a tunneling/hopping process, which is connected to an energy gain if $J_{ij} > 0$, which is typically the case, due to the delocalization. Usually discussions

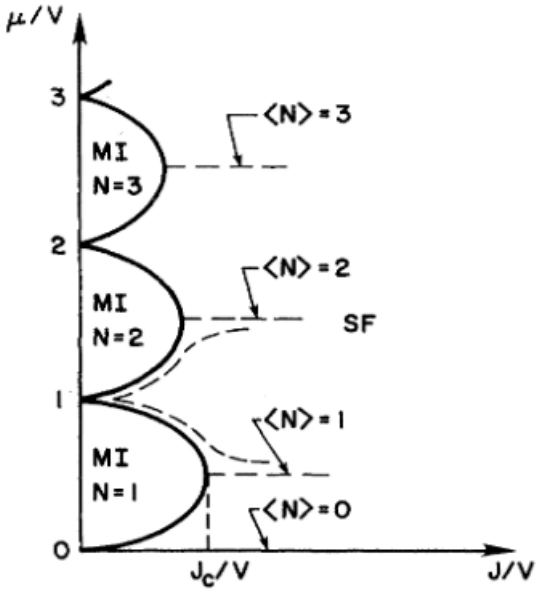

Figure 1.1: Zero temperature phase diagram of the Bose-Hubbard model with only nearest-neighbour hopping of strength J. The dashed lines, besides the one indicating the critical value of J, represent lines of constant particle number, MI is an abbreviation of Mott insulator and SF abbreviates superfluid. Taken from Ref. [33].

of the model are restricted to nearest neighbour hopping, which we will also do in the following. The second term describes the repulsive interaction if two or more bosons occupy the same state. The last term is simply added to go over to the grand-canonical ensemble, i.e. it fixes the mean particle number through introduction of a chemical potential μ. The J_0 is simply some offset which we will absorb into the chemical potential in the following.

Fisher *et al.* showed that this model also describes a phase transition from a superfluid phase to a Mott insulating phase. They constructed the phase diagram for the zero temperature case in the μ–J plane, see figure 1.1. You can clearly see that the Mott phases have lobe like shapes, one for each integer mean particle number per site. We will follow their arguments for constructing the phase diagram in section 2.4.

In 1998 then Jaksch *et al.* proposed that ultracold atoms in an optical lattice, to be introduced in section 1.3, should be an almost perfect realization of the Bose-Hubbard model [26]. Only four years later Greiner *et al.* reported the first experimental observation of the superfluid to Mott insulator transition using a Bose-Einstein condensate of ^{87}Rb atoms [7]. We will comment more on this in section 1.4.

After the publication of Fisher *et al.* there has been a lot of theoretical interest in the Bose Hubbard model, which was then revived again after the proposal of Jaksch *et al.* and the experiment of Greiner *et al.*.

Shortly after the original publication of the model, people started studying it using quantum Monte Carlo (QMC) simulations [34–38]. These works where mostly restricted to one-dimensional systems and zero temperature but also included effects of disorder and nearest neighbour interactions. After the experimental realization of Greiner *et al.*, Batrouni *et al.* expanded their QMC treatment to also include a

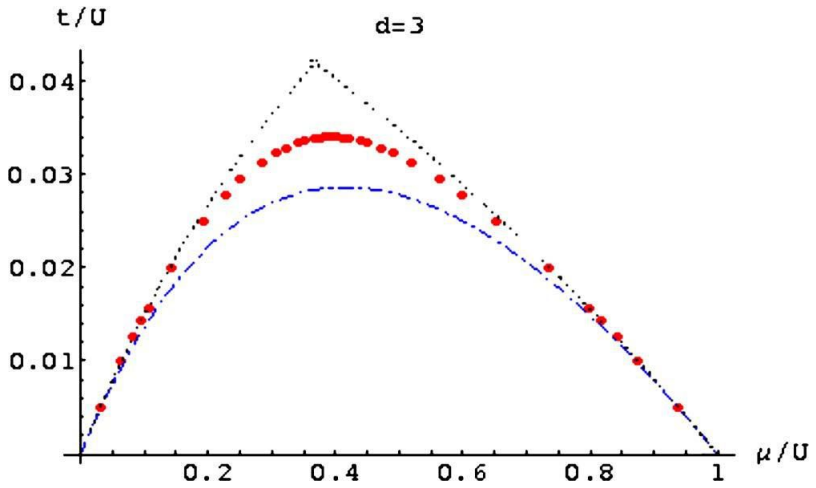

Figure 1.2: Comparison of the results for the $n = 1$ Mott lobe in three dimensions at $T = 0$. The dot-dashed blue line is the original mean-field result of Fisher *et al.* [33], the dotted black line is from a strong coupling expansion [46] and the red dots are from QMC simulations [27]. Here t denotes the hopping parameter and U the on-site repulsion. Taken from Ref. [47].

trapping potential [39]. A couple of years later Capogrosso-Sansone *et al.* investigated the Bose-Hubbard model at finite temperature, also including the effects of a trapping potential in two and three dimensions with QMC simulations, setting todays standard in accuracy of the Mott-superfluid phase boundary [27, 40]. Furthermore they also provided a discussion of the thermodynamics of the transition [27], which will also be the main topic of this thesis. Besides all these works relying on QMC simulations there have also been other numerical treatments, e.g. using the density matrix renormalization group (DMRG) [41–44] or dynamical mean-field theory [45].

Although these numerical methods provide accurate data, they can not provide the same physical insights that an analytical approach can. Thus, there has also been a lot of effort in treating the Bose-Hubbard model analytically. In the original paper, Fisher *et al.* made use of the mean-field approximation, to be discussed in detail in section 2.5, and also used the framework of the renormalization group. Further analytical treatments also often made use of mean-field type approximations [26, 48–51] but also renormalization group methods [52] and strong coupling expansions [46, 53, 54]. All of these analytical methods only investigated the $T = 0$ case. Works on the finite temperature case mostly started appearing only after 2000 [55–61].
It turned out that there was still a rather big discrepancy between the analytically found results and the (pretty much exact) QMC simulations, see figure 1.2. So, there was the need to go to higher order calculations in order to fit the QMC data better. There are some higher order analytic approaches for zero temperature [47, 62–66] but higher order results for finite temperature are still rather rare [67, 68].
Recent approaches made use of an effective action approach [67] and a strong coupling expansion based on the Green's function [68]. Both approaches made use of a perturbative expansion around the part of the Hamiltonian that is diagonal in the occupation number representation. This allows for an analytic treatment because the action of the creation and annihilation operators on these states is known. Our approach will differ from the previous ones, as we will treat the mean field

Hamiltonian exactly using numerical methods and then analytically find a perturbative expansion around it using the numerically known mean field eigenenergies and -states.

1.3 Optical Lattices

Atomic energy levels get shifted in external oscillating electric fields, like that of laser light, which is called the AC Stark effect [69]. This shift is proportional to the intensity of the electric field [6]. It follows from this that when two sufficiently detuned, to not induce unwanted energetic transitions, counter propagating laser beams interfere and form a standing wave, the generated intensity profile acts as a periodic potential on atoms in the intersection of the beams. A typical form of an optical lattice looks like

$$V_{\text{lat}}(\boldsymbol{x}) = V_0 \sum_{i=1}^{d} \sin^2(k_i x_i), \tag{1.3}$$

where $\boldsymbol{x} \in \mathbb{R}^d$ is the position vector, V_0 is the potential depth, the $k_i = \frac{2\pi}{\lambda_i}$ are the wave vectors and the λ_i are the wavelengths of the lasers generating the lattice in the ith direction.
One-dimensional lattices [71–74] can be generated by this but also higher dimensional lattices can be achieved using mutually orthogonal counter-propagating pairs of laser beams [75–77], see figure 1.3. Apart from these simple cubic geometries also others can be realized, for example hexagonal [78, 79], body-centered cubic [78], triangular [80] or more complex geometries like the Kagomé lattice [81]. Even periodic boundary conditions can be realized [82].
Due to their periodicity, atoms confined to an optical lattice, show a band structure in their spectrum and various other solid-state phenomena. It is thus possible to study condensed matter physics using ultracold atoms in optical lattices. There are however huge advantages of optical lattices over ordinary matter like crystals, etc.: Besides having no defects the big upside is the huge controllability of the system parameters. By varying the wavelength and the intensity of the generating lasers it is possible to change the lattice spacing and the potential height and with this also the interaction and tunneling strengths of the particles confined to the lattice. On-site interactions can further be controlled using Feshbach resonances, which allow the tuning of the scattering length with electromagnetic fields [83, 84]. Also long-range interactions can be realized by diple-dipole interactions [85] and three-body interactions are also possible [86]. Further you can create artificial magnetic fields by laser assisted tunneling allowing to test magnetic lattice models [87]. It is even possible to create phonon-like modes through atom-light interactions in an optical cavity [88]. It is nowadays also possible to address and manipulate single sites of a lattice and thus prepare states of arbitrary filling [89, 90].
Due to these great upsides, ultracold atoms in optical lattices provide a unique testing ground for solid-state phenomena. One great example of this is the observation of the superfluid-Mott insulator transition [7] but also a lot of other phenomena have been observed. In particular topological phases and other related topological phenomena, in which there has been a great interest in the last few decades, could be realized with ultracold atoms in optical lattices [10–13].

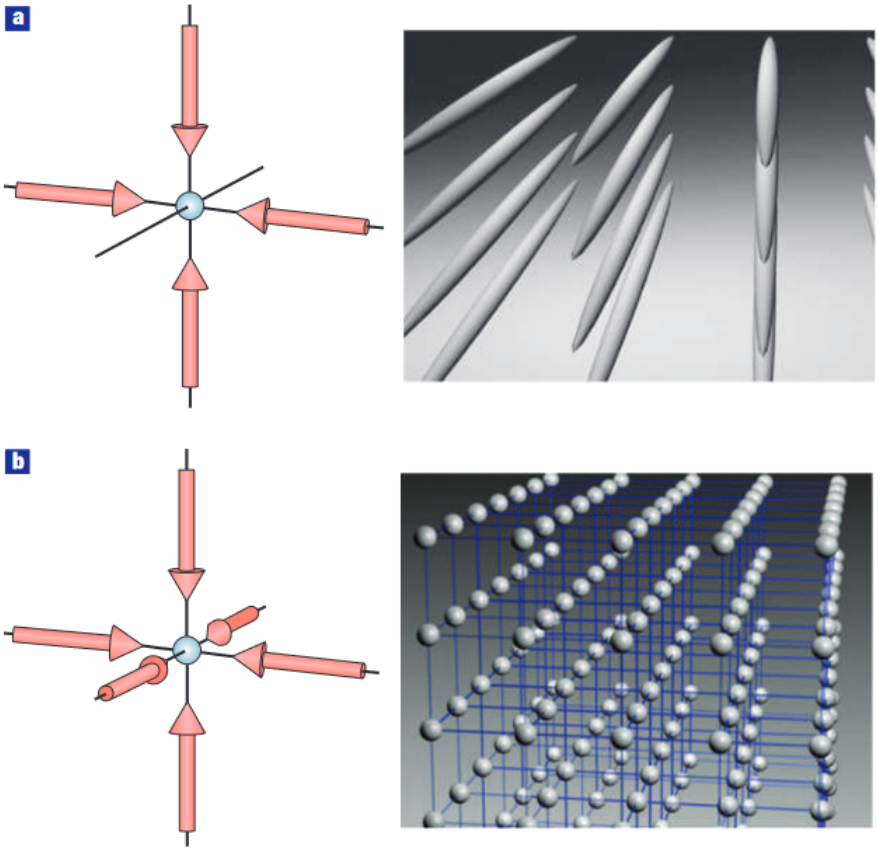

Figure 1.3: a) Two pairs of counter propagating laser beams create a lattice of one-dimensional tubes; b) three pairs generate a simple cubic structure. Taken from Ref. [70].

Maybe surprisingly also theories of high-energy physics and other seemingly unrelated areas of physics can be modeled and tested. For example abelian as well as non-abelian gauge theories like quantum chromodynamics or the other theories building the standard model of particle physics can be tested [21], possibly giving insights into outstanding problems like quark confinement. Recently it has even been proposed that it should be possible to test the AdS/CFT[1] correspondance with ultracold atoms [22], which is related to quantum gravity.

1.4 The Superfluid-Mott Insulator Transition

As already stated above, the Bose-Hubbard model shows a phase transition that was observed using ultracold atoms in an optical lattice. We can get an intuitive understanding for why there is a phase transition occurring in the Bose-Hubbard model by looking at two different limiting cases.
The first one is the case where $U/J \gg 1$. Note that we changed notation $U \equiv V$ from the notation of the original paper of Fisher *et al.* to the nowadays more commonly used one. In this limiting case we can neglect J, so that the remaining Hamiltonian decomposes into a sum over local one-site Hamiltonians (with an optical lattice in mind) that are diagonal in the occupation number representation. Thus, every site

[1] this is an abbreviation for anti-de Sitter/conformal field theory

is occupied by the same number n_0 of particles. The ground state of the system is thus given by

$$|\psi(J=0)\rangle = \prod_{i\in\Lambda} \frac{\left(\hat{a}_i^\dagger\right)^{n_0}}{\sqrt{n_0!}}|0\rangle. \tag{1.4}$$

This is a Mott insulating state, because the particles are prevented from hopping, and thus from conducting, by strong interactions between the particles. It is characterized by a finite excitation gap and zero compressibility $\partial\rho/\partial\mu \sim \partial n/\partial\mu$, where ρ is the particle density directly related to the number of particles per site.
If on the contrary $U/J \ll 1$ we can neglect U. The model then describes non-interacting bosons hopping freely through the lattice, which will of course all condense into the ground state with lattice momentum $\boldsymbol{q} = \mathbf{0}$, i.e. they form an ideal Bose-Einstein condensate. The ground state of the system is simply given by

$$|\psi(U=0)\rangle = \left(\hat{a}_{\boldsymbol{q}=\mathbf{0}}^\dagger\right)^N |0\rangle = \left(\frac{1}{\sqrt{N_\mathrm{S}}}\sum_{i\in\Lambda}\hat{a}_i^\dagger\right)^N |0\rangle, \tag{1.5}$$

where N is the number of particles and N_S is the number of sites. Due to the particles freely hopping through the lattice this state is superfluid. It is characterized by off diagonal long range order which is defined by the condition

$$\inf\left\{\langle\hat{a}_i^\dagger\hat{a}_j\rangle \;\middle|\; i,j\in\Lambda\right\} \neq 0, \tag{1.6}$$

which can be understood as particles on opposite ends of the lattice still affecting each other.
Because the system shows two different phases in the two limits investigated, somewhere in between a phase transition has to occur. Because we can achieve this by solely varying the system parameters, which we can (theoretically) also do at $T = 0$, this phase transition is not driven by thermal fluctuations like an ordinary phase transition. It is rather driven by quantum fluctuations and is thus called a quantum phase transition [91].
This transition is interesting in its own right, as it is the simplest quantum phase transition that can not be mapped to a known higher dimensional classical phase transition [91]. However, there are also multiple applications envisioned for this transition going beyond purely theoretical interest.
Jaksch *et al.* for example, proposed that the superfluid-Mott insulator transition could be used to prepare a large number of qubits for quantum computation and quantum information processing [23]. The Mott insulator states could also be used as a quantum memory [24]. Further it was argued, that the superfluid-Mott insulator transition could be used in high precision quantum interferometry [19]. Another application of the transition was proposed by Capogrosso-Sansone *et al.* They argued that it might be possible to use the transition at the tip of a Mott lobe to study scattering amplitudes of quantum field theories, calling it an "ultracold supercollider" [27].
In the lab the superfluid-Mott insulator transition can be observed through time-of-flight imaging [7], i.e. the optical lattice and the trap are shut down so that the atoms can expand freely and interfere. This interference pattern is then measured. In the superfluid phase, where the particles are coherently spread over the entire

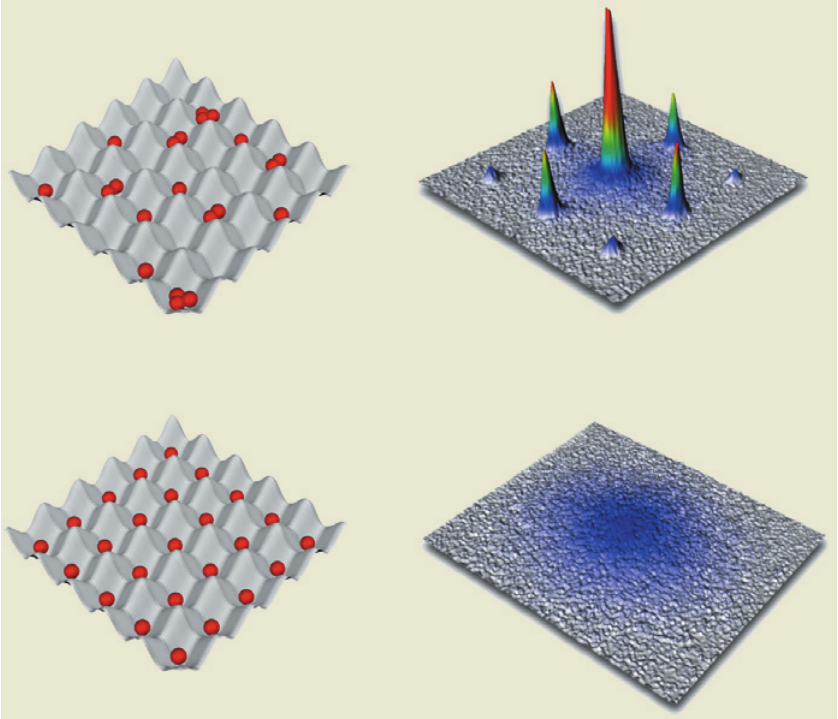

Figure 1.4: Lattice filling and interference pattern after shutting down the lattice and trap potentials in the two phases, top: superfluid, bottom: Mott insulator. Taken from Ref. [93].

lattice, an interference pattern is clearly visible. If the atoms were in the Mott phase prior to the shut down, you can just see an unstructured Gaussian distribution, due to the atoms being fully incoherent in the Mott phase. These two situations are depicted in figure 1.4. Note however that we need to be careful when imagining the atoms as spheres in the superfluid phase like depicted in the figure, as they are actually described by a wave function, which is spread out over the whole lattice. The actual interference patterns observed by Greiner *et al.* are shown in figure 1.5. The same group further showed experimentally, that it is also possible to restore the coherence of the wave function, i.e. to go from the superfluid phase to the Mott phase and back again [92].

When describing thermodynamical quantities at the phase transition, which we want to do extensively in this thesis, we need to decide which parameters we keep fixed and which we vary. The parameter space of interest is given by appropriate values for the quantities J, U, T, μ, which all have dimensions of energy in units where $k_\mathrm{B} = 1$, see section 2.1. We can always use one of these parameters to set the energy scale, i.e. set that parameter to 1, which simply means that we measure all energies in units of the energy set to 1. Thus, there are really only three independent parameters. We will almost always set the energy scale by J or U.
Through inverting the functions $n = n(J, U, T, \mu)$ and $S = S(J, U, T, \mu)$, we can interchange two quantities forming a thermodynamic pair, i.e. n with μ or S with T. In the following we will always consider thermodynamic quantities of interest in dependence of one of the three parameters, for different values of the other two. Most of the time we will vary J or U, which ever one we didn't use to set the scale, for different values of μ (or n) and T (or S).

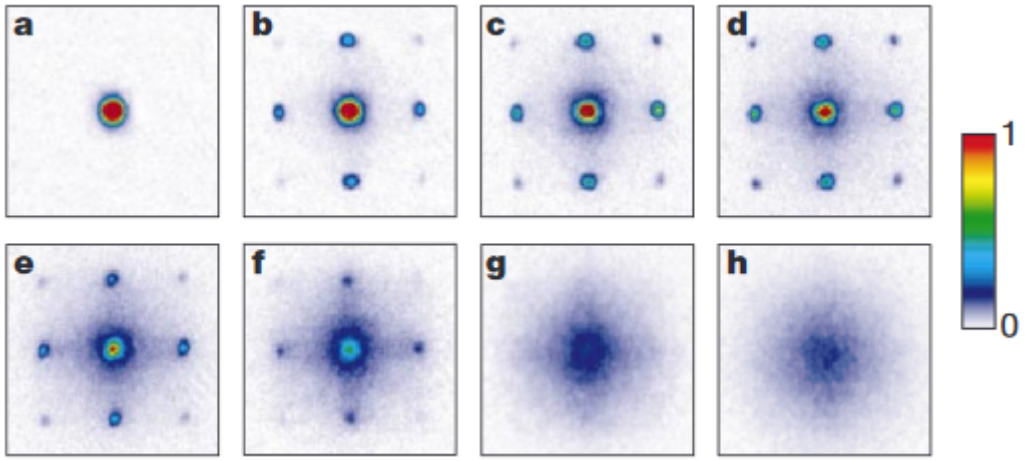

Figure 1.5: Absorption images after a time of flight of 15 ms demonstrating the superfluid-Mott insulator transition. The lattice depths in the images are **a** $0E_{\mathrm{R}}$; **b** $3E_{\mathrm{R}}$; **c** $7E_{\mathrm{R}}$; **d** $10E_{\mathrm{R}}$; **e** $13E_{\mathrm{R}}$; **f** $14E_{\mathrm{R}}$; **g** $16E_{\mathrm{R}}$; **h** $20E_{\mathrm{R}}$, where $E_{\mathrm{R}} = \frac{\hbar^2 k_{\mathrm{L}}^2}{2m}$ is the recoil energy, k_{L} is the wave vector of the lasers generating the optical lattice and m is the mass of the atoms. Taken from Ref. [7].

1.5 Outline

In the next chapter 2 we will review the theoretical background needed to deal with the superfluid-Mott insulator transition. We will review the framework of second quantization, with which we can then give a derivation of the Bose-Hubbard model, in order to see which approximations go into it. We will then give a more precise discussion of the superfluid-Mott insulator transition and construct the phase diagram. Finally we will introduce the mean-field approximation, which is often used to deal with the transition, and the interaction picture of quantum mechanics, which we will need in order to calculate post mean-field corrections.
In chapter 3 we then relate the grand-canonical partition function of the Bose-Hubbard model to a propagator in the interaction picture in imaginary time and then use a Dyson series to find a perturbative expansion around the mean-field grand-canonical partition function. We will see how to calculate the first two orders using a diagrammatic representation of the terms appearing, simplifying the calculation. We will then investigate the low-temperature limit and find that our calculation runs into problems in the case of degeneracies, which we will discuss. Finally we will calculate corrections to the mean-field spectrum for $T = 0$ using ordinary non-degenerate perturbation theory and compare the results with the limit obtained before, providing our calculations with a consistency check.
In chapter 4 we will investigate the consequences of the calculated corrections on thermodynamic quantities. After finding corrections to the phase diagrams we will consider horizontal and vertical lines through the fixed-J and fixed-U phase diagrams for different fixed temperatures and analyze the order parameter, the particle number and the entropy.
In chapter 5 we want to make a step closer to the experiment, where usually the particle number is fixed and not the chemical potential. Thus, we will numerically invert $n(\mu)$ and then consider lines of fixed particle number in the different phase diagrams. Again we will consider the order parameter as well as the entropy on

these lines.
In the final chapter 6 we will also invert $S(T)$ in order to consider the temperature for fixed particle number and fixed entropy. With this we can analyze how the temperature changes when adiabatically changing the system parameters. By considering a cosine-lattice potential we can explicitly calculate J and U in terms of the lattice depth, which allows us to analyze the temperature for varying lattice depth with fixed entropy and particle number. Further we can then give a prediction of the temperature of an ultracold Bose gas after adiabatically turning on an optical lattice, as long as the initial entropy and particle number are known.

Chapter 2

Theoretical Background

In this chapter we will develop the relevant theoretical background that is needed to deal with the phase transition of the Bose-Hubbard model.
After concisely introducing some conventions in section 2.1 we introduce the important framework of second quantization in section 2.2. With this we can then derive the Hamiltonian of the Bose-Hubbard model in section 2.3 and investigate the phase transition it describes in section 2.4. In section 2.5 we will then introduce the mean-field approximation with which we can numerically treat the model. To calculate corrections to this approximation we need to introduce the interaction picture of quantum mechanics which is done in the final section 2.6 of this chapter.

2.1 Conventions

In the following, we will work in natural units where the reduced Planck constant $\hbar$ and Boltzmann's constant k_B are set to 1. This means that temperatures are measured in units of energy and times are measured in units of inverse energy. This choice of units also makes entropies and actions dimensionless. In our analysis the energy scale will usually be set by one of the parameters of the Bose-Hubbard model. If we want to go back to SI units we must simply put in the missing factors of $\hbar$ and k_B, which we will do in all figures.
All vectors in $\mathbb{R}^d$, $d \in \mathbb{N}_{>0}$ will be bold, e.g. $\boldsymbol{x}$, and all operators $\mathcal{H} \to \mathcal{H}$ acting on some Hilbert space $\mathcal{H}$ will be denoted by a hat, e.g. $\hat{H}$. Furthermore we will follow the standard convention (Dirac notation) of denoting vectors in a Hilbert space $\mathcal{H}$ by a "ket", e.g. $|\psi\rangle$, and all elements of the corresponding dual space $\mathcal{H}^*$ by a "bra", e.g. $\langle\psi|$, where we use the same letter for elements connected by the Riesz isomorphism [94].
Also, we will always canonically extend operators acting on some space to operators acting on products involving this space. So, for an operator $\hat{A}_i$ acting on some space $\mathcal{H}_i$ we will let the (extended) operator act on some product space $\bigotimes_{j=1}^{N} \mathcal{H}_j$ as

$$\hat{A}_i = \mathbb{1} \otimes ... \otimes \mathbb{1} \otimes \underbrace{\hat{A}_i}_{\text{space } i} \otimes \mathbb{1} \otimes ... \otimes \mathbb{1}. \tag{2.1}$$

We will use the same symbol for both strictly speaking different operators, but this should never lead to confusion.

In the following, we will consider a finite lattice of N_S sites. We will assume periodic boundary conditions, so that we do not need to worry about boundary effects.

2.2 Second Quantization

The framework of second quantization makes it possible to deal with quantum many-body problems in a convenient way, in particular if the number of particles is not fixed. It is therefore not surprising that also the Bose-Hubbard model is typically discussed in terms of second quantization. In the following I will present the key aspects of second quantization of identical bosons, which will be the relevant case for this thesis. I will mostly present facts and make them plausible, more details and proofs can for example be found in Ref. [95].
We first choose an orthonormal basis $\{|\phi_i\rangle \mid i \in \mathbb{N}_{>0}\}$ of the one-particle Hilbert space $\mathcal{H}_1$. We then denote a state containing n_i identical bosons in state $|\phi_i\rangle$ for $i = 1, 2, ...$ by $|n_1, n_2, ...\rangle$. These states form a basis, the so called occupancy number basis $\{|n_1, n_2, ...\rangle \mid n_i \in \mathbb{N}, i \in \mathbb{N}_{>0}\}$ of the (bosonic) Fock space [96] $\mathcal{F} = \bigoplus_{N=0}^{\infty} \mathcal{H}_N$, where the Hilbert space completion is implied, see Ref. [94], and

$$\mathcal{H}_N = \sum_{\sigma \in S_N} \bigotimes_{i=1}^{N} \mathcal{H}_{\sigma(i)} \tag{2.2}$$

denotes the N-particle Hilbert space, which is just the symmetrized tensor product of the single-particle Hilbert spaces, due to the Pauli principle. Here, $S_N = \{\sigma : \{1, ..., N\} \to \{1, ..., N\} \text{ bijective}\}$ is the symmetric group of rank N [97]. The space $\mathcal{H}_0 = \text{span}(|0\rangle) \cong \mathbb{C}$ is spanned by the normalized vacuum state containing no particles.
In analogy to the algebraic solution of the harmonic oscillator [98] we can now define creation and annihilation operators on Fock space by their action on the occupation number basis states:

$$\begin{aligned} \hat{a}_i^\dagger |n_1, ..., n_i, ...\rangle &= \sqrt{n_i + 1} |n_1, ..., n_i + 1, ...\rangle, \\ \hat{a}_i |n_1, ..., n_i, ...\rangle &= \sqrt{n_i} |n_1, ..., n_i - 1, ...\rangle. \end{aligned} \tag{2.3}$$

In particular, it holds that

$$\hat{a}_i |0\rangle = 0 \text{ for all } i, \tag{2.4}$$

$$|n_1, n_2, ...\rangle = \prod_{i=1}^{\infty} \frac{\left(\hat{a}_i^\dagger\right)^{n_i}}{\sqrt{n_i!}} |0\rangle. \tag{2.5}$$

These operators obey the canonical commutation relations

$$\left[\hat{a}_i, \hat{a}_j\right] = 0, \tag{2.6}$$

$$\left[\hat{a}_i^\dagger, \hat{a}_j^\dagger\right] = 0, \tag{2.7}$$

$$\left[\hat{a}_i, \hat{a}_j^\dagger\right] = \delta_{ij}, \tag{2.8}$$

where δ_{ij} is the Kronecker delta. Note that the Pauli principle is now encoded in the commutation relations: because the creation operators commute it makes no difference in which order particles are created, i.e. how they are labeled. Thus the state does not change by interchanging two bosons as it should be. For fermions we would get analogous canonical anti-commutation relations so that states pick up a minus sign by interchanging two identical fermions.
In case we choose an uncountable basis $\{|\phi_\alpha\rangle \mid \alpha \in I,\ I \text{ uncountable}\}$ for $\mathcal{H}_1$, like for example the position basis, the occupation number kets are not well-defined anymore and it is more convenient to denote a state by all one-particle states involved. For example $|\boldsymbol{x}_1, ..., \boldsymbol{x}_N\rangle$ denotes a state with N particles, with the ith particle at position $\boldsymbol{x}_i$, which we do not require to be different. The action of the annihilation and creation operators is then given by

$$\begin{aligned} \hat{a}^\dagger(\alpha)|\psi_1, ..., \psi_N\rangle &= |\phi_\alpha, \psi_1, ..., \psi_N\rangle, \\ \hat{a}(\alpha)|\psi_1, ..., \psi_N\rangle &= \sum_{i=1}^{N} \langle\phi_\alpha|\psi_i\rangle |\psi_1, ...\psi_{i-1}, \psi_{i+1}, ..., \psi_N\rangle, \end{aligned} \tag{2.9}$$

where we used the notation $\hat{a}(\alpha) = \hat{a}_\alpha$. Note that the normalization is different from the one in the case of a countable basis. This will be justified by equation (2.14) connecting the two cases. We can now generate arbitrary states

$$|\phi_{\alpha_1}, ..., \phi_{\alpha_N}\rangle = \prod_{i=1}^{N} \hat{a}^\dagger_{\alpha_i}|0\rangle. \tag{2.10}$$

The commutation relations now change to

$$\left[\hat{a}_\alpha, \hat{a}_\beta\right] = 0, \tag{2.11}$$

$$\left[\hat{a}^\dagger_\alpha, \hat{a}^\dagger_\beta\right] = 0, \tag{2.12}$$

$$\left[\hat{a}_\alpha, \hat{a}^\dagger_\beta\right] = \delta(\alpha - \beta), \tag{2.13}$$

where $\delta(x)$ is the Dirac delta function. The kets showing all involved states are related to the occupation number kets by

$$|n_1, n_2, ...\rangle = \frac{|\overbrace{\phi_1, ..., \phi_1}^{n_1 \text{ times}}, \overbrace{\phi_2, ..., \phi_2}^{n_2 \text{ times}}, ...\rangle}{\sqrt{\prod_{i=1}^{\infty} n_i!}}. \tag{2.14}$$

From equations (2.5) and (2.10) is is clear that this choice justifies the different normalizations used in equations (2.3) and (2.9). Keep in mind though, that only for a countable basis both sides of this equation are well defined.
If we now change the basis of $\mathcal{H}_1$ from $\{|\phi_i\rangle \mid i \in \mathbb{N}_{>0}\}$ to $\{|\chi_i\rangle \mid i \in \mathbb{N}_{>0}\}$ the creation and annihilation operators transform as

$$\hat{a}^\dagger_{\chi_i} = \sum_{j \in \mathbb{N}_{>0}} \langle\phi_j|\chi_i\rangle \hat{a}^\dagger_{\phi_j}, \tag{2.15}$$

$$\hat{a}_{\chi_i} = \sum_{j \in \mathbb{N}_{>0}} \langle\chi_i|\phi_j\rangle \hat{a}_{\phi_j}. \tag{2.16}$$

The first equality can be immediately shown by acting on an arbitrary occupation number basis state, where the occupation numbers refer to the $|\phi_i\rangle$ basis, with the right hand side. The second equality follows from conjugation. In case of a continuous basis we would have to exchange sums by integrals. For example by changing from the position to the momentum basis the operators transform as

$$\hat{a}(\boldsymbol{p}) = \int_{\mathbb{R}^d} \mathrm{d}^d\boldsymbol{x}\ \frac{1}{(2\pi)^{d/2}} e^{-i\boldsymbol{p}\cdot\boldsymbol{x}} \hat{\Psi}(\boldsymbol{x}), \tag{2.17}$$

which is just a usual Fourier transform. Note that we use the standard convention to denote the annihilation and creation operator for position eigenstates (typically called field operator) differently: $\hat{\Psi}(\boldsymbol{x}) \equiv \hat{a}(\boldsymbol{x})$.
So, we have seen that we can express states using creation and annihilation operators. The convenience of this is that we do not have to deal with symmetrized wavefunctions, which is rather cumbersome for a large number of particles, but with operators that obey canonical commutation relations so that the Pauli principle is automatically satisfied.
We would now like to represent arbitrary one or two particle operators in terms of creation and annihilation operators, i.e. for an arbitrary operator acting on one- (two-) particle Hilbert space we would like to find a corresponding operator acting on Fock space that acts like the one- (two-) particle operator on one- (two-) particle states in Fock space. First we are looking for a corresponding Fock space operator for an arbitray one-particle operator $\hat{A}^{(1)} : \mathcal{H}_1 \to \mathcal{H}_1$. This operator is given by

$$\hat{A} = \sum_{i,j\in\mathbb{N}_{>0}} \langle\phi_i|\hat{A}^{(1)}|\phi_j\rangle \hat{a}_i^\dagger \hat{a}_j, \tag{2.18}$$

where again $\{|\phi_i\rangle \mid i \in \mathbb{N}_{>0}\}$ is a basis of $\mathcal{H}_1$ as before. It can straight-forwardly be checked that this choice makes sense:

$$\hat{A}|\phi_k\rangle = \sum_{i,j\in\mathbb{N}_{>0}} \langle\phi_i|\hat{A}^{(1)}|\phi_j\rangle \hat{a}_i^\dagger \hat{a}_j \hat{a}_k^\dagger|0\rangle = \sum_{i\in\mathbb{N}_{>0}} \hat{a}_i^\dagger|0\rangle\langle\phi_i|\hat{A}^{(1)}|\phi_k\rangle = \hat{A}^{(1)}|\phi_k\rangle. \tag{2.19}$$

In the second step we used the commutation relations and that $\hat{a}_j$ annihilates the vacuum. In the last step we used the completeness relation in $\mathcal{H}_1$.
The operator (2.18) can be interpreted as changing the state of a single particle from $|\phi_j\rangle$ to $|\phi_i\rangle$ with amplitude $\langle\phi_i|\hat{A}^{(1)}|\phi_j\rangle$. This can straight-forwardly be generalized to a two-particle operator which now changes the states of two particles:

$$\hat{A} = \sum_{i,j,k,l\in\mathbb{N}_{>0}} \left(\langle\phi_i| \otimes \langle\phi_j|\right) \hat{A}^{(2)} \left(|\phi_k\rangle \otimes |\phi_l\rangle\right) \hat{a}_i^\dagger \hat{a}_j^\dagger \hat{a}_k \hat{a}_l. \tag{2.20}$$

Here, $\hat{A}^{(2)} : \mathcal{H}_1 \otimes \mathcal{H}_1 \to \mathcal{H}_1 \otimes \mathcal{H}_1$ is now a two-particle operator. These types of operators can describe interactions like scattering events.

2.3 Bose-Hubbard Model

We will now derive the Bose-Hubbard model using the formalism of second quantization that was just introduced. This derivation can for example also be found in Ref. [15].

The single particle Hamiltonian of a non-relativistic particle of mass m in an optical lattice with potential $V_{\text{lat}}(\boldsymbol{x})$ is given by

$$\hat{H}^{(1)} = \frac{\hat{\boldsymbol{p}}^2}{2m} + \hat{V}_{\text{lat}}(\hat{\boldsymbol{x}}), \tag{2.21}$$

where $\hat{\boldsymbol{p}}$ is the usual momentum operator. Note that we do not include a trap potential, i.e. we consider a homogeneous system. Further we neglect the finite waist of the lasers generating the lattice, which would have an effect similar to a weak trapping potential [99]. Including these effects could be subject of further work.
If we now add a two particle interaction potential $\frac{1}{2}\hat{V}(\hat{\boldsymbol{x}}_1 - \hat{\boldsymbol{x}}_2)$ and go over to the second quantized Hamiltonian using the position basis as the basis of $\mathcal{H}_1$ by using equations (2.18) and (2.20) we get

$$\begin{aligned}\hat{H} = &\int_{\mathbb{R}^d} \mathrm{d}^d\boldsymbol{x}\ \hat{\Psi}^\dagger(\boldsymbol{x}) \left[-\frac{\nabla^2}{2m} + V_{\text{lat}}(\boldsymbol{x})\right] \hat{\Psi}(\boldsymbol{x}) \\ &+ \frac{1}{2}\int_{\mathbb{R}^d} d^d\boldsymbol{x}_1 \int_{\mathbb{R}^d} d^d\boldsymbol{x}_2 \hat{\Psi}^\dagger(\boldsymbol{x}_1)\hat{\Psi}^\dagger(\boldsymbol{x}_2)V(\boldsymbol{x}_1 - \boldsymbol{x}_2)\hat{\Psi}(\boldsymbol{x}_1)\hat{\Psi}(\boldsymbol{x}_2).\end{aligned} \tag{2.22}$$

We now assume that the interactions between the bosons are given by a contact potential

$$V(\boldsymbol{x}_1 - \boldsymbol{x}_2) = g\delta(\boldsymbol{x}_1 - \boldsymbol{x}_2) \tag{2.23}$$

with interaction strength $g = 4\pi a_{\text{s}}/m$ which is determined by the s-wave scattering length a_{s}. This is justified for small temperatures, which we are interested in [100]. This yields the Hamiltonian

$$\hat{H} = \int_{\mathbb{R}^d} \mathrm{d}^d\boldsymbol{x} \left\{\hat{\Psi}^\dagger(\boldsymbol{x}) \left[-\frac{\nabla^2}{2m} + V_{\text{lat}}(\boldsymbol{x})\right] \hat{\Psi}(\boldsymbol{x}) + \frac{g}{2}\hat{\Psi}^\dagger(\boldsymbol{x})\hat{\Psi}^\dagger(\boldsymbol{x})\hat{\Psi}(\boldsymbol{x})\hat{\Psi}(\boldsymbol{x})\right\}. \tag{2.24}$$

Due to the periodic lattice potential the energy spectrum will in general show a band structure. Because we are interested in the low-temperature regime, the thermal energy is generally smaller than the band gap between the lowest two bands, so occupation in the higher bands is exponentially suppressed. If we now introduce the Wannier functions of the lowest band (the band index will be suppressed) as Fourier transform of the Bloch functions of the lowest band [101]

$$w(\boldsymbol{x} - \boldsymbol{x}_i) = \frac{1}{\sqrt{N_{\text{S}}}} \sum_{\boldsymbol{k}\in 1.\text{BZ}} \phi_{\boldsymbol{k}}(\boldsymbol{x}) e^{-i\boldsymbol{k}\cdot\boldsymbol{x}_i} \tag{2.25}$$

we can expand the field operators in terms of these:

$$\hat{\Psi}(\boldsymbol{x}) = \sum_{i\in\Lambda} \hat{a}_i w(\boldsymbol{x} - \boldsymbol{x}_i). \tag{2.26}$$

Here, N_{S} is the number of sites in the optical lattice, 1.BZ is an abbreviation of the first Brillouin zone, $\hat{a}_i$ is the annihilation operator annihilating a particle on lattice site i, i.e. in the Wannier state of site i, $\boldsymbol{x}_i$ is the position of site i and Λ denotes the lattice itself. This expansion is essentially a basis change, as discussed in section 2.2, from the continuous position basis to the discrete basis of lattice sites. This means

that we are not interested in exact position eigenstates but only in the Wannier states which are localized on a lattice site.
If we now plug this decomposition into (2.24) we end up with

$$\hat{H} = -\sum_{i,j\in\Lambda} J_{ij}\hat{a}_i^\dagger\hat{a}_j + \frac{1}{2}\sum_{i,j,k,l\in\Lambda} U_{ijkl}\hat{a}_i^\dagger\hat{a}_j^\dagger\hat{a}_k\hat{a}_l, \tag{2.27}$$

where we defined

$$J_{ij} = -\int_{\mathbb{R}^d} \mathrm{d}^d\boldsymbol{x}\; w^*(\boldsymbol{x}-\boldsymbol{x}_i)\left[-\frac{\nabla^2}{2m} + V_{\mathrm{lat}}(\boldsymbol{x})\right] w(\boldsymbol{x}-\boldsymbol{x}_j), \tag{2.28}$$

$$U_{ijkl} = g\int_{\mathbb{R}^d} \mathrm{d}^d\boldsymbol{x}\; w^*(\boldsymbol{x}-\boldsymbol{x}_i)w^*(\boldsymbol{x}-\boldsymbol{x}_j)w(\boldsymbol{x}-\boldsymbol{x}_k)w(\boldsymbol{x}-\boldsymbol{x}_l). \tag{2.29}$$

If we assume that the lattice potential can be written as a sum over potentials that just depend on one coordinate $V_{\mathrm{lat}}(\boldsymbol{x}) = \sum_{i=1}^d V_{\mathrm{lat}}^{(i)}(x_i)$, which is definitely realistic, then the one-particle Hamiltonian also decomposes into a sum $\hat{H}^{(1)} = \sum_{i=1}^d \hat{H}_i^{(1)}$ and the Bloch functions factorize $\phi_{\boldsymbol{k}}(\boldsymbol{x}) = \prod_{i=1}^d \phi_{k_i}^{(i)}(x_i)$ and with this also the Wannier functions factorize in a similar fashion.
With this we can simplify the expression for J_{ij}. To this end we divide the d-dimensional integral in each term of the sum over the $\hat{H}_i^{(1)}$ into the one-dimensional part where the respective $\hat{H}_i^{(1)}$ acts and the rest.

$$\begin{aligned}
J_{ij} &= -\sum_{n=1}^d \int_{\mathbb{R}^d} \mathrm{d}^d\boldsymbol{x}\; w^*(\boldsymbol{x}-\boldsymbol{x}_i)\left[-\frac{\nabla_n^2}{2m} + V_{\mathrm{lat}}^{(n)}(x_n)\right] w(\boldsymbol{x}-\boldsymbol{x}_j) \\
&= -\sum_{n=1}^d \prod_{\substack{\alpha=1\\\alpha\neq n}}^d \int_{\mathbb{R}} \mathrm{d}x_\alpha\; (w^{(\alpha)}(x_\alpha - x_{i,\alpha}))^* w^{(\alpha)}(x_\alpha - x_{j,\alpha}) \\
&\quad\times \int_{\mathbb{R}} \mathrm{d}x_n\; (w^{(n)}(x_n - x_{i,n}))^* \left[-\frac{\nabla_n^2}{2m} + V_{\mathrm{lat}}^{(n)}(x_n)\right] w^{(n)}(x_n - x_{j,n}).
\end{aligned}$$

We can now use that the Bloch functions are eigenfunctions of the single particle Hamiltonian.

$$= -\frac{1}{N_{\mathrm{S}}}\sum_{n=1}^d \sum_{\boldsymbol{k}\in 1.\mathrm{BZ}} \sum_{\boldsymbol{q}\in 1.\mathrm{BZ}} \int_{\mathbb{R}^d} \mathrm{d}^d\boldsymbol{x}\; \phi_{\boldsymbol{k}}^*(\boldsymbol{x})\phi_{\boldsymbol{q}}(\boldsymbol{x}) e^{i\boldsymbol{k}\cdot\boldsymbol{x}_i} e^{-i\boldsymbol{q}\cdot\boldsymbol{x}_j} E^{(n)}(q_n).$$

This further simplifies because the Bloch functions are orthonormal.

$$J_{ij} = -\frac{1}{N_{\mathrm{S}}}\sum_{\boldsymbol{k}\in 1.\mathrm{BZ}} e^{i\boldsymbol{k}\cdot(\boldsymbol{x}_i-\boldsymbol{x}_j)} E(\boldsymbol{k}), \tag{2.30}$$

with $E(\boldsymbol{k}) = \sum_{n=1}^d E^{(n)}(k_n)$. This shows that $J_{\boldsymbol{\delta}} \equiv J_{ij}$ only depends on the difference $\boldsymbol{\delta} = \boldsymbol{x}_i - \boldsymbol{x}_j$ of the two sites. Typically $\boldsymbol{\delta}$ is measured in units of the nearest neighbour distance.
If the difference between two sites is large the exponential will oscillate fastly which will give a small J_{ij} due to the dispersion being a smooth function of $\boldsymbol{k}$. Thus, we are able to only keep the nearest neighbour and the on-site term as a first approximation. We will assume that this approximation is also valid for more general lattice potentials, which is definitely physically reasonable.
Further, we assume that the Wannier functions are sharply peaked on their respec-

tive site, which is reasonable for a deep enough lattice. With this assumption, we can also neglect all U_{ijkl} besides the on-site terms, see equation (2.29). Due to the homogeneity of the lattice all $J_{ij} \equiv J$, $J_{ii} \equiv \epsilon$ and $U_{iiii} \equiv U$ are the same, where i and j are nearest-neighbour sites.
The first J_{ij} and U_{ijkl} are depicted in figure 2.1. The figures were generated for the 1D lattice potential $V_{\text{lat}}(x) = \cos(2k_{\text{L}}x)$ (k_{L} being the wave vector of the laser generating the optical lattice), for which the dispersion and the Bloch functions can be straight-forwardly calculated, which is done in appendix A.
Both figures clearly show that the terms we have not neglected are the most dominant. In particular for higher lattice depths the approximations we made are well justified. Note that when the lattice depth is small, also the band gap between the lowest and the first excited band is small and it is not justified to neglect excitations into higher bands. Thus for the lattice depths where the lowest band approximation, which is crucial for the model, is justified also the other approximations are.
In appendix D we also consider higher order J_{ij} to get a better approximation. Higher order U_{ijkl} would correspond to non-local interactions involving multiple sites and they are generally more difficult to include. Similar models involving these higher order terms are usually called extended Hubbard models and they shall not be further considered in this thesis, as we have seen that they would make only a marginal difference.
By deploying the discussed approximations, splitting off the diagonal terms in the

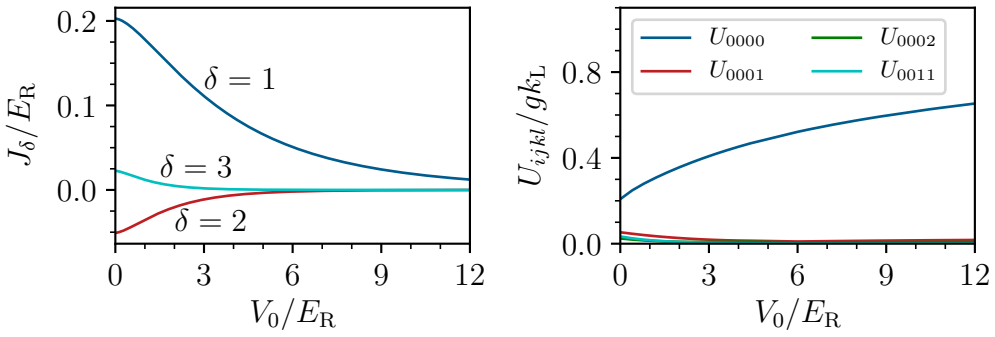

Figure 2.1: Comparison of the first J_{ij} and U_{ijkl}, generated for the 1D lattice potential $V_{\text{lat}}(x) = \cos(2k_{\text{L}}x)$, see appendix A. Here, k_{L} denotes the wave vector of the laser generating the optical lattice and $E_{\text{R}} = \frac{k_{\text{L}}^2}{2m}$ denotes the recoil energy.

first sum in equation (2.27) and using $\hat{a}_i^\dagger \hat{a}_i^\dagger \hat{a}_i \hat{a}_i = \hat{a}_i^\dagger \hat{a}_i \hat{a}_i^\dagger \hat{a}_i - \hat{a}_i^\dagger \hat{a}_i = \hat{n}_i(\hat{n}_i - 1)$, which directly follows from the canonical commutation relations, we arrive at

$$\hat{H} = -J \sum_{\langle i,j \rangle \in \Lambda^2} \hat{a}_i^\dagger \hat{a}_j + \frac{U}{2} \sum_{i \in \Lambda} \hat{n}_i(\hat{n}_i - 1) - \epsilon \sum_{i \in \Lambda} \hat{n}_i. \tag{2.31}$$

Here $\langle i, j \rangle$ denotes a pair of nearest neighbours and $\hat{n}_i = \hat{a}_i^\dagger \hat{a}_i$ is the occupation number operator. Finally we now go over to the grand-canonical ensemble, so we introduce a term $-\mu \hat{N} = -\mu \sum_{i \in \Lambda} \hat{n}_i$ fixing the mean particle number. If we now absorb the ϵ into the chemical potential μ we finally arrive at the Bose-Hubbard

Hamiltonian

$$\hat{H}_{\mathrm{BH}} = -J \sum_{\langle i,j\rangle \in \Lambda^2} \hat{a}_i^\dagger \hat{a}_j + \frac{U}{2} \sum_{i\in\Lambda} \hat{n}_i(\hat{n}_i - 1) - \mu \sum_{i\in\Lambda} \hat{n}_i. \tag{2.32}$$

We can interpret the first term as the energy the particles win for $J > 0$, which is typically the case, through delocalization by tunneling to a neighbouring site. The second term describes the energy loss for $U > 0$, which also is the case typically, due to the repulsive interaction of two or more bosons occupying the same site. The third term describes the energy win (loss) for $\mu > 0$ ($\mu < 0$) associated with an additional particle getting added to the system, which fixes the mean particle number as stated above. The physics that this model describes is dictated by the competition of these terms, in particular the first two.
Note also that this Hamiltonian possesses a continuous global U(1) symmetry $\hat{a}_i \to e^{i\theta}\hat{a}_i$, $\hat{a}_i^\dagger \to e^{-i\theta}\hat{a}_i^\dagger$. This symmetry will be spontaneously broken by a phase transition, which will be introduced in the next section.

2.4 The Superfluid - Mott Insulator Transition

To better understand the physics described by the Bose-Hubbard model we first restrict ourselves to the $T = 0$ case. Our discussion will be based on the one in the seminal paper of Fischer *et al.* [33].
First we look at the simple case $J = 0$. Here, the individual sites decouple and the one-site Hamiltonians are diagonal in the occupation number basis of the respective sites with eigenenergies

$$\epsilon(n) = \frac{U}{2} n(n-1) - \mu n. \tag{2.33}$$

So, each site is occupied by the same integer number of bosons n_0 that minimizes this energy. One approach to finding n_0 for some parameters μ and U is to realize that the following has to hold:

$$\begin{aligned} \epsilon(n_0+1) - \epsilon(n_0) &= Un_0 - \mu > 0, \\ \epsilon(n_0-1) - \epsilon(n_0) &= U(1-n_0) + \mu > 0. \end{aligned} \tag{2.34}$$

These equations simply state that it should not be energetically favorable to add or remove a boson. From these conditions it follows that for $n_0 - 1 < \mu/U < n_0$, n_0 will minimize the energy if $\mu > 0$, else $n_0 = 0$. We now study the lowest lying excitations of this state. To this end we fix μ/U such that the particle number is n, e.g. we set $\mu/U = n - \frac{1}{2} + \alpha$ with $\alpha \in \left(-\frac{1}{2}, \frac{1}{2}\right)$. The lowest lying excitations should be the state with one boson added or removed, i.e. a hole added. The excitation energies for these states are given by

$$\begin{aligned} \epsilon(n+1) - \epsilon(n) &= \left(\frac{1}{2} - \alpha\right) U, \\ \epsilon(n-1) - \epsilon(n) &= \left(\frac{1}{2} + \alpha\right) U. \end{aligned} \tag{2.35}$$

Thus, the smallest excitation energy is given by $\left(\frac{1}{2} - |\alpha|\right) U > 0$. This means that if we now increase J to a sufficiently small but non-zero value, this energy gap can not be overcome by the energy won through the hopping of the extra particle or hole. Because we can vary μ (or rather α) as well as J so that the ground state of the system is still given by every site being occupied by the same number of bosons, there should be a finite region in the μ–J plane where the mean number of bosons per site is a constant integer.
The lowest lying excitation at constant particle number is a particle-hole excitation with energy given by the energy difference between the state after a particle hopped from one site to a neighbouring one and the state before (both sites containing an equal number of bosons), i.e. $\epsilon(n+1) + \epsilon(n-1) - 2\epsilon(n) = U > \left(\frac{1}{2} - |\alpha|\right) U$. So, in these regions it is also not energetically favorable for the bosons to hop, which means that the system is insulating.
Furthermore, it follows from the constant particle number in these regions that the compressibility $\partial\rho/\partial\mu$ of the system vanishes. Here, $\rho \sim n$ is the particle density directly related to the number of particles per site. These properties (finite excitation gap and zero compressibility) are the characteristic properties of a Mott insulator [33].
If we now take a point in this Mott phase and increase (decrease) the chemical potential at fixed J we expect that at some point the energy won by adding a boson (hole) to the system together with the energy won through the hopping of this boson (hole) will overcompensate the energy cost through the on-site interaction. This extra boson (hole) can now freely hop through the lattice, not "seeing" the other bosons. So, the boson will fully delocalize and produce a superfluid state. Thus, we expect a phase transition from a Mott insulating state to a superfluid state to take place here.
Because this happens at $T = 0$, the transition can not be driven by thermal fluctuation like an ordinary phase transition but rather by quantum fluctuations, which is why it is called a quantum phase transition [91]. Furthermore it turns out that it is a second order phase transition, i.e. the first derivatives of the free energy (entropy, particle number, etc.) are all continuous at the transition and discontinuities only occur in the second derivatives of the free energy, e.g. the heat capacity.
For higher J a particle (hole) of course gains more energy through hopping, so this point of transition from Mott to superfluid will occur earlier. This leads to the conclusion, that the Mott phases have a lobe-like structure in the μ–J plane. In the discussion above, we excluded the cases $\alpha = \pm\frac{1}{2}$ corresponding to $\mu/U \in \mathbb{Z}$. Here, there exists no energy gap for adding/removing bosons as is apparent from (2.35). In these cases the system is in the superfluid phase for all values of J. This discussion can be summarized into a zero temperature phase diagram 2.2.

There are actually two kinds of phase transitions that occur. One of them occurs at the tip of the lobe and the other one occurs at any other point of the lobe boundary. During the second kind of transition the mean number of particles per site changes continously (strictly speaking only for $N_S \to \infty$, but approximately for N_S sufficiently large) as the system crosses the phase boundary. Thus, this transition is driven by extra particles (holes) getting added to the system that can then hop freely through the lattice producing a superfluid state.
The transition at the tip however, happens at constant particle number per site, it is thus driven differently. Here the particles in the Mott phase simply gain enough

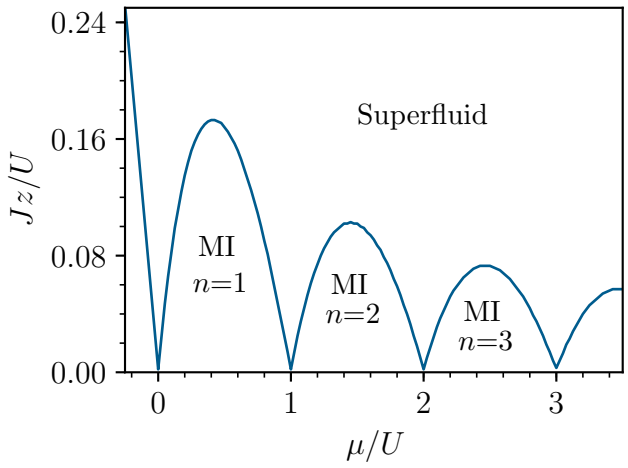

Figure 2.2: $T = 0$ phase diagram, generated using mean-field theory to be discussed in section 2.5, z denotes the number of nearest neighbour sites of one lattice site, MI is abbreviation of Mott insulator

energy through hopping so that they can overcome the repulsion and condense into a superfluid despite the integer mean particle number per site. The difference in the two transitions is also reflected in the fact that they lie in different universality classes i.e. have different critical exponents, which was also shown in Ref. [33].
If we look at a finite temperature, there is always the exponentially small possibility of the system crossing the excitation gap mentioned above, making it possible to add or remove a boson. Because of this the number of particles per site is only approximately constant and the compressibility is not exactly zero anymore. Thus, we conclude that at finite temperature there exists no exact Mott phase anymore. In the following we will refer to the not-superfluid phase as the normal phase to distinguish it from the exact Mott phase at $T = 0$.

2.5 Mean-Field Theory

Now that we have a qualitative understanding of the physics described by the Bose-Hubbard model and of the phase transition it inherits, we want to see how we can actually calculate the behaviour of thermodynamic quantities at the phase transition.
Due to the hopping term in equation (2.32) coupling neighbouring sites with each other the model can not be solved analytically and also a numerical treatment is demanding for a large number of sites. One common approximation simplifying the problem is the mean-field approximation. A discussion of the mean-field approximation in general terms as well as in the concrete context of the Bose-Hubbard model can for example also be found in Ref. [91].
The idea of this approximation is to get rid of non-local terms by approximating the involved operators by their expectation values. By this we neglect quantum as well as thermal fluctuations around these expectation values but we gain a local Hamiltonian which can be treated numerically. In the case of the Bose Hubbard

model we can approximate

$$\hat{a}_i \approx \langle \hat{a}_i \rangle \mathbb{1} + \delta \hat{a}_i, \tag{2.36}$$

where $\mathbb{1}$ is the identity operator, which will be omitted from now on. We now neglect terms that are at least second order in the fluctuations, so we find

$$\begin{aligned} 0 \approx \delta\hat{a}_i^\dagger \delta\hat{a}_j &= \hat{a}_i^\dagger \hat{a}_j - \langle \hat{a}_i^\dagger \rangle \hat{a}_j - \langle \hat{a}_j \rangle \hat{a}_i^\dagger + \langle \hat{a}_i^\dagger \rangle \langle \hat{a}_j \rangle \\ \Rightarrow \hat{a}_i^\dagger \hat{a}_j &\approx \langle \hat{a}_i^\dagger \rangle \hat{a}_j + \langle \hat{a}_j \rangle \hat{a}_i^\dagger - \langle \hat{a}_i^\dagger \rangle \langle \hat{a}_j \rangle. \end{aligned} \tag{2.37}$$

Because of the assumed homogeneity of the lattice the quantity $\psi = \langle \hat{a}_i \rangle$ is well-defined, or equivalently $\psi^* = \langle \hat{a}_i^\dagger \rangle$.
By deploying this approximation and renaming the summation indices we end up with the mean-field Hamiltonian

$$\hat{H}_{\mathrm{MF}} = \sum_{i \in \Lambda} \left\{ -zJ \left(\psi^* \hat{a}_i + \psi \hat{a}_i^\dagger - |\psi|^2 \right) + \frac{U}{2} \hat{n}_i \left(\hat{n}_i - 1 \right) - \mu \hat{n}_i \right\} \equiv \sum_{i \in \Lambda} \hat{H}_{\mathrm{MF},i}, \tag{2.38}$$

where z denotes the number of nearest neighbours of one site.
This Hamiltonian decouples into a sum of local one-site Hamiltonians which simplifies the problem drastically. Because of the homogeneity of the lattice each of these one-site Hamiltonians is equivalent. If we refer to one of these we will call it $\hat{H}_{\mathrm{MF,S}}$ instead of using a particular site index to stress the independence of the lattice site. Similarly, we will denote its grand-canonical partition function by $\mathcal{Z}_{\mathrm{MF,S}} \equiv \mathrm{Tr}\left(e^{-\beta \hat{H}_{\mathrm{MF,S}}} \right)$, where $\beta = 1/T$ is the inverse temperature.
Due to the decoupling in equation (2.38) it is now possible to numerically calculate the grand-canonical partition function and the grand-canonical potential for this Hamiltonian, which we will do in chapter 4. The numerical results for the mean-field case will be used as a reference for the results beyond this approximation calculated in chapter 3.
The mean-field parameter ψ would now have to be determined self-consistently, e.g. the correct value of $\psi = \psi_0$ is such that

$$\langle \hat{a}_i \rangle_{\mathrm{MF}}|_{\psi=\psi_0} \equiv \frac{1}{\mathcal{Z}_{\mathrm{MF}}} \mathrm{Tr}\left(\hat{a}_i e^{-\beta \hat{H}_{\mathrm{MF}}} \right) \Big|_{\psi=\psi_0} = \psi_0. \tag{2.39}$$

So, the mean-field parameter ψ is simply an unphysical parameter in our Hamiltonian and the "definition" of this parameter serves as a self consistency condition to determine its correct value.
In the following we will take a different approach to finding the correct value of ψ. It is known from thermodynamics that the entropy S must always be maximized in equilibrium. Statistically this follows from the fact that in equilibrium a system will always choose a macroscopic state such that the number of available microstates is maximized [102]. From the maximization of entropy it follows, that the grand-canonical potential $\Phi = E - TS - \mu N$ has to always be minimized with respect to its parameters in thermal equilibrium. If we now take ψ to be one of these thermodynamic parameters it follows that we can determine ψ by minimizing

the grand-canonical potential.

$$\psi_0 \in \left\{ \psi \in \mathbb{C} \;\middle|\; \Phi(\psi) = \min_{\psi \in \mathbb{C}}(\Phi(\psi)) \right\}. \tag{2.40}$$

It might be concerning that the set in equation (2.40) contains more than one element or is empty, and thus does not give a unique result for ψ. It turns out however that this set either only contains 0 or is a circle in the complex plane in which case all of the possible ψ are physically equivalent and observable quantities only depend on the absolute value $|\psi|$. This is a consequence of the already mentioned U(1) symmetry of the Bose-Hubbard Hamiltonian, we will also see this exemplarily in chapter 4.
By inspection of equation (2.38) you can see that the parameter ψ explicitly breaks the U(1) symmetry of the mean-field Hamiltonian, so for non-zero values of the parameter the Hamiltonian is not invariant under U(1) transformations. This makes ψ a suitable choice as an order parameter, because if it is zero it corresponds to a phase symmetric under U(1) transformations, and a non-zero value breaks this symmetry giving the system an order under the symmetry, which is the superfluid phase in this case [91]. It further turns out that $|\psi|^2$ is equal to the condensate density, i.e. the fraction of particles that are condensed into the lowest lying state and thus delocalized over the full lattice [100].
Furthermore, it is clear that the U(1) symmetry is connected to local particle number conservation, because the mean-field Hamiltonian commutes with the particle number operator $\hat{n}_i$ of an arbitrary site $i \in \Lambda$ if and only if $\psi = 0$.
One can also show analytically that the two approaches to determining ψ are equivalent. First note that because the grand-canonical potential only depends on the magnitude of ψ we can without loss of generality restrict ψ to real values to find the correct value ψ_0, i.e. we can find ψ_0 by taking the derivative of Φ in the sense of real analysis. Secondly note that differentiation with respect to ψ and taking the trace commutes, because the trace is basis independent and we could use a basis which is independent of ψ to take the trace. With this we can now show the equivalence:

$$\begin{aligned} \frac{\partial \Phi}{\partial \psi} &= \frac{1}{\mathcal{Z}_{\mathrm{MF}}} \mathrm{Tr}\left(\frac{\partial \hat{H}_{\mathrm{MF}}}{\partial \psi} e^{-\beta \hat{H}_{\mathrm{MF}}} \right) = -\frac{zJ}{\mathcal{Z}_{\mathrm{MF}}} \sum_{i \in \Lambda} \mathrm{Tr}\left[\left(\hat{a}_i^\dagger - \psi^* \right) e^{-\beta \hat{H}_{\mathrm{MF}}} \right] \\ &= -zJN_{\mathrm{S}} \left(\langle \hat{a}^\dagger \rangle_{\mathrm{MF}} - \psi^* \right). \end{aligned} \tag{2.41}$$

Here we omitted the index of $\hat{a}^\dagger$ in the expectation value because it can not depend on the lattice site due to the homogeneity of the lattice. Equation (2.41) now tells us that

$$\frac{\partial \Phi}{\partial \psi} = 0 \Leftrightarrow \psi^* = \langle \hat{a}^\dagger \rangle_{\mathrm{MF}}, \tag{2.42}$$

which shows the equivalence of the two approaches.

2.6 The Interaction Picture

We now want to go beyond the mean-field approximation and find a way to systematically expand around it in order to include the effect of quantum fluctuations. To

find this expansion we first need to introduce one important concept from ordinary quantum mechanics: the interaction picture. A discussion of the interaction picture can be found in almost every quantum mechanics textbook, for example in Ref. [98]. If the Hamiltonian $\hat{H}$, in the Schrödinger or Heisenberg picture, is decomposable into a possibly complicated interacting part $\hat{V}$ and a solvable, non-interacting part $\hat{H}_0$ then it turns out that the Schrödinger (time evolution in the states) or Heisenberg pictures (times evolution in the operators) of quantum mechanics are not the most beneficial choices. A better choice is to use the interaction picture, where the time evolution is split up between states and operators. In this picture we define the states by

$$|\psi_{\mathrm{I}}(t)\rangle = \hat{U}_0^{-1}(t,t_0)|\psi_{\mathrm{S}}(t)\rangle. \tag{2.43}$$

Here, $\hat{U}_0(t,t_0) = e^{-i(t-t_0)\hat{H}_0}$ is the free time evolution operator satisfying $\hat{U}_0^{-1}(t,t_0) = \hat{U}_0^{\dagger}(t,t_0) = \hat{U}_0(t_0,t)$, t_0 is an arbitrary reference time where the states in the interaction and the Schrödinger picture coincide and $|\psi_S(t)\rangle$ denotes a state in the Schrödinger picture. With this definition we aim to take the free evolution away from the states by evolving them backwards to the reference time using only the free Hamiltonian, so that "they only change when something interesting happens". Because expectation values have to be the same in the different pictures we can now deduce how the operators in the interaction picture have to look like. To this end we take an arbitrary operator in the Schrödinger picture $\hat{A}_{\mathrm{S}}$ and calculate:

$$\begin{aligned}\langle\psi_{\mathrm{S}}(t)|\hat{A}_{\mathrm{S}}|\psi_{\mathrm{S}}(t)\rangle &= \langle\psi_{\mathrm{I}}(t)|\hat{U}_0^{\dagger}(t,t_0)\hat{A}_{\mathrm{S}}\hat{U}_0(t,t_0)|\psi_{\mathrm{I}}(t)\rangle \equiv \langle\psi_{\mathrm{I}}(t)|\hat{A}_{\mathrm{I}}(t)|\psi_{\mathrm{I}}(t)\rangle \\ \Rightarrow \hat{A}_{\mathrm{I}}(t) &= \hat{U}_0^{\dagger}(t,t_0)\hat{A}_{\mathrm{S}}\hat{U}_0(t,t_0) = e^{i(t-t_0)\hat{H}_0}\hat{A}_{\mathrm{S}}e^{-i(t-t_0)\hat{H}_0}.\end{aligned} \tag{2.44}$$

We can find the time evolution of the states by differentiating them:

$$\begin{aligned}i\frac{\mathrm{d}}{\mathrm{d}t}|\psi_{\mathrm{I}}(t)\rangle &= \hat{U}_0^{-1}(t,t_0)(\hat{H}-\hat{H}_0)|\psi_{\mathrm{S}}(t)\rangle = \hat{U}_0^{-1}(t,t_0)\hat{V}_{\mathrm{S}}\hat{U}_0(t,t_0)\hat{U}_0^{-1}(t,t_0)|\psi_{\mathrm{S}}(t)\rangle \\ &= \hat{V}_{\mathrm{I}}(t)|\psi_{\mathrm{I}}(t)\rangle.\end{aligned} \tag{2.45}$$

Here, we used the Schrödinger equation $i\frac{\mathrm{d}}{\mathrm{d}t}|\psi_{\mathrm{S}}(t)\rangle = \hat{H}|\psi_{\mathrm{S}}(t)\rangle$ for $|\psi_{\mathrm{S}}(t)\rangle$. Equation (2.45) is just the Schrödinger equation for $|\psi_{\mathrm{I}}(t)\rangle$ with the interaction potential in the interaction picture acting as the Hamiltonian, which justifies the definition of the states from above.
The time evolution of the operators is given by

$$i\frac{\mathrm{d}}{\mathrm{d}t}\hat{A}_{\mathrm{I}}(t) = -\hat{H}_0\hat{A}_{\mathrm{I}}(t) + \hat{A}_{\mathrm{I}}(t)\hat{H}_0 = \left[\hat{A}_{\mathrm{I}}(t),\hat{H}_0\right]. \tag{2.46}$$

This is just the Heisenberg equation for $\hat{A}_{\mathrm{I}}(t)$ with the free Hamiltonian acting as the full Hamiltonian. Note that the free Hamiltonian is the same in the interaction picture and the Schrödinger picture.
So, in conclusion we have split up the time evolution so that the operators only evolve with the free Hamiltonian and the states only evolve with the interacting Hamiltonian as desired.
Because equation (2.45) looks like the Schrödinger equation with a time-dependent

Hamiltonian we can immediately write down the solution [98]

$$|\psi_{\mathrm{I}}(t)\rangle = \hat{U}_{\mathrm{I}}(t,t')|\psi_{\mathrm{I}}(t')\rangle, \tag{2.47}$$

with the propagator in the interaction picture

$$\hat{U}_{\mathrm{I}}(t,t') = \mathcal{T}\exp\left\{-i\int_{t'}^{t} \mathrm{d}\tau\ \hat{V}_{\mathrm{I}}(\tau)\right\}. \tag{2.48}$$

Here, $\mathcal{T}$ is the usual time ordering operator.
We can also find another expression for $\hat{U}_I(t,t')$ by relating it to the propagator in the Schrödinger picture $\hat{U}_{\mathrm{S}}(t,t')$:

$$\begin{aligned} &|\psi_{\mathrm{I}}(t)\rangle = \hat{U}_0^{-1}(t,t_0)|\psi_{\mathrm{S}}(t)\rangle = \hat{U}_0^{-1}(t,t_0)\hat{U}_S(t,t')\hat{U}_0(t',t_0)|\psi_{\mathrm{I}}(t')\rangle \\ &\Rightarrow \hat{U}_{\mathrm{I}}(t,t') = \hat{U}_0^{-1}(t,t_0)\hat{U}_{\mathrm{S}}(t,t')\hat{U}_0(t',t_0) = e^{-i(t_0-t)\hat{H}_0}e^{-i(t-t')\hat{H}}e^{-i(t'-t_0)\hat{H}_0}. \end{aligned} \tag{2.49}$$

In the next chapter we will relate the grand-canonical partition function to an expression of the form of equation (2.49) and then use equation (2.48) to find a systematic expansion around the mean-field grand-canonical partition function.

Chapter 3

Calculation of Corrections to the Mean-Field Approximation

With the theoretical background cleared we now want to calculate post mean field corrections to the grand-canonical partition function and correspondingly to the grand-canonical potential. We will first do this for finite temperature in section 3.1 and then investigate the low temperature limit of these results in section 3.2. We will find out that some regions of parameter space are problematic and that our results from section 3.1 are not physical there. These problems will be discussed in section 3.3. Finally in section 3.4 we will calculate corrections in the $T = 0$ case and investigate whether they match the $T \to 0$ limit obtained in section 3.2 to check our calculations for consistency.

3.1 Corrections for Finite Temperature

With the interaction picture from section 2.6 in mind we can now try to calculate the grand-canonical partition function for the Bose-Hubbard Hamiltonian by relating it to the one of the mean field Hamiltonian:

$$\mathcal{Z} = \mathrm{Tr}\left(e^{-\beta\hat{H}_{\mathrm{BH}}}\right) = \mathrm{Tr}\left\{e^{-\beta\hat{H}_{\mathrm{MF}}}e^{-(0-\beta)\hat{H}_{\mathrm{MF}}}e^{-(\beta-0)\hat{H}_{\mathrm{BH}}}e^{-(0-0)\cdot\hat{H}_{\mathrm{MF}}}\right\}. \tag{3.1}$$

The last three exponentials together have the form of equation (2.49) after performing a so called Wick rotation, i.e. introducing an imaginary time $\tau \equiv it$, with $\tau_0 = it_0 = 0 = \tau'$, $\hat{H}_0 = \hat{H}_{\mathrm{MF}}$ and $\hat{V} = \hat{H}_{\mathrm{BH}} - \hat{H}_{\mathrm{MF}}$ where

$$\hat{H}_{\mathrm{BH}} - \hat{H}_{\mathrm{MF}} = -J\sum_{\langle i,j\rangle\in\Lambda^2}\hat{a}_i^\dagger\hat{a}_j + zJ\sum_{i\in\Lambda}\left(\psi^*\hat{a}_i + \psi\hat{a}_i^\dagger - |\psi|^2\right), \tag{3.2}$$

giving us

$$\mathcal{Z} = \mathrm{Tr}\left\{e^{-\beta\hat{H}_{\mathrm{MF}}}\hat{U}_{\mathrm{I}}(\beta,0)\right\}. \tag{3.3}$$

But because equation (2.48) holds, we can also use that expression for the propagator:

$$\mathcal{Z} = \mathrm{Tr}\left\{e^{-\beta\hat{H}_{\mathrm{MF}}}\mathcal{T}\exp\left[-\int_0^\beta \mathrm{d}\tau\ \left(\hat{H}_{\mathrm{BH,I}}(\tau) - \hat{H}_{\mathrm{MF,I}}(\tau)\right)\right]\right\} \tag{3.4}$$

Here, $\mathcal{T}$ now denotes the imaginary time ordering operator defined analogously to the real time one. We can now expand the exponential to obtain a systematic expansion around the mean field grand-canonical partition function. Here, we also plug in the definition of the operators in the interaction picture, equation (2.44).

$$\begin{aligned}\mathcal{Z} = \mathrm{Tr}\Bigg\{ e^{-\beta \hat{H}_{\mathrm{MF}}} \Bigg[1 - \int_0^\beta \mathrm{d}\tau\ e^{\tau \hat{H}_{\mathrm{MF}}} (\hat{H}_{\mathrm{BH}} - \hat{H}_{\mathrm{MF}}) e^{-\tau \hat{H}_{\mathrm{MF}}} \\ + \int_0^\beta d\tau \int_0^\tau \mathrm{d}\tau_1\ e^{\tau \hat{H}_{\mathrm{MF}}} (\hat{H}_{\mathrm{BH}} - \hat{H}_{\mathrm{MF}}) e^{-(\tau-\tau_1)\hat{H}_{\mathrm{MF}}} (\hat{H}_{\mathrm{BH}} - \hat{H}_{\mathrm{MF}}) e^{-\tau_1 \hat{H}_{\mathrm{MF}}} + ... \Bigg] \Bigg\} \\ \equiv \mathcal{Z}_0 + \mathcal{Z}_1 + \mathcal{Z}_2 + ...\end{aligned} \tag{3.5}$$

The zeroth order $\mathcal{Z}_0$ is simply the mean field grand-canonical partition function $\mathcal{Z}_{\mathrm{MF}}$ and the higher orders are the first corrections to the mean field result that now include the effect of quantum fluctuations.
The traces have to be taken over the full lattice space $\mathcal{L} = \bigotimes_{i\in\Lambda} \mathcal{F} \equiv \mathcal{F}^{\otimes N_{\mathrm{S}}}$, where N_{S} is the number of lattice sites as in the previous chapter and $\mathcal{F}$ is the Fock space of one site as constructed in section 2.2. Note that we do not have to symmetrize this product as the sites are distinguishable.
In the following $\{|\chi_n\rangle \mid n \in \mathbb{N}\}$ and $\{\epsilon_n \mid n \in \mathbb{N}\}$ will denote the eigenstates and eigenvalues of the one-site mean field Hamiltonian $\hat{H}_{\mathrm{MF,S}}$. The eigenstates of the full mean-field Hamiltonian, which we will use to take the traces, are thus

$$\left\{ \bigotimes_{i\in\Lambda} |\chi_{n_i}\rangle \;\middle|\; n_i \in \mathbb{N} \right\} \tag{3.6}$$

with eigenvalues

$$\left\{ \sum_{i\in\Lambda} \epsilon_{n_i} \;\middle|\; n_i \in \mathbb{N} \right\}. \tag{3.7}$$

We will use the abbreviations $|\chi_{\vec{n}}\rangle = \bigotimes_{i\in\Lambda} |\chi_{n_i}\rangle$ and $\epsilon_{\vec{n}} = \sum_{i\in\Lambda} \epsilon_{n_i}$ with $\vec{n} \in \mathbb{N}^{N_{\mathrm{S}}}$. Note that if we have to take a trace, e.g. for an expectation value, over operators which act on different sites respectively, we can factorize the trace or expectation value, because the mean field Hamiltonian decomposes into a sum of local one-site Hamiltonians. We can exemplarily see this by taking the trace over a hopping term and decomposing the trace over the product space into a product of traces over the single site spaces:

$$\begin{aligned}\mathcal{Z}_{\mathrm{MF}} \langle \hat{a}_i^\dagger \hat{a}_j \rangle_{\mathrm{MF}} = \mathrm{Tr}\left(e^{-\beta \hat{H}_{\mathrm{MF}}} \hat{a}_i^\dagger \hat{a}_j \right) = \sum_{\vec{n}\in\mathbb{N}^{N_{\mathrm{S}}}} \langle \chi_{\vec{n}} | e^{-\beta \hat{H}_{\mathrm{MF}}} \hat{a}_i^\dagger \hat{a}_j | \chi_{\vec{n}} \rangle \\ = \sum_{n_i\in\mathbb{N}} \langle \chi_{n_i} | e^{-\beta \hat{H}_{\mathrm{MF},i}} \hat{a}_i^\dagger | \chi_{n_i} \rangle \sum_{n_j\in\mathbb{N}} \langle \chi_{n_j} | e^{-\beta \hat{H}_{\mathrm{MF},j}} \hat{a}_j | \chi_{n_j} \rangle \\ \times \prod_{\substack{k\in\Lambda \\ k\neq i,j}} \sum_{n_k\in\mathbb{N}} \langle \chi_{n_k} | e^{-\beta \hat{H}_{\mathrm{MF},k}} | \chi_{n_k} \rangle \\ = \mathcal{Z}_{\mathrm{MF}} \langle \hat{a}_i^\dagger \rangle_{\mathrm{MF},i} \langle \hat{a}_j \rangle_{\mathrm{MF},j}\end{aligned} \tag{3.8}$$

Here we used that $\mathcal{Z}_{\mathrm{MF}} = \prod_{i\in\Lambda} \mathcal{Z}_{\mathrm{MF},i} = \mathcal{Z}_{\mathrm{MF,S}}^{N_\mathrm{S}}$. Similarly it can be shown that it doesn't matter if you take mean-field expectation values of single-site operators over only the respective site or the whole lattice. Furthermore in single site expectation values it doesn't matter which site the operator acts on due to the homogeneity of the lattice. Therefore, we will from now on drop the subscripts on the operators in the single-operator expectation values and on the expectation value itself. For convenience we will define $\phi = \langle \hat{a} \rangle_{\mathrm{MF}}$ and correspondingly $\phi^* = \langle \hat{a}^\dagger \rangle_{\mathrm{MF}}$. Note that $\phi \neq \psi$: Because we are now including corrections, also the variational parameter ψ changes. You might be concerned that the two approaches to handling the self-consistency of mean-field theory mentioned in section 2.5 might not be equivalent anymore after including the corrections. However, it was shown analytically in [103] that the two approaches are still equivalent to first order. Extending these calculations to the second order would go beyond the scope of this thesis and could be subject of further work. In the following we will simply assume that the two approaches are still equivalent in second order, i.e. our calculations are still self-consistent.
With the preliminary work done we can now evaluate the higher order corrections to $\mathcal{Z}$ starting with $\mathcal{Z}_1$:

$$\mathcal{Z}_1 = -\mathrm{Tr}\left\{ e^{-\beta \hat{H}_{\mathrm{MF}}} \int_0^\beta \mathrm{d}\tau \; e^{\tau \hat{H}_{\mathrm{MF}}} (\hat{H}_{\mathrm{BH}} - \hat{H}_{\mathrm{MF}}) e^{-\tau \hat{H}_{\mathrm{MF}}} \right\}. \tag{3.9}$$

Because of the cyclic property of the trace we can cancel the τ-dependent exponentials and evaluate the integral. This leaves us with

$$\begin{aligned}
\mathcal{Z}_1 &= \beta J \sum_{\langle i,j\rangle \in \Lambda^2} \mathrm{Tr}\left(e^{-\beta \hat{H}_{\mathrm{MF}}} \hat{a}_i^\dagger \hat{a}_j \right) - \beta z J \sum_{i\in\Lambda} \Big[\psi^* \mathrm{Tr}\left(e^{-\beta \hat{H}_{\mathrm{MF}}} \hat{a}_i \right) + \psi \mathrm{Tr}\left(e^{-\beta \hat{H}_{\mathrm{MF}}} \hat{a}_i^\dagger \right) \\
&\qquad\qquad - |\psi|^2 \mathrm{Tr}\left(e^{-\beta \hat{H}_{\mathrm{MF}}} \right) \Big] \\
&= \mathcal{Z}_{\mathrm{MF}} \beta J N_\mathrm{S} z |\phi|^2 - \mathcal{Z}_{\mathrm{MF}} \beta J N_\mathrm{S} z \left(\psi^* \phi + \psi \phi^* - |\psi|^2 \right) \\
&= \mathcal{Z}_{\mathrm{MF}} \beta J N_\mathrm{S} z |\phi - \psi|^2.
\end{aligned} \tag{3.10}$$

We now want to evaluate the second order of the grand-canonical partition function. We will see that we can interpret the terms coming up as diagrams and find rules to assign a mathematical expression to each diagram, which simplifies the calculation. The second order of the grand-canonical partition function is given by

$$\begin{aligned}
\mathcal{Z}_2 = \mathrm{Tr}\Bigg\{ e^{-\beta \hat{H}_{\mathrm{MF}}} \int_0^\beta d\tau \int_0^\tau \mathrm{d}\tau_1 \; & e^{\tau \hat{H}_{\mathrm{MF}}} (\hat{H}_{\mathrm{BH}} - \hat{H}_{\mathrm{MF}}) e^{-(\tau-\tau_1)\hat{H}_{\mathrm{MF}}} \\
& \times (\hat{H}_{\mathrm{BH}} - \hat{H}_{\mathrm{MF}}) e^{-\tau_1 \hat{H}_{\mathrm{MF}}} \Bigg\}.
\end{aligned} \tag{3.11}$$

If we multiply out the product under the integral and use the linearity of the trace we end up with a sum of terms (with appropriate prefactors) of the form:

$$\mathcal{I}_{\hat{X},\hat{Y}} = \int_0^\beta \mathrm{d}\tau \int_0^\tau \mathrm{d}\tau_1 \; \mathrm{Tr}\left\{ e^{-\beta \hat{H}_{\mathrm{MF}}} e^{(\tau-\tau_1)\hat{H}_{\mathrm{MF}}} \hat{X} e^{-(\tau-\tau_1)\hat{H}_{MF}} \hat{Y} \right\} \tag{3.12}$$

Where $\hat{X}, \hat{Y} \in \left\{ \hat{a}_i^\dagger \hat{a}_j, \hat{a}_i, \hat{a}_i^\dagger, \mathbb{1} \;\middle|\; i,j \in \Lambda \right\}$. Because now two operators are involved we can not generally cancel the τ dependence like in the first order. In each of these

terms we now need to distinguish on which sites the respective operators act, e.g. if all operators act on different sites and the trace factorizes, the integral is trivial but if there are operators acting on the same site it is not. Each term will thus in general need a case distinction which we will do by drawing a diagram for each case, where each operator involved will be represented by a dot and a connection between two dots will denote that they act on the same site. We will then assign a mathematical expression to each diagram and simply add up all of these diagrams with appropriate factors of $\delta_{\cdot,\cdot}$ or $(1-\delta_{\cdot,\cdot})$ for the respective cases.
I now want to give a precise recipe how to draw the diagrams and assign an expression to each of them. The rules for this will first be stated and then proven.

1. Draw a dot for each single $\hat{a}$ or $\hat{a}^\dagger$ and draw a double dot for each $\hat{a}^\dagger\hat{a}$ hopping term in the arguments of the $\mathcal{I}$.

2. In this diagram all dots besides the ones from a double dot (hopping term) are allowed to be connected. The double dots are not even allowed to be connected indirectly. Draw all possible diagrams, i.e. one diagram for each possible combination of connections/disconnections.

3. Assign an expression to each diagram according to the following rules:

   (a) If the diagram contains no dots, i.e. $\hat{X} = \hat{Y} = \mathbb{1}$, assign

   $$\frac{1}{2}\beta^2 \mathcal{Z}_{\mathrm{MF}}. \tag{3.13}$$

   (b) If the diagram contains dots but no connection assign

   $$\frac{1}{2}\beta^2 \mathcal{Z}_{\mathrm{MF}} \times (\text{MF expectation values of all (discon.) operators}). \tag{3.14}$$

   (c) If there is one connection assign

   $$\begin{aligned}&\mathcal{Z}_{\mathrm{MF,S}}^{N_\mathrm{S}-1} \times S_{\text{connected operators}} \\ &\qquad \times (\text{MF expectation values of all disconnected operators}),\end{aligned} \tag{3.15}$$

   where $S_{\cdot,\cdot}$ is a function only depending on the operators involved and the mean field eigenenergies and -states. It is defined by

   $$S_{\hat{X},\hat{Y}} = \sum_{n,m\in\mathbb{N}} e^{-\beta\epsilon_n}\xi(\epsilon_n-\epsilon_m)\langle\chi_n|\hat{X}|\chi_m\rangle\langle\chi_m|\hat{Y}|\chi_n\rangle \tag{3.16}$$

   with

   $$\xi:\mathbb{R}\to\mathbb{R},\ x\mapsto \int_0^\beta \mathrm{d}\tau \int_0^\tau \mathrm{d}\tau_1\ e^{x(\tau-\tau_1)} = \begin{cases}\frac{e^{\beta x}-\beta x-1}{x^2}, & \text{for } x\neq 0\\ \frac{\beta^2}{2}, & \text{for } x=0.\end{cases} \tag{3.17}$$

   Note that $S_{\cdot,\cdot}$ is not symmetric in its arguments, so it is important that the connected operators have the same order as they have in $\mathcal{I}_{\cdot,\cdot}$. Furthermore it does not depend on the site on which the operators act, which is the same for the two operators by construction of the rule.

(d) If there are two connections assign

$$\mathcal{Z}_{\mathrm{MF,S}}^{N_\mathrm{S}-2} \times S_{\text{con. operator pair 1; con. operator pair 2}} \ , \tag{3.18}$$

where the S function is defined by

$$S_{\hat{X}_1,\hat{Y}_1;\hat{X}_2,\hat{Y}_2} = \sum_{n_1,m_1\in\mathbb{N}} \sum_{n_2,m_2\in\mathbb{N}} e^{-\beta(\epsilon_{n_1}+\epsilon_{n_2})}\xi(\epsilon_{n_1}+\epsilon_{n_2}-\epsilon_{m_1}-\epsilon_{m_2}) \tag{3.19}$$
$$\times \langle\chi_{n_1}|\hat{X}_1|\chi_{m_1}\rangle\langle\chi_{m_1}|\hat{Y}_1|\chi_{n_1}\rangle\langle\chi_{n_2}|\hat{X}_2|\chi_{m_2}\rangle\langle\chi_{m_2}|\hat{Y}_2|\chi_{n_2}\rangle.$$

The ordering in a pair is important as above but the ordering of the pairs themselves is not.

4. Sum up all of the terms with a respective factor of $\delta_{\cdot,\cdot}$ for each connection or $(1-\delta_{\cdot,\cdot})$ for each disconnection, with the involved sites as arguments. Redundant Kronecker deltas can of course be omitted as they are identically 1. For example the disconnection in a hopping term does not have to be made explicit because in the nearest neighbour sum the sites will never be equal.

You might be concerned that the β^2 terms coming from disconnected diagrams are unphysical because they are divergent in the low temperature limit. We will investigate this in section 3.2 and find that all terms coming from disconnected diagrams actually vanish in the $T \to 0$ limit. In fact they get cancelled from the terms in the sum of the S functions where the argument of ξ vanishes so that the ξ function also contributes a β^2 term.
To illustrate the recipe that was just introduced we will use the rules given to find an expression for $\mathcal{I}_{\hat{a}_i^\dagger\hat{a}_j,\hat{a}_k}$

1. We draw a double dot for the hopping term and a dot for the $\hat{a}_k$:

2. We draw all possible diagrams where i and j are not connected:

Note that the diagram where k is connected with i and j is forbidden as it also connects i and j indirectly.

3. We assign an expression to each diagram
First diagram: No connection so rule 3(b) applies:

$$\frac{1}{2}\beta^2\mathcal{Z}_{\mathrm{MF}}\phi^2\phi^* \tag{3.20}$$

Second diagram: $\hat{a}_i^\dagger$ and $\hat{a}_k$ are connected so rule 3(c) applies:

$$\mathcal{Z}_{\mathrm{MF,S}}^{N_\mathrm{S}-1} S_{\hat{a}^\dagger,\hat{a}}\phi \tag{3.21}$$

Third diagram: $\hat{a}_j$ and $\hat{a}_k$ are connected so rules 3(c) applies again:

$$\mathcal{Z}_{\mathrm{MF,S}}^{N_\mathrm{S}-1} S_{\hat{a},\hat{a}} \phi^* \tag{3.22}$$

4. We sum up all terms with appropriate factors of Kronecker deltas:

$$\begin{aligned}\mathcal{I}_{\hat{a}_i^\dagger \hat{a}_j, \hat{a}_k} = (1-\delta_{ik})(1-\delta_{jk})\frac{1}{2}\beta^2 \mathcal{Z}_\mathrm{MF}\phi^2\phi^* + \delta_{ik}\mathcal{Z}_{\mathrm{MF,S}}^{N_\mathrm{S}-1} S_{\hat{a}^\dagger,\hat{a}}\phi \\ + \delta_{jk}\mathcal{Z}_{\mathrm{MF,S}}^{N_\mathrm{S}-1} S_{\hat{a},\hat{a}}\phi^*.\end{aligned} \tag{3.23}$$

Note that in the second term for example we did not make the disconnection between j and k explicit because it is implied by the connection between i and k and the forced disconnection between i and j.

We now want to prove the rules stated above:
As already mentioned, the diagrams simply represent the different possibilities of the operators involved acting on the same site or not. Thus it is clear that the connections between the double dots of a hopping term are not allowed. Also it is clear that indirect connections are not allowed because acting on the same site is a transitive property. So, the only thing left to prove are the rules from point 3. Due to the possibility of a hopping term occurring we will decompose $\hat{X} = \hat{X}_i\hat{X}_j$ and $\hat{Y} = \hat{Y}_k\hat{Y}_l$. Here $\hat{X}_i, \hat{X}_j, \hat{Y}_k, \hat{Y}_l \in \left\{\hat{a}_s, \hat{a}_s^\dagger, \mathbb{1} \;\middle|\; s \in \Lambda\right\}$. The subscript of the operators denotes the site on which they act, so in particular $i \neq j$ and $k \neq l$. If one of the operators is the identity then we choose the "site it acts on" to be different from the other involved sites for convenience. This is justified because the identity can always be factorized out like a disconnected operator. We will now prove the three rules by simply calculating the $\mathcal{I}$ for the different cases:
Case 1: Disconnected diagram, i.e. i, j, k, l all unequal:

$$\begin{aligned}\mathcal{I}_{\hat{X},\hat{Y}} &= \int_0^\beta \mathrm{d}\tau \int_0^\tau \mathrm{d}\tau_1 \ \mathrm{Tr}\left\{e^{-\beta\hat{H}_\mathrm{MF}} e^{(\tau-\tau_1)\hat{H}_\mathrm{MF}} \hat{X}_i\hat{X}_j e^{-(\tau-\tau_1)\hat{H}_{MF}} \hat{Y}_k\hat{Y}_l\right\} \\ &= \mathcal{Z}_{\mathrm{MF,S}}^{N_\mathrm{S}-4} \int_0^\beta \mathrm{d}\tau \int_0^\tau \mathrm{d}\tau_1 \ \mathrm{Tr}\left(e^{-\beta\hat{H}_{\mathrm{MF},i}}\hat{X}_i\right)\mathrm{Tr}\left(e^{-\beta\hat{H}_{\mathrm{MF},j}}\hat{X}_j\right)\mathrm{Tr}\left(e^{-\beta\hat{H}_{\mathrm{MF},k}}\hat{Y}_k\right) \\ &\qquad \times \mathrm{Tr}\left(e^{-\beta\hat{H}_{\mathrm{MF},l}}\hat{Y}_l\right) \\ &= \frac{1}{2}\beta^2 \mathcal{Z}_{\mathrm{MF,S}} \langle\hat{X}_i\rangle_\mathrm{MF}\langle\hat{X}_j\rangle_\mathrm{MF}\langle\hat{Y}_k\rangle_\mathrm{MF}\langle\hat{Y}_l\rangle_\mathrm{MF}.\end{aligned} \tag{3.24}$$

Because of $\langle\mathbb{1}\rangle_\mathrm{MF} = 1$ this reproduces rule 3(b) as well as rule 3(a).
Case 2: Diagram with one connection (without loss of generality $i = k$, $j \neq l$):

$$\begin{aligned}\mathcal{I}_{\hat{X},\hat{Y}} &= \int_0^\beta \mathrm{d}\tau \int_0^\tau \mathrm{d}\tau_1 \ \mathrm{Tr}\left\{e^{-\beta\hat{H}_\mathrm{MF}} e^{(\tau-\tau_1)\hat{H}_\mathrm{MF}} \hat{X}_i\hat{X}_j e^{-(\tau-\tau_1)\hat{H}_{MF}} \hat{Y}_k\hat{Y}_l\right\} \\ &= \mathcal{Z}_{\mathrm{MF,S}}^{N_\mathrm{S}-1}\langle\hat{X}_j\rangle_\mathrm{MF}\langle\hat{Y}_l\rangle_\mathrm{MF}\int_0^\beta \mathrm{d}\tau \int_0^\tau \mathrm{d}\tau_1 \ \mathrm{Tr}\left\{e^{-\beta\hat{H}_{\mathrm{MF},i}} e^{(\tau-\tau_1)\hat{H}_{\mathrm{MF},i}} \hat{X}_i e^{-(\tau-\tau_1)\hat{H}_{MF,i}} \hat{Y}_i\right\} \\ &= \mathcal{Z}_{\mathrm{MF,S}}^{N_\mathrm{S}-1}\langle\hat{X}_j\rangle_\mathrm{MF}\langle\hat{Y}_l\rangle_\mathrm{MF}\sum_{n,m\in\mathbb{N}} e^{-\beta\epsilon_n}\langle\chi_n|\hat{X}_i|\chi_m\rangle\langle\chi_m|\hat{Y}_i|\chi_n\rangle \\ &\qquad \times \int_0^\beta \mathrm{d}\tau \int_0^\tau \mathrm{d}\tau_1 \ e^{(\tau-\tau_1)(\epsilon_n-\epsilon_m)} \\ &= \mathcal{Z}_{\mathrm{MF,S}}^{N_\mathrm{S}-1} S_{\hat{X}_i,\hat{Y}_i}\langle\hat{X}_j\rangle_\mathrm{MF}\langle\hat{Y}_l\rangle_\mathrm{MF}.\end{aligned} \tag{3.25}$$

Which is precisely rule 3(c). In the second step we inserted a completeness relation.
Case 3: Diagram with two connections (without loss of generality $i = k$, $j = l$):

$$\begin{aligned}
\mathcal{I}_{\hat{X},\hat{Y}} &= \int_0^\beta \mathrm{d}\tau \int_0^\tau \mathrm{d}\tau_1 \ \mathrm{Tr}\left\{e^{-\beta\hat{H}_{\mathrm{MF}}} e^{(\tau-\tau_1)\hat{H}_{\mathrm{MF}}} \hat{X}_i \hat{X}_j e^{-(\tau-\tau_1)\hat{H}_{MF}} \hat{Y}_k \hat{Y}_l\right\} \\
&= \mathcal{Z}_{\mathrm{MF,S}}^{N_\mathrm{S}-2} \int_0^\beta \mathrm{d}\tau \int_0^\tau \mathrm{d}\tau_1 \ \mathrm{Tr}\left\{e^{-\beta\hat{H}_{\mathrm{MF},i}} e^{(\tau-\tau_1)\hat{H}_{\mathrm{MF},i}} \hat{X}_i e^{-(\tau-\tau_1)\hat{H}_{MF},i} \hat{Y}_i\right\} \\
&\qquad\qquad \times \mathrm{Tr}\left\{e^{-\beta\hat{H}_{\mathrm{MF},j}} e^{(\tau-\tau_1)\hat{H}_{\mathrm{MF},j}} \hat{X}_j e^{-(\tau-\tau_1)\hat{H}_{MF},j} \hat{Y}_j\right\} \\
&= \mathcal{Z}_{\mathrm{MF,S}}^{N_\mathrm{S}-2} \sum_{n_1,m_1\in\mathbb{N}} \sum_{n_2,m_2\in\mathbb{N}} e^{-\beta(\epsilon_{n_1}+\epsilon_{n_2})} \langle\chi_{n_1}|\hat{X}_i|\chi_{m_1}\rangle\langle\chi_{m_1}|\hat{Y}_i|\chi_{n_1}\rangle \\
&\qquad \times \langle\chi_{n_2}|\hat{X}_j|\chi_{m_2}\rangle\langle\chi_{m_2}|\hat{Y}_j|\chi_{n_2}\rangle \int_0^\beta \mathrm{d}\tau \int_0^\tau \mathrm{d}\tau_1 \ e^{(\tau-\tau_1)(\epsilon_{n_1}+\epsilon_{n_2}-\epsilon_{m_1}-\epsilon_{m_2})} \\
&= \mathcal{Z}_{\mathrm{MF,S}}^{N_\mathrm{S}-2} S_{\hat{X}_i,\hat{Y}_i;\hat{X}_j,\hat{Y}_j}.
\end{aligned} \tag{3.26}$$

Which reproduces rule 3(d). With this we have proven the rules stated above.
The advantage of doing this calculation in terms of diagrams is that we have more control over the calculation, which leads to less mistakes. Also it provides a framework that can be generalized to higher orders. For example in the third order the $\mathcal{I}$'s would have 3 slots but the operators in each slot would be the same as before hence we have the same translation between an $\mathcal{I}$ and its corresponding diagram, with the only difference that there are now three columns in the diagrams. This allows more possibilities and also provides the need of higher order S's, which are probably also straightforward to calculate but will be more involved, and a new ξ function because of the triple integral. All of this makes the calculation more cumbersome but not conceptually harder. When the functional dependence of the S's is found, it could also be possible to teach a computer the (generalized) rules and automate great parts of the calculation. This could be subject of further work and shall not be further investigated in this thesis.
With these rules we can now straight-forwardly calculate the grand-canonical partition function to second order. To accomplish this we just have to plug in the rules for each $\mathcal{I}$ and evaluate the sums over the Kronecker deltas. Note that they are the only part of the $\mathcal{I}$'s that is site dependent. We then have to sum up all of these terms and simplify them. To make this less cumbersome we can separately look at the expressions from disconnected diagrams, diagrams with one and with two connections, because they all have different types of prefactors so that they can not interfere. After a quite lengthy calculation (more details are given in appendix B) we end up with

$$\begin{aligned}
\mathcal{Z}_{\leq 2} = \mathcal{Z}_{\mathrm{MF}} \Big\{ & 1 + \beta J N_\mathrm{S} z|\psi-\phi|^2 + \frac{1}{2}\beta^2 J^2 \left\{2N_\mathrm{S} z|\phi|^4 - N_\mathrm{S} z^2\left[(2\phi-\psi)\phi^* - \phi\psi^*\right]^2\right. \\
&\qquad \left. + N_\mathrm{S}^2 z^2 |\phi-\psi|^4\right\} \\
&+ \mathcal{Z}_{\mathrm{MF,S}}^{-1} J^2 \left\{N_\mathrm{S} z^2 \left[S_{\hat{a},\hat{a}}(\phi^*-\psi^*)^2 + S_{\hat{a},\hat{a}^\dagger}|\phi-\psi|^2 + S_{\hat{a}^\dagger,\hat{a}}|\phi-\psi|^2\right.\right. \\
&\qquad \left. + S_{\hat{a}^\dagger,\hat{a}^\dagger}(\phi-\psi)^2\right] \\
&\qquad - N_\mathrm{S} z \left[S_{\hat{a},\hat{a}}(\phi^*)^2 + S_{\hat{a},\hat{a}^\dagger}|\phi|^2 + S_{\hat{a}^\dagger,\hat{a}}|\phi|^2 + S_{\hat{a}^\dagger,\hat{a}^\dagger}\phi^2\right]\Big\} \\
&+ \mathcal{Z}_{\mathrm{MF,S}}^{-2} J^2 N_\mathrm{S} z (S_{\hat{a}^\dagger,\hat{a};\hat{a},\hat{a}^\dagger} + S_{\hat{a}^\dagger,\hat{a}^\dagger;\hat{a},\hat{a}})\Big\}.
\end{aligned} \tag{3.27}$$

With this we can now calculate the grand-canonical potential $\Phi = -T \log \mathcal{Z}$ by taking the natural logarithm. Because we brought the grand-canonical partition function into the form

$$\mathcal{Z} = \mathcal{Z}_{\mathrm{MF}} \left(1 + \frac{\mathcal{Z}_1}{\mathcal{Z}_{\mathrm{MF}}} + \frac{\mathcal{Z}_2}{\mathcal{Z}_{\mathrm{MF}}} + ...\right) \tag{3.28}$$

we can expand the logarithm as $\log(1+x) = x - \frac{x^2}{2} + ...$ to get an expansion of the grand-canonical potential.
The expansion of the logarithm is correct, i.e. it converges, as long as $\mathcal{Z} - \mathcal{Z}_{\mathrm{MF}} < \mathcal{Z}_{\mathrm{MF}}$ which should be true if the expansion of the partition function was justified in the first place. We will assume that this expansion always works[1]. With this we get

$$\begin{aligned}\Phi &= -\frac{1}{\beta}\log \mathcal{Z}_{\mathrm{MF}} - \frac{1}{\beta}\left(\frac{\mathcal{Z}_1}{\mathcal{Z}_{\mathrm{MF}}} + \frac{\mathcal{Z}_2}{\mathcal{Z}_{\mathrm{MF}}} + ...\right) + \frac{1}{2\beta}\left(\frac{\mathcal{Z}_1}{\mathcal{Z}_{\mathrm{MF}}} + \frac{\mathcal{Z}_2}{\mathcal{Z}_{\mathrm{MF}}} + ...\right)^2 \\ &= \Phi_{\mathrm{MF}} - \frac{1}{\beta}\frac{\mathcal{Z}_1}{\mathcal{Z}_{\mathrm{MF}}} + \frac{1}{\beta}\left[\frac{1}{2}\left(\frac{\mathcal{Z}_1}{\mathcal{Z}_{\mathrm{MF}}}\right)^2 - \frac{\mathcal{Z}_2}{\mathcal{Z}_{\mathrm{MF}}}\right] + ...\end{aligned} \tag{3.29}$$

The result up to second order is

$$\begin{aligned}\Phi_{\leq 2} = \Phi_{\mathrm{MF}} &- JN_{\mathrm{S}}z|\psi-\phi|^2 - \frac{1}{2}\beta J^2\left\{2N_{\mathrm{S}}z|\phi|^4 - N_{\mathrm{S}}z^2[(2\phi-\psi)\phi^* - \phi\psi^*]^2\right\} \\ &- \frac{1}{\beta}\mathcal{Z}_{\mathrm{MF,S}}^{-1}J^2\left\{N_{\mathrm{S}}z^2\left[S_{\hat{a},\hat{a}}(\phi^*-\psi^*)^2 + S_{\hat{a},\hat{a}^\dagger}|\phi-\psi|^2 + S_{\hat{a}^\dagger,\hat{a}}|\phi-\psi|^2\right.\right. \\ &\qquad\qquad \left. + S_{\hat{a}^\dagger,\hat{a}^\dagger}(\phi-\psi)^2\right] \\ &\qquad - N_{\mathrm{S}}z[S_{\hat{a},\hat{a}}(\phi^*)^2 + S_{\hat{a},\hat{a}^\dagger}|\phi|^2 + S_{\hat{a}^\dagger,\hat{a}}|\phi|^2 + S_{\hat{a}^\dagger,\hat{a}^\dagger}\phi^2]\Big\} \\ &- \frac{1}{\beta}\mathcal{Z}_{\mathrm{MF,S}}^{-2}J^2N_{\mathrm{S}}z(S_{\hat{a}^\dagger,\hat{a};\hat{a},\hat{a}^\dagger} + S_{\hat{a}^\dagger,\hat{a}^\dagger;\hat{a},\hat{a}}).\end{aligned} \tag{3.30}$$

Starting in chapter 4 we will numerically analyze the consequences of these corrections on thermodynamic quantities like the entropy and compare them to the mean field results.
Note that all terms containing an N_{S}^2 cancelled in the grand-canonical potential leaving it extensive as it should be. Further note that, in contrast to mean-field theory, where J and z only occurred in a product such that you could simply rescale J to get rid of z, here now also terms containing Jz^2 occur. Hence, even when rescaling J, there is still a z dependence, and thus a dependence on the geometry and dimensionality of the problem, remaining.
This is typical for theories going beyond the mean-field approximation, as mean-field theory is independent of the dimension and geometry, so we expect this dependence to enter in the corrections.
Further you might be concerned about the terms containing a β, which come exactly from the disconnected diagrams, because they make it seem like our result might diverge in the $T \to 0$ limit. We will now further investigate this limit and it will turn out that the diagonal terms in the sums of the S functions where the argument of ξ gets zero will also contribute β terms and in the case of no degeneracy these terms will all cancel in the limit $\beta \to \infty$.

[1] There are regions of parameter space where this is actually not the case and our calculation does not work. We will discuss this issue in section 3.3

3.2 Zero-Temperature Limit

We will now investigate what happens when the temperature gets small and consequently β gets big. We will for now assume that the mean field energies are non-degenerate. This does not have to be the case and I will comment on what happens in the case of degeneracy at the end of this section and in section 3.3.
Without loss of generality we will shift the energy scale so that $\epsilon_0 = 0$. First note that when β gets large we can neglect every term in the partition function except the ground state:

$$\mathcal{Z}_{\mathrm{MF,S}} = \sum_{n\in\mathbb{N}} e^{-\beta\epsilon_n} \approx 1. \tag{3.31}$$

This gets exact in the limit $\beta \to \infty$. Note that already here we needed the non-degeneracy of the ground state.
Next note that $\phi = \langle\hat{a}\rangle_{\mathrm{MF}}$ goes over into a mean-field ground-state expectation value for large β:

$$\phi = \frac{1}{\mathcal{Z}_{\mathrm{MF,S}}} \sum_{n\in\mathbb{N}} \langle\chi_n|\hat{a}|\chi_n\rangle e^{-\beta\epsilon_n} \approx \langle\chi_0|\hat{a}|\chi_0\rangle \equiv \langle\hat{a}\rangle_{\mathrm{MF},0}. \tag{3.32}$$

Because the partition function becomes 1 in the limit, terms with different powers of $\mathcal{Z}_{\mathrm{MF,S}}$ can now mix. Because of this we will regroup the terms in equation (3.30) into terms with z and z^2 as prefactors because these still can not mix.

$$\begin{aligned}\Phi_{\leq 2} = \Phi_{\mathrm{MF}} &- JN_{\mathrm{S}}z|\psi-\phi|^2 + J^2N_{\mathrm{S}}z^2\left\{\frac{1}{2}\beta\left[(2\phi-\psi)\phi^* - \phi\psi^*\right]^2\right.\\
&\left.-\frac{1}{\beta}\mathcal{Z}^{-1}_{\mathrm{MF,S}}\left[S_{\hat{a},\hat{a}}(\phi^*-\psi^*)^2 + S_{\hat{a},\hat{a}^\dagger}|\phi-\psi|^2 + S_{\hat{a}^\dagger,\hat{a}}|\phi-\psi|^2 + S_{\hat{a}^\dagger,\hat{a}^\dagger}(\phi-\psi)^2\right]\right\}\\
&+ J^2N_{\mathrm{S}}z\left\{\frac{1}{\beta}\mathcal{Z}^{-1}_{\mathrm{MF,S}}\left[S_{\hat{a},\hat{a}}(\phi^*)^2 + S_{\hat{a},\hat{a}^\dagger}|\phi|^2 + S_{\hat{a}^\dagger,\hat{a}}|\phi|^2 + S_{\hat{a}^\dagger,\hat{a}^\dagger}\phi^2\right] - \beta|\phi|^4\right.\\
&\left.-\frac{1}{\beta}\mathcal{Z}^{-2}_{\mathrm{MF,S}}\left(S_{\hat{a}^\dagger,\hat{a};\hat{a},\hat{a}^\dagger} + S_{\hat{a}^\dagger,\hat{a}^\dagger;\hat{a},\hat{a}}\right)\right\}.\end{aligned} \tag{3.33}$$

We will now show that the different terms are finite in the $\beta \to \infty$ limit. It is justified to look at the different terms individually because if the limits of all terms exist then also the limit of the sum of these terms exists and is given by the sum of the limits [104], which is sometimes called the algebraic limit theorem.
The zeroth order actually vanishes for $\beta \to \infty$ due to the fact that we chose $\epsilon_0 = 0$:

$$\Phi_{\mathrm{MF}} = -\frac{1}{\beta}\log\mathrm{Tr}\left(e^{-\beta\hat{H}_{\mathrm{MF}}}\right) = -\frac{N_{\mathrm{S}}}{\beta}\log\left(\sum_{n\in\mathbb{N}} e^{-\beta\epsilon_n}\right) \xrightarrow{\beta\to\infty} 0. \tag{3.34}$$

The first order stays finite as the only change happens in the ϕ as mentioned above. We will now turn to the z^2 terms in the second order. To find their limit we first investigate what happens to $\frac{1}{\beta}S_{\hat{X},\hat{Y}}$ in the limit ($S_{\hat{X},\hat{Y}}$ was defined in equation (3.16)). To this end we divide the sum over $m, n \in \mathbb{N}$ up into the terms where $m = n$ and the ones with $m \neq n$ and use the fact that $\xi(0) = \beta^2/2$ (note that the assumed

non-degeneracy is again crucial here):

$$\frac{1}{\beta}S_{\hat{X},\hat{Y}} = \sum_{\substack{n,m\in\mathbb{N}\\ n\neq m}} \langle\chi_n|\hat{X}|\chi_m\rangle\langle\chi_m|\hat{Y}|\chi_n\rangle \frac{1}{(\epsilon_n-\epsilon_m)^2}\left[\frac{1}{\beta}e^{-\beta\epsilon_m} - \frac{1}{\beta}e^{-\beta\epsilon_n} - (\epsilon_n-\epsilon_m)e^{-\beta\epsilon_n}\right] + \sum_{n\in\mathbb{N}}\langle\chi_n|\hat{X}|\chi_n\rangle\langle\chi_n|\hat{Y}|\chi_n\rangle\frac{\beta}{2}e^{-\beta\epsilon_n}. \tag{3.35}$$

The $1/\beta$ terms become negligible for large β and will vanish in the limit. In the other two sums we just have to consider the ground state term because also here the others with $\epsilon_i > 0$ will vanish in the limit. For β large enough we get

$$\frac{1}{\beta}S_{\hat{X},\hat{Y}} \approx \frac{\beta}{2}\langle\hat{X}\rangle_{\mathrm{MF},0}\langle\hat{Y}\rangle_{\mathrm{MF},0} - S^{(0)}_{\hat{X},\hat{Y}}, \tag{3.36}$$

where we defined

$$S^{(0)}_{\hat{X},\hat{Y}} = -\sum_{n\in\mathbb{N}_{>0}}\frac{1}{\epsilon_n}\langle\chi_0|\hat{X}|\chi_n\rangle\langle\chi_n|\hat{Y}|\chi_0\rangle. \tag{3.37}$$

The minus sign is introduced for further convenience. By plugging this into equation (3.33) we can now see that the terms that would diverge in the $\beta\to\infty$ limit cancel:

$$\begin{aligned}(z^2 \text{ terms in } \Phi_2) \approx J^2 N_{\mathrm{S}} z^2 \Big\{ & S^{(0)}_{\hat{a},\hat{a}}(\phi^*-\psi^*)^2 + S^{(0)}_{\hat{a},\hat{a}^\dagger}|\phi-\psi|^2 + S^{(0)}_{\hat{a}^\dagger,\hat{a}}|\phi-\psi|^2 \\ & + S^{(0)}_{\hat{a}^\dagger,\hat{a}^\dagger}(\phi-\psi)^2 \\ & \underbrace{+\frac{\beta}{2}\left[[(2\phi-\psi)\phi^* - \phi\psi^*]^2 - \left[\phi^2(\phi^*-\psi^*)^2 + 2|\phi|^2|\phi-\psi|^2 + (\phi^*)^2(\phi-\psi)^2\right]\right]}_{\equiv 0}\Big\} \\ = J^2 N_{\mathrm{S}} z^2 \Big\{ & S^{(0)}_{\hat{a},\hat{a}}(\phi^*-\psi^*)^2 + S^{(0)}_{\hat{a},\hat{a}^\dagger}|\phi-\psi|^2 + S^{(0)}_{\hat{a}^\dagger,\hat{a}}|\phi-\psi|^2 \\ & + S^{(0)}_{\hat{a}^\dagger,\hat{a}^\dagger}(\phi-\psi)^2\Big\}. \end{aligned} \tag{3.38}$$

In the limit this is exact, so we see that the β terms exactly cancel and the limit stays finite.

Finally we want to take the limit for the z terms in the second order. To do this we first need to find out what happens to $\frac{1}{\beta}S_{\hat{X}_1,\hat{Y}_1;\hat{X}_2,\hat{Y}_2}$ in the limit ($S_{\hat{X}_1,\hat{Y}_1;\hat{X}_2,\hat{Y}_2}$ was defined in equation (3.20)). To this end we again split off the terms where the argument of ξ gets zero. These definitely include the terms where $n_1 = m_1,\ n_2 = m_2$ and those where $n_1 = m_2,\ n_2 = m_1$, where the case $n_1 = n_2 = m_1 = m_2$ that would be included in both cases will be split off separately. But even in the case of non-degenerate mean field eigenenergies there could be terms where $n_1 + n_2 = m_1 + m_2$ with n_1, n_2, m_1, m_2 all unequal. These would correspond to degenerate two site mean field states and they can occur. For now we will assume that this does not happen however and as mentioned before I will comment more on this at the end of the section. If we assume that these two-site degeneracies do not occur then, after splitting off the terms mentioned above where $n_1 + n_2 - m_1 - m_2 = 0$ trivially, the remaining sum will stay finite in the $\beta\to\infty$ limit. We will denote the remaining sum with a prime to indicate that there are terms missing. The terms remaining in the sum are

the ones were n_1, n_2, m_1, m_2 are all unequal, the ones were three of them are equal and the fourth different and the ones where $n_1 = n_2$ and $m_1 = m_2$, but the pairs are different.

$$\begin{aligned}
\frac{1}{\beta} S_{\hat{X}_1,\hat{Y}_1;\hat{X}_2,\hat{Y}_2} = & \sum_{n_1,m_1\in\mathbb{N}} \sum_{n_2,m_2\in\mathbb{N}} e^{-\beta(\epsilon_{n_1}+\epsilon_{n_2})} \xi(\epsilon_{n_1}+\epsilon_{n_2}-\epsilon_{m_1}-\epsilon_{m_2}) \\
& \times \langle\chi_{n_1}|\hat{X}_1|\chi_{m_1}\rangle\langle\chi_{m_1}|\hat{Y}_1|\chi_{n_1}\rangle\langle\chi_{n_2}|\hat{X}_2|\chi_{m_2}\rangle\langle\chi_{m_2}|\hat{Y}_2|\chi_{n_2}\rangle \\
= & \sum_{n_1,m_1,n_2,m_2\in\mathbb{N}}{}' \frac{1}{(\epsilon_{n_1}+\epsilon_{n_2}-\epsilon_{m_1}-\epsilon_{m_2})^2} \left[\frac{1}{\beta}\left(e^{-\beta(\epsilon_{m_1}+\epsilon_{m_2})} - e^{-\beta(\epsilon_{n_1}+\epsilon_{n_2})}\right)\right. \\
& \left. -(\epsilon_{n_1}+\epsilon_{n_2}-\epsilon_{m_1}-\epsilon_{m_2}) e^{-\beta(\epsilon_{n_1}+\epsilon_{n_2})}\right] \\
& \times \langle\chi_{n_1}|\hat{X}_1|\chi_{m_1}\rangle\langle\chi_{m_1}|\hat{Y}_1|\chi_{n_1}\rangle\langle\chi_{n_2}|\hat{X}_2|\chi_{m_2}\rangle\langle\chi_{m_2}|\hat{Y}_2|\chi_{n_2}\rangle \\
& + \sum_{\substack{n_1,n_2\in\mathbb{N} \\ n_1\neq n_2}} \Big[\langle\chi_{n_1}|\hat{X}_1|\chi_{n_2}\rangle\langle\chi_{n_2}|\hat{Y}_1|\chi_{n_1}\rangle\langle\chi_{n_2}|\hat{X}_2|\chi_{n_1}\rangle\langle\chi_{n_1}|\hat{Y}_2|\chi_{n_2}\rangle \\
& + \langle\chi_{n_1}|\hat{X}_1|\chi_{n_1}\rangle\langle\chi_{n_1}|\hat{Y}_1|\chi_{n_1}\rangle\langle\chi_{n_2}|\hat{X}_2|\chi_{n_2}\rangle\langle\chi_{n_2}|\hat{Y}_2|\chi_{n_2}\rangle\Big] \\
& \times \frac{\beta}{2} e^{-\beta(\epsilon_{n_1}+\epsilon_{n_2})} \\
& + \sum_{n\in\mathbb{N}} \frac{\beta}{2} e^{-2\beta\epsilon_n} \langle\chi_n|\hat{X}_1|\chi_n\rangle\langle\chi_n|\hat{Y}_1|\chi_n\rangle\langle\chi_n|\hat{X}_2|\chi_n\rangle\langle\chi_n|\hat{Y}_2|\chi_n\rangle. \qquad (3.39)
\end{aligned}$$

For large β we can now again neglect the terms containing a $1/\beta$ and in the other terms we only need to consider the ground state terms. For the sums over n_1, n_2 this means that both n_1 and n_2 have to be 0 because else the sum $\epsilon_{n_1} + \epsilon_{n_2} > 0$ would be positive and the exponential would suppress the term. In particular this means that the second sum vanishes in the limit due to the constraint $n_1 \neq n_2$. For the primed sum this means that from all the terms listed above only the ones with $n_1 = n_2 = m_1 \neq m_2$ or $n_1 = n_2 = m_2 \neq m_1$ and the ones with $m_1 = m_2 \neq n_1 = n_2$ survive. These will give the three different sums remaining. For large β we thus get

$$\begin{aligned}
\frac{1}{\beta} S_{\hat{X}_1,\hat{Y}_1;\hat{X}_2,\hat{Y}_2} \approx & \sum_{n\in\mathbb{N}_{>0}} \frac{1}{\epsilon_n} \langle\chi_0|\hat{X}_2|\chi_n\rangle\langle\chi_n|\hat{Y}_2|\chi_0\rangle\langle\hat{X}_1\rangle_{\mathrm{MF},0}\langle\hat{Y}_1\rangle_{\mathrm{MF},0} \\
& + \sum_{n\in\mathbb{N}_{>0}} \frac{1}{\epsilon_n} \langle\chi_0|\hat{X}_1|\chi_n\rangle\langle\chi_n|\hat{Y}_1|\chi_0\rangle\langle\hat{X}_2\rangle_{\mathrm{MF},0}\langle\hat{Y}_2\rangle_{\mathrm{MF},0} \\
& + \sum_{n_1,n_2\in\mathbb{N}_{>0}} \frac{1}{\epsilon_{n_1}+\epsilon_{n_2}} \langle\chi_0|\hat{X}_1|\chi_{n_1}\rangle\langle\chi_{n_1}|\hat{Y}_1|\chi_0\rangle\langle\chi_0|\hat{X}_2|\chi_{n_2}\rangle\langle\chi_{n_2}|\hat{Y}_2|\chi_0\rangle \\
& + \frac{\beta}{2} \langle\hat{X}_1\rangle_{\mathrm{MF},0}\langle\hat{Y}_1\rangle_{\mathrm{MF},0}\langle\hat{X}_2\rangle_{\mathrm{MF},0}\langle\hat{Y}_2\rangle_{\mathrm{MF},0} \\
\equiv & -S^{(0)}_{\hat{X}_2,\hat{Y}_2}\langle\hat{X}_1\rangle_{\mathrm{MF},0}\langle\hat{Y}_1\rangle_{\mathrm{MF},0} - S^{(0)}_{\hat{X}_1,\hat{Y}_1}\langle\hat{X}_2\rangle_{\mathrm{MF},0}\langle\hat{Y}_2\rangle_{\mathrm{MF},0} - \tilde{S}^{(0)}_{\hat{X}_1,\hat{Y}_1;\hat{X}_2,\hat{Y}_2} \\
& + \frac{\beta}{2} \langle\hat{X}_1\rangle_{\mathrm{MF},0}\langle\hat{Y}_1\rangle_{\mathrm{MF},0}\langle\hat{X}_2\rangle_{\mathrm{MF},0}\langle\hat{Y}_2\rangle_{\mathrm{MF},0}, \qquad (3.40)
\end{aligned}$$

with $S^{(0)}_{\hat{X},\hat{Y}}$ as defined in (3.37). Here we further defined

$$\tilde{S}^{(0)}_{\hat{X}_1,\hat{Y}_1;\hat{X}_2,\hat{Y}_2} = -\sum_{n_1,n_2\in\mathbb{N}_{>0}} \frac{1}{\epsilon_{n_1}+\epsilon_{n_2}} \langle\chi_0|\hat{X}_1|\chi_{n_1}\rangle\langle\chi_{n_1}|\hat{Y}_1|\chi_0\rangle \times \langle\chi_0|\hat{X}_2|\chi_{n_2}\rangle\langle\chi_{n_2}|\hat{Y}_2|\chi_0\rangle. \tag{3.41}$$

Also here we introduced a minus sign for further convenience. Note that we used a tilde to distinguish this function from $S^{(0)}_{\hat{X}_1,\hat{Y}_1;\hat{X}_2,\hat{Y}_2}$ to be defined in equation (3.52). Together with the large β approximation for $\frac{1}{\beta}S_{\hat{X},\hat{Y}}$ we can now show that also the z terms remain finite in the limit. For β sufficiently large we can approximate

$$\begin{aligned}(z \text{ terms in } \Phi_2) \approx J^2 N_S z\Big\{ &-\Big[S^{(0)}_{\hat{a},\hat{a}}(\phi^*)^2 + S^{(0)}_{\hat{a},\hat{a}^\dagger}|\phi|^2 + S^{(0)}_{\hat{a}^\dagger,\hat{a}}|\phi|^2 + S^{(0)}_{\hat{a}^\dagger,\hat{a}^\dagger}\phi^2\Big] \\ &+ S^{(0)}_{\hat{a},\hat{a}}(\phi^*)^2 + S^{(0)}_{\hat{a},\hat{a}^\dagger}|\phi|^2 + S^{(0)}_{\hat{a}^\dagger,\hat{a}}|\phi|^2 + S^{(0)}_{\hat{a}^\dagger,\hat{a}^\dagger}\phi^2 \\ &+ \tilde{S}^{(0)}_{\hat{a}^\dagger,\hat{a};\hat{a},\hat{a}^\dagger} + \tilde{S}^{(0)}_{\hat{a}^\dagger,\hat{a}^\dagger;\hat{a},\hat{a}} + \underbrace{4\cdot\frac{\beta}{2}|\phi|^4 - \beta|\phi|^4 - 2\cdot\frac{\beta}{2}|\phi|^4}_{\equiv 0}\Big\} \\ = J^2 N_S z &\left(\tilde{S}^{(0)}_{\hat{a}^\dagger,\hat{a};\hat{a},\hat{a}^\dagger} + \tilde{S}^{(0)}_{\hat{a}^\dagger,\hat{a}^\dagger;\hat{a},\hat{a}}\right).\end{aligned} \tag{3.42}$$

As before, this gets exact in the limit which shows that also this term remains finite. In conclusion this means that the grand-canonical potential remains finite in the $\beta\to\infty$ ($T\to 0$) limit which is given by

$$\begin{aligned}\Phi_{\leq 2}|_{T=0} = &-JN_S z|\psi-\phi|^2 + J^2 N_S z\left(\tilde{S}^{(0)}_{\hat{a}^\dagger,\hat{a};\hat{a},\hat{a}^\dagger} + \tilde{S}^{(0)}_{\hat{a}^\dagger,\hat{a}^\dagger;\hat{a},\hat{a}}\right) \\ &+ J^2 N_S z^2\Big\{S^{(0)}_{\hat{a},\hat{a}}(\phi^*-\psi^*)^2 + S^{(0)}_{\hat{a},\hat{a}^\dagger}|\phi-\psi|^2 + S^{(0)}_{\hat{a}^\dagger,\hat{a}}|\phi-\psi|^2 \\ &+ S^{(0)}_{\hat{a}^\dagger,\hat{a}^\dagger}(\phi-\psi)^2\Big\}.\end{aligned} \tag{3.43}$$

It is important to stress that we made strong assumptions in taking this limit. We needed to assume that the mean field energy levels are non-degenerate and that there are no two-site degeneracies in the mean field energy spectrum. Each degeneracy of one of the types mentioned will result in another β term due to the argument of the ξ function becoming zero. There is *a priori* no reason why these terms should cancel in the case of arbitrary degeneracy and in general they will not. In the parts of parameter space where these degeneracies occur our calculation thus has no well-defined $T\to 0$ limit and gets unreliable for small temperatures. We will see consequences of this in our analysis in the following chapters. The low temperature limit is not the only reason why degeneracies in the one-site or multiple-site spectrum are problematic. This will be discussed in the following section.

3.3 Problems of the Calculation

In the preceding calculations we have made assumptions where I have already commented that they will not always be justified. For the perturbative expansion around the mean-field partition function we of course needed to assume that the expansion converges i.e. the Bose-Hubbard Hamiltonian does not "differ too much" from the mean field one. Furthermore we needed to assume that the expansion of the loga-

rithm in the grand-canonical potential converges, which quantitatively means that $\mathcal{Z} - \mathcal{Z}_{\mathrm{MF}} < \mathcal{Z}_{\mathrm{MF}}$ which is of course closely related to the first assumption and quantifies it.
Further we found that our calculation does not seem to have a well-defined low temperature limit if either the single site or the two site mean field spectrum is degenerate. These assumptions are all related to each other which can be seen as follows: if our perturbative expansion, or correspondingly the logarithm expansion, does not converge this means that the mean field approximation was not a good basis to expand around, i.e. the full Bose-Hubbard Hamiltonian differs substantially from its mean field approximation so $\hat{H}_{\mathrm{BH}} - \hat{H}_{\mathrm{MF}}$ is not a small perturbation. If the mean field energies, in particular the two-site, or multiple-site, energies are degenerate this means that there are many-particle states with similar or even the same energies, meaning that the states are not very different. The correct eigenstates of the system are then in general some entangled, i.e. not factorizable, combinations of these closely related states rather than the fully factorized mean field states. This means that in the regions of parameter space where the (many site) mean field spectrum is degenerate we do not expect the mean field approximation to be good and can not expect the perturbative expansion to converge.
The connection between degeneracies and divergence of the perturbative expansion gets clearer in the $T = 0$ case. The second order correction to the ground state energy in non-degenerate perturbation theory has the form [98]

$$\sum_{\vec{n} \in \mathbb{N}^{N_S} \setminus \{\vec{0}\}} \frac{|\langle \chi_{\vec{0}} | \hat{H}_{\mathrm{BH}} - \hat{H}_{\mathrm{MF}} | \chi_{\vec{n}} \rangle|^2}{\epsilon_{\vec{0}} - \epsilon_{\vec{n}}} \tag{3.44}$$

with $\vec{0} = (0, ..., 0) \in \mathbb{N}^{N_S}$. It is clear that this series does not converge if the mean field energies are of order $|\langle \chi_{\vec{n}} | \hat{H}_{\mathrm{BH}} - \hat{H}_{\mathrm{MF}} | \chi_{\vec{n}} \rangle|$ or even smaller. This occurs precisely when either the many-site mean-field energies close to the ground state are (almost) degenerate and when the Bose-Hubbard Hamiltonian differs substantially from the mean field one, here quantified through the matrix elements. What we would have to do in the $T = 0$ case is to take the degenerate many site subspaces and diagonalize the Hamiltonian in each of them. In general it will then not be possible to write these new eigenstates as simple product states, i.e. they are entangled, in contrast to the mean field product states around which we tried to perturb.
The question now arises where in parameter space these degeneracies (divergences) occur. We already saw in the preceding section that the problem will get worse with lower temperature but the question still stands where it happens at all. In section 2.4 we already saw that for $J = 0$ and μ/U integer we get a degeneracy between the state with $n_0 - 1$ bosons occupying each site and the state with n_0 bosons on each site. If we now increase J we still expect to have almost degenerate states which is still problematic as we saw above. Further we would expect that the local mean field approximation will not be good in the deep superfluid phase where all bosons delocalize i.e. for high J. We will see in the following sections that the problematic zone in the fixed-temperature phase diagram for fixed U, almost fills the space in between the lobes and gets bigger for higher J. In the deep superfluid phase the zone then in fact stretches over all values of μ.
Recently a group used a projector operator formalism to deal with degeneracies between the lobes for zero temperature [105] and finite temperature [106], but only

for the mean field case. So, they dealt with degeneracies between the eigenstates of the particle number operator. Here, we are dealing with degeneracies between the eigenstates of the mean-field Hamiltonian, so that these two degeneracies only coincide for $\psi = 0$, i.e. in the Mott/normal phase. It could be subject of further work to generalize their framework in order to also deal with degeneracies between mean-field eigenstates for $\psi \neq 0$, which would be necessary to solve the problems of our calculations.

3.4 Corrections for Zero Temperature

Finally we now want to do a consistency check for our results. We want to calculate corrections to the ground state energy E_0, which corresponds to the grand-canonical potential for $T = 0$, due to the $-\mu\hat{N}$ term in the Hamiltonian, using ordinary quantum mechanical perturbation theory [98] and see if the $T \to 0$ limit of our finite temperature result coincides with these results. To do this we will use non-degenerate perturbation theory because we have used the assumption of no degeneracy in taking the limit so we would not expect that degenerate perturbation theory would reproduce our limit albeit being the more correct framework to use, as argued in the preceding section. The corrected ground state energy up to second order is given by

$$E_{0,\leq 2} = \epsilon_{\vec{0}} + \langle\chi_{\vec{0}}|\hat{H}_{\mathrm{BH}} - \hat{H}_{\mathrm{MF}}|\chi_{\vec{0}}\rangle + \sum_{\vec{n}\in\mathbb{N}^{N_{\mathrm{S}}}\setminus\{\vec{0}\}} \frac{|\langle\chi_{\vec{n}}|\hat{H}_{\mathrm{BH}} - \hat{H}_{\mathrm{MF}}|\chi_{\vec{0}}\rangle|^2}{\epsilon_{\vec{0}} - \epsilon_{\vec{n}}}. \tag{3.45}$$

The zeroth order is simply the mean field ground state energy $\epsilon_{\vec{0}} = N_{\mathrm{S}}\epsilon_0$. The first order can also be readily calculated:

$$\begin{aligned} E_{0,1} &= -J \sum_{\langle i,j\rangle\in\Lambda} \langle\chi_0|\hat{a}_i^\dagger|\chi_0\rangle\langle\chi_0|\hat{a}_j|\chi_0\rangle\langle\chi_0|\chi_0\rangle^{N_{\mathrm{S}}-2} \\ &\quad + zJ\sum_{i\in\Lambda}\left(\psi^*\langle\chi_0|\hat{a}_i|\chi_0\rangle + \psi\langle\chi_0|\hat{a}_i^\dagger|\chi_0\rangle - |\psi|^2\langle\chi_0|\chi_0\rangle\right)\langle\chi_0|\chi_0\rangle^{N_{\mathrm{S}}-1} \\ &= -JN_{\mathrm{S}}z|\phi|^2 + JN_{\mathrm{S}}z\left(\psi^*\phi + \psi\phi^* - |\psi|^2\right) = -JN_{\mathrm{S}}z|\psi - \phi|^2. \end{aligned} \tag{3.46}$$

We can already see that this coincides with the $T \to 0$ limit of our finite temperature first order results (remember that $\phi|_{T=0} = \langle\chi_0|\hat{a}_i|\chi_0\rangle$ with $i \in \Lambda$ arbitrary), see equation 3.43. To evaluate the second order we proceed similarly as in the finite temperature case. First notice that we now have to deal with terms of the form

$$\mathcal{T}_{\hat{X},\hat{Y}} = \sum_{\vec{n}\in\mathbb{N}^{N_{\mathrm{S}}}\setminus\{\vec{0}\}} \frac{1}{\epsilon_{\vec{0}} - \epsilon_{\vec{n}}}\langle\chi_{\vec{0}}|\hat{X}|\chi_{\vec{n}}\rangle\langle\chi_{\vec{n}}|\hat{Y}|\chi_{\vec{0}}\rangle. \tag{3.47}$$

As in the finite temperature case we can now calculate each of these terms using a diagrammatic representation for each of the possible combinations of the involved operators acting on the same or different lattice sites. The only difference to the finite temperature rules is in rule 3, i.e. the translation from diagram to mathematical expression apart from the Kronecker delta factors (rules 4 stays the same). Thus I will only state and prove the modified rule 3, the rest is completely analogous to the finite temperature case. The modified rule 3 is:

(a) If the diagram contains no dots or no connections assign

$$0. \tag{3.48}$$

(b) If the diagram contains one connection assign

$$S^{(0)}_{\text{con. operators}} \times (\text{MF ground state expectation values of discon. operators}), \tag{3.49}$$

with $S^{(0)}_{\cdot,\cdot}$ defined as in equation (3.37). Note that in the definition the energy scale was shifted so that $\epsilon_0 = 0$. For arbitrary ϵ_0 we would have

$$S^{(0)}_{\hat{X},\hat{Y}} = \sum_{n\in\mathbb{N}_{>0}} \frac{1}{\epsilon_0 - \epsilon_n} \langle\chi_0|\hat{X}|\chi_n\rangle\langle\chi_n|\hat{Y}|\chi_0\rangle. \tag{3.50}$$

(c) If the diagram contains two connections assign

$$S^{(0)}_{\text{con. operator pair 1; con. operator pair 2}}\ , \tag{3.51}$$

with

$$S^{(0)}_{\hat{X}_1,\hat{Y}_1;\hat{X}_2,\hat{Y}_2} = \sum_{(n,m)\in\mathbb{N}^2\setminus\{0\}} \frac{1}{2\epsilon_0 - (\epsilon_n + \epsilon_m)} \langle\chi_0|\hat{X}_1|\chi_n\rangle\langle\chi_n|\hat{Y}_1|\chi_0\rangle \times \langle\chi_0|\hat{X}_2|\chi_m\rangle\langle\chi_m|\hat{Y}_2|\chi_0\rangle, \tag{3.52}$$

which is related to the $\tilde{S}^{(0)}_{\hat{X}_1,\hat{Y}_1;\hat{X}_2,\hat{Y}_2}$ defined in equation (3.41) by

$$S^{(0)}_{\hat{X}_1,\hat{Y}_1;\hat{X}_2,\hat{Y}_2} = S^{(0)}_{\hat{X}_1,\hat{Y}_1}\langle\hat{X}_2\rangle_{\text{MF},0}\langle\hat{Y}_2\rangle_{\text{MF},0} + S^{(0)}_{\hat{X}_2,\hat{Y}_2}\langle\hat{X}_1\rangle_{\text{MF},0}\langle\hat{Y}_1\rangle_{\text{MF},0} + \tilde{S}^{(0)}_{\hat{X}_1,\hat{Y}_1;\hat{X}_2,\hat{Y}_2}. \tag{3.53}$$

Note that the disconnected diagrams that, in the finite temperature case, did not have a well defined low temperature limit and only cancelled when going to that limit vanish identically in the $T = 0$ case.
We now again prove these rules by calculating the $\mathcal{T}$ for the different cases. As in section 3.1 we decompose $\hat{X} = \hat{X}_i\hat{X}_j$, $\hat{Y} = \hat{Y}_k\hat{Y}_l$ with $i \neq j$, $k \neq l$.

Case 1: Disconnected diagram, i.e. i, j, k, l all unequal:

$$\begin{aligned}\mathcal{T}_{\hat{X},\hat{Y}} &= \sum_{\vec{n}\in\mathbb{N}^{N_S}\setminus\{\vec{0}\}} \frac{1}{\epsilon_{\vec{0}}-\epsilon_{\vec{n}}} \langle\chi_0|\hat{X}_i|\chi_{n_i}\rangle\langle\chi_0|\hat{X}_j|\chi_{n_j}\rangle \left(\prod_{\substack{\alpha\in\Lambda\\ \alpha\notin\{i,j\}}} \delta_{0,n_\alpha}\right) \\ &\qquad \times \langle\chi_{n_k}|\hat{Y}_k|\chi_0\rangle\langle\chi_{n_l}|\hat{Y}_l|\chi_0\rangle \left(\prod_{\substack{\alpha\in\Lambda\\ \alpha\notin\{k,l\}}} \delta_{n_\alpha,0}\right) \\ &= \sum_{\vec{n}\in\mathbb{N}^{N_S}\setminus\{\vec{0}\}} \frac{1}{\epsilon_{\vec{0}}-\epsilon_{\vec{n}}} \langle\chi_0|\hat{X}_i|\chi_{n_i}\rangle\langle\chi_0|\hat{X}_j|\chi_{n_j}\rangle\langle\chi_{n_k}|\hat{Y}_k|\chi_0\rangle\langle\chi_{n_l}|\hat{Y}_l|\chi_0\rangle \underbrace{\left(\prod_{\alpha\in\Lambda} \delta_{0,n_\alpha}\right)}_{=0} \\ &= 0. \end{aligned} \tag{3.54}$$

The last product over Kronecker deltas is zero because it would enforce $\vec{n} = \vec{0}$ which is excluded from the sum. This case again includes both the case with no connections and the case with no dots at all because the latter just corresponds to all operators being the identity which act on different sites by definition, as already argued in the proof of the corresponding finite temperature rules. So this shows the new rule 3(a).
Case 2: Diagram with one connection (without loss of generality $i = k$, $j \neq l$):

$$\begin{aligned}\mathcal{T}_{\hat{X},\hat{Y}} &= \sum_{\vec{n}\in\mathbb{N}^{N_S}\setminus\{\vec{0}\}} \frac{1}{\epsilon_{\vec{0}}-\epsilon_{\vec{n}}} \langle\chi_0|\hat{X}_i|\chi_{n_i}\rangle\langle\chi_0|\hat{X}_j|\chi_{n_j}\rangle \left(\prod_{\substack{\alpha\in\Lambda\\ \alpha\notin\{i,j\}}} \delta_{0,n_\alpha}\right) \\ &\qquad \times \langle\chi_{n_i}|\hat{Y}_i|\chi_0\rangle\langle\chi_{n_l}|\hat{Y}_l|\chi_0\rangle \left(\prod_{\substack{\alpha\in\Lambda\\ \alpha\notin\{i,l\}}} \delta_{n_\alpha,0}\right) \\ &= \sum_{\vec{n}\in\mathbb{N}^{N_S}\setminus\{\vec{0}\}} \frac{1}{\epsilon_{\vec{0}}-\epsilon_{\vec{n}}} \langle\chi_0|\hat{X}_i|\chi_{n_i}\rangle\langle\chi_0|\hat{X}_j|\chi_{n_j}\rangle\langle\chi_{n_i}|\hat{Y}_i|\chi_0\rangle\langle\chi_{n_l}|\hat{Y}_l|\chi_0\rangle \left(\prod_{\substack{\alpha\in\Lambda\\ \alpha\neq i}} \delta_{0,n_\alpha}\right) \\ &= \sum_{n_i\in\mathbb{N}\setminus\{0\}} \frac{1}{\epsilon_0-\epsilon_{n_i}} \langle\chi_0|\hat{X}_i|\chi_{n_i}\rangle\langle\chi_{n_i}|\hat{Y}_i|\chi_0\rangle\langle\hat{X}_j\rangle_{\mathrm{MF},0}\langle\hat{Y}_l\rangle_{\mathrm{MF},0} \\ &\equiv S^{(0)}_{\hat{X}_i,\hat{Y}_i}\langle\hat{X}_j\rangle_{\mathrm{MF},0}\langle\hat{Y}_l\rangle_{\mathrm{MF},0}. \end{aligned} \tag{3.55}$$

This shows rule 3(b).
Case 3: Diagram with two connections (without loss of generality $i = k$, $j = l$):

$$\begin{aligned}
\mathcal{T}_{\hat{X},\hat{Y}} = &\sum_{\vec{n}\in\mathbb{N}^{N_S}\setminus\{\vec{0}\}} \frac{1}{\epsilon_{\vec{0}} - \epsilon_{\vec{n}}} \langle\chi_0|\hat{X}_i|\chi_{n_i}\rangle\langle\chi_0|\hat{X}_j|\chi_{n_j}\rangle \left(\prod_{\substack{\alpha\in\Lambda\\ \alpha\notin\{i,j\}}} \delta_{0,n_\alpha}\right) \\
&\times \langle\chi_{n_i}|\hat{Y}_i|\chi_0\rangle\langle\chi_{n_j}|\hat{Y}_j|\chi_0\rangle \left(\prod_{\substack{\alpha\in\Lambda\\ \alpha\notin\{i,j\}}} \delta_{n_\alpha,0}\right) \\
= &\sum_{\vec{n}\in\mathbb{N}^{N_S}\setminus\{\vec{0}\}} \frac{1}{\epsilon_{\vec{0}} - \epsilon_{\vec{n}}} \langle\chi_0|\hat{X}_i|\chi_{n_i}\rangle\langle\chi_0|\hat{X}_j|\chi_{n_j}\rangle\langle\chi_{n_i}|\hat{Y}_i|\chi_0\rangle\langle\chi_{n_j}|\hat{Y}_j|\chi_0\rangle \left(\prod_{\substack{\alpha\in\Lambda\\ \alpha\notin\{i,j\}}} \delta_{0,n_\alpha}\right) \\
= &\sum_{(n_i,n_j)\in\mathbb{N}^2\setminus\{(0,0)\}} \frac{1}{2\epsilon_0 - (\epsilon_{n_i} + \epsilon_{n_j})} \langle\chi_0|\hat{X}_i|\chi_{n_i}\rangle\langle\chi_{n_i}|\hat{Y}_i|\chi_0\rangle\langle\chi_0|\hat{X}_j|\chi_{n_j}\rangle\langle\chi_{n_j}|\hat{Y}_j|\chi_0\rangle \\
\equiv &\, S^{(0)}_{\hat{X}_i,\hat{Y}_i;\hat{X}_j,\hat{Y}_j}. \qquad (3.56)
\end{aligned}$$

This proves rule 3(c), so the only thing left to show is the relation (3.53). To do this first note that $S_{\cdot,\cdot;\cdot,\cdot}$ and $\tilde{S}_{\cdot,\cdot;\cdot,\cdot}$ only differ from each other in the terms where one of the summation indices is 0. Thus, we divide the sum over n, m in $S^{(0)}_{\hat{X}_1,\hat{Y}_1;\hat{X}_2,\hat{Y}_2}$ up into the terms where $n = 0,\ m > 0$ the ones with $n > 0,\ m = 0$ and the ones with $n > 0,\ m > 0$ in order to relate it to $\tilde{S}^{(0)}_{\hat{X}_1,\hat{Y}_1;\hat{X}_2,\hat{Y}_2}$.
After renaming indices we get

$$\begin{aligned}
S^{(0)}_{\hat{X}_1,\hat{Y}_1;\hat{X}_2,\hat{Y}_2} = &- \sum_{n\in\mathbb{N}_{>0}} \frac{1}{\epsilon_n} \Big\{ \langle\chi_0|\hat{X}_1|\chi_n\rangle\langle\chi_n|\hat{Y}_1|\chi_0\rangle\langle\hat{X}_2\rangle_{\mathrm{MF},0}\langle\hat{Y}_2\rangle_{\mathrm{MF},0} \\
&\qquad + \langle\chi_0|\hat{X}_2|\chi_n\rangle\langle\chi_n|\hat{Y}_2|\chi_0\rangle\langle\hat{X}_1\rangle_{\mathrm{MF},0}\langle\hat{Y}_1\rangle_{\mathrm{MF},0} \Big\} \\
&- \sum_{n,m\in\mathbb{N}_{>0}} \frac{1}{2\epsilon_0 - (\epsilon_n + \epsilon_m)} \langle\chi_0|\hat{X}_1|\chi_n\rangle\langle\chi_n|\hat{Y}_1|\chi_0\rangle\langle\chi_0|\hat{X}_2|\chi_m\rangle \\
&\qquad \times \langle\chi_m|\hat{Y}_2|\chi_0\rangle \\
\equiv &\, S^{(0)}_{\hat{X}_1,\hat{Y}_1}\langle\hat{X}_2\rangle_{\mathrm{MF},0}\langle\hat{Y}_2\rangle_{\mathrm{MF},0} + S^{(0)}_{\hat{X}_2,\hat{Y}_2}\langle\hat{X}_1\rangle_{\mathrm{MF},0}\langle\hat{Y}_1\rangle_{\mathrm{MF},0} \\
&+ \tilde{S}^{(0)}_{\hat{X}_1,\hat{Y}_1;\hat{X}_2,\hat{Y}_2}. \qquad (3.57)
\end{aligned}$$

Note again the shift in the energy scale in the definition of $\tilde{S}^{(0)}_{\hat{X}_1,\hat{Y}_1;\hat{X}_2,\hat{Y}_2}$ (equation (3.41)).
With these modified rules we can now calculate every $\mathcal{T}$ like in the finite temperature case. This is less cumbersome though, because all disconnected diagrams identically vanish. After plugging in the $\mathcal{T}$s, evaluating the sums over the Kronecker deltas and

simplifying the expression we end up with (details are given in appendix C)

$$\begin{aligned} E_{0,\leq 2} = \epsilon_{\vec{0}} - JN_{\mathrm{S}}z|\psi-\phi|^2 + J^2N_{\mathrm{S}}z\left(\tilde{S}^{(0)}_{\hat{a}^\dagger,\hat{a};\hat{a},\hat{a}^\dagger} + \tilde{S}^{(0)}_{\hat{a}^\dagger,\hat{a}^\dagger;\hat{a},\hat{a}}\right) \\ + J^2N_{\mathrm{S}}z^2\left\{S^{(0)}_{\hat{a},\hat{a}}(\phi^*-\psi^*)^2 + S^{(0)}_{\hat{a},\hat{a}^\dagger}|\phi-\psi|^2 + S^{(0)}_{\hat{a}^\dagger,\hat{a}}|\phi-\psi|^2 \right. \\ \left. + S^{(0)}_{\hat{a}^\dagger,\hat{a}^\dagger}(\phi-\psi)^2\right\}. \end{aligned} \tag{3.58}$$

This matches the result (3.43) found by taking the $T \to 0$ limit of the grand-canonical potential at finite temperature assuming no degeneracies in the one and two site spectra. This shows that our calculations are consistent, at least when no degeneracies are involved. We already saw that we can not assume this anymore if there are degeneracies as discussed in section 3.3.

Chapter 4

First Analysis of Thermodynamic Quantities

With the results found in Chapter 3 we can now calculate thermodynamic quantities including post mean-field corrections. Here and in the following chapters all extensive quantities will always be measured per site, which will not always be explicitly stated. For example when we refer to the entropy S we mean the entropy per site $S_{\text{total}}/N_{\text{S}}$. Further, we will refer to the mean-field Hamiltonian of one site as $\hat{H}_{\text{MF,S}}$, like in the previous chapter. Also note that we will absorb a factor of z into J because in the mean-field case these quantities only occur in a product. In the corrected case there also occur terms containing $J^2 z$ which are z dependent even after absorbing z into J, we thus have to pick a specific z. We will always choose $z = 6$ in the following, corresponding for example to a simple cubic 3D lattice. So, for example, in order to translate a critical point on the J/U axis in one of the following figures into the "real" value of J/U, without the factor of z, you must simply divide by $z = 6$.
This choice of z is justified, because mean-field theory is expected to give a better approximation in higher dimensions [102]. Thus, by considering a three dimensional lattice, we can expect our mean-field results to deviate less from the correct values than if we would have considered a one- or two-dimensional lattice.
Before using the results from the previous chapter we start by numerically calculating thermodynamic quantities using the mean-field Hamiltonian so we have a reference for the results including corrections. For all numerical calculations to be described here and in the following, the program Mathematica was used.
To calculate thermodynamic quantities in mean-field approximation we restrict the Hilbert space of one site to a finite number of states (dimension d_{num}) so that we can generate finite matrices. As basis we used the eigenbasis of the particle number operator of the respective site $\hat{n}$. The choice of basis of course does not affect the results as we only need the eigenenergies and eigenstates, which are independent of the choice of basis. The eigenbasis of $\hat{n}$ is simply a convenient choice, as we know how the creation and annihilation operators act on the eigenstates. As cutoff we chose $d_{\text{num}} = 7$ and regularly checked that our figures are robust against increasing this number. This choice of cutoff means that we use the states $\{|0\rangle, ..., |6\rangle\}$ for generating the matrices. The cutoff is then justified by the fact that we will restrict our analysis in the following to regions of parameter space around the $n = 1$ lobe, where it is to expect that states with $n > 6$ do not play a relevant role.

In this finite-dimensional Hilbert space we can now numerically diagonalize the matrix corresponding to the one-site mean-field Hamiltonian and determine the corresponding grand-canonical partition function

$$\mathcal{Z}_{\mathrm{MF,S}} = \mathrm{Tr}\left(e^{-\beta \hat{H}_{\mathrm{MF,S}}}\right) = \sum_{i=0}^{\infty} e^{-\beta \epsilon_i} \approx \sum_{i=0}^{d_{\mathrm{num}}-1} e^{-\beta \epsilon_i} \tag{4.1}$$

and the grand-canonical potential

$$\Phi = -\frac{1}{\beta} \log \mathcal{Z}_{\mathrm{MF,S}}. \tag{4.2}$$

Here, $\{\epsilon_i \mid i \in \mathbb{N}\}$ are again the eigenvalues of the one-site mean-field Hamiltonian. We can also calculate the mean particle number per site

$$n = \frac{1}{\mathcal{Z}_{\mathrm{MF,S}}} \mathrm{Tr}\left(\hat{n} e^{-\beta \hat{H}_{\mathrm{MF,S}}}\right). \tag{4.3}$$

The entropy can be simply obtained by

$$\Phi = E - TS - \mu n \Rightarrow S = \frac{E - \mu n - \Phi}{T}, \tag{4.4}$$

with

$$E = \frac{1}{\mathcal{Z}_{\mathrm{MF,S}}} \mathrm{Tr}\left(\hat{H}_{\mathrm{MF,S}} e^{-\beta \hat{H}_{\mathrm{MF,S}}}\right). \tag{4.5}$$

Alternatively we could also compute these quantities as derivatives of the grand-canonical potential

$$n = -\left(\frac{\partial \Phi}{\partial \mu}\right)_T \tag{4.6}$$

$$S = -\left(\frac{\partial \Phi}{\partial T}\right)_\mu, \tag{4.7}$$

where $\left(\frac{\partial}{\partial \cdot}\right)\Big|_x$ means that the quantity x is kept fixed while taking the derivative. Note that, as already mentioned in the introduction, J and U do not have to be independent parameters as we can use one of them to set the energy scale, i.e. set it to one. In our numerical implementation we have set $U = 1$, so that all quantities with dimension of energy are measured in units of U. However when we want to set the scale with J, i.e. analyze thermodynamic quantities for fixed J, which we will start doing in section 4.2, we need to translate. For example from the grand-canonical potential for fixed U, i.e. the one calculated as in equation (4.2) with $U = 1$ in the Hamiltonian, we can get a corresponding grand-canonical potential function where J is fixed:

$$\frac{\Phi}{J}\left(\frac{U}{J}, \frac{\mu}{J}, \frac{T}{J}, \psi\right) = \frac{\Phi}{U}\left(1\Big/\frac{U}{J}, \frac{\mu}{J}\Big/\frac{U}{J}, \frac{T}{J}\Big/\frac{U}{J}, \psi\right)\frac{U}{J}, \tag{4.8}$$

where Φ/J and Φ/U take all arguments with dimensions of energy in units of J and U, respectively.
In order to calculate thermodynamic quantities with corrections, we first computed the corrected grand-canonical potential found in equation (3.30), which simply depends on the mean-field eigenenergies and eigenstates, as well as the standard ther-

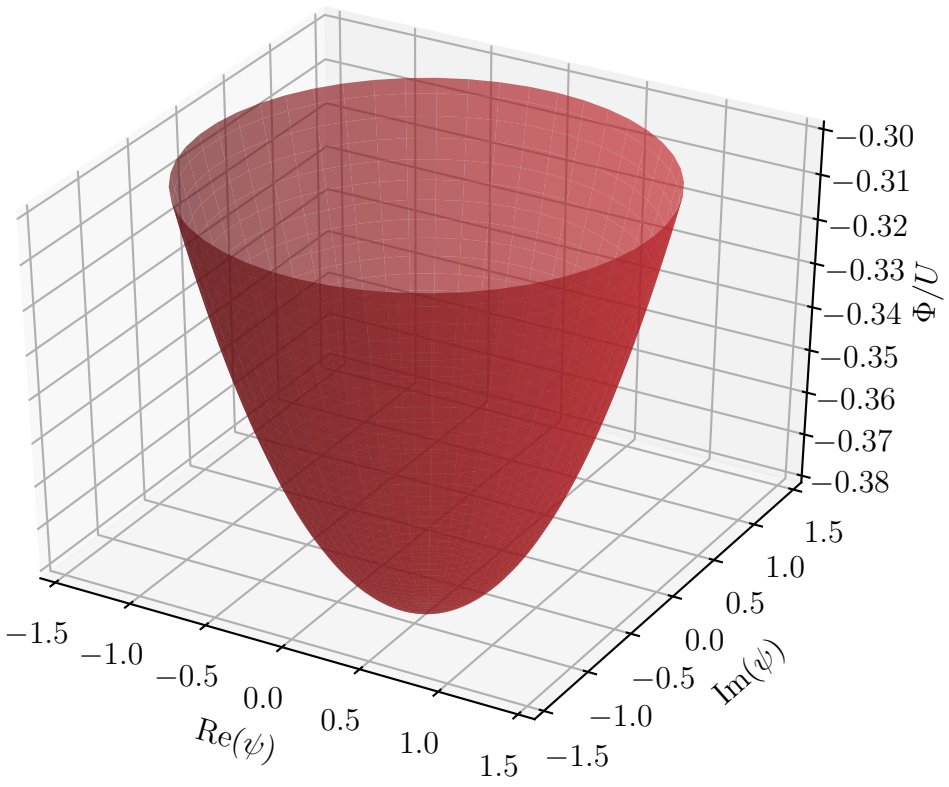

Figure 4.1: Grand-canonical potential in mean-field approximation in the complex ψ-plane for $J = 0.1U,\ T = 0.01U,\ \mu = 0.4U$, corresponding to the normal phase.

modynamic quantities including ψ. We then determined the particle number and entropy using equations (4.6) and (4.7). To compute the derivatives we made use of the centered differences formulae. Higher order formulae were found to make no substantial difference.
At the moment all of these functions depend on the mean-field parameter ψ. To determine the correct value of this parameter we have to numerically minimize the grand-canonical potential with respect to it, as explained in section 2.5. If the minimum is at $\psi = 0$ the system is in the disordered, normal phase. By entering the superfluid phase we obtain $|\psi| \neq 0$, so ψ "has to choose" a phase, which breaks the U(1) symmetry.

Figure 4.1 shows the grand-canonical potential in mean-field approximation in the complex ψ plane for $J = 0.1U$, $T = 0.01U$, $\mu = 0.4U$. We did not show the corrected results for clarity because they show the same qualitative behaviour. The minimum is at $\psi = 0$, so the system is in the normal phase. Also the U(1) symmetry is apparent from the figure.

If we now increase the value of J to $J = 0.4U$ the grand-canonical potential qualitatively changes, see figure 4.2. Now there is no single minimum at the origin, but a circle in the complex plane where the grand-canonical potential is minimized. Whatever the value of ψ is, it has to pick a certain phase breaking the symmetry. It is clear though that it does not matter which phase ψ chooses, which is of course also a consequence of the symmetry. So without loss of generality we can in the following always assume that ψ is real.

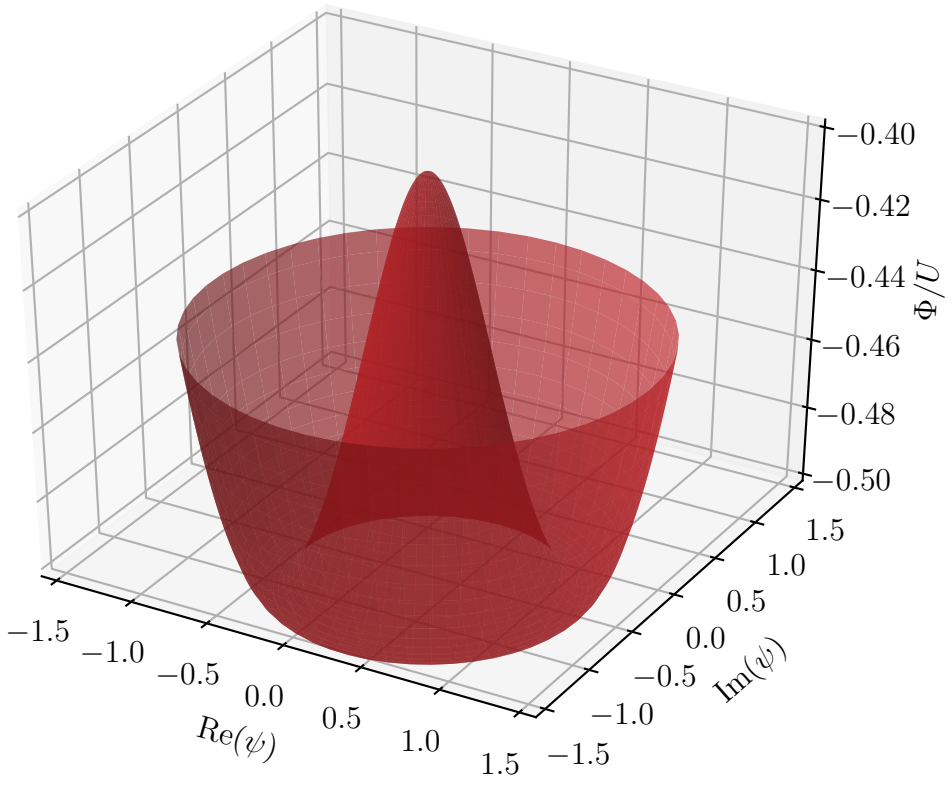

Figure 4.2: Grand-canonical potential in mean-field approximation in the complex ψ-plane for $J = 0.4U,\ T = 0.01U,\ \mu = 0.4U$ corresponding to the superfluid phase.

Figure 4.3 shows the grand-canonical potential as a function of $\psi \in \mathbb{R}$, for the same two sets of parameters as before. Also the results for the corrected grand-canonical potential are now shown. The corrections seem quite large but keep in mind that only the minimum value is physical. At the minima the corrections lower the grand-canonical potential only slightly. On the other hand the non-zero value of ψ in the superfluid phase gets appreciably shifted by the corrections.
We now want to calculate the critical parameter values, where exactly the phase transition introduced in section 2.4 occurs. To achieve this we fix a temperature T and a chemical potential μ. We then increase J or decrease the U, keeping the other one fixed, starting from the normal phase, until the minimum of the grand-canonical potential jumps from $\psi = 0$ to $\psi \neq 0$. To precisely find the point of transition we interpolated the grand-canonical potential by a fourth order polynomial $\Phi(\psi) = a_0 + a_2\psi^2 + a_4\psi^4,\ a_4 > 0$, which is essentially a Taylor expansion, using that ψ is real, where the odd powers are left out because they violate the U(1) symmetry, which reduces to a $\mathbb{Z}_2$ symmetry $\psi \to -\psi$ over $\mathbb{R}$. The coefficient a_4 has to be positive because else the energies would be unbounded from below, which is unphysical. The truncation after the fourth order is justified because ψ is zero in the normal phase and small in the vicinity of the phase transition, which is the point we are interested in. This expansion of the grand-canonical potential is the basic idea of Landau's theory of second-order phase transitions [102]. Note however, that we will use this expansion only to determine the phase boundary. In order to calculate thermodynamic quantities in arbitrary regions of the phase diagram, where

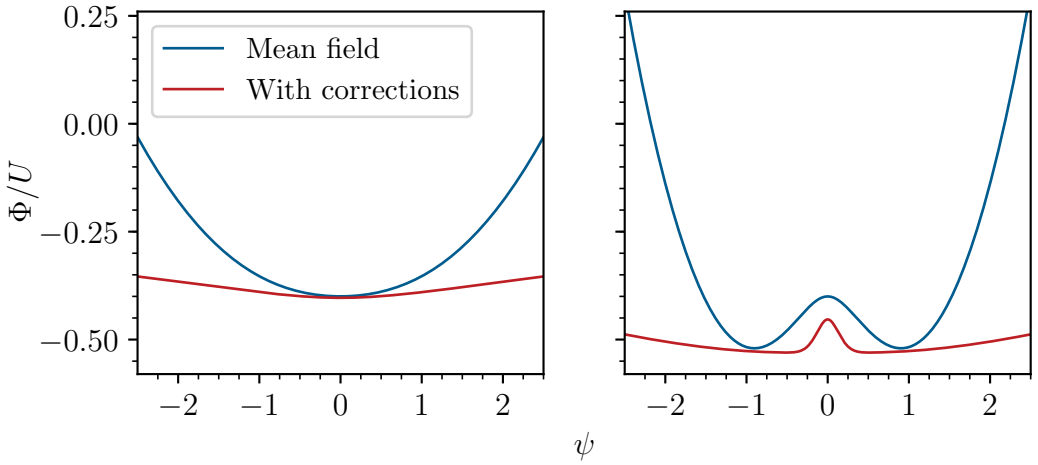

Figure 4.3: Grand-canonical potential in the two phases. On the left side the parameters are $J = 0.1U,\ T = 0.01U,\ \mu = 0.4U$ corresponding to the normal phase. On the right side the parameters are $J = 0.4U,\ T = 0.01U,\ \mu = 0.4U$ corresponding to the superfluid phase

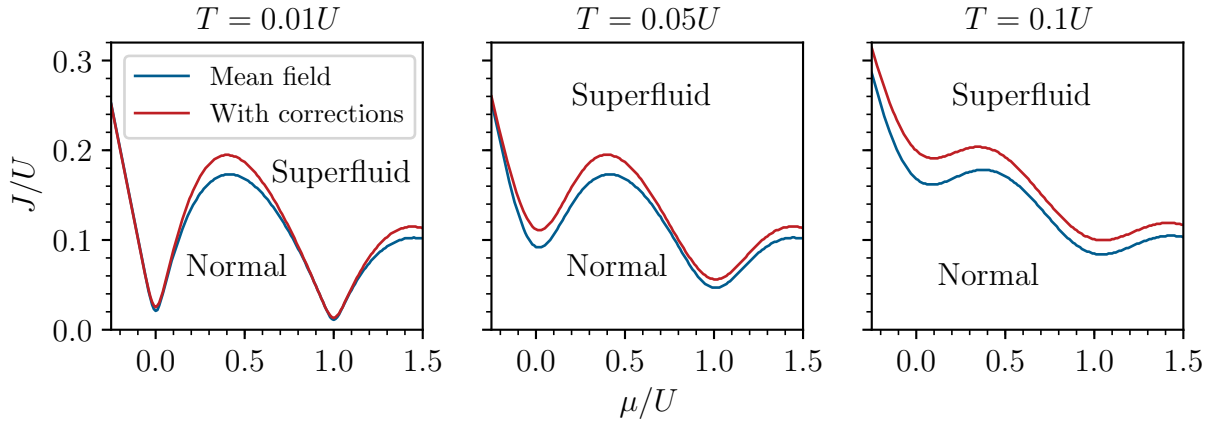

Figure 4.4: Fixed-temperature phase diagrams for fixed U and three different temperatures.

this expansion would not work, we still numerically minimize the grand-canonical potential in order to find the correct value of ψ.
The extrema of the polynomial we use to interpolate, lie at $\psi = 0, \pm\sqrt{-a_2/2a_4}$. For $a_2 > 0$ the only extremum over the real numbers is at $\psi = 0$, being a minimum, as $\partial^2\Phi/\partial\psi^2(\psi = 0) = 2a_2 > 0$, which corresponds to the normal phase. If $a_2 < 0$ there is a maximum at $\psi = 0$ and minima at $\psi = \pm\sqrt{-a_2/2a_4}$, as $\partial^2\Phi/\partial\psi^2\left(\psi = \pm\sqrt{-a_2/2a_4}\right) = -4a_2 > 0$, which corresponds to the superfluid phase. Clearly $a_2 = 0$ marks the point of the phase transition. So, by checking the coefficient a_2 from the interpolation we can determine to which phase the current value of J or U corresponds, and find the point of phase transition. We can then repeat this procedure for many μ to obtain a fixed-temperature phase diagram.
Figure 4.4 shows the fixed-temperature phase diagrams for fixed U for three different temperatures. For low temperature you can observe a lobe like structure like in

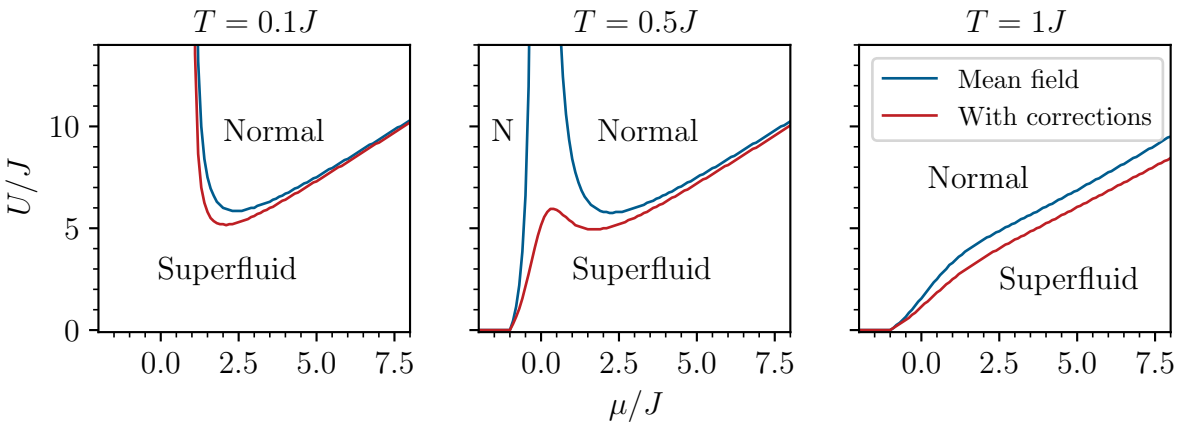

Figure 4.5: Fixed-temperature phase diagrams for fixed U and three different temperatures. N is an abbreviation for normal.

the $T = 0$ case, see figure 2.2. This structure disintegrates for higher temperature. There are now non-superfluid states even at integer μ/U in contrast to the $T = 0$ case. Thus, there is now the possibility of a phase transition at constant integer μ/U. Because this was not possible for $T = 0$, this transition is not a quantum phase transition but rather a classical one.
For higher temperature the critical value of J generally increases, i.e. the phase boundary is shifted to higher values of J, so for more thermal fluctuations the particles need to gain more energy through hopping to condense into a superfluid state. Furthermore it is apparent that the phase boundary is shifted to higher J when including the corrections, so the quantum fluctuations also prevent the system from condensing. It is already visible for low temperature but becomes more apparent for higher temperature, that for higher μ, i.e. for a higher particle number and with this also a higher density the particles can undergo the phase transition for lower values of J. So, a higher particle density supports the phase transition, like in the case of an ideal Bose gas.

Figure 4.5 shows the fixed-temperature phase diagrams for fixed J for three different temperatures. Also here you can observe a "lobe" for small T, although it is formed differently.
It is consistent with the findings of the fixed-U phase diagrams, that the phase transition now occurs for lower values of U when including the corrections. Furthermore it is consistent that for higher values of μ, i.e. a higher particle density a higher U is needed for the system to enter the normal phase.
One striking difference to the fixed-U phase diagrams is that for $T = 0.1J$, there is a region where the system does not enter the normal phase even for high values of U/J. For higher temperature the lobe opens up, leading to the disappearance of this region. This happens for a smaller temperature, when including the corrections. This leads to the interesting circumstance, that for $T = 0.5J$ such a region still exists in mean-field approximation but it has already fully vanished when including the corrections.
Another difference concerns the regions with $\mu < 0$. In the fixed-U case we see that the phase boundary there is a straight line. This means that for a more negative μ, i.e. a larger energy cost to add particles to the system, a higher J is needed to

overcompensate this cost through the hopping of the particles. In the fixed-J phase diagrams there is essentially no superfluid phase at all for $\mu < 0$. An exception to this is of course the low temperature case $T = 0.1J$, as already mentioned.
The temperatures in the phase diagrams discussed above were partly chosen as in Ref. [61] in order to provide a qualitative comparison and sanity check of our calculations. It turns out that our results for the phase diagrams qualitatively agree with those from the reference.

In order to also quantitatively classify our calculations, we compared the critical J/U value at the tip of the $n = 1$ lobe with the beyond mean field results of other groups, see table 4.1. We did not include the results from Ref. [61] in the table as they also made use of a mean-field type approximation. In the table we compare our corrected and mean-field results with quantum Monte-Carlo (QMC) data [27, 40], a variational $T = 0$ approach [47] and one of the two analytical finite-temperature beyond mean-field approaches mentioned in the introduction [68]. We did not include results from the other group because they reproduced the mean-field phase boundary to the order they investigated. Although the QMC group dealt with the finite-temperature case, they computed the critical J/U value only in the zero-temperature limit, which is why we do not have any exact data to compare our finite-temperature results with.
Our corrected results are already notably better than the mean-field results, see also table 4.2, they are however, slightly inferior to those of the Green's function approach but still comparable with them. We note that our results effectively coincide with those of the variational approach from dos Santos *et al.* That approach however, is based on a Landau expansion, it thus only works in the Mott phase and the vicinity of the phase boundary whereas our approach still works in the superfluid phase. We did not include further $T = 0$ results, as this thesis will be concerned with the finite-temperature case only.
Further note, that table 4.2 also shows that not only the mean-field results but also our corrected results show more deviation from the QMC value for lower dimension. Hence this further justifies our choice of $z = 6$.
We conclude that our calculations already significantly improve the mean-field results for the critical value of J/U at the $n = 1$ lobe tip. Beyond this, with our approach we can further also calculate thermodynamic quantities like the entropy, which we will do in the following.
In the rest of this chapter we will analyze the order parameter, the particle number and the entropy on different lines in the different phase diagrams. Due to the qualitative difference between the phase diagrams for fixed J and fixed U we will examine these cases separately starting with the former.

Table 4.1: Comparison of the critical J/U value, without the factor of z, at the tip of the $n = 1$ lobe for different dimensionalities and temperatures. We compare our exact results from mean-field theory (MFT) and our corrected results with quantum Monte-Carlo (QMC) data, the results from a Green's function approach by Ohlinger and Pelster and from a variational approach by dos Santos *et al.* The numbers in the brackets denote an error estimate of the last given digit. For the Green's function approach they were estimated by me, as I had to read off the critical value from the phase diagram. The error estimate of the variational approach was computed using the one from the QMC data as they did not give explicit values but only the deviation of their results from the QMC ones.

d	T/U	MFT	Our calc.	QMC [27, 40]	Green [68]	Var. [47]
2	0	0.04290(1)	0.05204(1)	0.05974(3)	-	0.05197(3)
3	0	0.028600(8)	0.032375(5)	0.03408(2)	0.0330(1)	0.03238(2)
3	0.1	0.2947(2)	0.032417(8)	-	0.0335(8)	-

Table 4.2: Deviation from the quantum Monte-Carlo results of our mean-field and corrected results for the critical J/U value, without the factor of z, at the tip of the $n = 1$ lobe for zero temperature and different dimensionalities.

d	T	MFT	Our calc.
2	0	28%	13%
3	0	17%	5%

4.1 Fixed On-Site Interaction Strength

We will start our analysis with the fixed-U case. There are two straight-forward choices of lines through the phase diagram: horizontal and vertical. Additionally to U we keep J fixed on the horizontal lines and we keep μ fixed on the vertical lines. We will now investigate both of these cases separately, starting with the horizontal lines.

4.1.1 Horizontal lines

We will investigate three different horizontal lines in the fixed-temperature phase diagrams, see figure 4.6. We take one line to be rather low in the lobe at $J = 0.06U$, one line to be rather high in the lobe at $J = 0.16U$ and one in between at $J = 0.12U$. Because on horizontal lines both U and J are fixed we will only look at them in this section as they contain exactly the same information as horizontal lines, i.e. fixed-U lines, in the fixed-J phase diagrams. We will now look at different thermodynamic quantities on these lines starting with the order parameter ψ.

Figures 4.7-4.9 show the order parameter on the horizontal lines in the three different fixed-temperature phase diagrams. You can clearly see the two phases as expected from looking at the phase diagrams, figure 4.6. In the normal phase the order parameter is identically zero and when μ/U gets to a critical value the order parameter changes in a non-analytic way and gets a non-zero value in the superfluid phase. The observed jump in the derivative is typical for a phase transition.

The order parameter is generally smaller when including the corrections. This is clear because quantum fluctuations prevent the particles from condensing into the ground state and thus the condensate density $|\psi|^2$ and with this also the order parameter ψ get decreased by quantum fluctuations.

Furthermore, the corrections make the normal phases bigger in general, which is of course also clear from the phase diagrams. This can also be explained by the quantum fluctuations preventing the particles from condensing, and thus making the normal phases larger. The effect of quantum fluctuations on the critical value of μ, where the phase transition occurs on horizontal lines, increases for higher J,

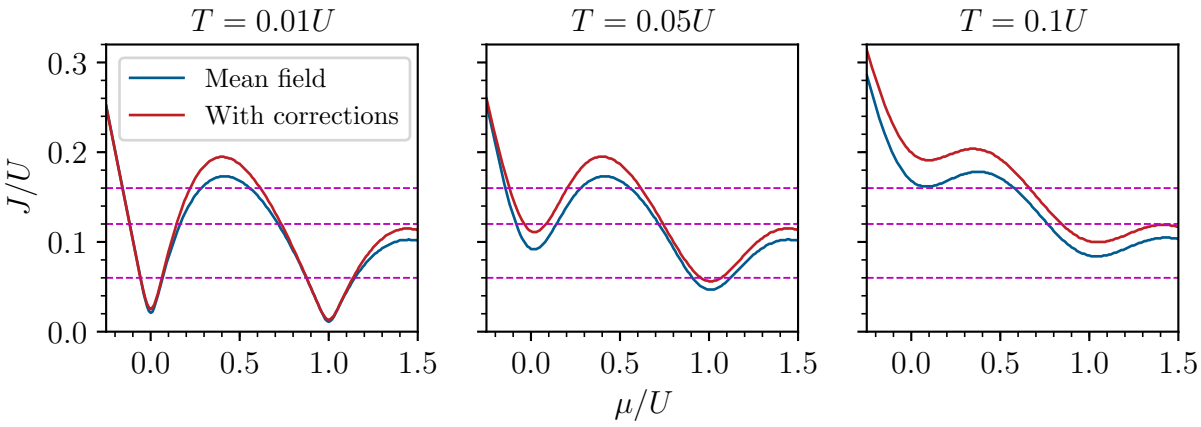

Figure 4.6: Horizontal lines in the fixed-U phase diagrams for different temperatures. J takes the values $0.06U$, $0.12U$, $0.16U$ on these lines, respectively.

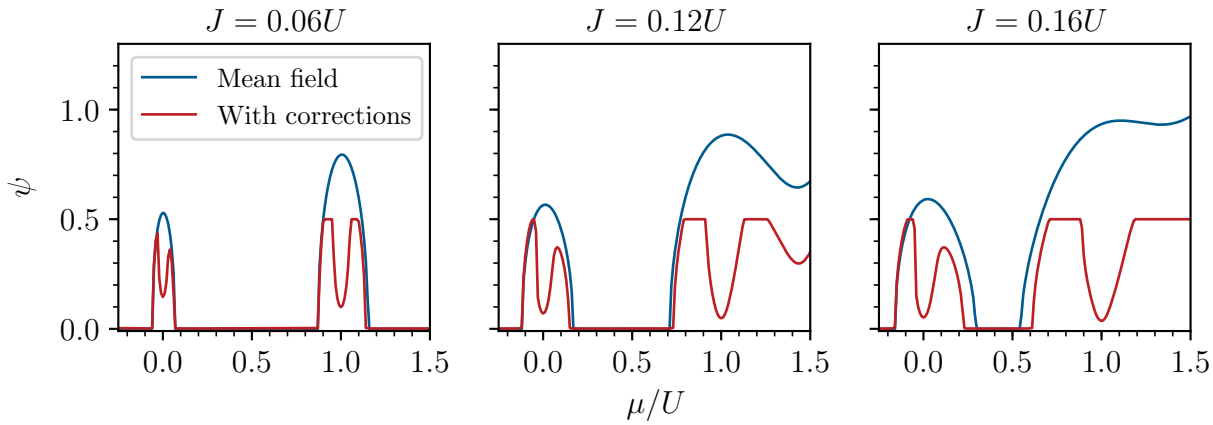

Figure 4.7: Order parameter on horizontal lines in the fixed-U phase diagram at $T = 0.01U$.

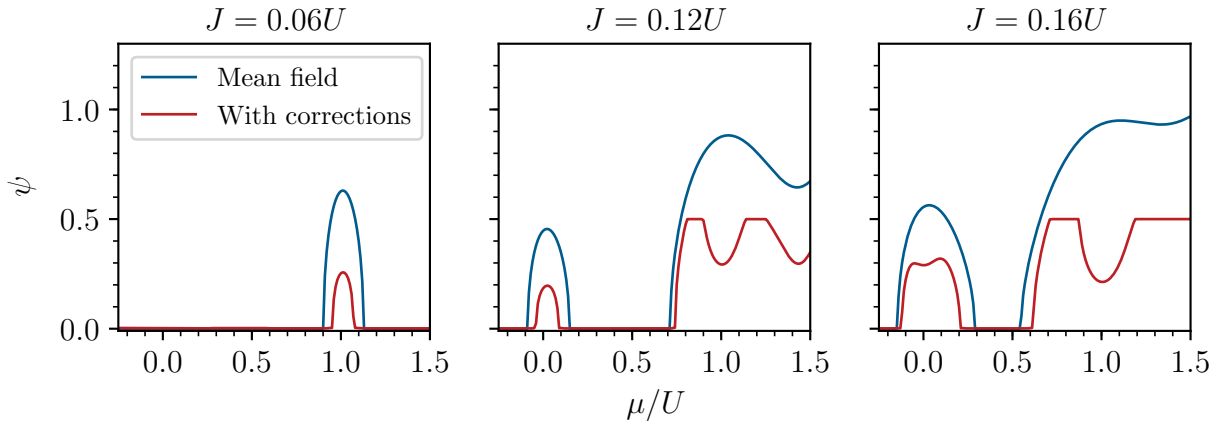

Figure 4.8: Order parameter on horizontal lines in the fixed-U phase diagram at $T = 0.05U$.

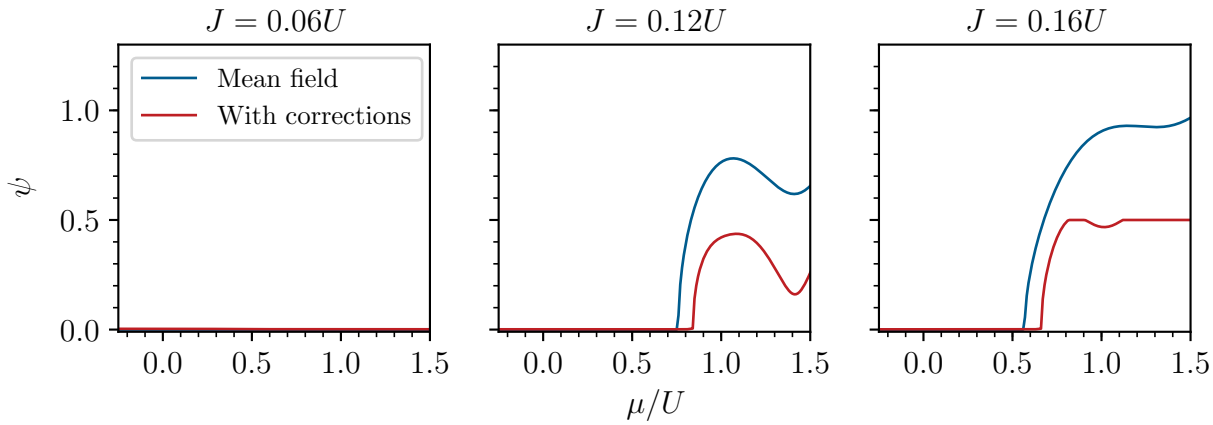

Figure 4.9: Order parameter on horizontal lines in the fixed-U phase diagram at $T = 0.1U$.

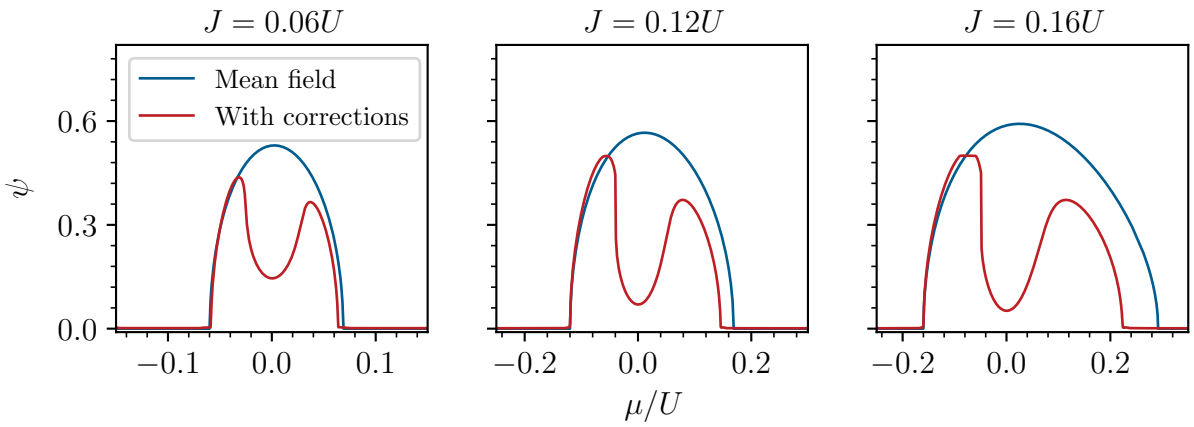

Figure 4.10: Order parameter in the vicinity of the superfluid phase left to the $n = 1$ lobe on horizontal lines in the fixed-U phase diagram at $T = 0.01U$.

i.e. higher in the lobe, and for higher T, i.e. when more thermal fluctuations are involved.
Thermal fluctuations have a similar effect, i.e. they also prevent particles from condensing. This has for example a big effect on the superfluid phase for lower μ, which fully disappears even on the highest horizontal line, for $T = 0.1U$.
You can notice, that at the values $\mu/U = 0$ and $\mu/U = 1$ there is a big discrepancy between the corrected results and the mean-field results. These dips in the corrected results are clearly not physical and reflect the fact that the calculation of the corrections is not valid in these parameter regions, i.e. our expansion does not converge due to (many-site) degeneracies in between the lobes, as explained in section 3.3. This effect is strongest for small T and high J, as we already expected there.
Some of these unphysical dips are connected to plateaus around them. They are probably also due to degeneracy effects and thus unphysical. This is consistent with the fact that they are more prominent where the problems due to degeneracies are also stronger. Another indicator that they are unphysical is the fact that they are connected to further non-analyticities which are not due to a phase transition.
For $J = 0.12U$ there is another dip at $\mu \approx 1.4U$, which is physical and reflects the fact that the line runs close to the tip of the corresponding lobe.
Figure 4.10 again shows the order parameter on the horizontal lines for $T = 0.01U$ but with the focus on the left superfluid phase. It is apparent that for $J = 0.06U$ the corrected results fit the mean-field ones extremely well especially on the left side of the superfluid phase. On the right side there is a small discrepancy, until the line enters the problematic zone and the order parameter shows the unphysical dip. For higher J we can see that on the left side of the dip the corrected order parameter is actually bigger than in mean-field approximation in contrast to it being smaller on the rest of the lines. This seems unphysical and might also be due to degeneracies because it happens close to the dip. This explanation is supported by the fact that the difference increases for larger J.

After investigating the order parameter, we next want to analyze the particle number on the same horizontal lines. Figures 4.11-4.13 show an overview of our results. You directly notice that there exist plateaus where the particle number is approximately constant, as expected in section 2.4. When J increases these plateaus

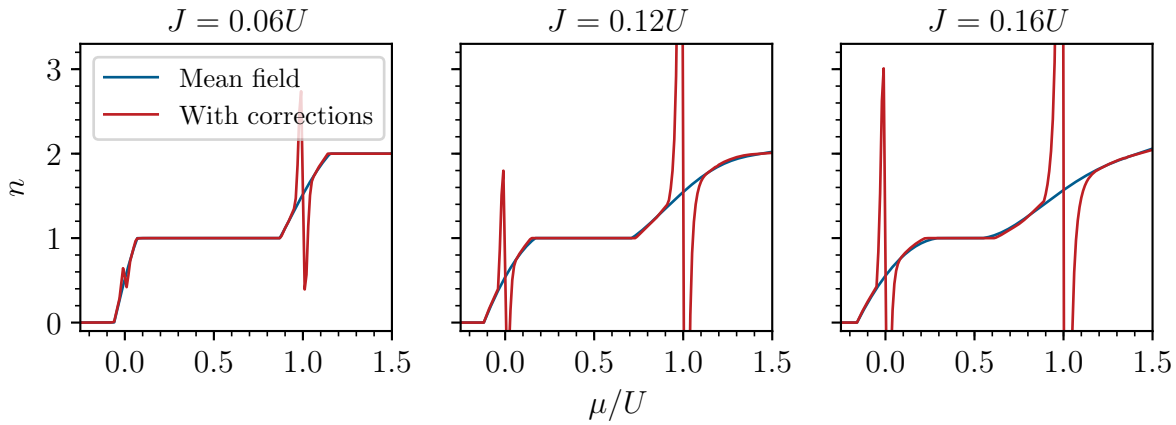

Figure 4.11: Particle number on horizontal lines in the fixed-U phase diagram at $T = 0.01U$.

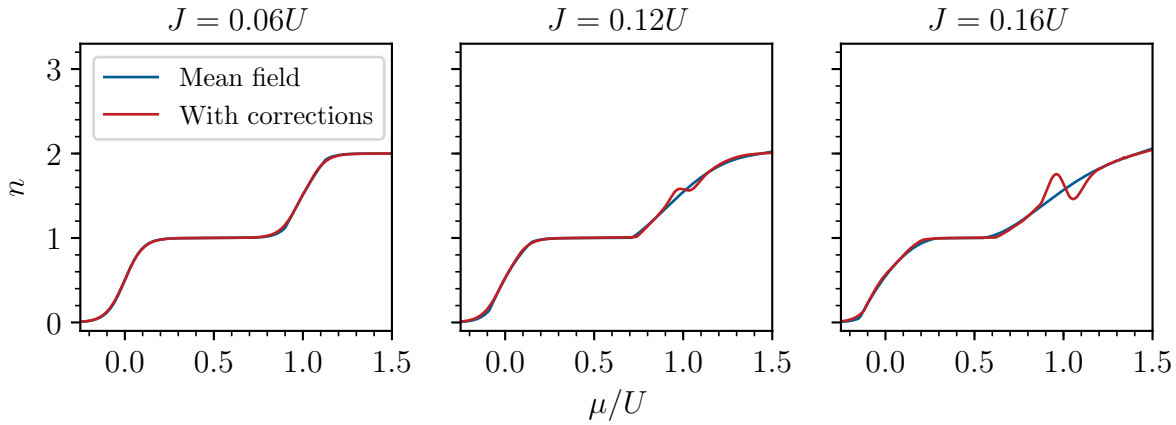

Figure 4.12: Particle number on horizontal lines in the fixed-U phase diagram at $T = 0.05U$.

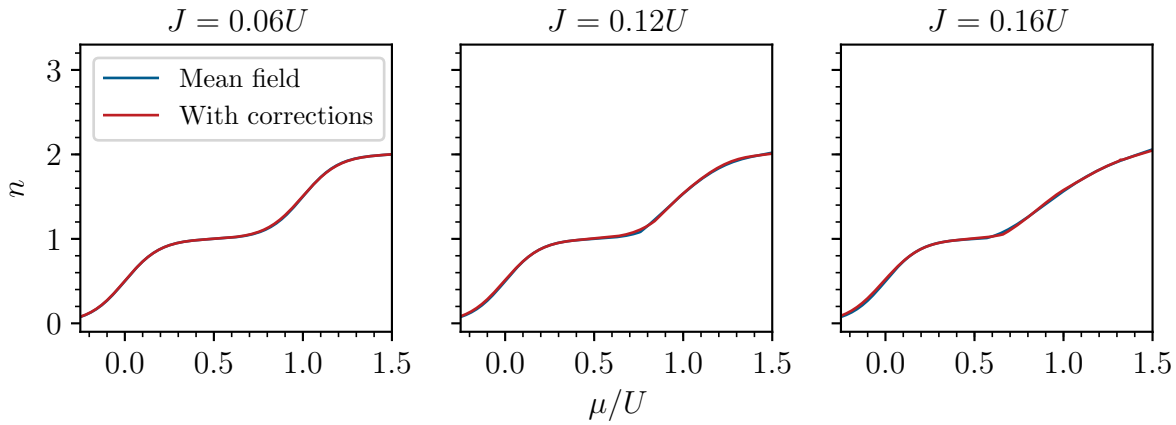

Figure 4.13: Particle number on horizontal lines in the fixed-U phase diagram at $T = 0.1U$.

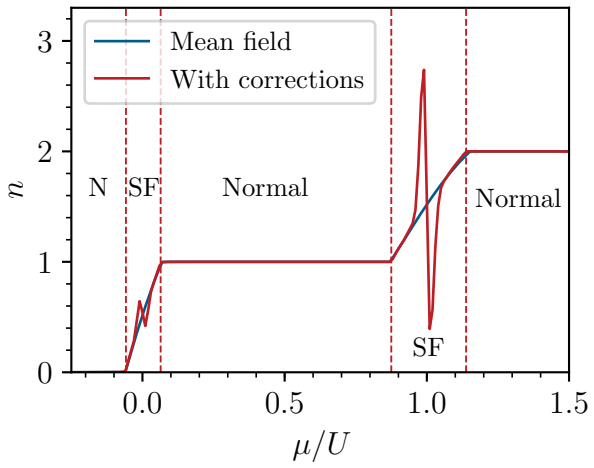

Figure 4.14: Low-temperature behaviour of the particle number on the $J = 0.06U$ horizontal line in the fixed-U phase diagram for $T = 0.01U$, with phase transitions indicated by dashed lines. N is an abbreviation of normal and SF abbreviates superfluid.

get smaller, i.e. it needs less deviation of μ to make it energetically favorable to add/remove particles and let the resulting extra particles/holes hop through the lattice. For higher temperature you can very well observe the non-zero slope that we expected in section 2.4, which is the reason why there is no exact Mott phase anymore.
Furthermore, in the unproblematic regions, the differences between mean-field and the corrected results for the particle number are small compared to the differences in the results for the order parameter. Thus, quantum fluctuations do not really influence the particle number in total but rather the fraction of particles in the ground state, which is physically plausible.
In the particle number figures it becomes especially clear where degeneracies occur and render our corrected results unphysical. Due to this, it might be possible to map out the problematic zones in the phase diagram using the particle number. Unfortunately, by comparison of figure 4.9 and 4.13, it is already clear, that although the particle number does not show any unphysical behaviour, the order parameter still shows the unphysical dip mentioned above. So, we can already conclude here, that this mapping using the particle number alone will still not fully capture the problematic zone. We will not further investigate this in this thesis.
Figure 4.14 again shows the particle number for $J = 0.06U$ and $T = 0.01U$. The dashed lines indicate where the phase transition occurs. They were calculated using the corrected results because we already saw above that the corrected and the mean-field phase transitions essentially happen at the same point for these parameters. In order to find the point of transition we used the same method as for the phase diagrams, as outlined at the beginning of this chapter.
The figure captures the low temperature behaviour of the particle number well. There are normal phases, which are close to the exact Mott phase, where the particle number is approximately constant, i.e. the compressibility is almost zero. Further there are superfluid regions between the normal phases where the particle number is non integer and continously changes from the particle number of one lobe to the

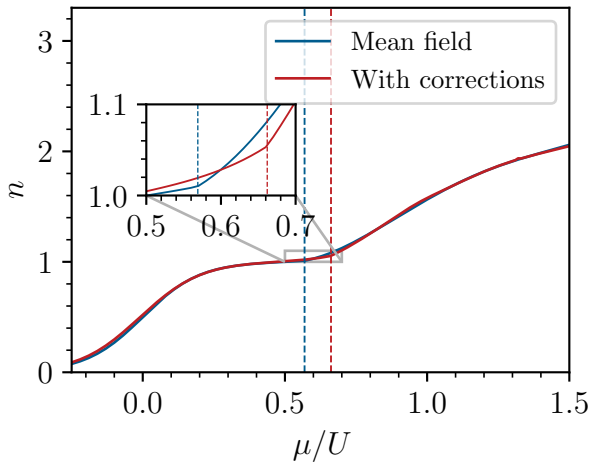

Figure 4.15: High-temperature behaviour of the particle number on the $J = 0.16U$ horizontal line in the fixed-U phase diagram for $T = 0.1U$, with phase transitions indicated by dashed lines.

one of the other. The point of phase transition is exactly where the derivative of the particle number jumps, i.e. where the particle number is not analytic.

In contrast to this figure 4.15 shows the particle number for $J = 0.16U$ and $T = 0.1U$. This time the critical value of μ/U is shown both in mean-field approximation and including the corrections, indicated with blue and red dashed lines respectively, because here there is a substantial discrepancy between the two. The particle number still shows a similar behaviour to the low temperature case, having regions with bigger and regions with smaller slope, but these are not generally divided by a phase transition anymore. For example, the particle number changes from $n = 0$ to $n = 1$ without entering the superfluid phase at all.

A big difference between the high and the low temperature behaviour resulting from this, is that for high temperature, there are parts of the phase diagram where the mean particle number is non-integer but the system is not in the superfluid phase. These regions get smaller for lower T and fully vanish for $T = 0$. We can explain this observation through thermal fluctuations, that prevent the system from getting a long-range order, which is what characterizes the superfluid phase. This is analogous to a spin system, where a high temperature also prevents the spins from aligning and forming an ordered phase, a ferromagnet, only that the notion of order in the Bose-Hubbard model is less intuitive. Another explanation for this is that the particles get prevented from condensing into the ground state by excitations through thermal activation.

From figure 4.15 is is clear that for high temperature, the particle number is generally a smoother function of J/U than in the low temperature case. However, there is still a point of non-analyticity at the phase transition, which can be seen in the inset. The inset also shows that there are some discrepancies between the corrected and the mean-field results in the vicinity of the phase transition but they are on a much smaller scale than differences in the order parameter for example.

Lastly, we investigate the entropy on the horizontal lines. Figures 4.16 and 4.17 show our results for $T = 0.05U$ and $T = 0.1U$, respectively. Note that we do not show the entropy for $T = 0.01U$. This is because at low temperature the entropy

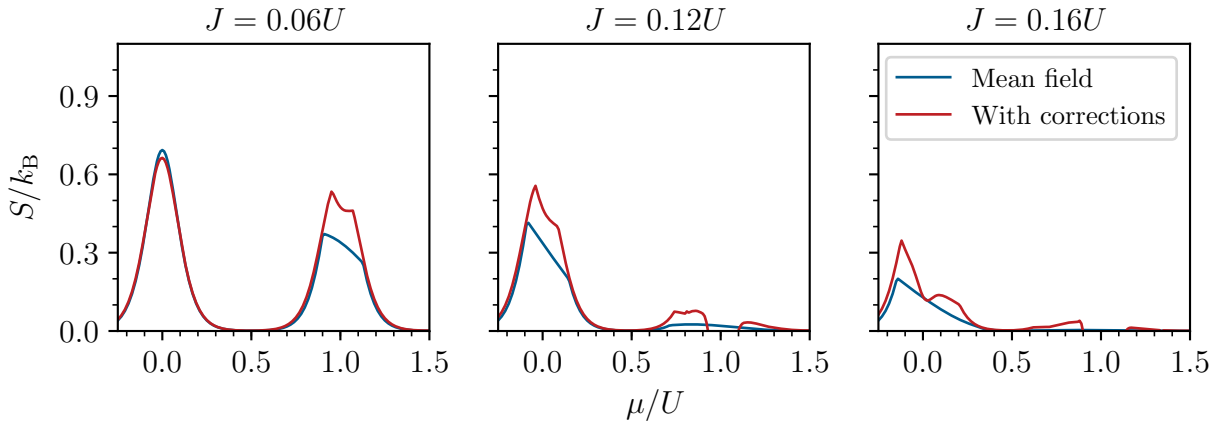

Figure 4.16: Entropy on horizontal lines in the fixed-U phase diagram at $T = 0.05U$.

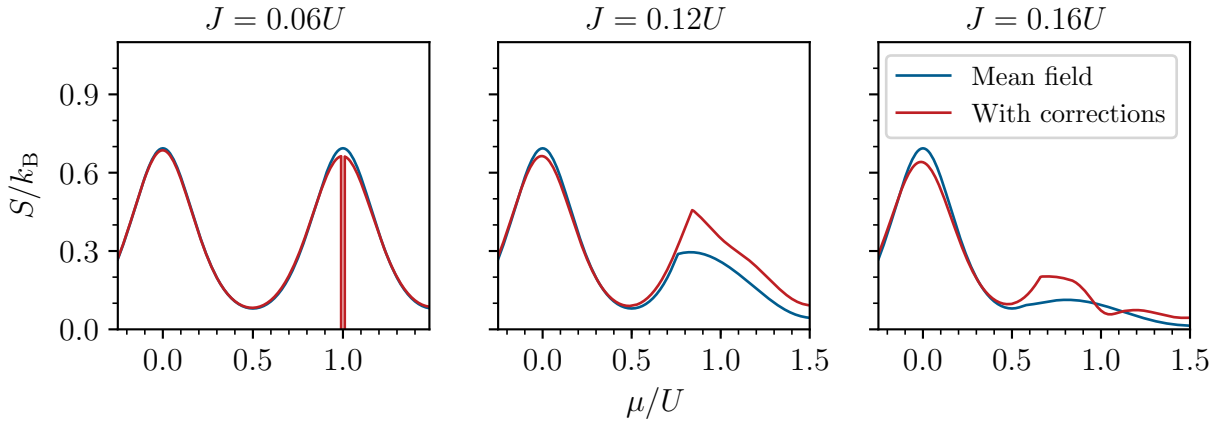

Figure 4.17: Entropy on horizontal lines in the fixed-U phase diagram at $T = 0.1U$.

is simply too small to see any structures besides those coming from degeneracies i.e. the entropy is of the order of the machine precision in the regions where our calculation works.
In all of the figures, the entropy has a lower value in the normal phase and peaks between the lobes. By comparison with the particle number figures 4.11-4.13, it is clear that the peaks in the entropy occur, where the particle number is non-integer and the entropy is small where the particle number is approximately integer.
The small entropy in the regions of integer particle number can be explained as follows: The ground state of the system for integer particle number is the state where each lattice site is occupied by the same integer number of particles. This state can only be realized in one way and it thus has no entropy. Hence, all entropy for integer particle number comes from excited states, which are however separated by some excitation gap. For small temperature this can practically not be overcome, resulting in a very small entropy. When increasing the temperature, the gap can be overcome more often, increasing the entropy. The quantum fluctuations also allow the particles to occasionally cross the excitation gap, slightly increasing the entropy, which can be seen in figure 4.17 or in the inset of figure 4.19.
We can further explain the peak in between the lobes by the following reasoning: If there are no particles in the system there is of course no entropy. If one particle is added it will now somewhat delocalize but not fully as thermal fluctuations prevent the condensation. There are now a lot of degenerate states possible how this particle can delocalize, giving rise to some finite entropy. If further particles are added they will also mostly delocalize just partly, which gives rise to even more possibilities of different states. Thus the entropy keeps increasing by increasing the chemical potential, i.e. adding more and more particles to the system, until a mean particle number per site of $1/2$ is reached, where the entropy is maximized. If now more particles are added we can view this as holes, that are hopping through the mostly filled lattice, being removed, again reducing the entropy. For higher J the particles will delocalize more, which reduces the number of possible states and thus the entropy .
It might be concerning that the entropy peak on the right side of the lobe is not symmetric, contradicting the reasoning just given. This is due to the fact that on the right side of the lobe the particles comprising the non-integer filling state are additional to an existing integer filling, instead of being the only particles in the lattice. But because also the particles comprising the integer filling can occasionally hop out of it and contribute to the entropy the situation gets more complicated. The general idea is the same however and can still explain why there is an entropy peak at all.
As the different states of the particles being spread out differently are essentially degenerate, we would expect that thermal activation does not change the height of the peaks. We can however observe that the height of the peaks changes with temperature, especially the height of the peak on the right side of the lobe. By comparison with the figures showing the order parameter on the horizontal lines, figures 4.8 and 4.9, it is clear that the height of the peak is correlated with the order parameter. If the system is in the normal phase the peak is the highest, but with increasing order parameter, when the system is superfluid, the height of the peak decreases. This is clear as $|\psi|^2$ is the condensate density, or the fraction of particles occupying the ground state, i.e. the fraction of particles that are delocalized over the whole

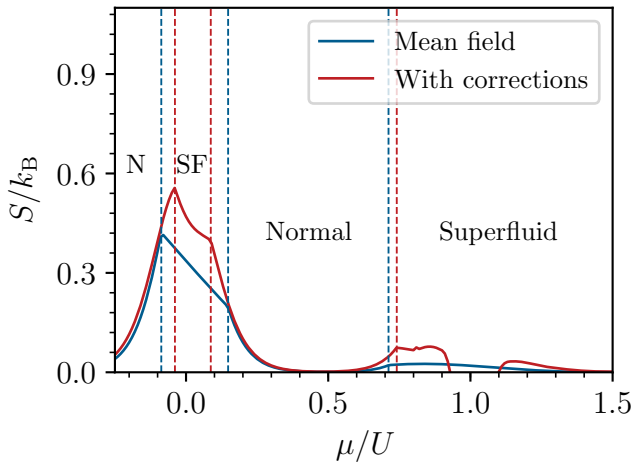

Figure 4.18: Entropy on the $J = 0.12U$ horizontal line in the fixed-U phase diagram at $T = 0.05U$, with phase transitions indicated by dashed lines. N is an abbreviation for normal and SF abbreviates superfluid.

lattice. As we already argued above, particles in the single-particle ground state, do not contribute to the entropy. For increasing temperature, we have seen that the phase boundary moves to higher values of J and thus the order parameter should generally decrease, because the horizontal lines we investigate stay the same. This can also be observed in the respective figures 4.7-4.9. This explains the observation that the entropy peaks are generally higher for higher temperature.
As the entropy peaks occur at integer μ/U, which is exactly where our calculations might not work properly due to degeneracies, we need to be careful when interpreting the corrected results here. Especially for low T and high J the entropy shows highly unphysical behaviour, see for example figure 4.19.
However, there are also non-analyticities in the entropy that are actually physical and are associated with a phase transition, see figures 4.18 and 4.19. In figure 4.18 you can further notice a small peak at $\mu \approx 0.8U$, which is probably a numerical error. It is however robust against using higher order differentiation formulae, using a larger Hilbert space and slight parameter changes.
The inset in figure 4.19 focuses on the phase transition that is not visible in the full figure as the entropy is small there. Here, the relative difference between mean-field and corrected results is rather large. For $\mu \approx 0.7U$ you can spot another non-analyticity not connected to a phase transition. This might already be a result of degeneracies, which could be possible as J is rather large.

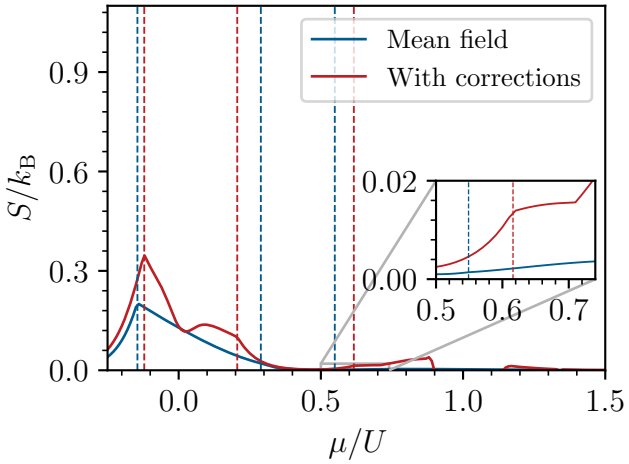

Figure 4.19: Entropy on the $J = 0.16U$ horizontal line in the fixed-U phase diagram at $T = 0.05U$, with phase transitions indicated by dashed lines. The inset focuses on one particular transition where the entropy is small.

4.1.2 Vertical lines

After analyzing thermodynamic quantities on horizontal lines we will now turn to vertical lines, see figure 4.20. We take one line to be on the left side of the lobe at $\mu = 0.1U$, one on the right side at $\mu = 0.9U$ and one that goes approximately through the tip at $\mu = 0.4U$. As we already argued in section 3.3 our calculation will not work for high J. Further we expect the critical J where we enter the problematic zone, to be lower at the sides of the lobe than it is in the middle. In the following we thus have to use different J/U-axis limits for the different lines, especially for low temperature. You should keep that in mind in the following as it will not always be explicitly stated. Note however, that it is in general hard to distinguish where exactly deviations of the corrected results from the mean-field expectations are physical and where they become unphysical, so we need to generally be cautious when interpreting the corrected results for high J.

As before we start our analysis with the order parameter, shown in figures 4.21-4.23.

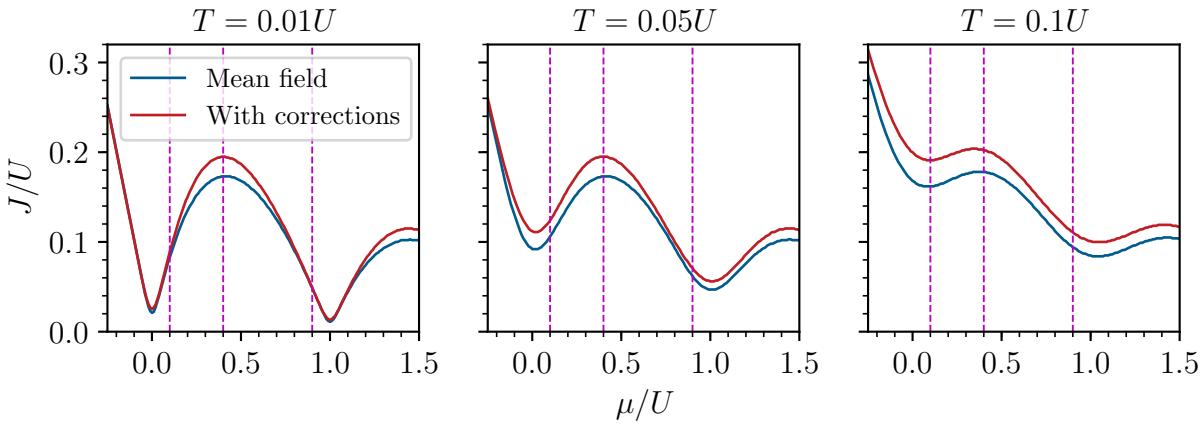

Figure 4.20: Vertical lines in the fixed-U phase diagrams for different temperatures, μ takes the values $0.1U$, $0.4U$, $0.9U$ on these lines respectively.

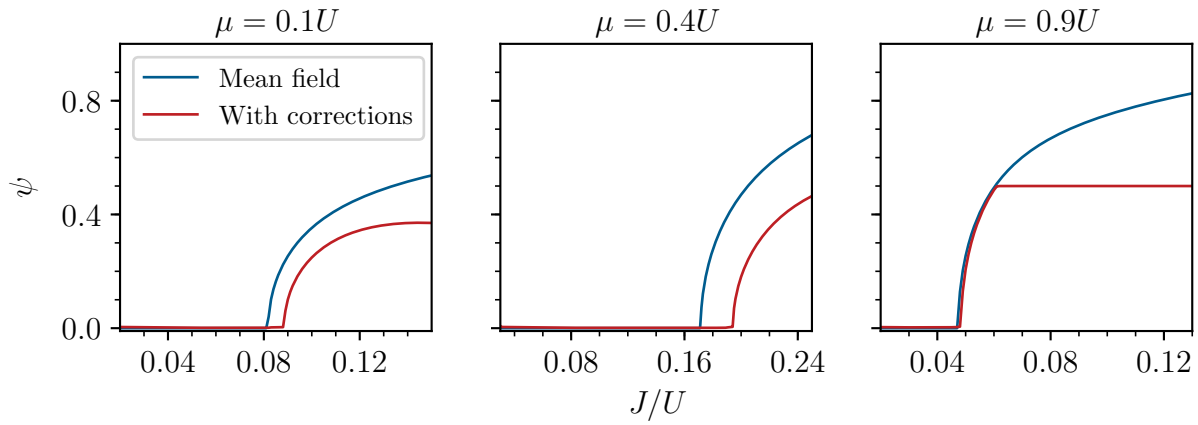

Figure 4.21: Order parameter on vertical lines in the fixed-U phase diagram at $T = 0.01U$.

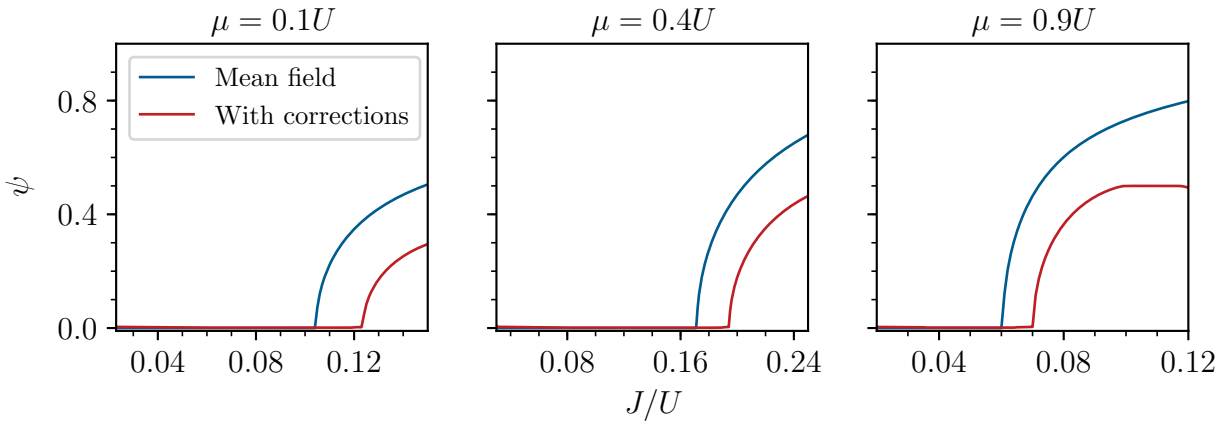

Figure 4.22: Order parameter on vertical lines in the fixed-U phase diagram at $T = 0.05U$.

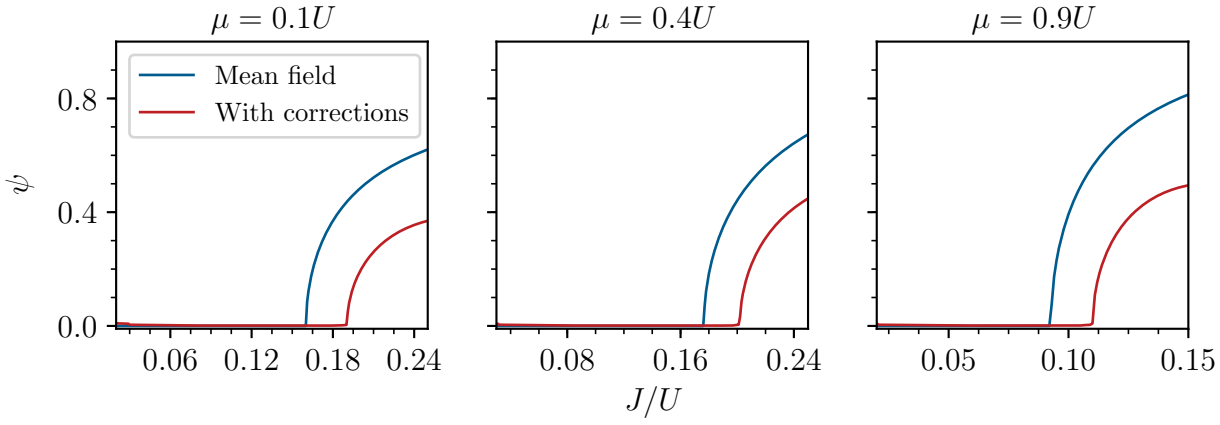

Figure 4.23: Order parameter on vertical lines in the fixed-U phase diagram at $T = 0.1U$.

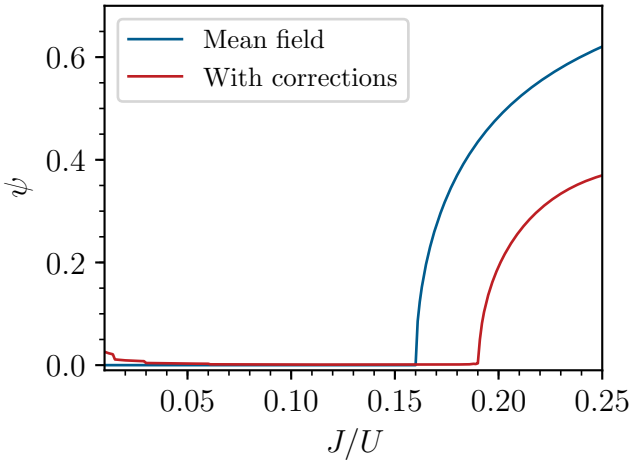

Figure 4.24: Unphysical behaviour of the order parameter for J close to 0, here for $\mu = 0.9U$ and $T = 0.01U$.

First note that the starting limit of the J/U-axis sometimes varies slightly. This is due to unphysical behaviour of the order parameter near $J = 0$, see figure 4.24. This is a consequence of numerical mistakes. We calculate the order parameter as the value ψ that minimizes the grand canonical potential $\Phi(\psi)$. For $J = 0$ however the grand canonical potential does not depend on ψ at all as is clear from the mean-field Hamiltonian (2.38), i.e. $\Phi(\psi)$ is simply constant. For small values of J, $\Phi(\psi)$ is then still approximately constant which results in a noticeable error in numerically determining the minimum.
In the figures 4.21-4.23 you can see that, as expected, ψ is zero until we reach a critical J where the particles start macroscopically occupying the ground state. Also here we can observe the characteristic non-analytic change of the order parameter at the phase transition. At the center of the lobe, the critical J is generally higher than at higher or lower μ, as was already discussed in section 2.4.
As on the horizontal lines, the order parameter is generally smaller when including the corrections. Furthermore we observe that quantum as well as thermal fluctuations delay the transition to higher J, i.e. the fluctuations prevent the particles from condensing.
It is notable that the order parameter seems to obey the same scaling law in the vicinity of the critical point, both in the corrected and the mean-field results. This would mean that our calculations still predict the order parameter critical exponent β to have the mean field value $\beta = 1/2$ [102]. This is correct for most transitions as they fall into the mean-field universality class. Those at the tip of the lobes however fall into the universality class of the four-dimensional XY model for a three-dimensional lattice, and thus should not have mean-field critical exponents [33]. However, to properly discuss this, the critical exponents of our corrected results should be investigated more carefully, which could be subject of further work and will not be done in this thesis.
Figure 4.25 exemplarily shows what happens for large J. You can observe that the order parameter goes through a plateau and then decreases in the deep superfluid phase when including the corrections which is clearly non-physical, as we expected. Note that the unphysical behaviour already starts at $J \approx 0.135U$, which is lower

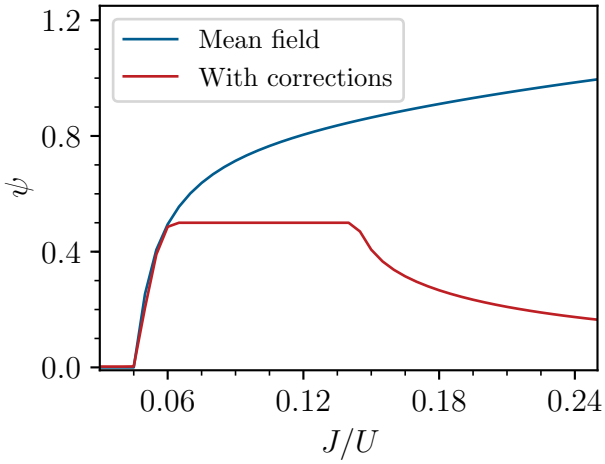

Figure 4.25: Unphysical behaviour of the order parameter in the deep superfluid phase, here for $\mu = 0.9U$ and $T = 0.01U$.

than the critical J of the phase transition for the $\mu = 0.4U$ line at the same temperature, which is approximately $\mu \approx 0.175U$. This justifies the different J/U-axis limits used, as mentioned at the beginning of this section.

Figures 4.26-4.28 show an overview of our results for the particle number on the different vertical lines. At low temperature the particle number shows a plateau for small J, while it already has a non-zero slope there at higher temperature. This reflects what was already found on the horizontal lines, that the n-plateaus get smaller for higher temperature.

It is apparent that on the right side of the n-plateau, i.e. on the right side of the lobe, the particle number increases after the transition and that it decreases on the left side. This is consistent with the statement from section 2.4, that on the right (left) side of the lobe, the transition is driven by extra particles (holes) getting added to the system, producing a superfluid state.

Close to the center of the plateau, the particle number almost doesn't change. Here, the other type of transition occurs, which is not driven by extra particles or holes getting added but by the existing particles overcoming the repulsive interaction to condense into a superfluid anyway. Of course after the transition the particle number still changes because we are investigating a vertical line which is not an exact constant particle number line. We will turn to these in chapter 5.

Figure 4.29 shows the particle number with a focus on the transition at the tip of the lobe. Here it is clearly visible, that the particle number increases after the transition on this line. An interesting feature that did not get captured by the overview is that the particle number in mean-field approximation undergoes a minimum after the phase transition which the corrected results do not. The same behaviour can also be seen for $\mu = 0.1U$, $T = 0.1U$, see figure 4.30.

In general on the vertical lines, the effect of the corrections on the particle number is more clearly visible than on the horizontal lines. This is probably due to the fact that the n-axis limits are different in the two cases. The corrections are especially notable in the vicinity of the phase transition, where fluctuations become more important.

Lastly, we now analyze the entropy on vertical lines through the fixed-U phase

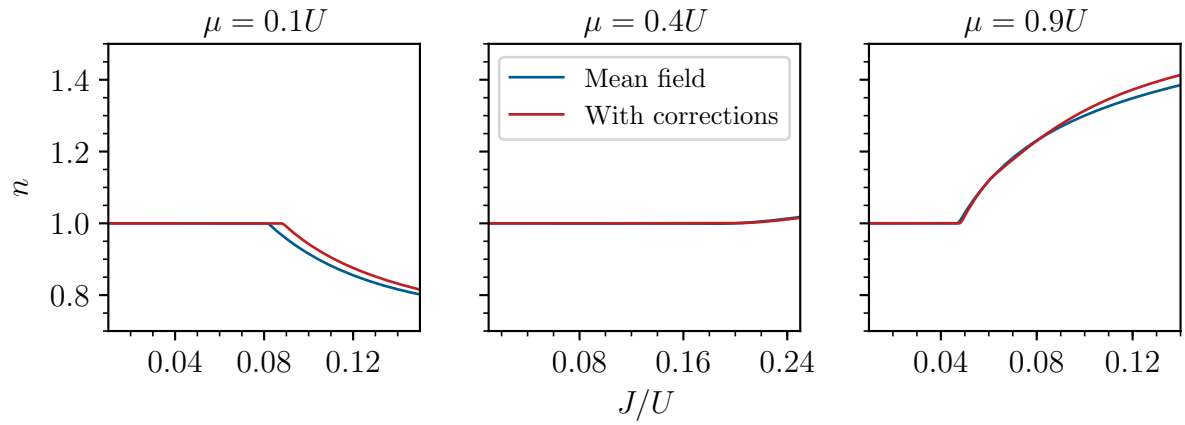

Figure 4.26: Particle number on vertical lines in the fixed-U phase diagram at $T = 0.01U$.

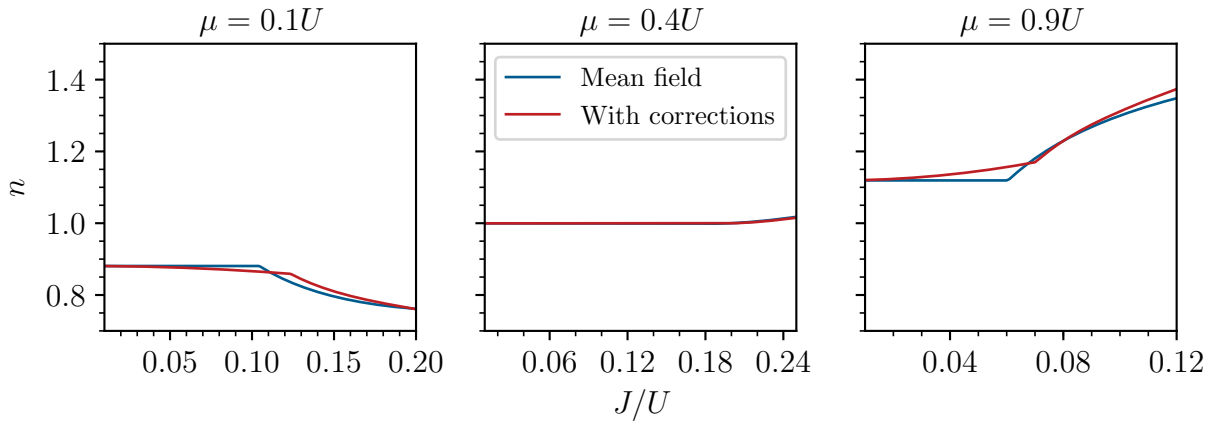

Figure 4.27: Particle number on vertical lines in the fixed-U phase diagram at $T = 0.05U$.

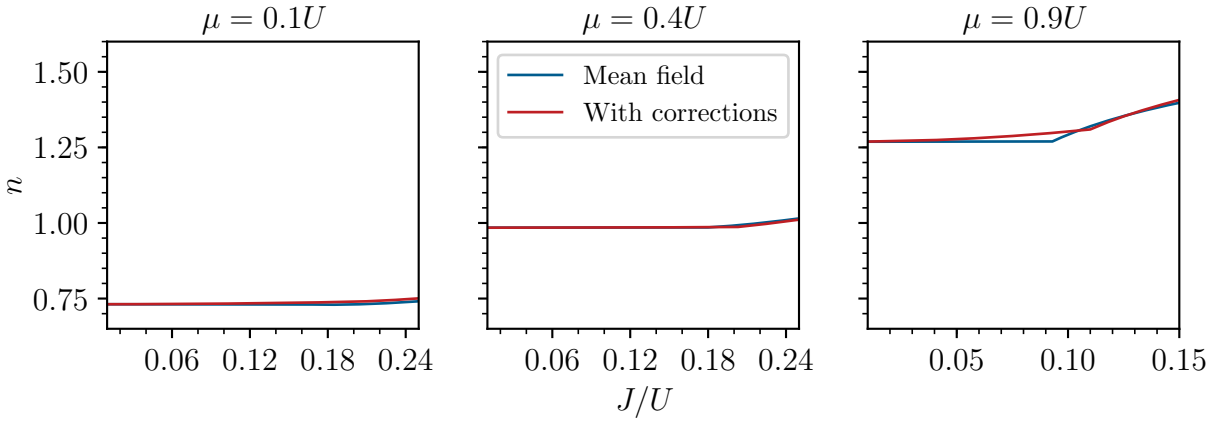

Figure 4.28: Particle number on vertical lines in the fixed-U phase diagram at $T = 0.1U$.

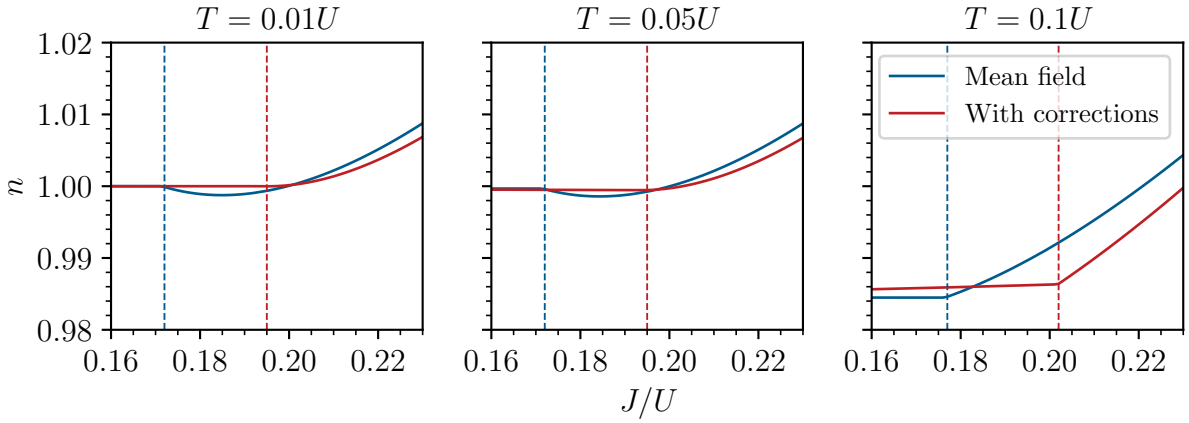

Figure 4.29: Particle number on the $\mu = 0.4U$ vertical lines in the fixed-U phase diagrams in the vicinity of the phase transition at the tip of the lobe. The phase transition is indicated by a dashed line.

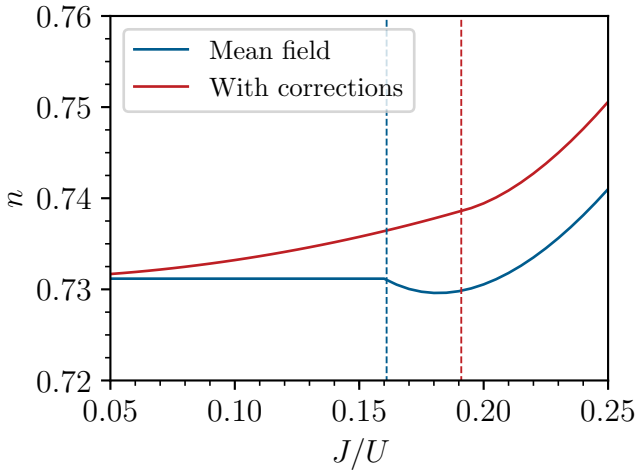

Figure 4.30: Minimum in the particle number in mean-field approximation on the $\mu = 0.1U$ vertical line in the fixed-U phase diagram at $T = 0.1U$ after the phase transition. The phase transition is indicated by a dashed line.

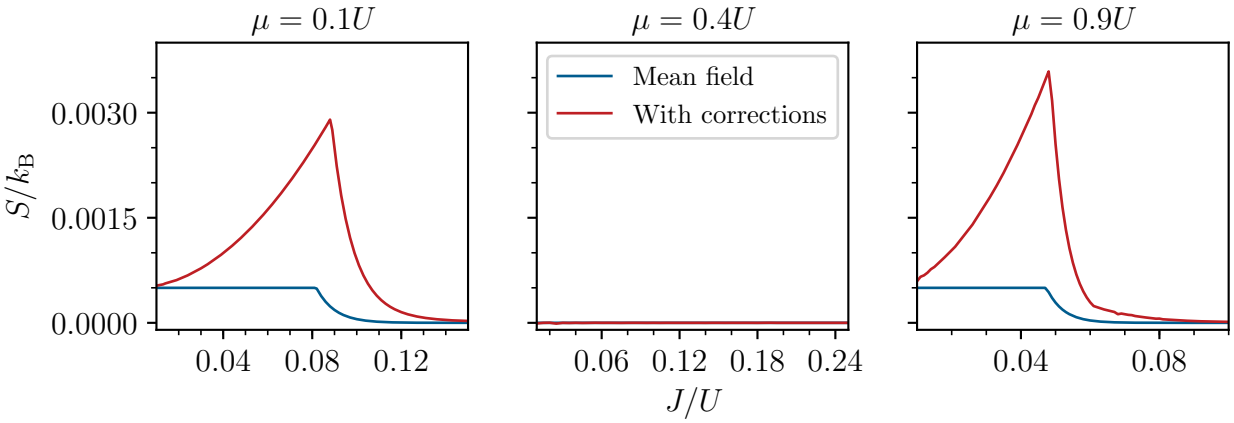

Figure 4.31: Entropy on vertical lines in the fixed-U phase diagram at $T = 0.01U$.

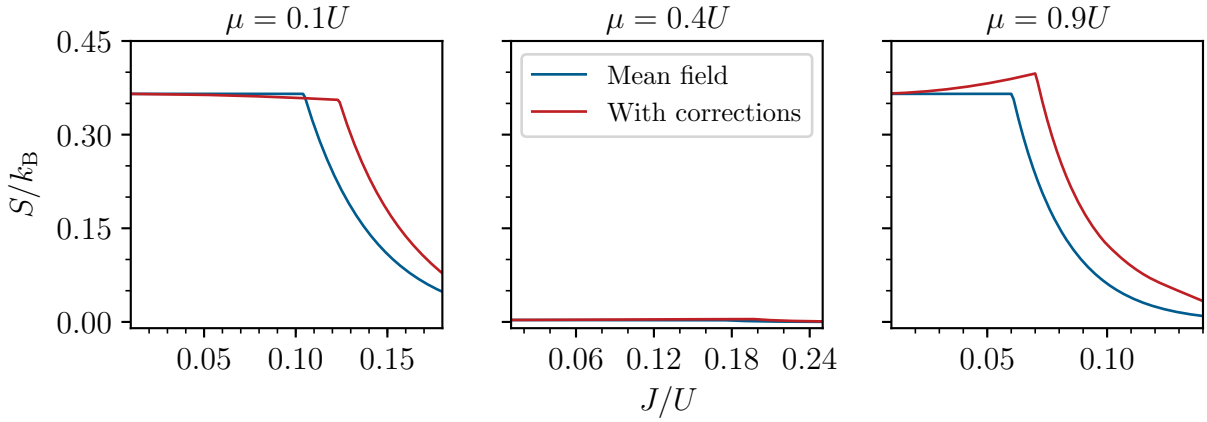

Figure 4.32: Entropy on vertical lines in the fixed-U phase diagram at $T = 0.05U$.

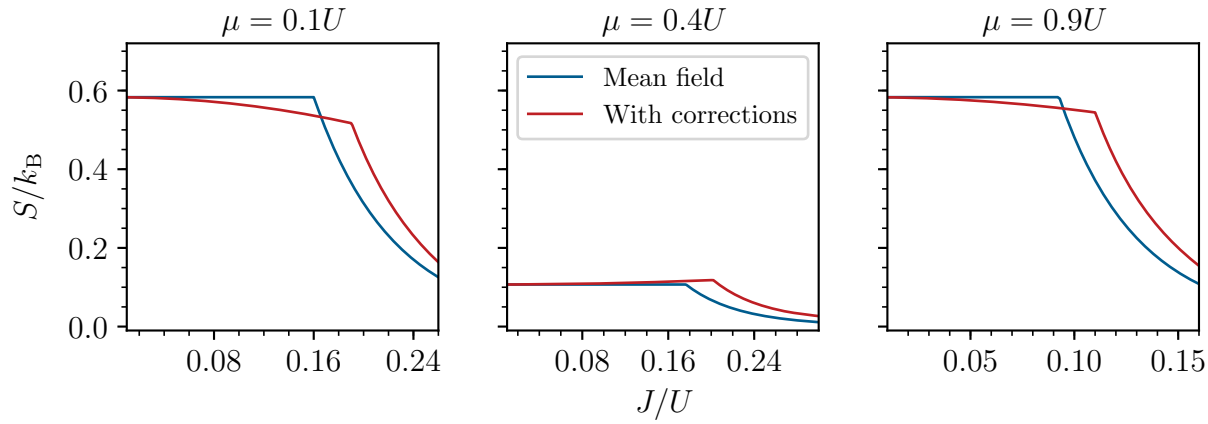

Figure 4.33: Entropy on vertical lines in the fixed-U phase diagram at $T = 0.1U$.

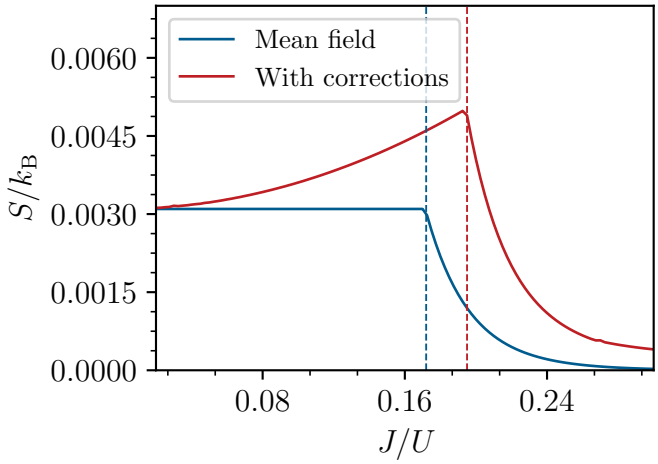

Figure 4.34: Entropy on the $\mu = 0.4U$ vertical line in the fixed-U phase diagram at $T = 0.05U$. The phase transition is indicated by a dashed line.

diagrams. Figures 4.31-4.33 show an overview of our results. Generally, the entropy is non-zero in the normal phase and then falls to zero after the phase transition because for increasing J more and more bosons delocalize throughout the whole lattice and condense into the lowest lying state where they do not contribute to the entropy. Furthermore you can observe that the non-central values for μ lead to a larger entropy than $\mu = 0.4U$. This is because in the center of the lobe the system usually has a non-integer particle number which allows for more states and thus a higher entropy. This was discussed in more detail in our analysis of the horizontal lines. Also a higher temperature generally leads to a higher entropy, which is clear because the thermal fluctuations allow for higher energetic states to be populated more.
The corrected entropy shows two different behaviours in the normal phase, whereas the entropy in mean-field approximation is always constant there. In some figures the entropy has a positive slope in the normal phase with a maximum at the phase transition. In the other figures the entropy already has a negative slope in the normal phase, which then jumps at the phase transition.
From the overview it already gets clear that the entropy on the non-central vertical lines, tends to show the former behaviour for lower temperature, while it mostly shows the latter for high temperature.

Figures 4.34 and 4.35 show the entropy on the central vertical line on a more appropriate scale. Note that we do not show the entropy for $T = 0.01U$, as it is too small to see any structure. From these two figures it gets clear, that the entropy on these lines shows a positive slope in the normal phase and a maximum at the phase transition even for high temperature. However, also on these lines the maximum gets suppressed by higher temperature.
We will postpone the discussion of these two behaviours and their physical interpretation to section 5.1, where we discuss lines of constant particle number. On those lines we observe the same two behaviours but it will get more clear when the entropy shows which of the two.

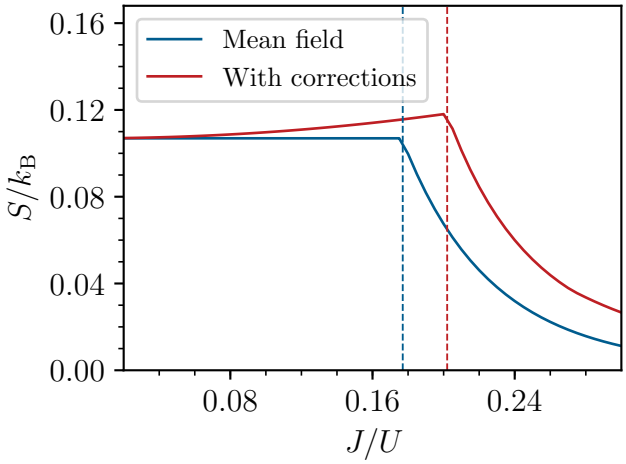

Figure 4.35: Entropy on the $\mu = 0.4U$ vertical line in the fixed-U phase diagram at $T = 0.1U$. The phase transition is indicated by a dashed line.

4.2 Fixed Hopping Amplitude

Now that we have analyzed different lines in the fixed-U phase diagram we will do the same with the fixed-J one. As already briefly mentioned at the beginning of section 4.1, we will only look at vertical lines through the fixed-J phase diagrams, as we can simply relate a horizontal line through the fixed-J phase diagram to one through the fixed-U phase diagram. We simply have to translate the fixed-J quantities to fixed-U quantities. For example:

$$\frac{T}{U} = \frac{T}{J}\frac{J}{U} = \frac{T}{J}\frac{1}{U/J}. \tag{4.9}$$

As vertical lines we choose those with $\mu = 0.4J$, $\mu = 2J$ and $\mu = 4J$, see figure 4.36. Due to the degeneracy problems, we have to expect unphysical results for low U/J. In the following we will thus have to use different U/J-axis limits for the different figures, which will not be explicitly stated every time.

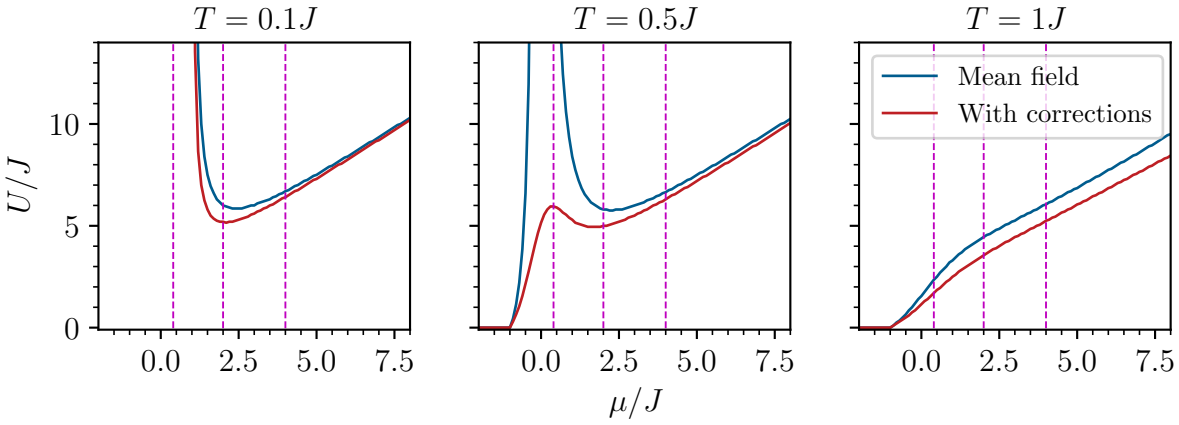

Figure 4.36: Vertical lines in the fixed-J phase diagrams for different temperatures, μ takes the values $0.4J$, $2J$, $4J$ on these lines respectively.

As before we start our analysis with the order parameter. An overview of our results is given in figures 4.37-4.39. As expected, we observe an inverse behaviour compared to the fixed-U case. For small U the system is in the superfluid phase and enters the normal phase for a critical value of U/J, where the strong on-site repulsion prevents the particles from condensing. This transition now occurs earlier, i.e. for a smaller value of U, when the corrections are included. Thermal fluctuations have a similar effect, i.e. a higher temperature also makes the transition occur earlier. As before, the corrected result is generally smaller than the mean-field one. All of these observations are consistent with the corresponding ones made in the fixed-U case.
For $T = 0.1J$, $\mu = 0.4J$ the fact that the system never enters the normal phase is clearly visible. It is notable that the mean-field results have a negative slope, while the corrected results have a positive slope, i.e. the corrected results predict that the number of condensed particles increases for increasing U, which is quite counterintuitive. This might also be a consequence of degeneracies.
The line for $T = 0.5J$, $\mu = 0.4J$ does not enter the normal phase in mean-field approximation but it does so when including the corrections. Thus, on this line mean-field theory and the corrected results make qualitatively different predictions for the behaviour of the system, which was never observed on the fixed-U lines.
As in the fixed-U case we observe unphysical plateaus in the superfluid phase, here for small U, which are probably due to degeneracies. Figure 4.40 shows further unphysical behaviour for small U, exemplarily justifying the different axis limits used.
Next we investigate the particle number. An overview is given in figures 4.41-4.43. The particle number decreases with rising U in all figures, in contrast to the fixed-U case, where we saw that the particle number can increase or decrease in the superfluid phase after the transition, depending on which side of the lobe the transition occurs. Also we do not observe the phase transition at constant mean particle number on the lines investigated. The fact that we can only observe one type of phase transition will get clear in section 5.2, where we consider constant particle number lines. Essentially the reason is that the lobe of constant particle number is formed differently. Because of this, the $n = 1$ line for example, is not approximately vertical like in the fixed-U case and we can thus not observe the corresponding transition on a vertical line.
As in the fixed-U case the particle number admits a plateau with $n = 1$ after entering the lobe, at least for low temperature. This plateau gets smaller for increasing temperature. For example the $\mu = 4J$ line for $T = 1J$ does not show a plateau anymore.
Furthermore, the differences between corrected and mean-field results are again most visible at the phase transition. They are particularly prominent on the line that does not enter the normal phase at all, i.e. for $\mu = 0.4J$, $T = 0.1J$.
Figure 4.44 shows another feature that we already saw in the fixed-U case. The particle number in mean-field approximation goes through a minimum on the superfluid side of the phase transition. In these figures also further quantitative differences between the mean-field and the corrected results are visible. This is also the case in figure 4.45, which shows the particle number with focus on the phase transition on two vertical lines for $T = 1J$. In the two figures, the corrections lead to a lower particle number in the superfluid phase and to a higher particle number in the normal phase

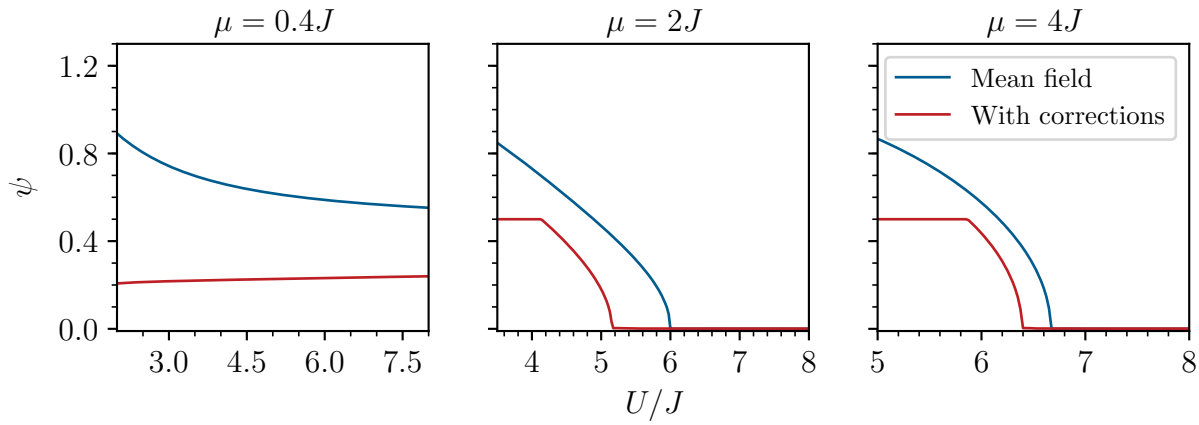

Figure 4.37: Order parameter on vertical lines in the fixed-J phase diagram at $T = 0.1J$.

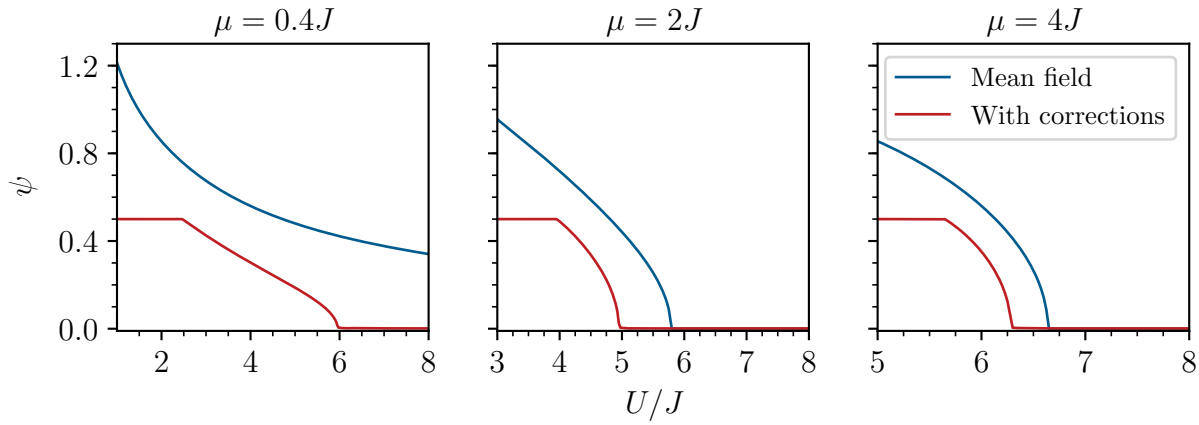

Figure 4.38: Order parameter on vertical lines in the fixed-J phase diagram at $T = 0.5J$.

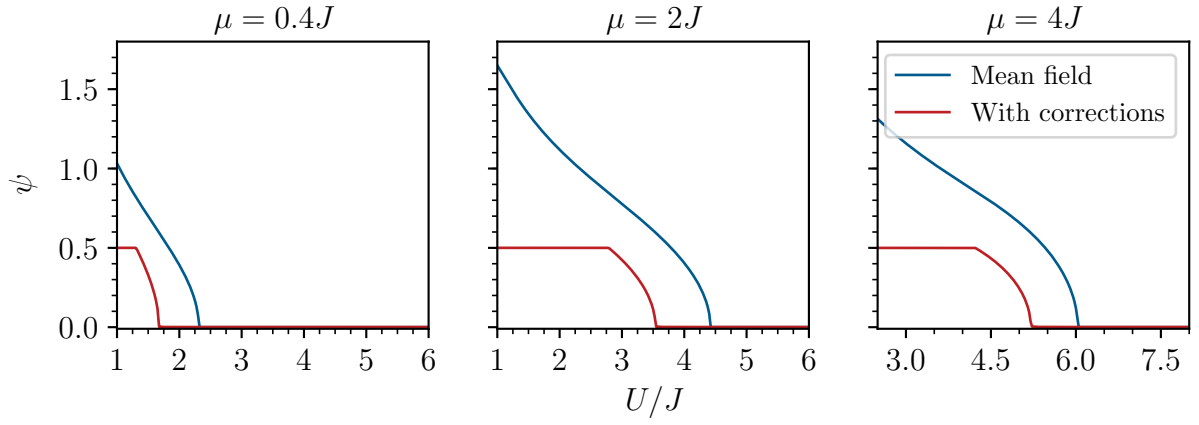

Figure 4.39: Order parameter on vertical lines in the fixed-J phase diagram at $T = 1J$.

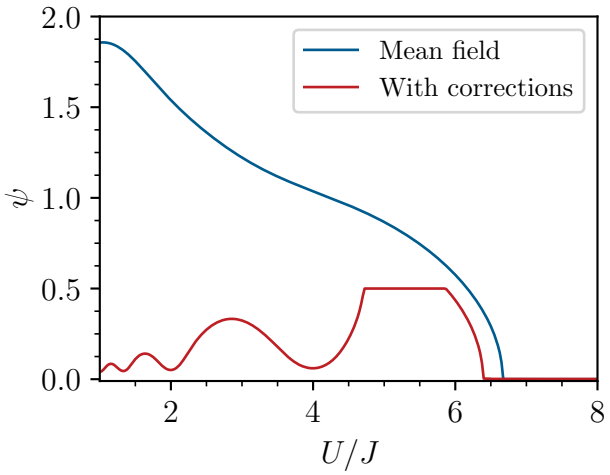

Figure 4.40: Unphysical behaviour of the order parameter for small U, here for $\mu = 4J$, $T = 0.1J$ and fixed J.

Lastly, we investigate the entropy on the vertical lines in the fixed-J phase diagrams. An overview is given in figures 4.46 and 4.47. Note that we again excluded the low temperature case $T = 0.01U$ as the entropy is too small there, at least for the two lines that enter the lobe.
For $T = 0.5J$ the entropy shows qualitatively different behaviours on the different lines. On the $\mu = 0.4J$ line it generally has a positive slope, the corrected entropy then reaches a plateau after the phase transition. The mean-field results do not show a plateau, which is probably due to the fact that the line does not enter the normal phase in mean-field approximation.

On the $\mu = 2J$ line, which is shown with focus on the phase transition in figure 4.48 the entropy shows a similar behaviour in mean-field approximation and when including the corrections. The entropy has a positive slope in the superfluid phase, has a maximum at the phase transition and then shows a plateau in the normal phase. The corrected results are generally larger in the superfluid phase, and then align with the mean-field results in the normal phase.
The behaviour of the entropy on the $\mu = 4J$ line is only slightly different. Also here the two results show a plateau in the normal phase where they align. The entropy on this plateau is however smaller than for $\mu = 2J$. In the superfluid phase the entropy shows a negative slope in mean-field approximation and a small positive slope when including the corrections. Again, the corrections increase the entropy in the superfluid phase.

For $T = 1J$ the behaviour is qualitatively similar for all μ. The entropy increases in the superfluid phase with a maximum at the phase transition and the decreases to some plateau in the normal phase. This plateau has a lower entropy for higher μ. The differences between mean-field and corrected results for $T = 1J$ are more noticable in the superfluid phase, where the quantum fluctuations increase the entropy. In the normal phase the two results align and the corrections decrease the entropy only slightly. Figure 4.49 again shows the entropy on the vertical lines at $T = 1J$, with focus on the phase transition. Here also the differences in the normal phase get visible.
As before we will postpone the physical discussion of the entropy to the next chapter,

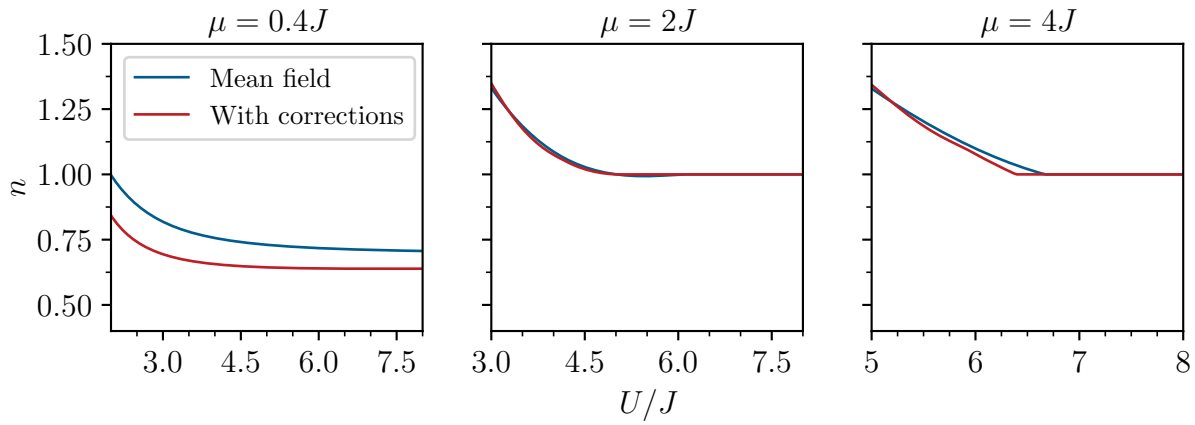

Figure 4.41: Particle number on vertical lines in the fixed-J phase diagram at $T = 0.1J$.

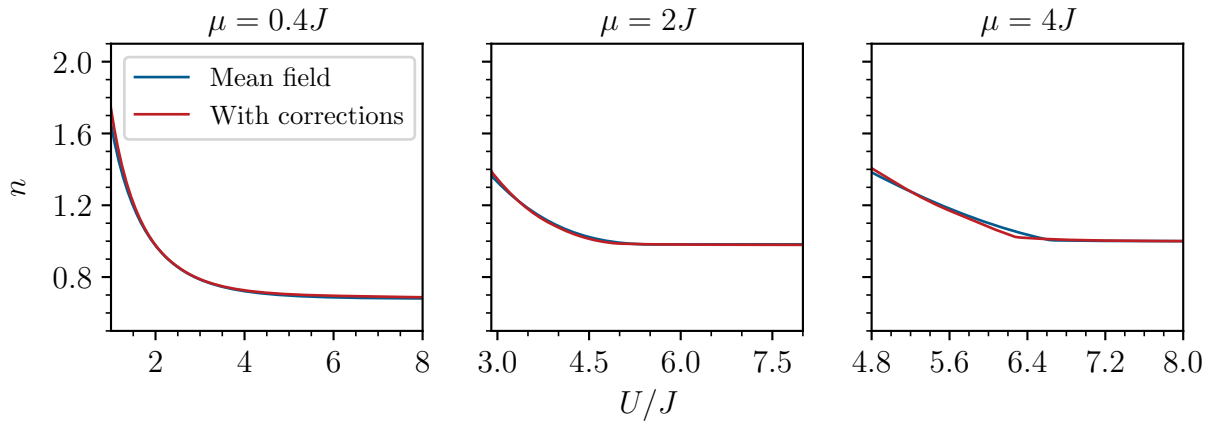

Figure 4.42: Particle number on vertical lines in the fixed-J phase diagram at $T = 0.5J$.

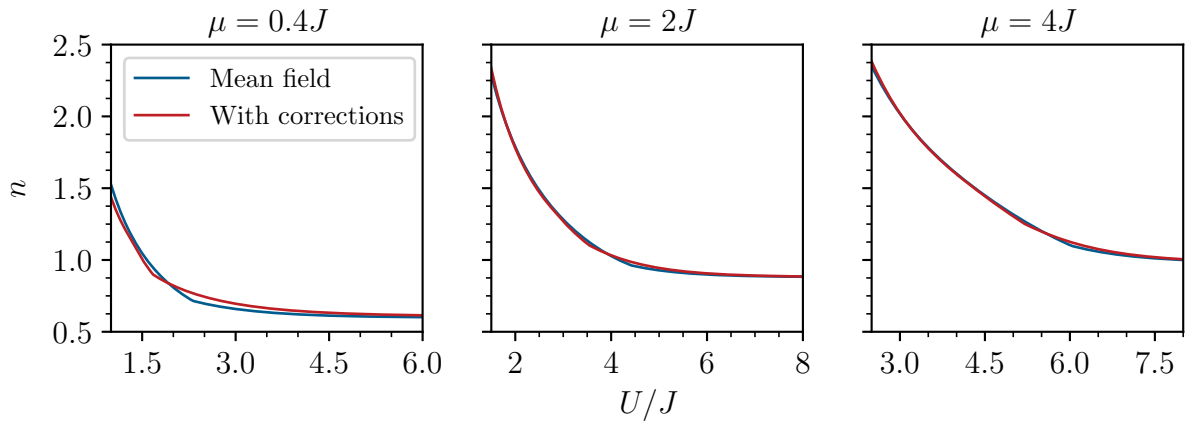

Figure 4.43: Particle number on vertical lines in the fixed-J phase diagram at $T = 1J$.

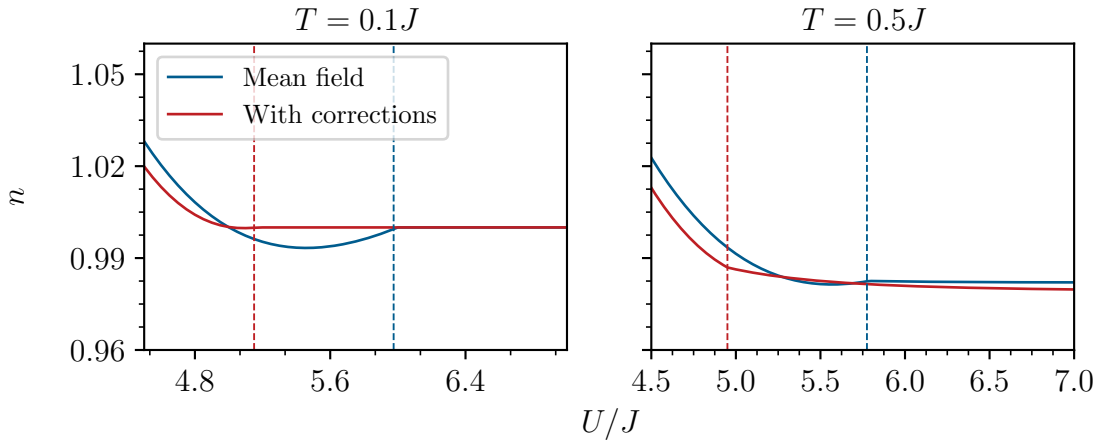

Figure 4.44: Minimum in the particle number in mean-field approximation on the superfluid side of the phase transition. Here on the $\mu = 2J$ vertical line in the fixed-J phase diagrams at $T = 0.1J$ and $T = 0.5J$. The phase transitions are indicated by dashed lines.

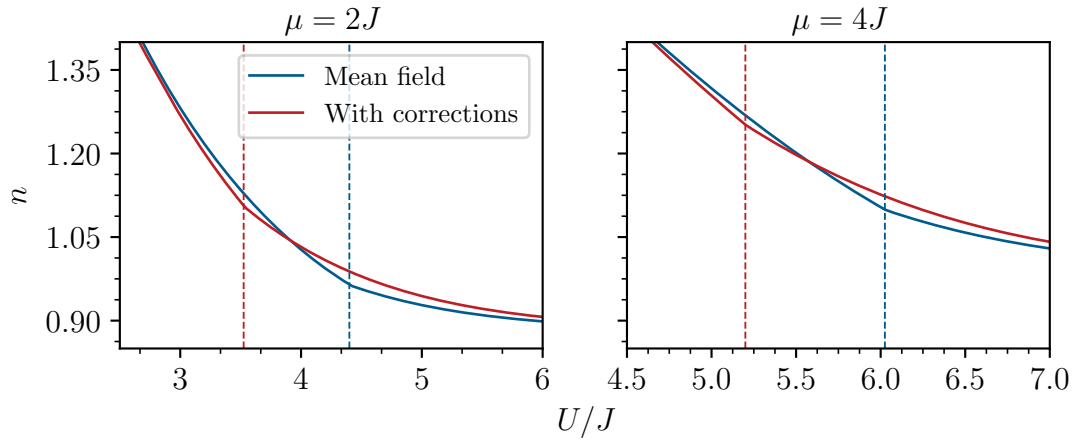

Figure 4.45: Particle number on the $\mu = 2J$ and $\mu = 4J$ vertical lines in the fixed-J phase diagram at $T = 1J$ in the vicinity of the phase transition. The phase transitions are indicated by dashed lines.

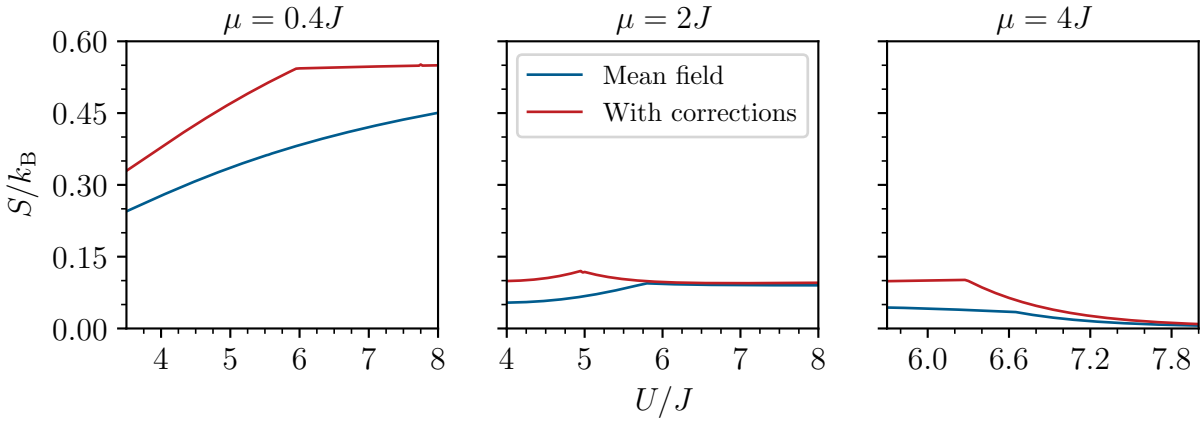

Figure 4.46: Entropy on vertical lines in the fixed-J phase diagram at $T = 0.5J$.

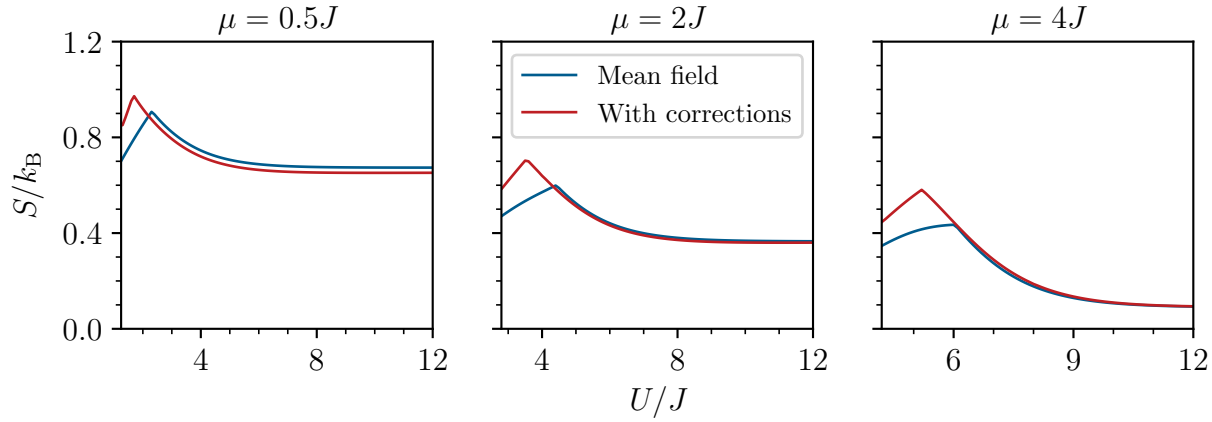

Figure 4.47: Entropy on vertical lines in the fixed-J phase diagram at $T = 1J$.

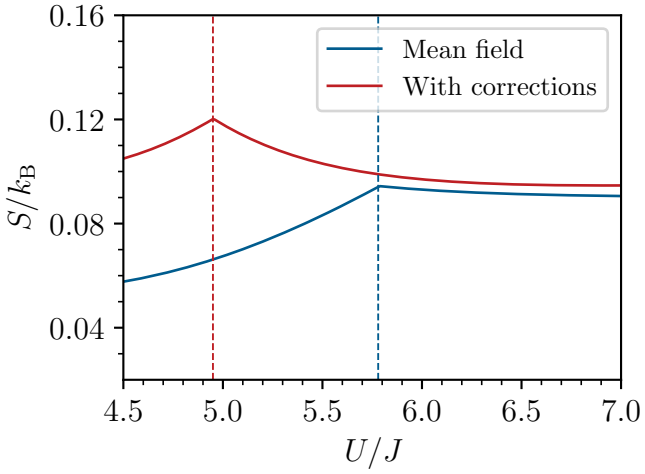

Figure 4.48: Entropy on the $\mu = 2J$ vertical line in the fixed-J phase diagram at $T = 0.5J$ in the vicinity of the phase transition. The phase transition is indicated by a dashed line.

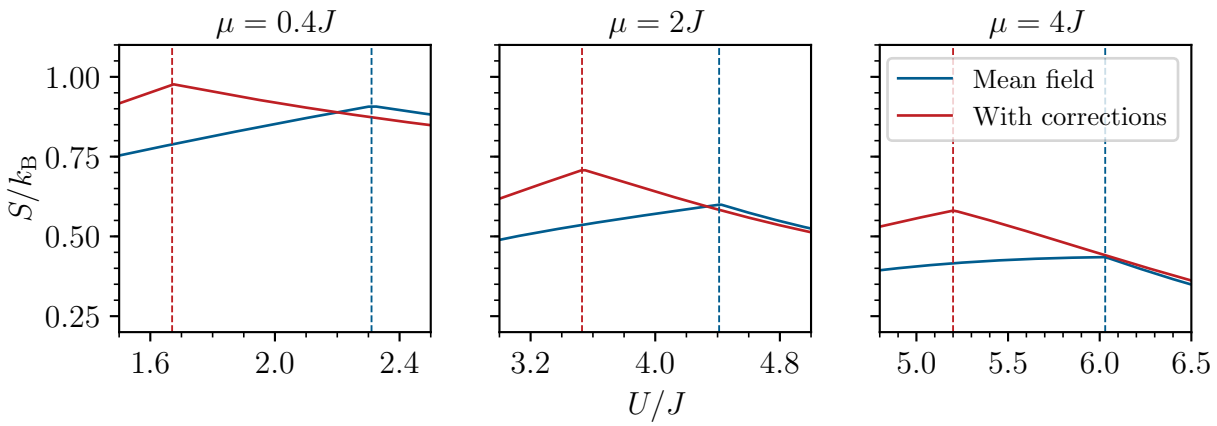

Figure 4.49: Entropy on vertical lines in the fixed-J phase diagram at $T = 1J$ in the vicinity of the phase transition. The phase transition is indicated by a dashed lines.

i.e. section 5.2, where we study lines of constant particle number. As already seen, the lines of constant particle number differ notably from vertical lines in the fixed-J phase diagram. Thus, the behaviour of the entropy will be somewhat different from the one observed here, but it will become more clear. If wanted, the entropy figures in this section can then be understood by combining the arguments from section 5.2 and the particle number figures in this section. We will not further discuss this in this thesis because the constant particle number case is more interesting, as it is more realistic in the experiment.

4.3 Summary

I now want to summarize what we have seen in this chapter. After computing the fixed-temperature phase diagrams, we have investigated the order parameter, the particle number and the entropy on horizontal and vertical lines for both fixed J and fixed U. In particular, we have investigated the influence of the corrections we calculated.
The order parameter generally showed what can be expected from the phase diagrams. It is zero in the normal phase and non-analytically obtains a non-zero value in the superfluid phase, as the particles start condensing into the ground state. Fluctuations generally prevent the particles from condensing. This leads to the order parameter getting decreased by the corrections and the phase boundary getting shifted to higher values of J or smaller values of U by the corrections and higher temperature.
On horizontal lines the particle number shows a very characteristic behaviour. For small temperature it is approximately constant and integer in the normal phases and continously changes between the respective integer values in the superfluid phases in between. For higher temperature the slope in the normal phase increases. Furthermore the regions where the particle number is approximately integer are not generally divided by a superfluid region anymore, as thermal fluctuations prevent the system from getting an order or the particles from condensing, despite the non-integer particle number.

On the vertical lines for fixed U the particle number is approximately constant in the normal phase and then either decreases (increases) in the superfluid phase, when the phase transition occurs on the left (right) side of the lobe, because these transitions are driven by extra holes (particles) getting added to the system. At the tip the transition is driven by the particles simply overcoming the repulsive interactions and they thus condense into a superfluid at approximately constant particle number.
On the vertical lines fixed J we only observed the particle number increasing on the superfluid side of the transition. This is due to the different lobe shape in the phase diagram, and will become more clear in section 5.2, where we will see the constant particle number lines in the fixed-J phase diagram.
The quantum fluctuations mostly do not have a big influence on the particle number. They affect the number of condensed particles more than the total number of particles. The most notable differences between mean-field and corrected results for the particle number occur at the phase transition, where fluctuations are particularly prominent.
The entropy on the horizontal lines is small in the regions where the particle number is approximately integer and shows peaks where the particle number is non-integer. We explained the behaviour in between the peaks with the relatively large energy gap in case of integer particle number, which can only occasionally be overcome by thermal excitation. The peaks could be explained by the different number of degenerate states that a non-integer amount of particles delocalizing over differently many lattice sites, can realize for different particle numbers. The quantum fluctuations generally increase the number of possible states and thus also the entropy.
On the vertical lines for fixed U the entropy in mean-field approximation is generally constant in the normal phase and then falls to zero in the superfluid phase due to the particles condensing into the ground state, where they do not contribute to the entropy. The corrections change this behaviour in two different ways. For some parameters the entropy shows a positive slope in the normal phase with a maximum at the phase transition. For other parameters the entropy already has a negative slope in the normal phase. In both cases however, the entropy then falls to zero in the superfluid phase also when including the corrections. We have postponed the physical discussion of these two behaviours to the next chapter.
On the vertical lines for fixed J we also observed different behaviours for different parameter choices. The entropy generally increases with increasing U in the superfluid phase. For some parameters it then shows a maximum at the phase transition, for other parameters it does not. For all parameter choices however the entropy admits a plateau for large U. Also here we postponed the physical discussion to the next chapter because the behaviour of the entropy on lines of fixed particle number will become more clear. Furthermore, the constant particle number case is more realistic and thus more interesting.
We, have however not always observed physical behaviour. In some regions of parameter space we have observed unphysical behaviour due to degeneracies. This can manifest itself in plateaus of the order parameter, huge peaks in the particle number or dips in the entropy. The problems occur in between the lobes and for large J/U or small U/J. Further, they get worse for small temperature. We have expected and explained these problems in section 3.3.
In the following chapter we will now investigate lines of constant particle number,

which will make our results more realistic. Furthermore, as already mentioned, the behaviour of the entropy will be more clear and will be physically discussed.

Chapter 5

Lines of Fixed Particle Number

In the preceding chapter we have analyzed the order parameter, the particle number and the entropy on different vertical and horizontal lines through the fixed-J as well as the fixed-U phase diagram for different fixed temperatures. Through this, we have now gained some intuition for the behaviour of these thermodynamic quantities in different regions of the phase diagrams. We also saw the first consequences of the corrections calculated. On the lines we either varied the chemical potential μ for fixed J and fixed U or we fixed μ and varied J or U. In the experiment however the chemical potential is not directly accessible. There it is more common to load some number of particles into the optical lattice and then keep this particle number fixed. To make predictions for those experiments we thus need not consider vertical or horizontal lines in the phase diagram but rather lines on which the particle number is constant, which we will do in this chapter. Note that, as in the previous chapter, we will measure all extensive quantities per site.

In order to consider constant particle number lines we need to invert the function $n = n(J/U, T/U, \mu/U)$, as in equation (4.3) or (4.6), to get a function $\mu/U = \mu/U(J/U, T/U, n)$ in the case when U is fixed, the fixed-J case is of course analogous. Because we have seen that $n(\mu)$ increases monotonically for U, J and T fixed, where we do not make the division by U explicit for brevity, we can implement a bisection type algorithm to achieve this: first we choose a starting interval for μ which contains the correct value, i.e. the value μ_0 such that $n(\mu_0) = n_0$, where n_0 is the fixed particle number of interest. In our case the interval $[-0.1U, 1.1U]$ was sufficient for this, i.e. it always contained μ_0. We then check if $n(\mu_{\text{mid}})$ is greater or less than the wanted $n = n_0$, where μ_{mid} is the middle point of the μ interval. We then change either the left or the right limit of the interval to be μ_{mid} such that the correct $\mu = \mu_0$ is still in the interval. We repeat this procedure iteratively until the interval is smaller than some threshold, which we chose to be $\Delta\mu_{\text{goal}} = 0.05U$. On this small interval the function $n(\mu)$ is then approximately linear and can easily be interpolated. From the interpolation we can then deduce the correct value of $\mu = \mu_0$. To make sure that our algorithm converges correctly we then always check that $n(\mu_0) = n_0$. Due to degeneracy effects this does not always have to be the case. In conclusion, this algorithm gives us a function $\mu/U = \mu/U(J/U, T/U, n)$, as desired.

As before we next analyze thermodynamic quantities but now on lines of constant particle number. Note that we could now analyze the chemical potential as one of these quantities but we will not do so, as it is not a quantity that is really of interest. We will thus focus only on the order parameter and the entropy. For

the fixed particle numbers we chose $n = 1$, i.e. integer filling as well as $n = 1.1$ and $n = 0.9$, i.e. integer filling with some particles/holes added, and $n = 1.3$ and $n = 0.7$. We are not able to deviate much more from integer filling as it will get the lines closer and eventually into to the problematic regions in the phase diagrams, i.e. our calculations would become less reliable. As in the previous chapter we will investigate the cases for fixed U and fixed J separately.

5.1 Fixed On-Site Interaction Strength

As before we start with lines in the fixed-U phase diagram. Figures 5.1-5.3 show the lines for fixed particle number in the three fixed-temperature phase diagrams. Note that the $n = 1$ line for low temperature, i.e. in figure 5.1, stops at the phase boundary. This is because, as we saw before, for low temperature the slope of the $n(\mu)$ function is small in the lobe and at $T = 0.01U$ the slope is actually too small to properly invert the function as the slope is of the same order as the numerical errors that we make. However, because the order parameter is zero in the normal phase no matter where exactly in the lobe, we can still show it with axis limits not limited to the phase boundary. Furthermore the entropy for $T = 0.01U$ is of the order of the machine precision on the $n = 1$ line, which is why we can not analyze it at all and will leave it out. The fact that we have no unique $n = 1$ line in the lobe for $T = 0.01U$ hence does not really affect our following analysis.

In figure 5.1 you can further see, that for low temperature the non-integer particle number lines run along the boundary of the lobe, running closer to it for n closer to the corresponding integer, and only enter the normal phase for a small value of J. In the case $T = 0$, they would not enter the Mott phase at all and land on the μ/U-axis at integer values. The fact that there are now phase transitions at constant non-integer particle number which did not exist for $T = 0$ shows that these transitions are ordinary phase transition in contrast to being quantum phase transitions.

For higher temperature, as the phase boundary gets shifted to higher values of J and the lobes deform, the non-integer particle number lines enter the normal phase for higher values of J and then become approximately vertical. Thus, in the normal phase, the vertical lines were a good approximation of constant particle lines. Further, the distance between these vertical constant particle number lines gets smaller for higher temperature. This simply reflects the fact that the plateaus of constant integer particle number get smaller for higher temperature, which we have already seen before.

The integer particle number line goes through the tip of the lobe. As already mentioned before, the phase transition occurring here is genuinely different from the transition occurring at any other point of the phase boundary, which is also reflected in the respective critical exponents or their universality classes [33]. An interesting thing to observe, is that the lines abruptly change their direction after entering their respective normal phases. After this change these lines also become approximately vertical, especially the mean-field lines. Through this abrupt change at the respective phase boundaries, there is a discrepancy between the constant integer particle number lines in mean-field approximation and the corrected ones, in between the two phase boundaries. In the normal phase however, the two lines then again converge towards each other.

In the superfluid phase, the integer particle number lines in mean-field approxima-

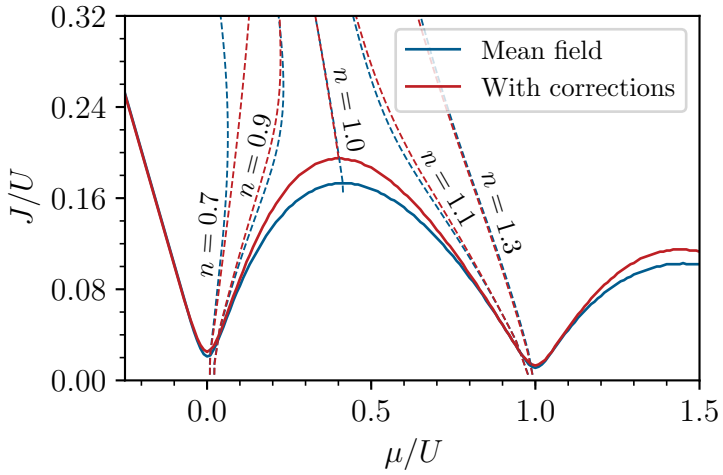

Figure 5.1: Fixed particle number lines in the fixed-U phase diagram for $T = 0.01U$.

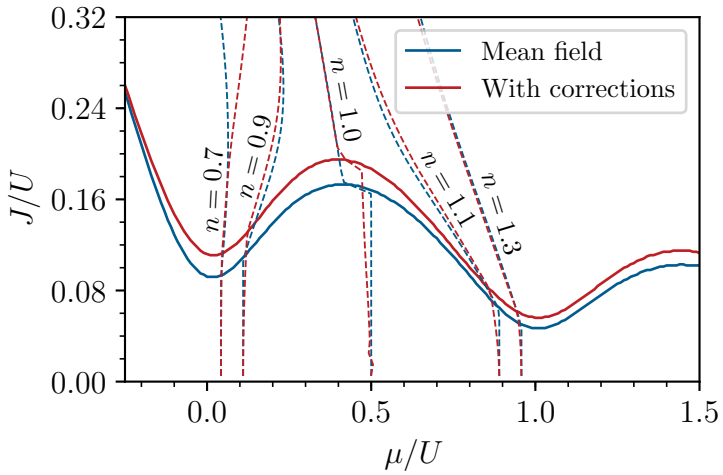

Figure 5.2: Fixed particle number lines in the fixed-U phase diagram for $T = 0.05U$.

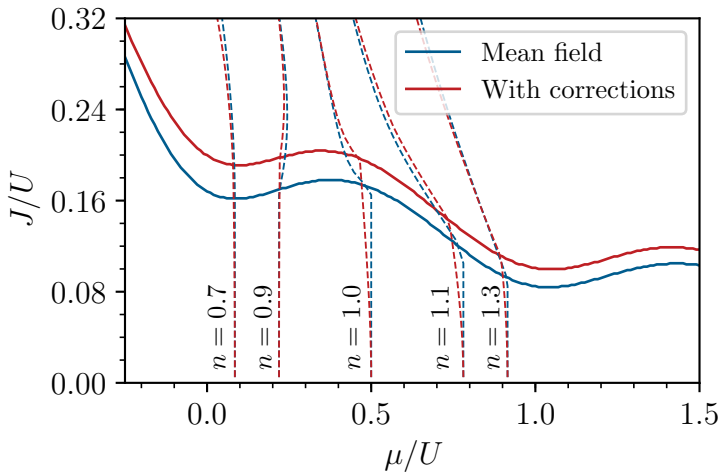

Figure 5.3: Fixed particle number lines in the fixed-U phase diagram for $T = 0.1U$.

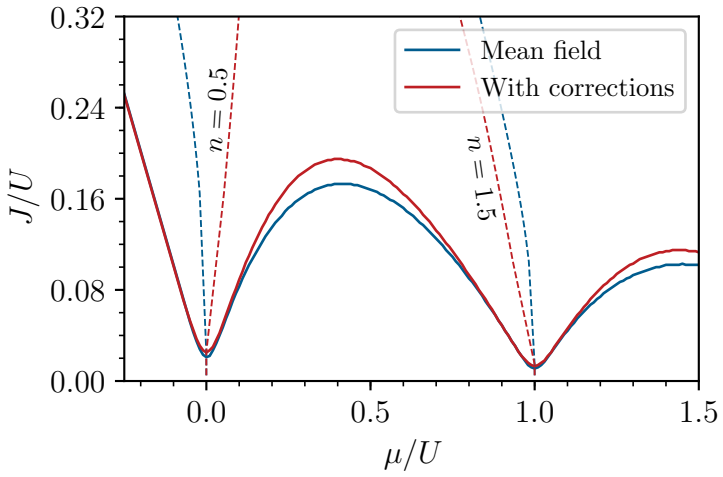

Figure 5.4: Fixed $n = 0.5$ and $n = 1.5$ lines in the fixed-U phase diagram for $T = 0.01U$.

tion and the ones with the corrections do not really differ. The non-integer particle lines on the other hand show some discrepancy in the superfluid phase but are essentially the same in the normal phase. The largest discrepancy can be seen for the $n = 0.7$ lines for $T = 0.01U$ and $T = 0.05U$ in the deep superfluid phase, see figures 5.1 and 5.2. This might be due to degeneracies, which is plausible as it occurs for large J, small T and μ/U close to an integer value.
Another observation to make here is that for large J, i.e. in the deep superfluid phase, the different constant particle number lines look like they would asymptotically run towards parallel linear lines. These have a negative slope in the μ/U–J/U diagram, i.e. for larger J it needs a lower chemical potential μ for the system to have the same number of particles.

Figure 5.4 shows the lines of constant particle number $n = 0.5$ and $n = 1.5$ in the $T = 0.01U$ phase diagram. As we already expected these lines start exactly between the lobes on the μ/U-axis and stay in the problematic zone of the phase diagram. The fact that the corrected lines differ substantially from the respective mean-field lines is also a sign that the degeneracy problems are particularly severe on these lines. This figure thus justifies that we restrict our following discussion to constant particle number lines with n closer to an integer value.
We will now study both the order parameter and the entropy on these lines. In the following we will distinguish between non-integer and integer particle number lines, i.e. we will investigate the four non-integer particle number lines for all temperatures and then look at the three respective integer particle number lines for the three different temperatures afterwards. We will do this in this way because the system is qualitatively different for integer and non-integer filling. As before we will now start our analysis with the order parameter.

Figures 5.5-5.7 show an overview of our results for the order parameter on the non-integer particle number lines and figure 5.8 shows them on the integer particle number ones. As before we see the typical behaviour of an order parameter at a second-order phase transition. Also, as before, the corrections generally make the order parameter smaller and delay the transition to larger values of J. Furthermore we again observe the plateaus and other unphysical behaviours, which are probably

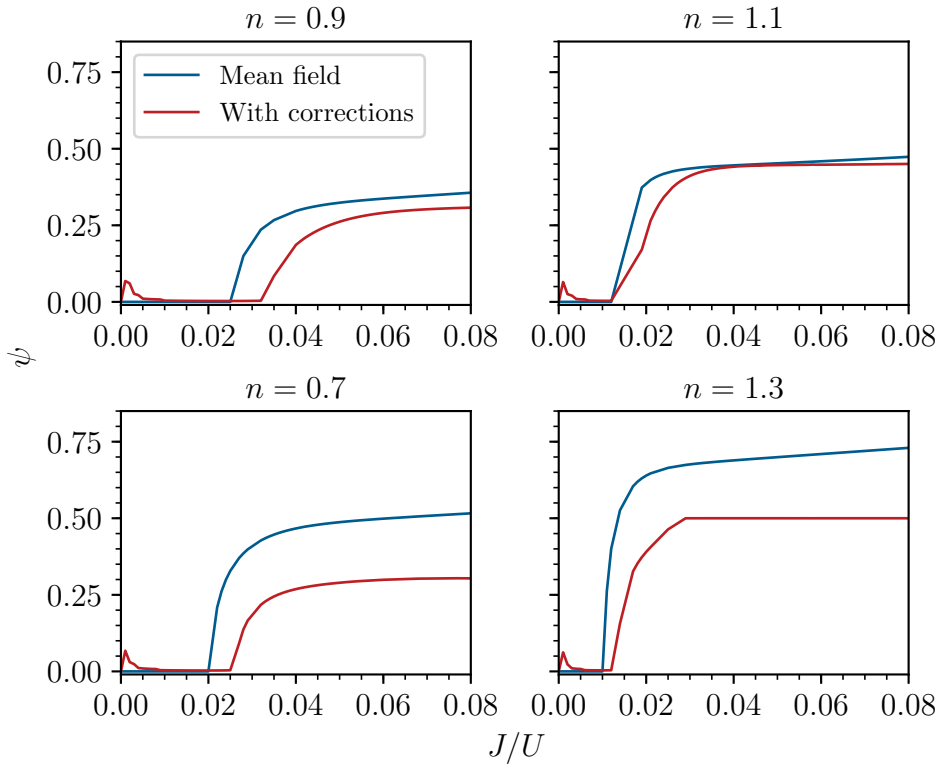

Figure 5.5: Order parameter on constant non-integer particle number lines in the fixed-U phase diagram for $T = 0.01U$.

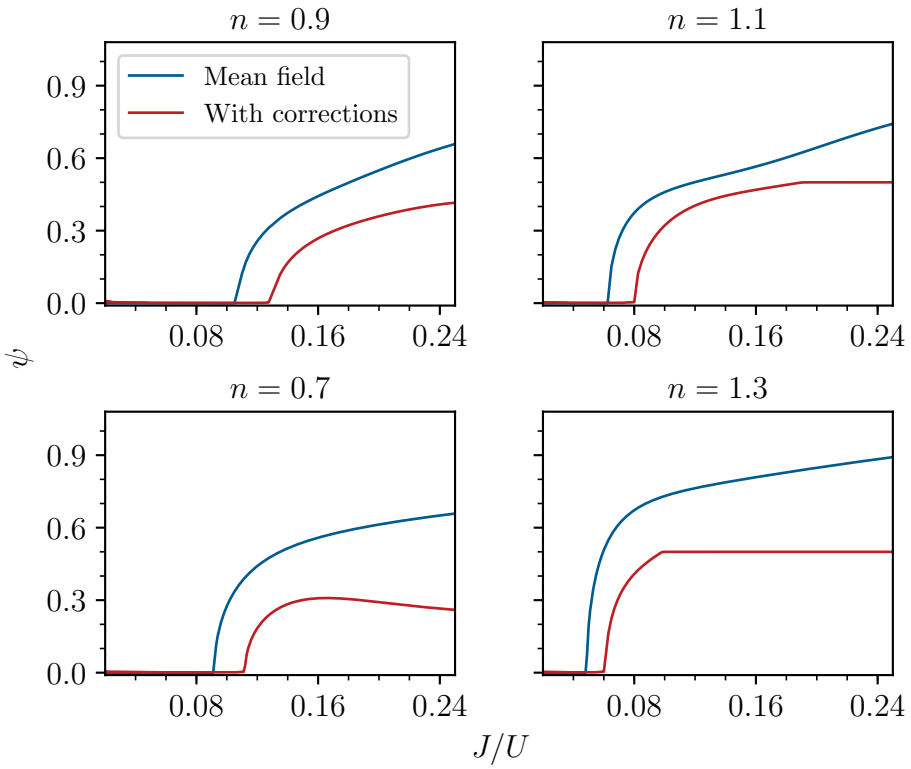

Figure 5.6: Order parameter on constant non-integer particle number lines in the fixed-U phase diagram for $T = 0.05U$.

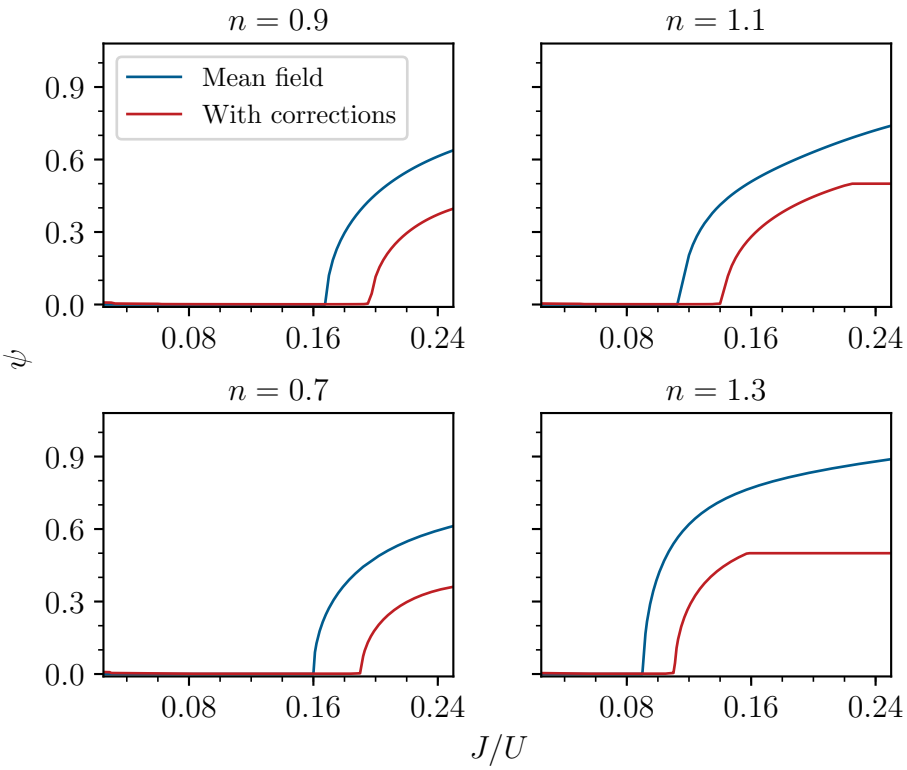

Figure 5.7: Order parameter on constant non-integer particle number lines in the fixed-U phase diagram for $T = 0.1U$.

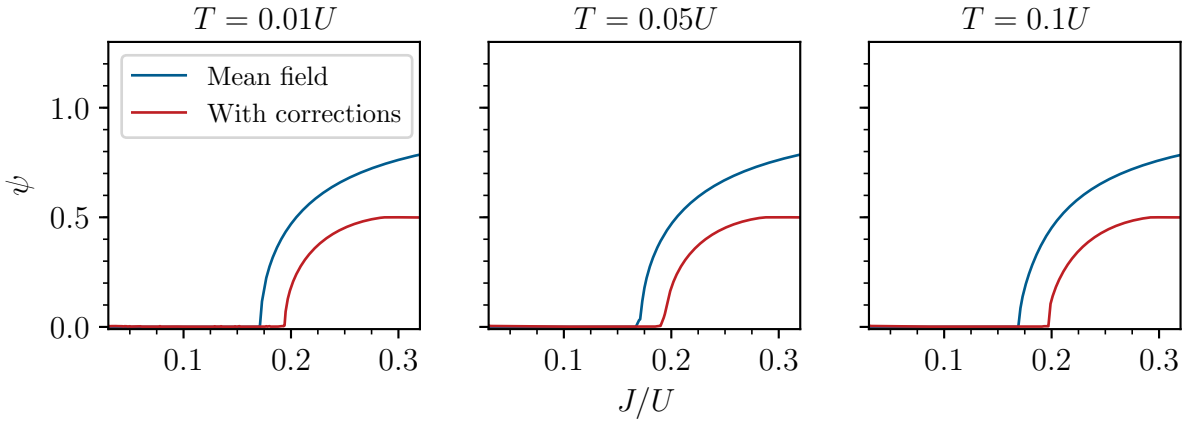

Figure 5.8: Order parameter on the constant $n = 1$ line in the fixed-U phase diagram for different temperatures.

due to degeneracy effects. We can make all of these observations both in the non-integer as well as in the integer particle number figures.
Another obvious mistake we can observe are the peaks in the corrected results for low J in figure 5.5. We already encountered this behaviour in section 4.1 and argued that this is due to numerical mistakes stemming from the fact that $\Phi(\psi)$ is approximately constant for small J. In the previous figures we simply adjusted the limits, i.e. started with a larger value of J to circumvent these problems. In figure 5.5 although, as the phase transition occurs for a particularly small value of J, we also included this unphysical region. In the other figures we again adjusted the lower limit in order to exclude the regions where this occurs.

As before we next analyze the entropy. Figures 5.9-5.11 show an overview of our results for non-integer particle number. Figure 5.12 shows our results for integer particle number. We can see the same two behaviours as in section 4.1 on the vertical lines, although now it is clear that the entropy decreases in the normal phase for non-integer particle number and increases for integer particle number. We will now physically discuss the two cases starting with the former.
First, observe that the entropy in the normal phase is of the same order of magnitude for the two corresponding constant particle number lines i.e. for $n = 0.7$ and $n = 1.3$ as well as for $n = 0.9$ and $n = 1.1$, for all temperatures, where it is larger on the lines where the particle number deviates more from an integer value. They are of the same order of magnitude because it does not make a big difference for the number of possible states whether there are additional holes or particles added to an integer filling. Further the orders of magnitude of the two pairs of lines differ due to the fact that for more deviation from integer filling there are more states possible. For example two particles added to an integer filling can realize more states than one particle added to an integer filling can. The fact that this order of magnitude of the entropy changes only slightly with the temperature, reflects the fact that thermal activation does not really enable any new states. This makes sense because there is a large degeneracy for the non-integer particle states, as the particles can be distributed differently over the lattice sites. Due to this the entropy mostly comes from these degenerate states and the impact of thermal activation is not that large.
In the superfluid phase the entropy is generally larger when including the corrections, which is probably, at least partly, due to the fact that the transition and with this the strong decrease in entropy, occurs for higher J. For large J the difference between mean-field and corrected results decreases, although for $T = 0.1U$, $n = 1.3$, i.e. in figure 5.11, you can still observe a notable difference between the two. At the same temperature for $n = 0.7$ you can see that the corrected results actually cross the mean-field ones and tend to zero more rapidly. This is unphysical and probably again due to degeneracy effects as it occurs for rather big deviation from an integer particle number and large J.
We now turn to the negative slope in the normal phase. For higher temperature, as the J-interval where the system is in the normal phase increases, this slope becomes less negative. Also less deviation from integer filling makes the slope less negative, as can for example be seen in figure 5.11. We can understand the negative slope as follows. On the $n = 1.1$ lines for example, there are some particles in the system additionally to an integer filling. These will somewhat delocalize throughout the lattice depending on the fraction J/U. For a higher J the amplitude of the particles passing each other increases and with this also the "delocalization length". Then

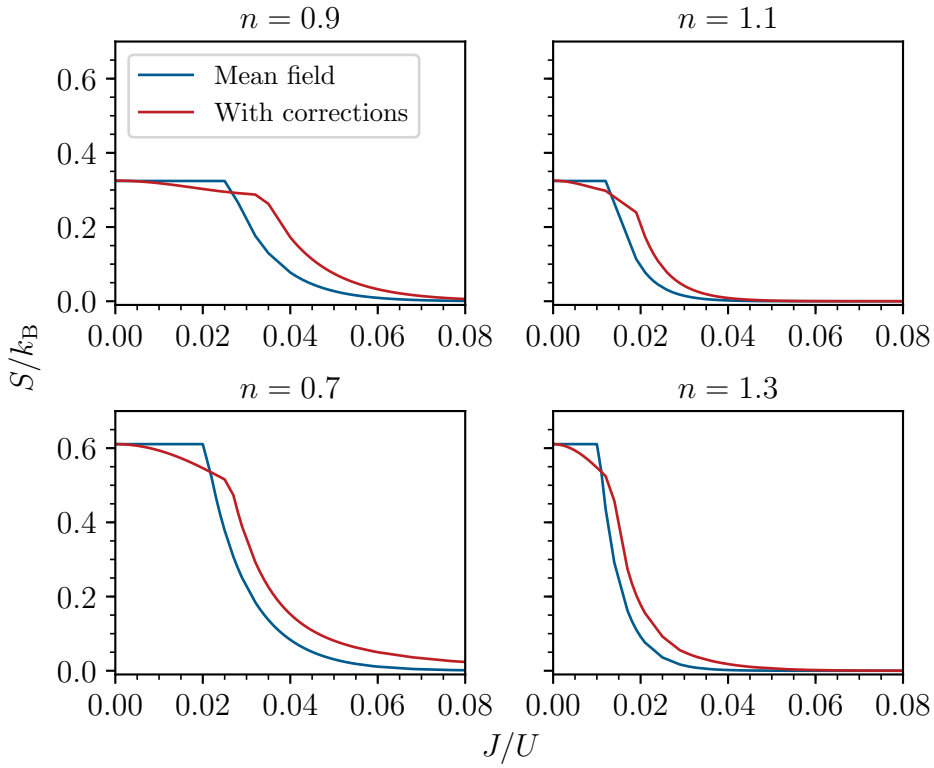

Figure 5.9: Entropy on constant non-integer particle number lines in the fixed-U phase diagram for $T = 0.01U$.

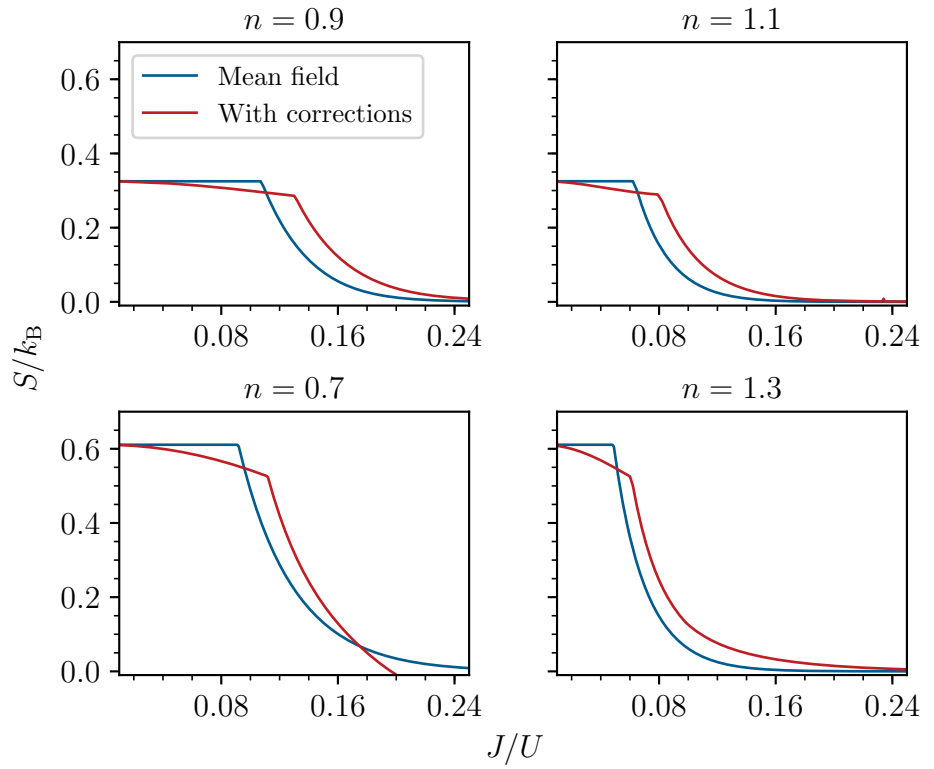

Figure 5.10: Entropy on constant non-integer particle number lines in the fixed-U phase diagram for $T = 0.05U$.

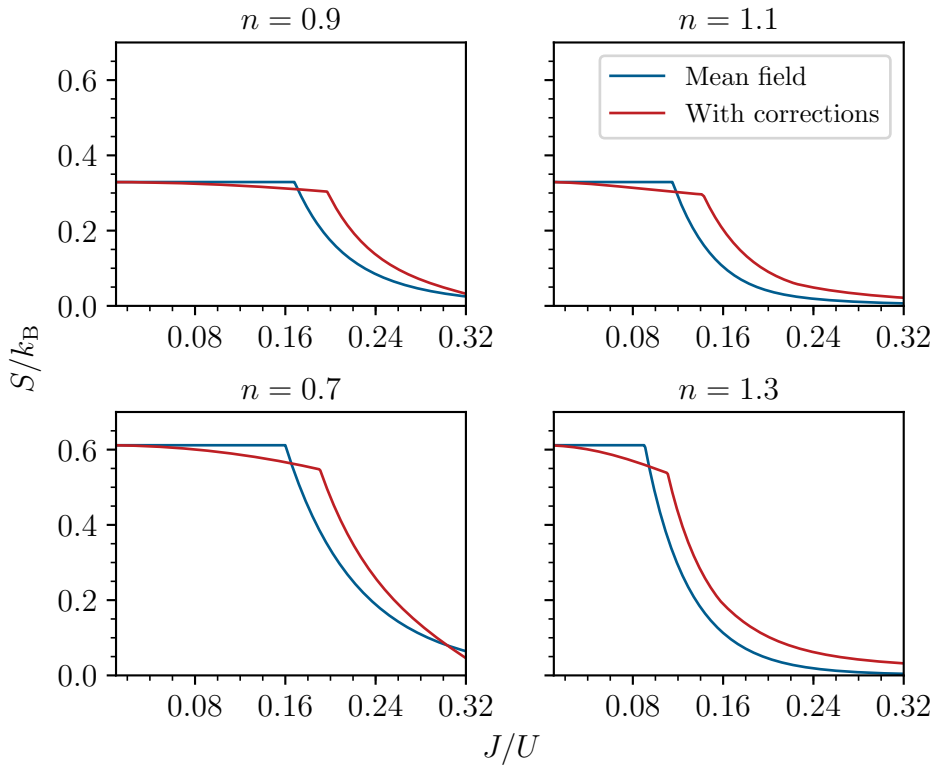

Figure 5.11: Entropy on constant non-integer particle number lines in the fixed-U phase diagram for $T = 0.1U$.

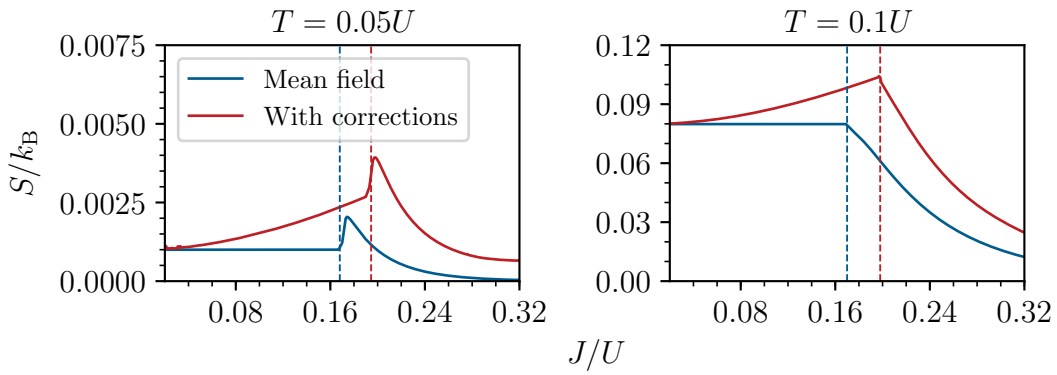

Figure 5.12: Entropy on the constant $n = 1$ line in the fixed-U phase diagram with phase transitions indicated by dashed lines.

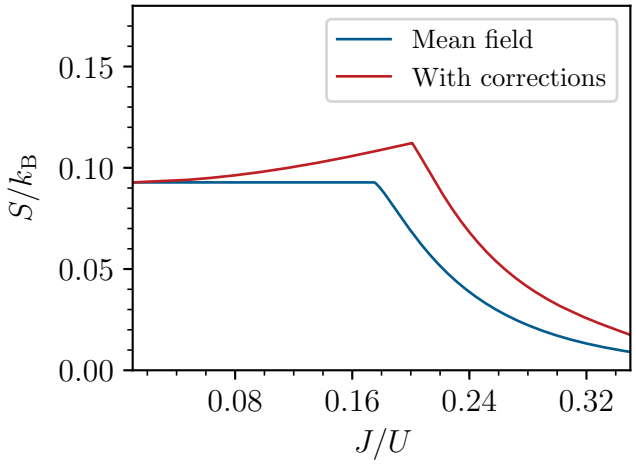

Figure 5.13: Entropy on the constant $n = 0.99$ line in the fixed-U phase diagram at $T = 0.1U$. The entropy shows the integer particle number behaviour also for particle numbers close to an integer value.

also the number of possible states gets reduced. For example a particle spread out over the entire lattice can be described by only one state, while a particle which is fully localized on a lattice site can have N_S states, one for each lattice site. This thus explains the observed negative slope.
Without quantum fluctuations the particles would not be able to pass each other at all, as they actually do not have enough energy to do so, until J reaches a critical value. This explains that the effect can only be observed when including the corrections, i.e. quantum fluctuations.

If the particle number gets closer to integer filling this delocalization effect decreases as the system approaches the integer filling state where the particles can not delocalize at all for low J and T. Thus the slope in the normal phase is less negative for particle numbers closer to an integer. When the particle number gets close enough to an integer value we can actually observe the integer value behaviour of the entropy, see figure 5.13. Thus, the positive slope can not only be observed in the somewhat artificial limit an exact integer particle number per site, but also for sufficiently small deviations from integer particle number.
For lower temperature, where the normal phase is shorter, this process of increasing delocalization has to take place on a shorter J-interval, which gives rise to a more negative slope.
Now, we will physically interpret the observed positive slope of the entropy in the normal phase for integer particle number, see figure 5.12. For low temperature the system is simply in the approximate Mott state. There is one particle on each site and the particles can only rarely cross the excitation gap and hop out of this state due to thermal activation. Because the integer filling state is not degenerate, this results in the entropy being small as the only additional states, and with this the only entropy, come these few additional states. For higher temperature the particles can more often hop out of the integer filling state due to thermal activation, increasing the entropy.
When increasing J, the entropy now increases because, due to the higher energy gain from hopping, the particles will hop out of the Mott-like state more often producing

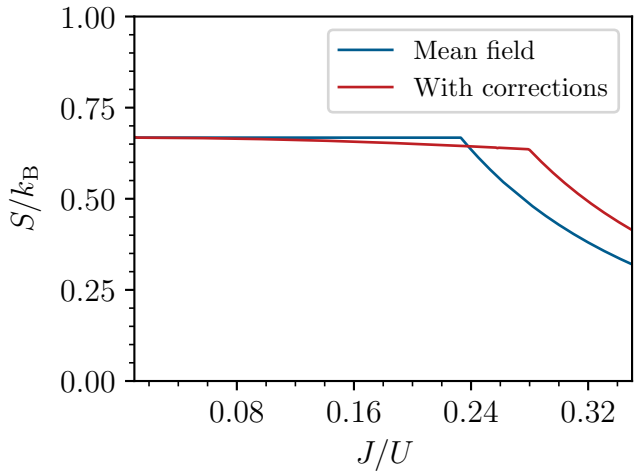

Figure 5.14: Entropy on the constant $n = 1$ line in the fixed-U phase diagram for $T = 0.25U$. The maximum of the corrected entropy gets suppressed for high temperature.

more entropy. The entropy increases for increasing J until a critical value is reached where the particles gain enough energy though hopping so that they can simply all hop out of the integer filling. Many of them will fully delocalize, i.e. condense into the ground state, producing a superfluid state. Then the entropy will fall off, as only the remaining excited particles still contribute to the entropy, like we already saw before. The fact that this positive slope only occurs when including the corrections indicates that the additional states that get available through increasing J are only available due to quantum fluctuations.
Further you can see that for $T = 0.05U$ in figure 5.12, there is a peak occurring both in mean-field approximation and in the corrected results, in addition to the maximum in the corrected results, which we discussed before. From the figure it is clear that the phase transition actually occurs before the peak reaches its maximum. From this peak we can infer that for this temperature right after the phase transition, i.e. for J slightly larger than needed for the particles to delocalize over the full lattice, suddenly some additional states get available, before the particles start condensing into the ground state, which is quite interesting.
Figure 5.14 shows the entropy for integer particle number and a higher temperature than previously investigated. You can clearly see, that the maximum at the phase transition gets suppressed by the temperature. This is because at a high temperature, the particles can often hop out of the Mott-like state and delocalize despite the integer particle number. Thus the system qualitatively behaves like a non-integer particle number system explaining the similar behaviour of the entropy.

5.2 Fixed Hopping Amplitude

After analyzing the fixed-U case we will now again turn to the fixed-J one. Figures 5.15-5.17 show the same constant particle number lines as before but in the fixed-J phase diagram. As in the fixed-U case we can not invert $n(\mu)$ in the lobe for low temperature, i.e. we can not find a unique $n = 1$ line. Thus, as before, the $n = 1$ line ends at the phase boundary for $T = 0.1J$. Further you can see that we do

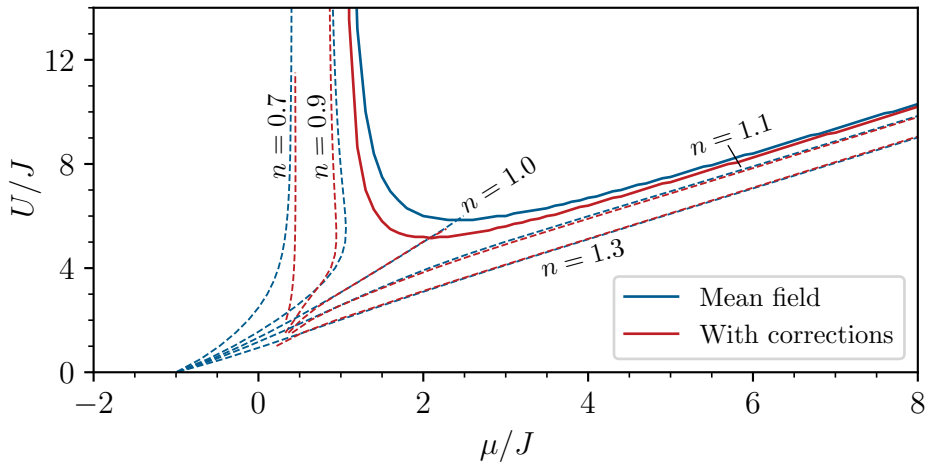

Figure 5.15: Fixed particle number lines in the fixed-J phase diagram for $T = 0.1J$.

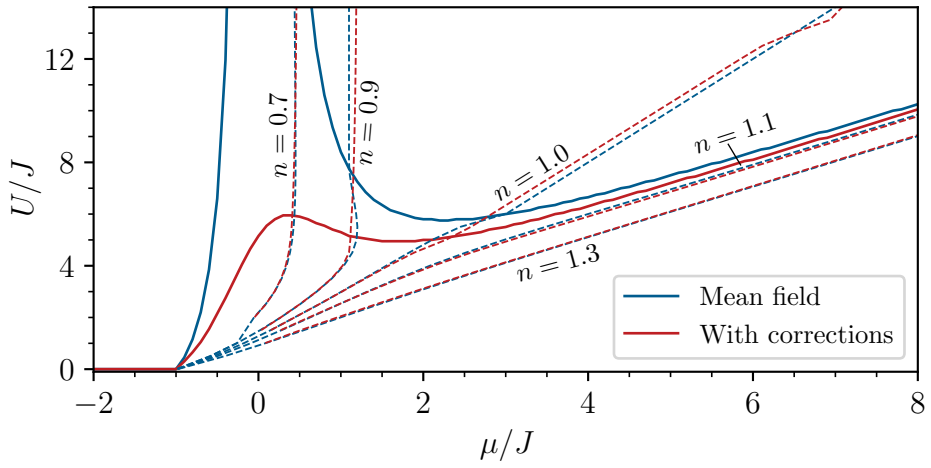

Figure 5.16: Fixed particle number lines in the fixed-J phase diagram for $T = 0.5J$.

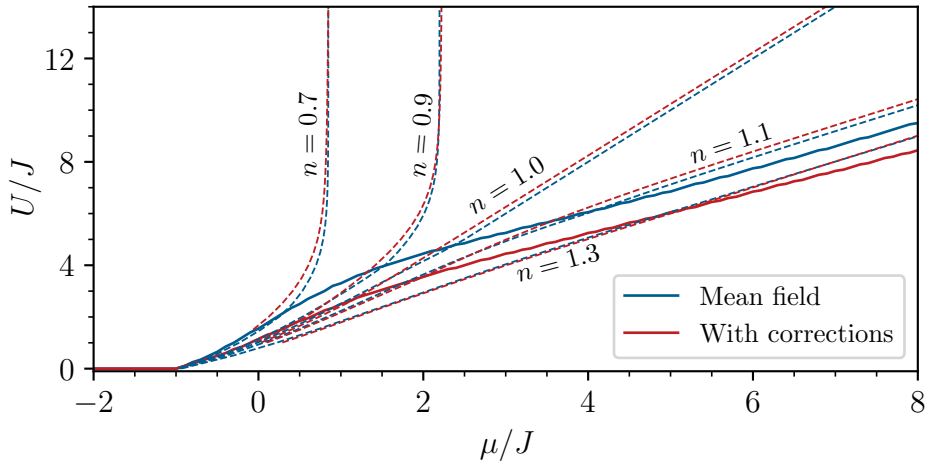

Figure 5.17: Fixed particle number lines in the fixed-J phase diagram for $T = 1J$.

not show the corrected lines for low U which is due to the fact that we could not invert $n(\mu)$ here because the errors due to degeneracies became too large. For the same reason also the corrected $n = 0.7$ line in the $T = 0.1J$ phase diagram ends at $U \approx 11J$. You can further spot, that the corrected $n = 1$ line in the $T = 0.5J$ phase diagram deviates from a straight line and crosses the mean-field one at $U \approx 13J$, which is however probably just a numerical mistake.
We see that in contrast to the fixed-U case the non-integer particle number lines never enter the normal phase for $T = 0.1J$. For $T = 0.5J$ the $n = 0.9$ line then enters the normal phase due to the lobe opening up but the $n = 1.1$ and $n = 1.3$ ones still only run along the boundary and never enter the normal phase in the investigated parameter regions. The $n = 0.7$ line is particularly interesting here as it enters the normal phase only when including the corrections due to the qualitative difference in the phase diagrams which we already noticed before.
Another thing to notice here, is that the lines in mean-field approximation and when including the corrections do not differ too much but sometimes the respective lines cross each other between the respective phase boundaries, see for example the $n = 0.9$ lines for $T = 0.5J$. For low U you can see that the mean-field lines converge towards one point which ends up to be $\mu \approx -J$ for all investigated temperatures for $U = 0$.
As before we will now analyze the order parameter and the entropy on these lines starting with the former.

Figures 5.18-5.20 show an overview of our results for the order parameter on the constant non-integer particle number lines and figure 5.21 shows them on the integer particle number line. The main observations are the same as before. The corrected order parameter is generally smaller than the one in mean-field approximation and you can see that the quantum fluctuations shift the phase transition to smaller values of U, i.e. they destroy the long-range order for a lower value of U. Also we can again observe unphysical plateaus in the superfluid phase.
Furthermore, we can see that the system never enters the normal phase on the lines already mentioned above. The order parameter generally has a negative slope on these lines in mean-field approximation, which makes sense as we expect the repulsive interaction to prevent particles from condensing. There are however lines where the order parameter is approximately constant or even has a positive slope when including the corrections which seems unphysical, see for example the $n = 1.3$ and $n = 0.7$ lines in figure 5.18. As we generally observe this for the larger deviations from integer filling and low temperature this could also be the effect of degeneracies. The $n = 0.7$ and $n = 0.9$ lines for $T = 1J$ enter the normal phase already for a very small value of U. As explained above, we can not invert $n(\mu)$ for small values of U due to degeneracies, which is why the phase transition in the corrected results in figure 5.20 can only barely be seen for the $n = 0.9$ line and can not be seen at all for the $n = 0.7$ line.

Now we again investigate the entropy. Figures 5.22 and 5.23 show the entropy on the fixed non-integer particle number lines for the higher two temperatures. For $T = 0.1J$ the entropy was again simply too small, i.e. of order of the machine precision which is why we do not analyze it here.
For the lower temperature, $T = 0.5J$, the entropy shows two different behaviours. First the entropy decreases with increasing U and then, for larger U, starts increasing again. In the $n = 1.1$ and $n = 1.3$ figures the entropy then keeps this positive

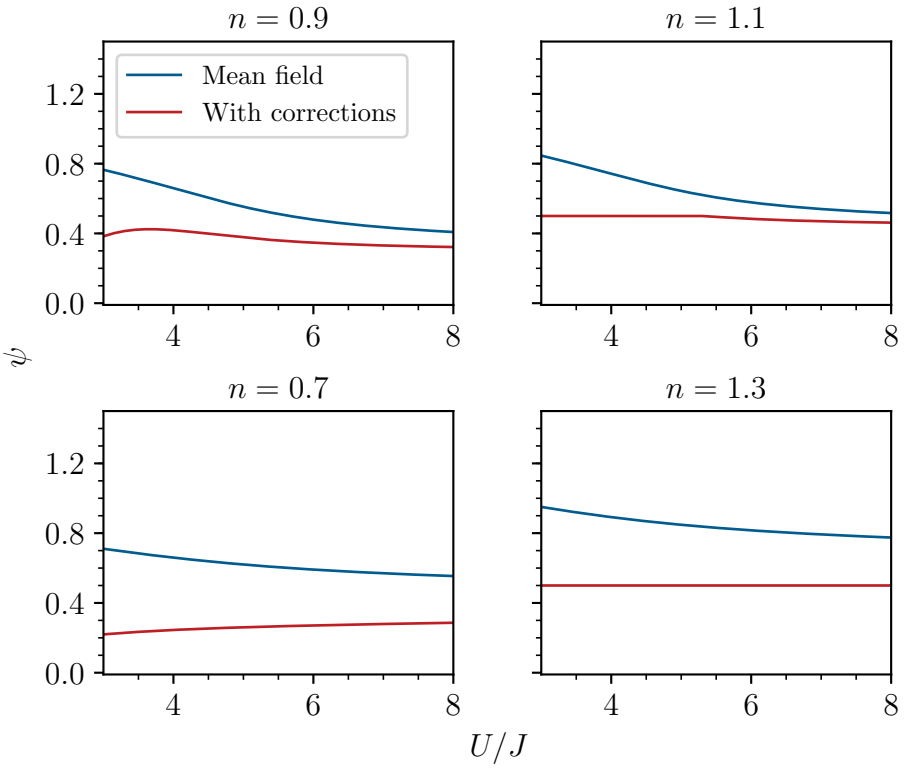

Figure 5.18: Order parameter on constant non-integer particle number lines in the fixed-J phase diagram for $T = 0.1J$.

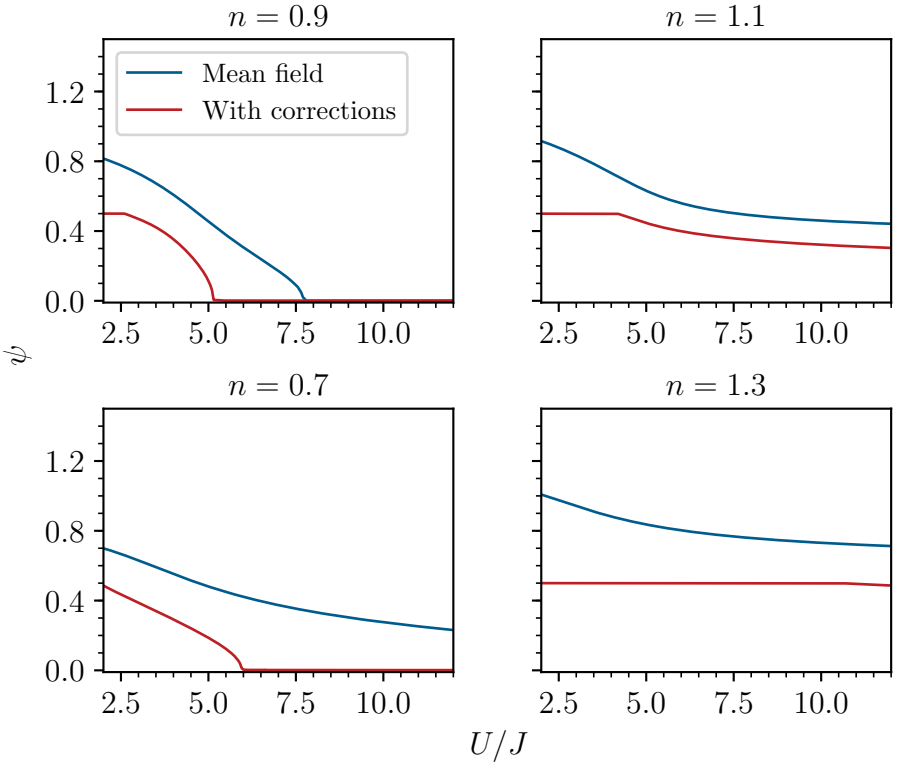

Figure 5.19: Order parameter on constant non-integer particle number lines in the fixed-J phase diagram for $T = 0.5J$.

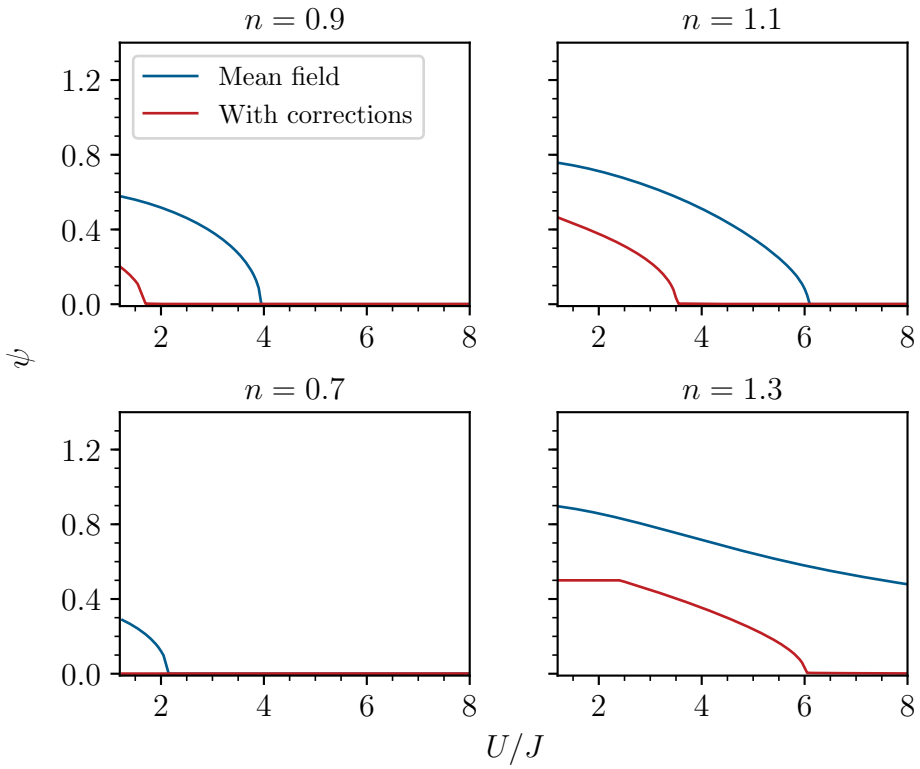

Figure 5.20: Order parameter on constant non-integer particle number lines in the fixed-J phase diagram for $T = 1J$.

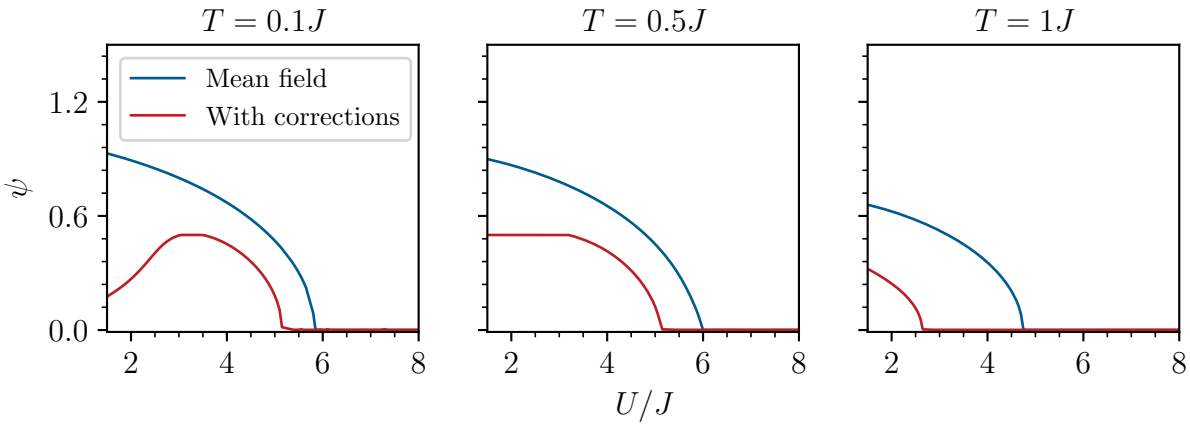

Figure 5.21: Order parameter on the constant $n = 1$ particle number line in the fixed-J phase diagram for different temperatures.

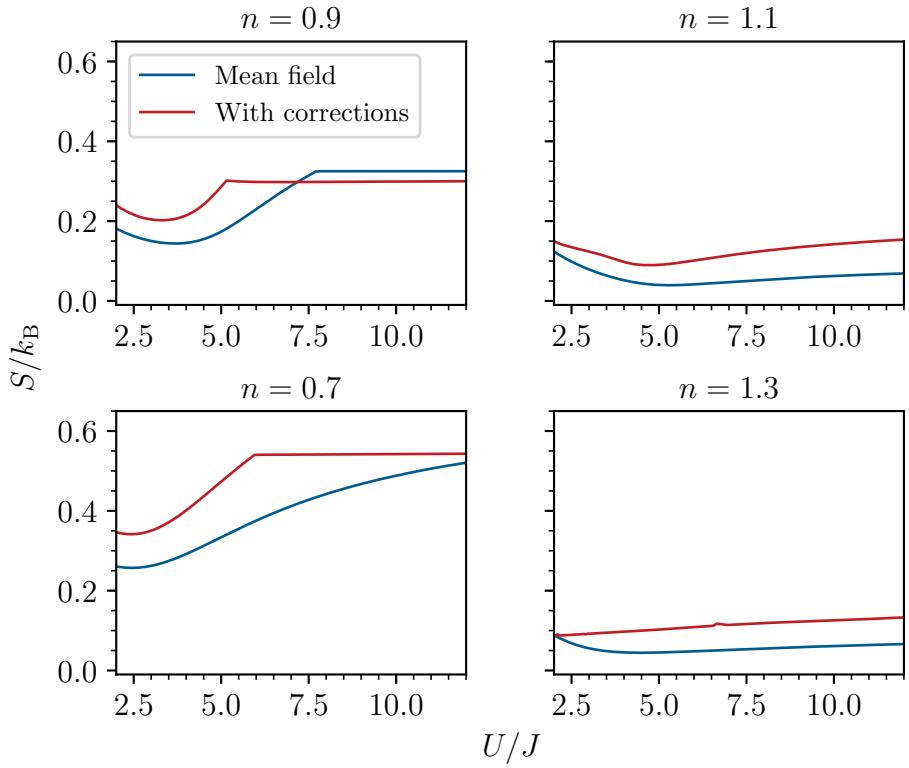

Figure 5.22: Entropy on constant non-integer particle number lines in the fixed-J phase diagram for $T = 0.5J$.

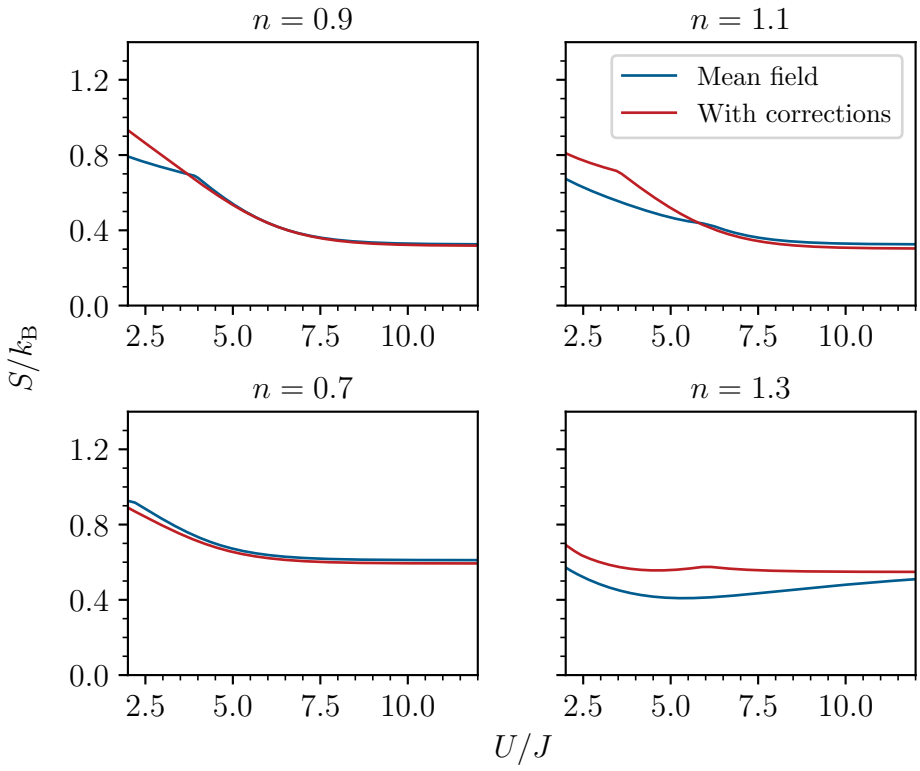

Figure 5.23: Entropy on constant non-integer particle number lines in the fixed-J phase diagram for $T = 1J$.

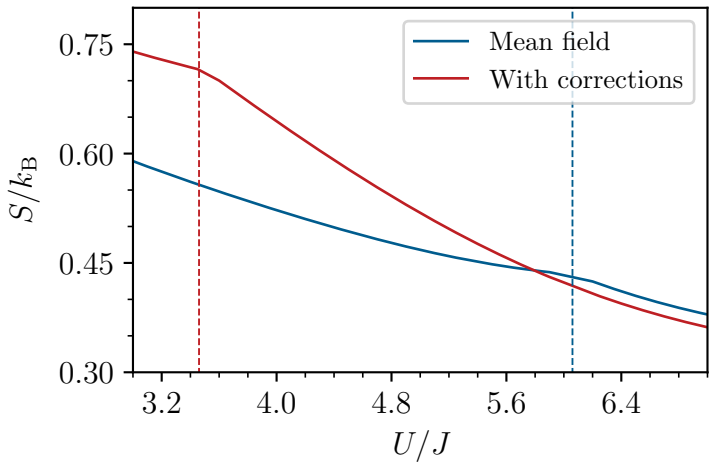

Figure 5.24: Entropy in the vicinity of the phase transition on the $n = 1.1$ line in the fixed-J phase diagram for $T = 1J$. The phase transitions are indicated by dashed lines.

slope whereas in the other two figures, the entropy admits a plateau after a critical value of U, at least when including the corrections. By comparison with the corresponding order parameter figure 5.19 it is clear that the entropy admits a plateau after undergoing a phase transition. The figures where the entropy generally shows a positive slope for large U are those where the system never enters the normal phase. This is also the reason why the entropy in mean-field approximation also does not show a plateau for $n = 0.7$, whereas the corrected entropy does.
For the higher temperature, $T = 1J$, the entropy shows a somewhat different behaviour. For small U the entropy also decreases, it then however does not increase again but it undergoes a phase transition and keeps decreasing after. For large U the entropy then again reaches a non-zero plateau. One exception to this is the $n = 1.3$ line, where the corrected results increase slightly prior to the phase transition and the mean-field results keep increasing also for large U, which is consistent with the observations from the $T = 0.5J$ figure as the mean-field line never enters the normal phase.

The effect of the quantum fluctuations is to increase the entropy in the superfluid phase as they prevent the particles from condensing, and to decrease it in the normal phase where they allow the particles to delocalize more reducing the entropy. This can also be seen in figure 5.24, which gives a close-up view of the entropy in the vicinity of the phase transition for $n = 1.1$ and $T = 1J$.
There are two different effects dictating the behaviour of the entropy. First note that as U is the interaction strength, we would expect the excitation gap to increase with increasing U. We have also exemplarily seen this for the excitation gap of the Mott state in section 2.4. An increase in the excitation gap will then lead to a decrease in the entropy, as there will be less particles able to cross the gap and thus less states possible.
Increasing U has another effect on the entropy. A large repulsive interaction strength of the particles, prevents them from condensing. Thus increasing the interaction strength U reduces the condensate fraction, as we already saw in our analysis of the order parameter. These additional particles that are not in the ground state

anymore, can then again contribute to the entropy, which leads to an increase in the entropy. We will now explain the behaviour of the entropy for non-integer particle number, starting with $T = 0.5J$, using these two competing effects.
For small values of U the system is superfluid and many particles are condensed into the ground state. The entropy comes only from the excited particles. Increasing U now decreases the number of particles in the excited states as well as the number of particles in the condensate, as we just argued. It is clear from figure 5.22 that the former effect dominates for small U leading to a decrease in the entropy. After some point the entropy then starts increasing due to the latter effect. For $n = 1.3$ you can see a positive slope in the corrected results already for small U. As this does not happen in mean-field approximation and can not be explained with the argument from above we conclude that this is unphysical and due to degeneracy effects. Further, on the same line, you can spot a small peak at $U \approx 7J$, which is probably a numerical mistake.
The increase of the energy gap does not have any impact anymore at some point. This is because if effectively no particles can cross it anymore due to thermal activation it of course does not change anything if the gap increases even more. Thus, on the lines that do not enter the normal phase, the entropy simply keeps slightly increasing for higher U, due to the particles slowly being prevented from condensing. It is clear from the order parameter figure 5.19 that the number of condensed particles decreases only slightly explaining the small positive slope in the entropy.
On the lines that enter the normal phase the ground state is not macroscopically occupied anymore. Thus also the second effect mentioned does not have an influence anymore and with the argument from above now both effects do net contribute and thus the entropy does not change with increasing U anymore, explaining the plateau. This plateau is non-zero because, as we argued in the previous section, there are many degenerate many-particle ground states possible for non-integer particle number in the normal phase.
For $T = 1J$, i.e. in figure 5.23, the argumentation is similar to before. For small increasing U the entropy decreases, due to the first effect mentioned. Because the phase transition already occurs for small values of U we can not observe the second effect as there is no condensate anymore before the second effect would dominate the first one. An exception to this is $n = 1.3$ where you can notice a small increases in the corrected entropy before the phase transition is reached. In the mean-field results you can clearly see the second effect as this line never enters the normal phase in the investigated limits. On the other lines you can again observe a plateau after the energy gap becomes too large and also has no effect on the entropy anymore.
Figure 5.25 shows the entropy for integer particle number. Also here the entropy decreases in the superfluid phase, undergoes a phase transition, and then keeps decreasing. After the phase transition, the entropy falls to zero for large U. As before the quantum fluctuations, i.e. the corrections, increase the entropy in the superfluid phase. In contrast to the non-integer particle number figures however the quantum fluctuations also increase the entropy in the normal phase, especially for $T = 0.5J$. This can simply be explained by the quantum fluctuations allowing the particles to hop out of the Mott-like state more often, giving rise to more possible states.
The behaviour of the entropy for integer particle number can be explained with the same two arguments as before. As in the non-integer particle number case, at low U, the entropy starts at some value determined by the excited states occupied by

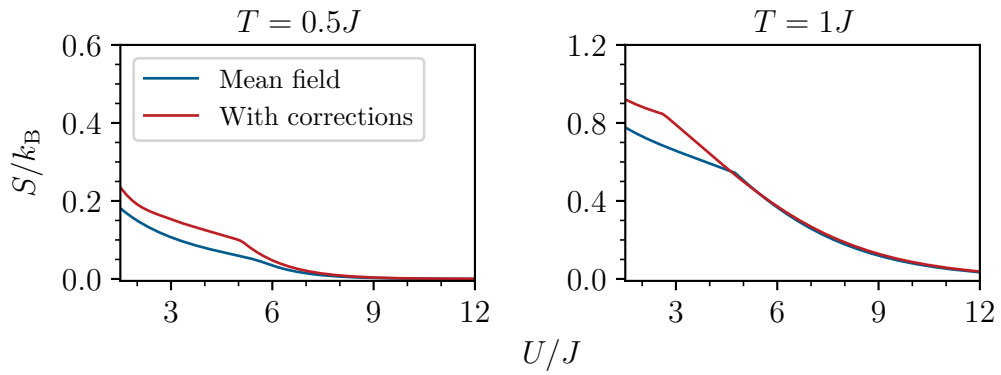

Figure 5.25: Entropy on the constant $n = 1$ line in the fixed-J phase diagram for different temperatures.

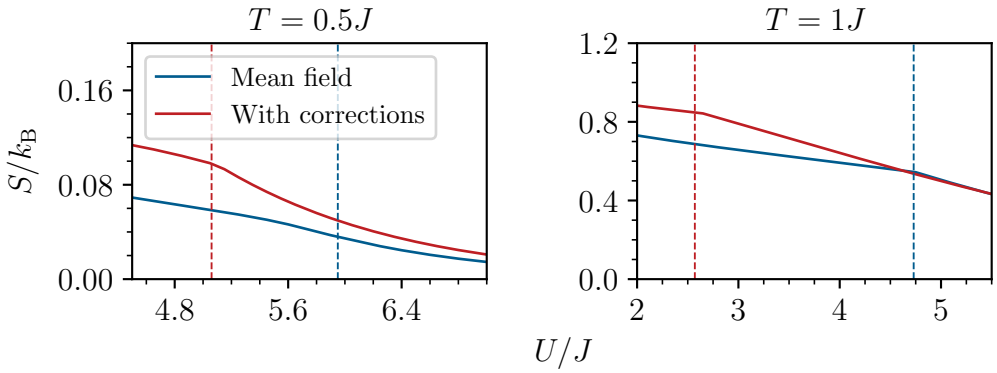

Figure 5.26: Entropy on the constant $n = 1$ line in the fixed-J phase diagram for different temperatures with phase transitions indicated by dashed lines.

the particles that are not condensed, and the decreases due to an increasing energy gap. The second effect can again not be observed as the system undergoes a phase transition before the second effect starts dominating over the first one. After the phase transition the system is then in the approximate Mott states with the only entropy coming from thermal excitations allowing particles to cross the energy gap. As the gap increases the entropy thus falls to zero because the integer filling state is non-degenerate.

Figure 5.26 again shows the entropy on the integer particle number lines but with focus on the phase transition. Here you can very well see that the corrections increase the entropy also in the normal phase for $T = 0.5J$, but for $T = 1J$ it is still hard to distinguish the mean-field and the corrected results.

One might be concerned that we saw in the previous section that the entropy decreases when increasing J/U starting from the phase transition and here we now see that it increases with decreasing U/J, i.e. with increasing J/U, which seems like a contradiction. These different observations do not contradict each other however, as the former figures were generated with T/U fixed and the ones in this section with T/J fixed. We exemplarily show how to solve apparent contradictions like this by investigating the entropy in the deep superfluid phase, i.e. for large J/U or small U/J.

In the previous section we saw that the entropy falls to zero for large J as the par-

ticles mostly condense into the ground state. In this section however the entropy has a large value for small U and then falls off. Also here the entropy only comes from the excited particles, there are however a lot more than in the fixed U case. To understand this we need to translate the temperature. Because the number of excited particles through thermal activation is determined by the relation of the temperature and the excitation gap it is more natural to view T/U as the "real" temperature and translate T/J. We get

$$\frac{T}{U} = \frac{T}{J}\frac{1}{U/J}. \tag{5.1}$$

Thus for small U/J and fixed T/J, T/U is large. There are thus many different excited states possible, leading to a large entropy despite many particles being condensed into the ground state. All other seemingly contradictory observations you might occur can be explained in a similar way.

5.3 Summary

In this chapter we investigated lines of constant particle number in the fixed-temperature phase diagrams both for fixed J and fixed U. Besides the order parameter, which showed no new behaviour, we analyzed the entropy and physically interpreted it as promised in the previous chapter.
For fixed U we saw two qualitatively different behaviours. For non-integer particle number the entropy started decreasing from some initial value in the normal phase, due to an increasing "delocalization length". For some critical value of J the particles could then simply overcome the repulsion and delocalize completely resulting in the entropy decreasing to zero quickly.
On the integer particle number lines however we observed positive slope in the normal phase and a maximum at the phase transition when including the corrections. This was due to the fact that for increasing J the particles can more often hop out of the Mott-like state, increasing the entropy, until a critical value of J is reached and may particles condense into the ground state which decreases the entropy as already stated above.
On the same line for $T = 0.05U$ we observed an additional peak which also occurred in mean-field approximation. This peak only formed after the phase transition in the superfluid phase. We can infer from this peak that right after the phase transition, suddenly some new states get available before the particles all condense into the ground state.
In the fixed-J case we found two different effects dictating the behaviour of the entropy. The first one is concerned with the energy gap. We argued that for increasing U, the energy gap increases, allowing for less excited states leading to a decrease in entropy. On the other hand, increasing U reduces the number of particles condensed into the ground state, which can then contribute to the entropy, leading to an increase in the entropy.
For small values of U the first effect dominated, decreasing the entropy. Then at some point when the energy gap is too big in order for the particles to cross it at all, a further increase does not change anything anymore so that this effect does not contribute anymore. After the phase transition, in the normal phase, also the

second effect does not contribute as there is no condensate anymore.
This leads to different behaviours for lines that enter the normal phase for different values of U. On those that enter is very quickly we never observe the second effect and on those that never enter it we observe only the second effect for large U.
In the normal phase for U large enough so that both effect do not contribute anymore the entropy becomes constant. The constant is non-zero for non-integer particle number as there are many degenerate ground states available. If the particle number is integer this constant is zero as there is only one non-degenerate ground state, the Mott state.
I want to stress that we used quite different arguments in the fixed-U and the fixed-J case to explain seemingly contrary behaviours. We argued that these different behaviours actually do not contradict each other as we have to keep in mind to transform the temperature from one case to the other. Physically speaking it makes a qualitative difference if the interaction of the particles is fixed and the tunneling strength changes, controlling the delocalization of the particles or if the tunneling strength is fixed and the interaction strength changes, changing the excitation gap.
In the following chapter we will now use our won understanding of the entropy on constant particle number lines to discuss the temperature for constant entropy and constant particle number.

Chapter 6

Temperature for Fixed Particle Number and Entropy

In the previous chapter we took a step closer to the experiment by considering lines of fixed particle number instead of fixed chemical potential. Now that we have gained some understanding of the thermodynamics on these constant particle number lines we want to address a question mentioned in the introduction. We want to be able to predict the temperature of a Bose gas after adiabatically turning on an optical lattice. In section 6.1 we will, as in the previous sections, fix either J or U and vary the other for fixed particle number and entropy, which already allows us to gain a qualitative understanding of the temperature for varying lattice depth. In the second section 6.2 we will make the discussion more quantitative, by considering a three-dimensional simple cubic lattice structure, which allows us to directly study the temperature as a function of the lattice depth. With this we are then able to predict the temperature of a Bose gas after an adiabatic ramp up of an optical lattice.

6.1 Fixed Hopping Amplitude or On-Site Interaction Strength

In order to consider adiabatic processes we need to be able to fix the entropy. For now, we will keep U fixed. Then, we need to invert the function $S = S(J/U, T/U, n)$ to get a function $T/U = T/U(J/U, S, n)$. Beforehand let us first take a look at the function we want to invert, i.e. $S(T/U)$ for all other arguments fixed. On the one hand we need to check that $S(T/U)$ is monotonically increasing so that we can make use of the same algorithm we used in the previous chapter. On the other hand, there is quantum Monte Carlo data available for this function so that we can compare our calculation with exact results [27].

Figures 6.1 and 6.2 show the entropy as a function of temperature for J fixed for integer filling $n = 1$ and $U = 6.667Jz$ or $U = 4.329Jz$, respectively. Because in the paper from which the figures we are comparing with, are taken, there is no factor of z absorbed into J, we have also made it explicit in our results.

Indeed the entropy increases monotonically with the temperature. For small temperature the entropy is zero because the system is in the ground state, i.e. all particles are condensed in the superfluid phase, or the system is in the Mott state in the nor-

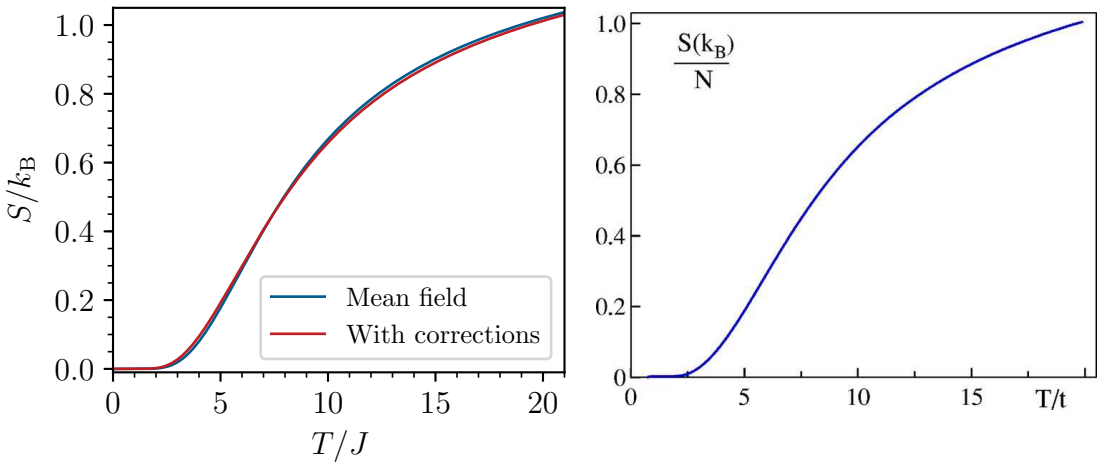

Figure 6.1: Entropy for varying temperature with $n = 1$, $U = 6.667Jz$, $d = 3$, corresponding to the superfluid phase. Left side: Our calculation. Right side: QMC calculation, image taken from Ref. [27], with the notation $t = J$. In both figures the factor of z is made explicit, i.e. not absorbed into J.

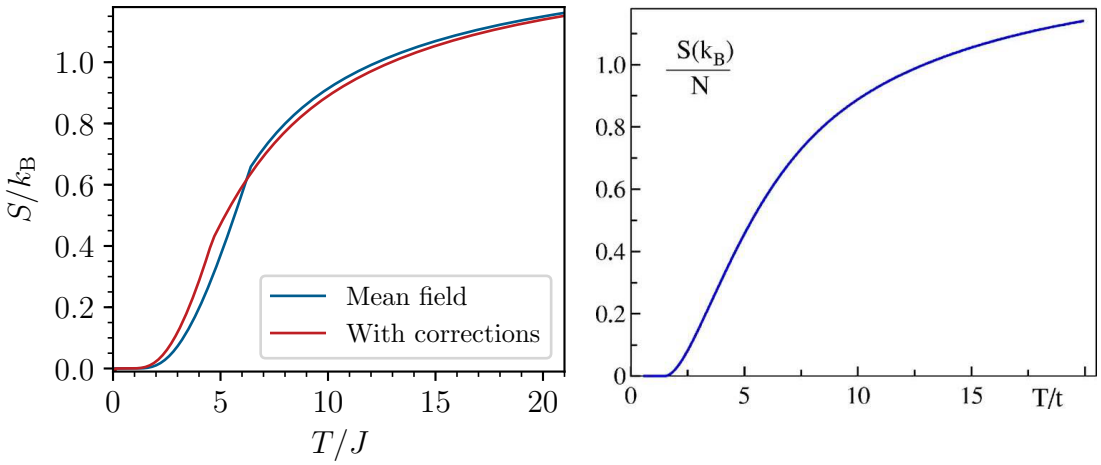

Figure 6.2: Entropy for varying temperature with $n = 1$, $U = 4.329Jz$, $d = 3$ corresponding to the normal phase in the QMC simulations. Left side: Our calculation. Right side: QMC calculation, image taken from Ref. [27], with the notation $t = J$. In both figures the factor of z is made explicit, i.e. not absorbed into J.

mal phase. After the temperature gets larger than some critical value the entropy starts increasing, i.e. the particles get out of the condensate or the Mott state due to thermal activation.
In figure 6.1 the corrected and the mean-field results are essentially the same. Further they agree well with the QMC results. In figure 6.2 however, there is some discrepancy between corrected and mean-field results and also a qualitative difference to the QMC data. Our calculations, both the mean-field and the corrected ones predict a phase transition. The QMC data however predict the particles to stay in the normal phase. This discrepancy is consistent with the observation we made in chapter 4. There we saw that the correct (QMC) phase boundary is at a larger value of J/U than our calculations predict. As the value of U/J for which the entropy is shown in the figure is close to the correct phase boundary, which is also stated in the paper from which the figure is taken, it is already in the superfluid phase for some higher temperature in our calculation. Besides this qualitative difference and the non-analyticity connected to the phase transition, our results again agree pretty well with the QMC ones.
We have exemplarily seen that the entropy is indeed monotonically increasing with temperature, which is also to be expected from physical reasoning. We can thus use the same bisection type algorithm as described at the beginning of chapter 5 to invert $S(T)$. For the starting interval of the temperature, we most oftenly chose $[0.001U,\ 0.3011U]$ but also sometimes varied the interval, in particular for high entropies, where we have to expect high temperatures. For the goal threshold we mostly used $\Delta T_{\text{goal}} = 0.002U$ but also here we sometimes varied the value.
Note however that our algorithm did not always converge. This is partly due to degeneracy problems but partly also simply due to numerical mistakes. In the following, we will use the same axis limits for all figures, so that it gets clear where the algorithm does not converge as there are then no data points. Interesting points like phase a transition are always shown however.
Note that because we are fixing n and S, which are both dimensionless, lines with fixed U and lines with fixed J carry the same information, i.e. we can relate the the temperature for fixed U to a corresponding temperature function with fixed J:

$$\frac{T}{J}\left(\frac{U}{J}\right) = \frac{T}{U}\left(1\Big/\frac{U}{J}\right)\frac{U}{J}. \tag{6.1}$$

This is in contrast to before, where we for example kept T and n fixed. Because the temperature has dimensions of energy, it will change when translating from one case to the other, and so the two cases contain different information. Because this is not the case here, we will mostly restrict our discussion to to the fixed J case. However, although both lines contain the same information, the temperature will still show different behaviour, so sometimes we will also show figures for fixed J in order to show how different aspects of the fixed-U figures translate over. The fixed-J figures are simply generated from the fixed-U data using the translation given in equation (6.1).
In the following we will look at four different entropies $S \in \{0.01,\ 0.1,\ 0.3,\ 0.6\}$ at the same particle numbers as in the previous chapter: $n \in \{0.7,\ 0.9,\ 1.0,\ 1.1,\ 1.3\}$. Note that the two entropies $S = 0.3$ and $S = 0.6$ are approximately equal but slightly smaller than the values of entropy on the plateaus it shows in mean-field approximation in the normal phase for $n = 0.9,\ 1.1$ and $n = 0.7,\ 1.3$, respectively, see

figures 5.9-5.11. Additionally we chose one entropy value which is slightly smaller and one which is an order of magnitude smaller.
In the previous chapter we have investigated the entropy depending on J/U for different fixed particle numbers and temperatures. From our observations there, we can already argue how the temperature should qualitatively behave as a function of J/U for fixed particle number and entropy. To this end let us quickly recapitulate the key observations concerning the entropy in the fixed-U case.
For non-integer particle number the corrected entropy shows a negative slope for increasing J in the normal phase, until a critical value of J is reached where the system undergoes a phase transition to a superfluid. In the superfluid phase the entropy then falls even quicker to zero. The key difference in the mean-field results is that there the entropy is constant in the normal phase and only obtains a negative slope in the superfluid phase.
On the integer particle number lines, the corrected entropy shows a positive slope in the normal phase with a maximum at the phase transition. After that the entropy again falls off in the superfluid phase. The entropy in mean-field approximation does not show this positive slope, however for a specific temperature it shows a peak at the phase transition. This also occurs in the corrected results in addition to the maximum due to the positive slope.
With these observations in mind we can now try to qualitatively predict the behaviour of the temperature for fixed entropy. Let us first investigate the case of non-integer particle number. As the entropy starts at some rather large value for $J = 0$, we would expect that we need a small temperature to compensate that for small fixed entropies. For increasing J we then recalled, that the corrected entropy falls off for fixed temperature. We would thus expect the temperature to increase in order to keep the entropy constant. The entropy in mean-field approximation however is approximately constant throughout the normal phase. We could thus expect that the temperature also stays constant. This is not that clear however because the constant value of the entropy in the normal phase does not really change much with changing the temperature. Thus it is not that easy to estimate the behaviour of the mean-field entropy.
After going through the phase transition it is then clear however that the temperature both in mean-field approximation and when including the corrections, has to increase in order to keep the entropy constant, as it falls quickly to zero in the superfluid phase.
On the integer particle number lines we would expect a somewhat different behaviour than for non-integer particle number. In this case the entropy is generally smaller, thus the temperature for small J does need to be as small as for the non-integer particle number case. Further the entropy then starts increasing in the corrected results so that we expect a decrease in temperature. In the mean-field results we however have the same problem as before, that the entropy does not change much with changing J or T.
After the phase transition we then, as before, expect the temperature to increase again, as the entropy decreases quickly. Because of this we can expect the temperature to show a minimum at the phase transition when including the corrections. In the mean-field results it is not that clear if we can expect a minimum. Recall that we also observed a peak in the mean-field entropy for a particular temperature. However, as this peak is clearly temperature sensitive, we can not *a priori* expect a

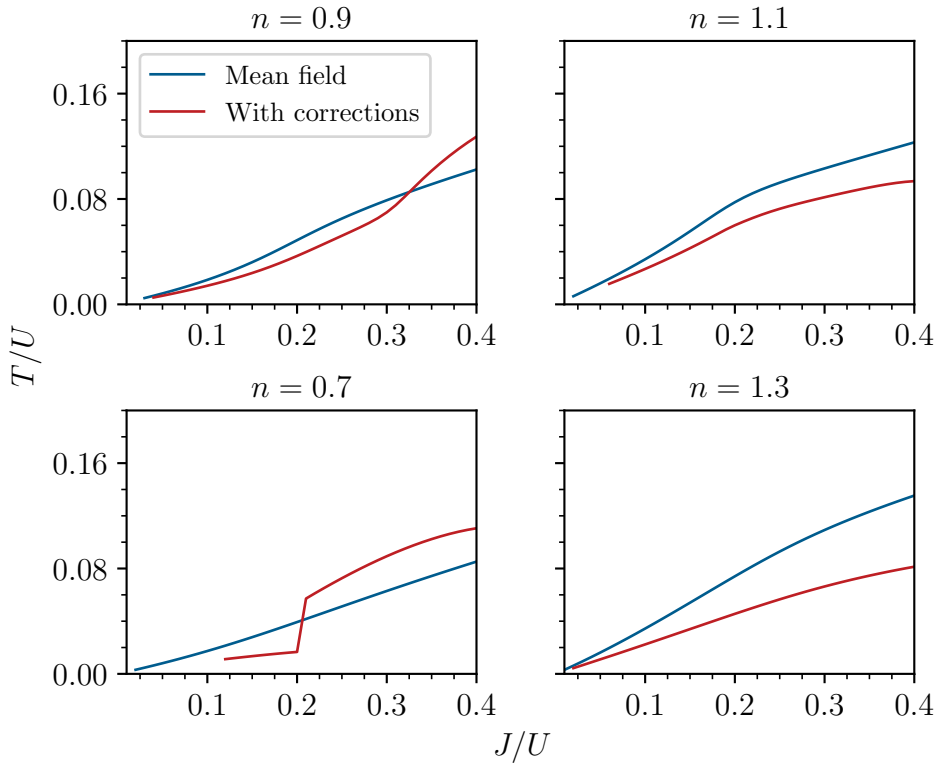

Figure 6.3: Temperature for varying hopping amplitude for $S = 0.01k_B$ and different non-integer particle numbers with U fixed.

dip in the temperature due to it.
We have now estimated the behaviour of the entropy in the two phases. You have to keep in mind however, that the phase boundary moves to higher values of J for increasing temperature. Thus it is not that clear in which phase the system starts for low J because although J is small we also argued the temperature to be small, at least for small entropy, and we have previously seen that the non-integer particle number lines cross the phase boundary for small values of J at low temperature, see figures 5.1-5.3. Besides the fact that we can not directly say in which phase the system starts, we can further not say if a phase transition will occur when increasing J, because, although J is increasing, we argued that also the temperature increases, leading to the phase boundary also moving to higher J. Because we can not say which of the two effects is stronger we can not generally expect a phase transition to occur.
We now take a look at the numerical results for the temperature and compare them to our expectations. Note that, because we expect the temperature to increase for increasing J we might be able to investigate higher values of J. This is because we have observed in the previous chapter, that although the problems of our calculation due to degeneracies get worse for larger J, they also get better for higher T. Thus, we will take our axis limits such that higher values of J will be investigated. We need to be careful with our results however as we can not be sure, which of the two effects mentioned is stronger.
As before we will first investigate the non-integer particle number case. Figure 6.3 shows the temperature for non-integer particle number and a low entropy $S = 0.01$.

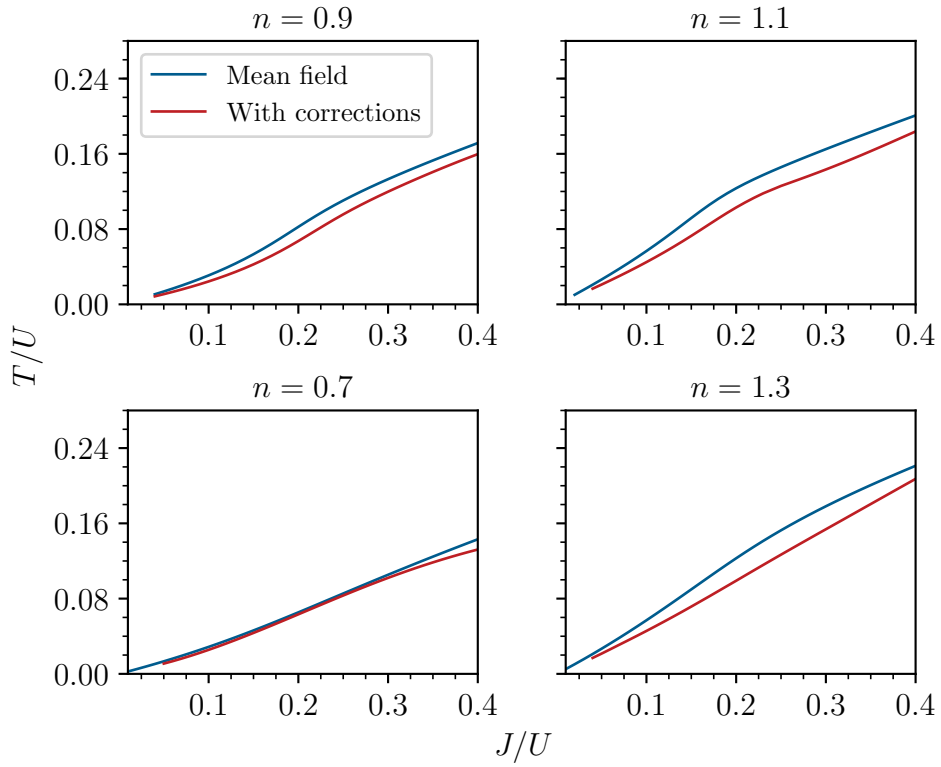

Figure 6.4: Temperature for varying hopping amplitude for $S = 0.1k_B$ and different non-integer particle numbers with U fixed.

Indeed, as expected, the temperature starts at a small value for small J and then increases. By also computing the order parameter it turns out that the system is in the superfluid phase for all investigated J, i.e. the increase in temperature is not sufficient to overcome the condensation through the increase in J.
The corrections generally lower the entropy, which is consistent with our observation, that the corrections increase the entropy in the superfluid phase. You can however observe two exceptions to this. For $n = 0.9$, the slope of the corrected temperature starts increasing for $J \approx 0.3U$, which leads to the corrected temperature being larger than the one in mean-field approximation. This might very well be due to degeneracy effects as it occurs for high J and is qualitatively different from the other figures. The second exception can be observed for $n = 0.7$. Here the temperature jumps non-analytically for $J \approx 0.2U$. Because the system is generally in the superfluid phase and there is thus no phase transition occurring, the jump in the temperature is probably due to the degeneracies. This is plausible as the temperature where this occurs is rather low and further, we have previously seen that the degeneracy problems on the non-integer particle number lines occur already for smaller J, in particular for larger deviation for $n = 1$. Generally we can see that the differences between the corrected temperature and the temperature in mean-field approximation increase for higher J. This might also indicate that for this low entropy the temperature increase is too small to make it possible to go to higher values of J.
Figure 6.4 shows the temperature for the same non-integer particle numbers for a higher entropy, $S = 0.1$. The general behaviour looks similar to the previously in-

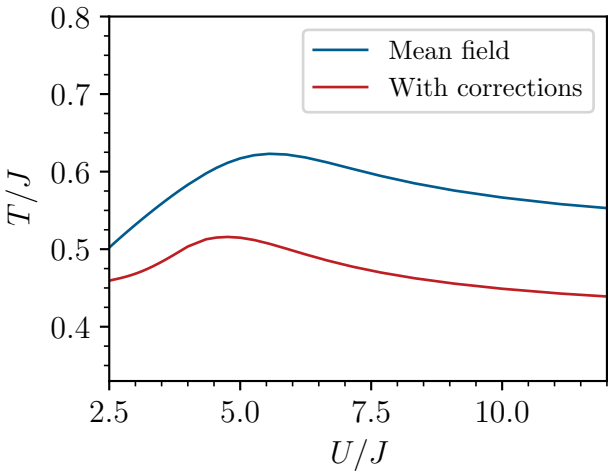

Figure 6.5: Temperature for varying on-site interaction strength for $S = 0.1k_B$ and $n = 1.1$ with J fixed.

vestigated entropy, $S = 0.01$. Here however, the temperatures are generally slightly larger, which had to be expected for higher entropy. As in the previous figure the system is generally superfluid, so the temperature increase again not enough to overcompensate the increase in J and prevent the particles from condensing.
The differences between the corrected and the mean-field results are smaller than for the previously investigated entropy. Furthermore, they do not really increase for higher J on the $n = 0.9$ and $n = 1.1$ lines. This might be an indicator that here even the results for high J are actually physical because the temperature increase allows our calculation to work even here, as we hoped at the beginning of the chapter. On the $n = 0.7$ line however, the corrections again start deviating more from the mean-field results for large J, which might be due to degeneracies. This is consistent because it only happens for larger deviation from $n = 1$.

Figure 6.5 shows how this typical increase in temperature translates to the fixed-J case. Here, the temperature first increases with increasing U, then shows a maximum and then also decreases like in the fixed-J case. This is as could be expected from the fixed-J entropy figures that never enter the normal phase, see for example the $n = 1.1$ plot in figure 5.22. There the entropy first decreases with increasing U, so we expect a temperature increase. For larger U the entropy then increases with increasing U so we expect a decrease in temperature. These two behaviours then of course lead to a maximum in between, which is exactly what we observe.

Figure 6.6 shows an even higher entropy, $S = 0.3$. Note that this is slightly smaller than the entropy of the plateaus on the $n = 0.9$ and $n = 1.1$ lines, we observed in section 5.1. Also here the temperature increases with increasing J, as expected. A key difference to before can be seen in the $n = 0.9$ and the $n = 1.1$ figures. Here, there is a non-analyticity in the corrected temperature for $J \approx 0.2U$ and $J \approx 0.15U$ respectively. Computing the order parameter yields that there is a phase transition from the normal to the superfluid phase occurring there for increasing J. The mean-field results on all lines and the corrected results on the $n = 0.7$ and $n = 1.3$ lines however again predict the system to always be in the superfluid phase.
You might be concerned, that the temperature on the $n = 0.9$ and $n = 1.1$ lines tends to zero for small J although we have chosen the entropy approximately equal

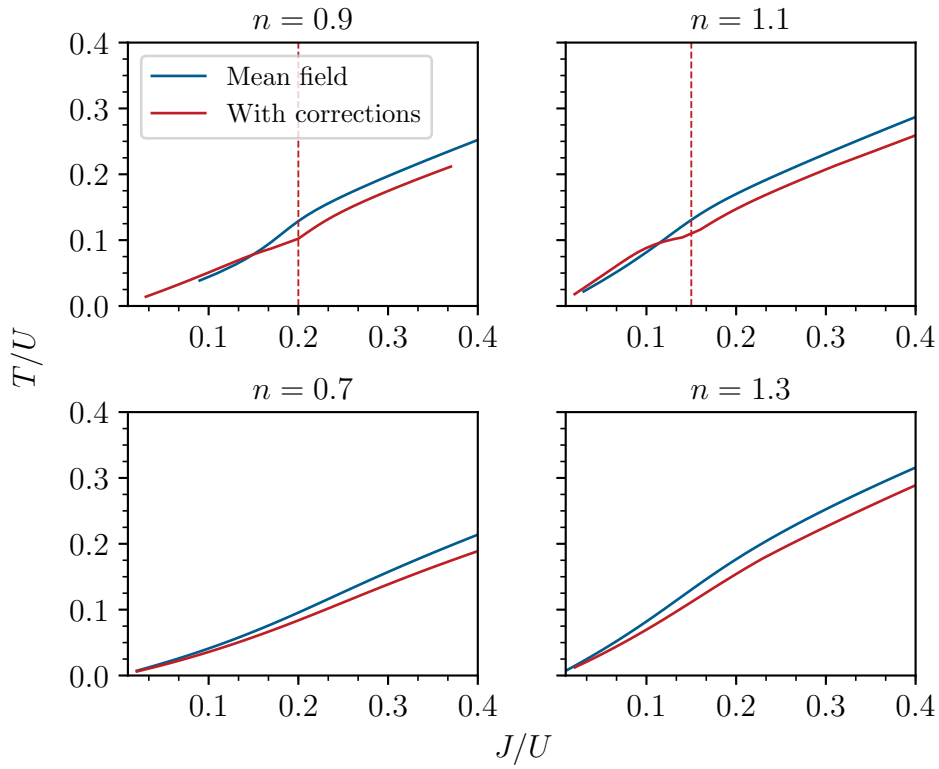

Figure 6.6: Temperature for varying hopping amplitude for $S = 0.3k_\mathrm{B}$ and different non-integer particle numbers with U fixed. Phase transitions are indicated by dashed lines.

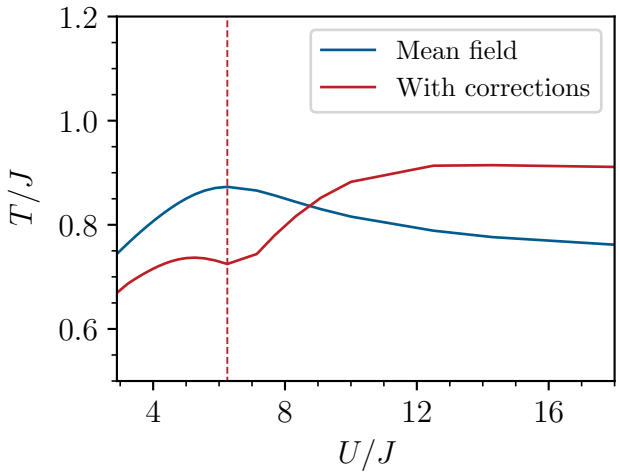

Figure 6.7: Temperature for varying on-site interaction strength for $S = 0.3k_B$ and $n = 1.1$ with J fixed. Phase transitions are indicated by dashed lines.

to the value on the plateaus. However the entropy on the plateaus was slightly bigger and because this value does not change much with the temperature, still a small temperature is needed to compensate this slight entropy difference. In the next figure however, where we investigate $S = 0.6$, we can then expect that the $n = 0.9$ and $n = 1.1$ lines have a larger temperature for small J because the entropy is then notably larger than the entropy value on the observed plateaus.

Figure 6.7 shows the implication of phase transition for the temperature in the fixed-J case. It is clear that the non-analyticity in the corrected temperature for fixed U leads to a non analytic minimum of the temperature for fixed J. After the phase transition, we have observed in section 5.2, that the entropy decreases further and eventually reaches a constant value. This is consistent with the temperature further increasing after the phase transition and then showing an approximate plateau. However, you can spot a slight negative slope, which could be connected to the entropy also not being perfectly constant. Because the mean-field results do not predict a phase transition they show the same behaviour as in the previous fixed-J figure.

Figure 6.8 shows the temperature for $S = 0.6$, which is approximately the entropy of the plateaus on the $n = 0.7$ and $n = 1.3$ lines, that we observed in section 5.1. Indeed, as expected, the temperature on the $n = 0.9$ and $n = 1.1$ lines is now rather large already for small values of J. Furthermore it then shows a different behaviour to before. The mean-field results are approximately constant, and the corrected results only show a small positive slope. After some critical value of J/U the temperature then non-analytically starts increasing with a larger slope, like in the previous figures. A computation of the order parameter yields that this point, where the derivative of the temperature jumps, is again connected to a phase transition from normal to superfluid, both in the corrected and the mean-field results. On the $n = 0.7$ and $n = 1.3$ lines the behaviour is similar to the behaviour for the lower entropies. In particular the temperature is again small for small J, due to the entropy being slightly smaller than the entropy on the plateaus for $n = 0.7$ and $n = 1.3$, as argued for $S = 0.3$. The differences between the mean-field and corrected results for small J are however larger than before. These differences are

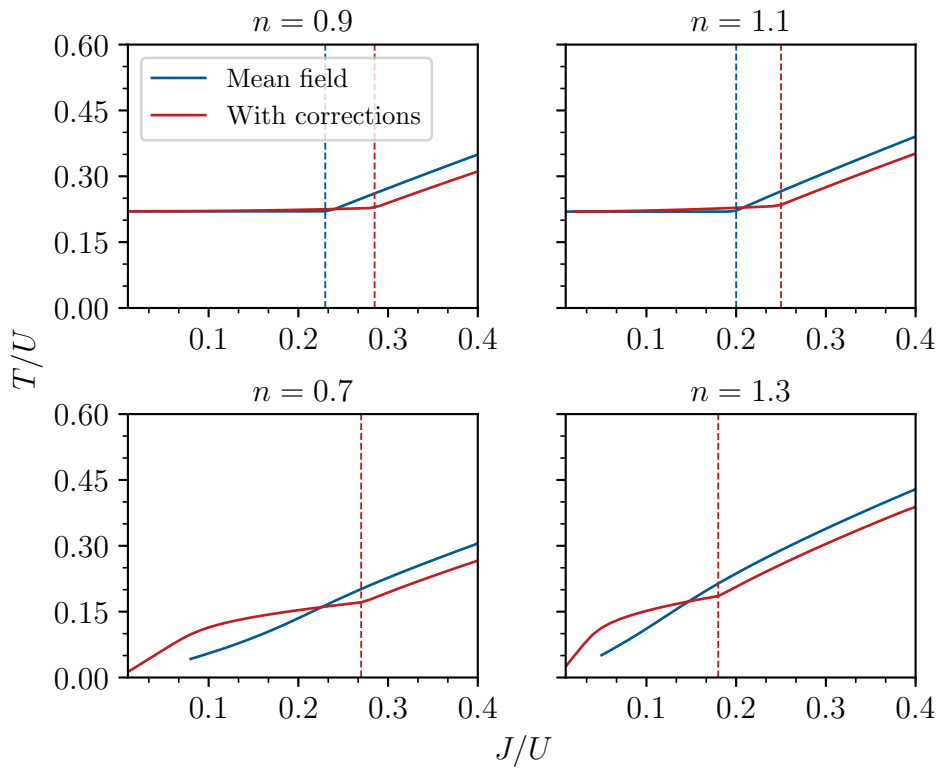

Figure 6.8: Temperature for varying hopping amplitude for $S = 0.6k_\mathrm{B}$ and different non-integer particle numbers with U fixed. Phase transitions are indicated by dashed lines.

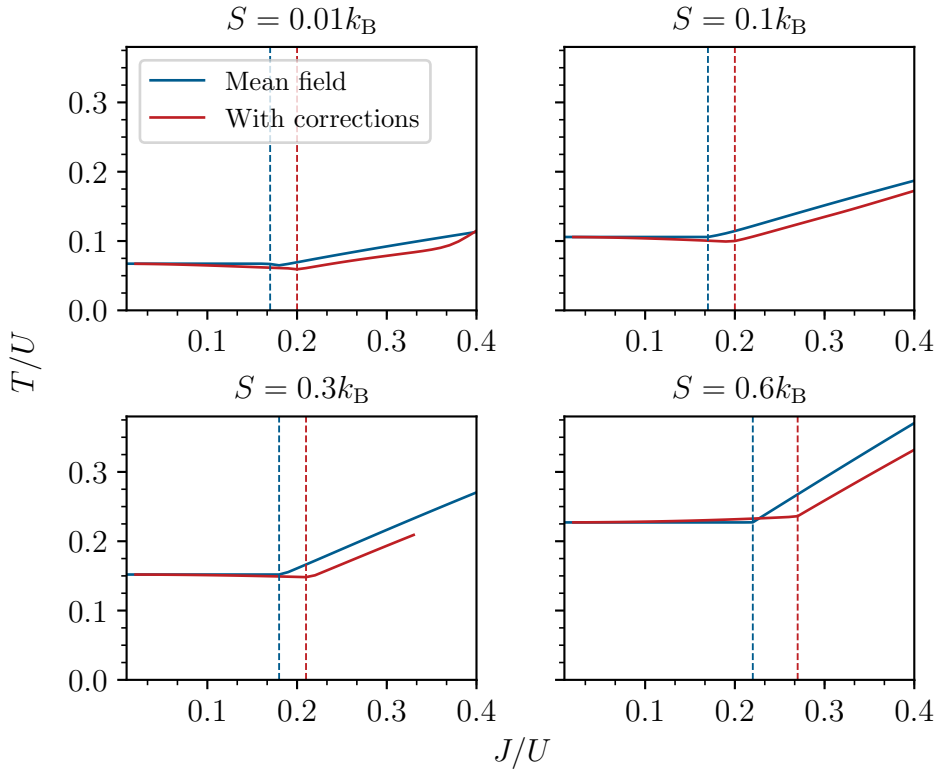

Figure 6.9: Temperature for $n = 1$ and different entropies with U fixed. Phase transitions are indicated by dashed lines.

connected to the corrected results having a negative curvature and the mean-field results having a positive curvature. For some critical value of J the corrected results then change in a non-analytic way after which they are approximately parallel to the mean-field results, but smaller. Again there is a phase transition from normal to superfluid occurring here. In contrast to the $n = 0.9$ and $n = 1.1$ lines, this transition however only occurs in the corrected results here.

Figure 6.9 shows the temperature for integer particle number and for the same entropies as before. The entropy in mean field-approximation is approximately constant for small J and then obtains a positive slope after some critical point where it changes non-analytically. The corrected results show a negative slope for J smaller than the critical point, which gives rise to a minimum at the phase transition. We have expected this behaviour at the beginning of this chapter. Further, it is clearly visible that the temperature generally increases with increasing entropy.
In the normal phase the quantitative difference between the mean-field and corrected results is rather small, due to the slope of the corrected results being only slightly non-zero. In the superfluid phase the two results show the same qualitative behaviour as temperature has approximately the same slope in mean-field approximation and when including the corrections. The corrected temperature is however smaller, as also seen in the previous figures.

Figure 6.10 again shows the temperature for integer particle number but only for the three lower entropies, where the temperature shows a minimum, and with focus on the phase transition. In these figures the minimum can be seen more clearly. Further it is clear that the minimum disappears for larger entropy and thus larger

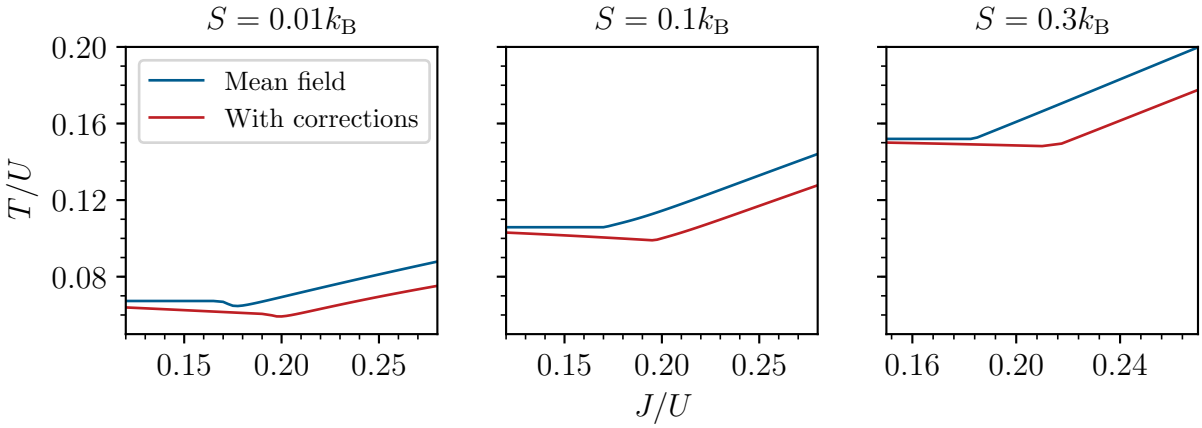

Figure 6.10: Temperature for $n = 1$ and different entropies with focus on the minimum at the phase transition and U fixed.

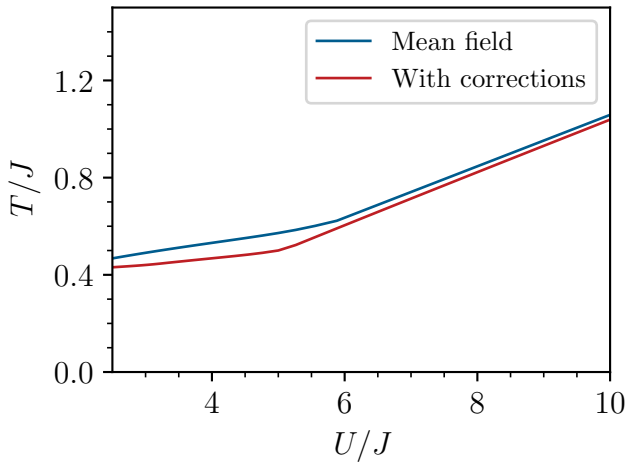

Figure 6.11: Temperature for $S = 0.1k_B$ and $n = 1.0$ for fixed J.

temperature, which is consistent with the entropy peak, which gives rise to the temperature minimum, disappearing for larger temperature, as we saw in section 5.1. For $S = 0.01$ you can see a dip at the phase transition, which is visible both in mean-field approximation and the corrected results. Because this happens at a low temperature, this is probably connected to the peak in the entropy which we observed for $T = 0.05U$ in figure 5.12. This peak was also visible both in mean-field approximation and the corrected results additionally to the positive slope of the corrected entropy which gives rise to the negative slope of the corrected temperature here.

Figure 6.11 shows the integer particle number behaviour of the temperature for fixed J, here for $S = 0.1$. Again this can be explained by the corresponding entropy figure 5.25. There, we saw that the entropy decreases in the superfluid phase and then, changes its slope but keeps decreasing in the normal phase. This implies for the temperature to generally increase, but change the slope at the phase transition, which is what we observe here.

Now that we have investigated the temperature for varying J or U, we can get a qualitative understanding of the temperature for varying lattice depth. When the

lattice depth increases we would expect, that J decreases because the Wannier functions should decay more rapidly. This will then result in more on-site overlap so that U should increase with increasing lattice depth. We have also exemplarily seen this in section 2.3, see figure 2.1. Thus when increasing the lattice depth the temperature should decrease. For integer particle number we further expect the temperature to increase again after undergoing a phase transition from the superfluid to the normal phase. In the following section we will investigate this more thoroughly.

6.2 Varying the Lattice Depth

Up to now we have analyzed T/U for varying J/U, or T/J for varying U/J while keeping S and n fixed. This can be understood as also keeping U or J fixed while varying the other one and measuring all energies in units of the fixed parameter. This does not yet fit the experiment however, because changing the lattice depth changes both J and U so the idea of one of them being fixed is not realistic. Alternatively you could argue, that when both J and U change both T/U and T/J are not a good measure for the "real" temperature because the scale we are using, is changing.
So, in order to investigate the temperature depending on the lattice depth V_0 we need to find the dependence of J/U on V_0 and then use some other energy to set the scale. We will use the recoil energy $E_\mathrm{R} = k_\mathrm{L}^2/2m$ for this, where $k_\mathrm{L} = 2\pi/\lambda_\mathrm{L}$ is the wave vector of the lasers generating the optical lattice, λ_L is the corresponding wavelength and m is the mass of the particles.
The first step is to find the dependence of J and U on the lattice depth. To calculate these parameters we need to solve the eigenvalue problem of the single-particle Hamiltonian, so we need to choose a concrete lattice potential. For simplicity and because it is very well a realistic choice we will choose a simple cosine potential:

$$V(\boldsymbol{x}) = \frac{V_0}{2} \sum_{i=1}^{d} \cos(2k_\mathrm{L} x_i), \tag{6.2}$$

where d is the dimensionality of the lattice. For the sake of generality the following discussion will be for arbitrary dimension but for the concrete computations and the generated figures we will restrict to $d = 3$.
In appendix A it is shown how to calculate the eigenenergies and eigenfunctions of the Hamiltonian for this specific lattice potential. There, the computation is done in terms of dimensionless variables, i.e. we have calculated the dimensionless dispersion $E(\boldsymbol{k})/E_\mathrm{R}$ and the dimensionless wavefunction $\phi_{\boldsymbol{\nu}}(\boldsymbol{z})$ with the dimensionless lattice momentum $\boldsymbol{\nu} = \boldsymbol{k}/k_\mathrm{L}$ and the dimensionless coordinate $\boldsymbol{z} = k_\mathrm{L}\boldsymbol{x}$.
With the dimensionless dispersion we can now calculate the hopping amplitude in units of the recoil energy using equation (2.30):

$$\frac{J}{E_\mathrm{R}} = -\frac{1}{N_\mathrm{S}} \sum_{\boldsymbol{k}\in 1.\mathrm{BZ}} e^{i\boldsymbol{k}\cdot\boldsymbol{\delta}} \frac{E(\boldsymbol{k})}{E_\mathrm{R}}. \tag{6.3}$$

Here, N_S is the number of lattice sites and $\boldsymbol{\delta}$ is the position-difference vector between arbitrary nearest-neighbour sites. J does not depend on the choice of these sites due to the homogeneity and isotropy of the lattice.
We can reduce the numerical effort needed for evaluating J, by noticing that J

does not depend on the dimensionality of the lattice and we can thus evaluate it in one dimension. This can be shown as follows: First note that for the given lattice potential, equation (6.2), corresponding to a simple cubic lattice structure we can always choose the coordinate system such that $\boldsymbol{\delta} = a\hat{\boldsymbol{e}}_n$ for an $n \in \{1, ..., d\}$, where $a = \lambda_\mathrm{L}/2$ is the lattice constant and $\hat{\boldsymbol{e}}_n$ is the unit vector in the direction of the nth coordinate. If we then use that the energy decomposes into a sum $E(\boldsymbol{k}) = \sum_{i=1}^{d} E_i(k_i)$, we can divide up both the sum and the product over the different dimensions into the term of the direction in which $\boldsymbol{\delta}$ is pointing, i.e. $i = n$, and the rest:

$$
\begin{aligned}
J_{d\mathrm{D}} &= -\frac{1}{N_\mathrm{S}} \sum_{\boldsymbol{k}\in 1.\mathrm{BZ}} E(\boldsymbol{k}) e^{ia\boldsymbol{k}\cdot\hat{\boldsymbol{e}}_n} = -\frac{1}{N_\mathrm{S}} \sum_{i=1}^{d} \left\{ \prod_{\substack{j=1 \\ j\neq n}}^{d} \sum_{k_j\in 1.\mathrm{BZ(1D)}} \sum_{k_n\in 1.\mathrm{BZ(1D)}} E_i(k_i) e^{iak_n} \right\} \\
&= -\frac{1}{N_\mathrm{S}} \sum_{\substack{i=1 \\ i\neq n}}^{d} \left\{ \prod_{\substack{j=1 \\ j\neq n}}^{d} \sum_{k_j\in 1.\mathrm{BZ(1D)}} E_i(k_i) \underbrace{\sum_{k_n\in 1.\mathrm{BZ(1D)}} e^{iak_n}}_{=0} \right\} \\
&\qquad - \frac{1}{N_\mathrm{S}} \underbrace{\prod_{\substack{j=1 \\ j\neq n}}^{d} \sum_{k_j\in 1.\mathrm{BZ(1D)}}}_{=N_{\mathrm{S,1D}}^{d-1}} \sum_{k_n\in 1.\mathrm{BZ(1D)}} E_i(k_n) e^{iak_n} \\
&= -\frac{1}{N_{\mathrm{S,1D}}} \sum_{k_n\in 1.\mathrm{BZ(1D)}} E_n(k_n) e^{iak_n} = J_{1\mathrm{D}}.
\end{aligned} \tag{6.4}
$$

Here, we used the relation

$$
\sum_{k\in 1.\mathrm{BZ}} e^{ika} = 0, \tag{6.5}
$$

which follows straight-forwardly from the geometric sum formula, where $a \neq 0$. Further, 1.BZ denotes the Brillouin zone of the full lattice given by $[-\pi/a, \pi/a)^d$, 1.BZ(1D) denotes the Brillouin zone of an arbitrary one-dimensional chain taken out of the lattice along one of the coordinate axes, given by $[-\pi/a, \pi/a)$ and $N_{\mathrm{S,1D}}$ denotes the number of sites the direction of an arbitrary coordinate axis, satisfying $N_\mathrm{S} = N_{\mathrm{S,1D}}^d$. Further we used that there are $N_{\mathrm{S,1D}}$ k-values in the one-dimensional Brillouin zone.

We can further calculate U using the definition (2.29) after computing the Wannier functions using their definition (2.25). Here we need to keep in mind that we computed the dimensionless Bloch and correspondingly the dimensionless Wannier functions. Because a wave function always has to have its dimension such that the normalization is dimensionless we need to introduce a length scale in order to relate the wavefunction in the dimensionless to the one in the dimensional coordinate. The most natural and convenient choice is to use the same length scale as used for defining the dimensionless coordinate:

$$
w(\boldsymbol{z}) = \left(\frac{1}{k_\mathrm{L}}\right)^{\frac{d}{2}} w(\boldsymbol{x}). \tag{6.6}
$$

With this we can also relate the integral in U to a dimensionless one:

$$U = g \int \mathrm{d}^d\boldsymbol{x}\ |w(\boldsymbol{x})|^4 = g k_\mathrm{L}^{2d} \int \mathrm{d}^d\boldsymbol{x}\ |w(\boldsymbol{z}(\boldsymbol{x}))|^4 = g k_\mathrm{L}^d \int \mathrm{d}^d\boldsymbol{z}\ |w(\boldsymbol{z})|^4. \tag{6.7}$$

Because the Wannier functions factorize $w(\boldsymbol{z}) = \prod_{i=1}^d w_i(z_i)$ due to the special choice of lattice potential we can also relate the d-dimensional integral to a one-dimensional one:

$$U = g k_\mathrm{L}^d \int \mathrm{d}^d\boldsymbol{z}\ |w(\boldsymbol{z})|^4 = g k_\mathrm{L}^d \prod_{i=1}^d \int \mathrm{d}z_i\ |w_i(z_i)|^4 = g k_\mathrm{L}^d \left(\int \mathrm{d}z_i\ |w_i(z_i)|^4 \right)^d, \tag{6.8}$$

where the choice of i is unimportant due to the isotropy.
So, we can numerically calculate J/E_R and $U/g k_\mathrm{L}^d$. In order to relate the fraction of these two to the real fraction J/U we can use the definitions of $E_\mathrm{R} = k_\mathrm{L}^2/2m$ and $g = 4\pi a_\mathrm{s}/m$ with the scattering length a_s as well as the relation $k_\mathrm{L} = \pi/a$. We get, now with restriction to three dimensions:

$$\frac{J}{E_\mathrm{R}} \frac{g k_\mathrm{L}^3}{U} = \frac{J}{U} 8\pi a_\mathrm{s} k_\mathrm{L} = 8\pi^2 \frac{J}{U} \frac{a_\mathrm{s}}{a}. \tag{6.9}$$

Thus we need to know the ratio of the scattering length and the lattice constant. To determine realistic values we take the setup from the original experiment of Greiner *et al.* [7]. They used a laser of wave length $\lambda_\mathrm{L} = 852\,\mathrm{nm}$ and $^{87}\mathrm{Rb}$ as bosons. As scattering length we use $a_\mathrm{s} = 95.44 a_0$, where a_0 is the Bohr radius [107]. This results in $a_\mathrm{s}/a \approx 1.186 \cdot 10^{-2}$. Now we only need to translate the temperature axis from T/U to T/E_R. To this end we calculate:

$$\frac{T}{U} \frac{U}{g k_\mathrm{L}^3} \frac{E_\mathrm{R}}{E_\mathrm{R}} = \frac{1}{8\pi^2} \frac{a}{a_\mathrm{s}} \frac{T}{E_\mathrm{R}}. \tag{6.10}$$

Thus, we can translate the temperature by multiplying with the numerically calculated value $U/g k_\mathrm{L}^3$ and the numerical factor $8\pi^2 a_\mathrm{s}/a$. In conclusion, this allows us to plot T against V_0 using E_R as energy scale, as desired.

Before turning to the temperature, we will take a look at the just calculated dependence of J/U on the lattice depth. This is shown in figure 6.12, where, as in the previous chapters, we absorbed a factor of $z = 6$ into J. As expected, the fraction decreases for increasing lattice depth. This decrease seems to be exponential.
By inspection of the J/U axis it is clear that for small lattice depths, the fraction is way bigger than the J/U values previously investigated. In particular we can not expect our calculation to work for these extraordinary large values of J/U. Furthermore, for small lattice depths also the band gap in between the energy bands of the single particle spectrum are rather small. Recall, that the Bose-Hubbard model needs as one of the assumptions, that we can only consider one band, i.e. neglect excitations into higher bands. Thus, besides our calculation not working there, we can not even expect the Bose-Hubbard model to be valid in the regime of small lattice depths. We will thus in the following restrict to lattice depths in a more appropriate interval where J/U is of order 1, as we have analyzed before.

Figure 6.13 shows again shows the fraction J/U for varying lattice depth but now restricted to a more appropriate interval of lattice depths where J/U is of the same order of magnitude as investigated in the previous chapters.

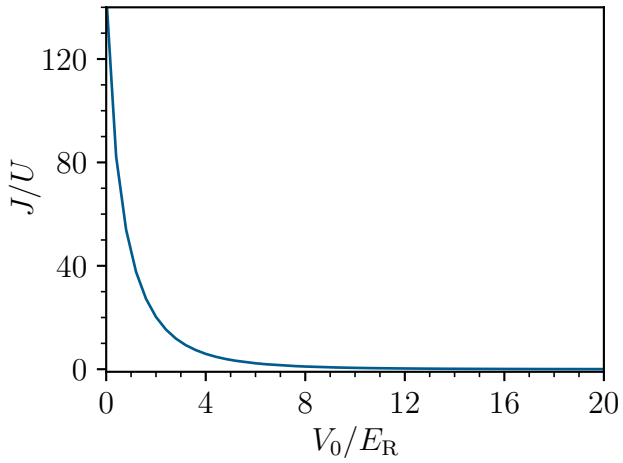

Figure 6.12: Fraction J/U with a factor of z absorbed into J for different lattice depths V_0 in units of the recoil energy E_R.

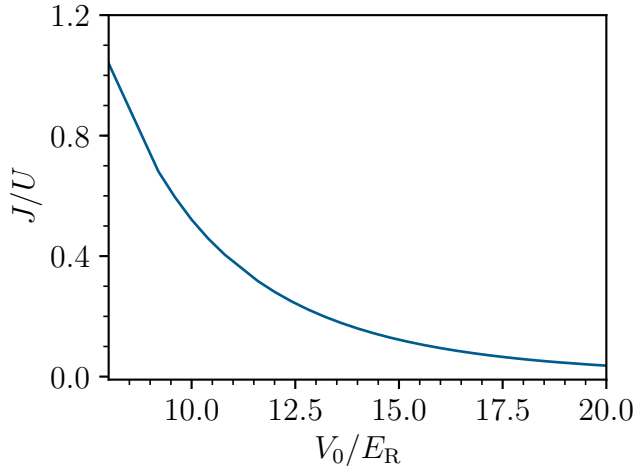

Figure 6.13: Fraction J/U with a factor of z absorbed into J for different lattice depths V_0 in units of the recoil energy E_R with focus on lattice depths corresponding to J/U values that allow our calculation to be physical.

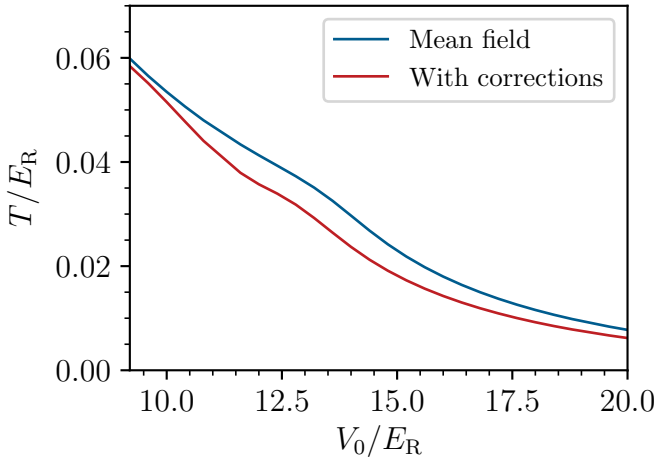

Figure 6.14: Temperature for varying lattice depth for $S = 0.1k_B$ and $n = 1.1$.

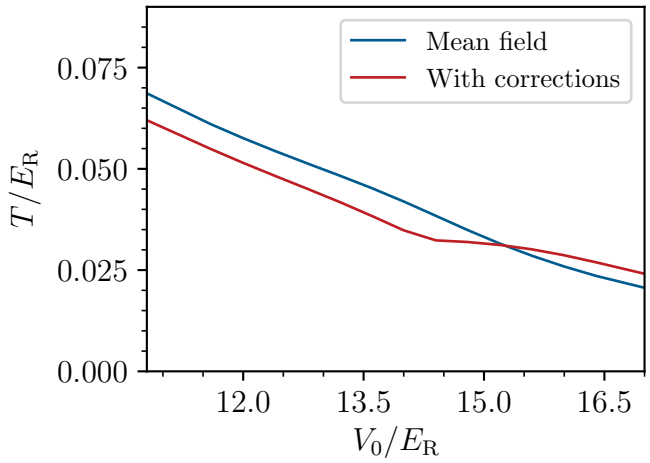

Figure 6.15: Temperature for varying lattice depth for $S = 0.3k_B$ and $n = 1.1$.

We now analyze the temperature as a function of the lattice depth. We will restrict to only some representative parameter choice, because we have seen that the temperature often shows similar behaviour, so the qualitative behaviour will be the same in the figures not shown. Further we will exclude the lowest entropy value $S = 0.01$, because we argued that we have to expect unphysical behaviour already for relatively small values of J/U corresponding to large values of V_0.

Figure 6.14 shows the temperature for $S = 0.1$ and $n = 1.1$. The behaviour is exactly as expected: The system simply cools off for increasing lattice depth. For large lattice depth we can already observe a saturating behaviour, which of course has to happen at some point because the temperature can not get negative. The quantum fluctuations lower the temperature, as before.

A similar behaviour can also be seen in figure 6.15, where $S = 0.3$ and $n = 1.1$. In the corresponding fixed-U figure 6.6 we have observed a phase transition in the corrected results, connected to a non-analytic change in temperature. This also translates to this figure, where the corrected temperature also jumps at the transition. The temperature in mean-field approximation shows the same behaviour as in the previous figure, due to not undergoing a phase transition. Again the corrections

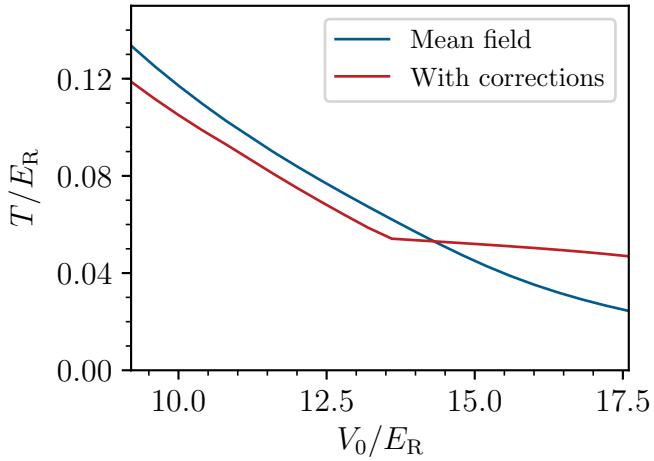

Figure 6.16: Temperature for varying lattice depth for $S = 0.6k_B$ and $n = 1.3$.

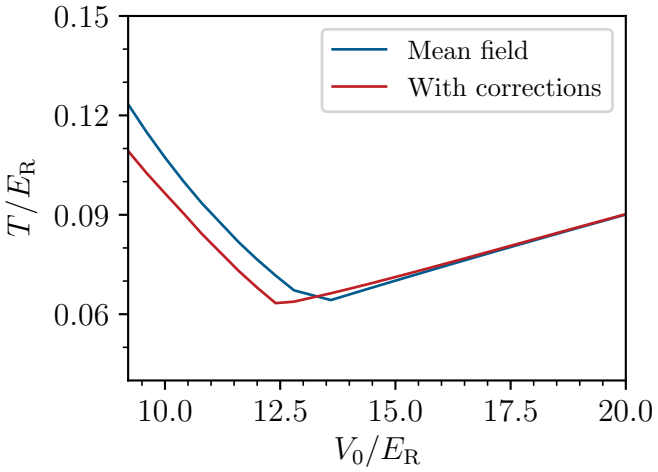

Figure 6.17: Temperature for varying lattice depth for $S = 0.6k_B$ and $n = 1.1$.

lower the temperature in the superfluid phase. In the normal phase however, after the phase transition, the corrected results then increase the temperature.

For $S = 0.6$ and $n = 1.3$, see figure 6.16, the behaviour is similar to the previous figure. Again we observe the decrease of the temperature and the non-analyticity of the corrected results due to the phase transition. The jump in the derivative is however larger than previously. This also leads to a notable difference between the corrected and the mean-field results, which do not enter the normal phase for the investigated parameters, as in the corresponding fixed-U figure 6.8.

Figure 6.17 shows the temperature for $S = 0.6$ and $n = 1.1$. Here, we observe a different behaviour in the normal phase. The temperature increases after undergoing a minimum, both in mean-field approximation and in the corrected results. Here we observe, that the corrections do not really change the temperature in the normal phase, as also the mean-field results enter it. Because the corresponding fixed-U figure 6.8 already showed the integer particle number behaviour, we can also here expect that the temperature for varying lattice depth and integer particle number shows a behaviour similar to figure 6.17.

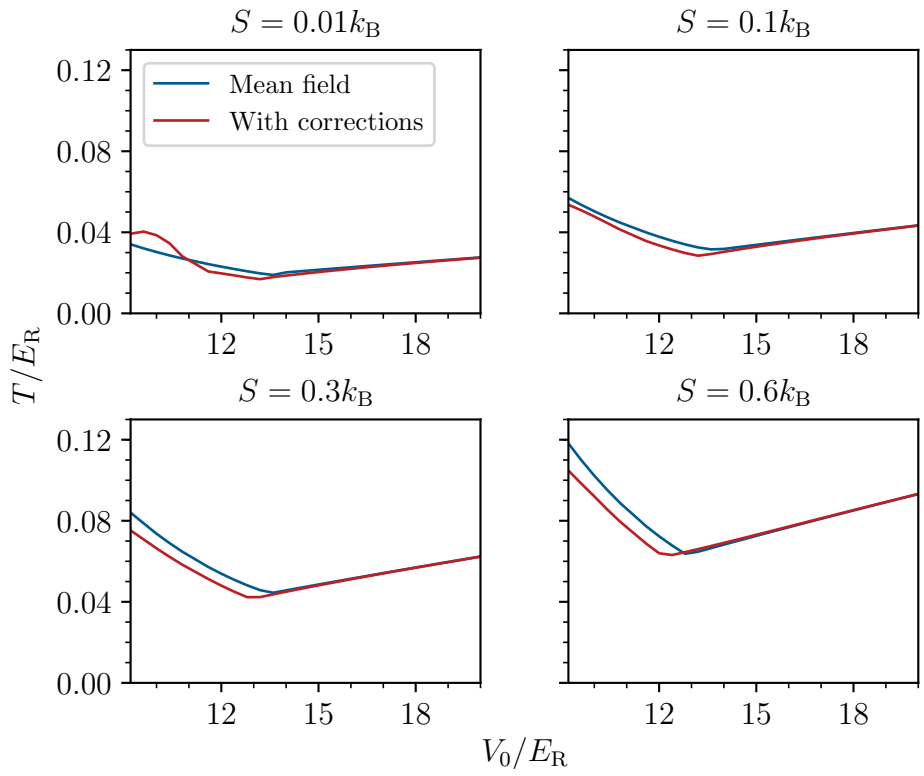

Figure 6.18: Temperature for varying lattice depth for $n = 1$ for different entropies.

Figure 6.18 shows the temperature for integer particle number for all entropies investigated. Indeed the behaviour is similar to the previous figure. The temperature falls off in the superfluid phase, shows a minimum at the phase transition and then increases again in the normal phase. The steepness of the decrease in the superfluid phase and the increase in the normal phase gets larger as the entropy and correspondingly the general temperature increases, which leads to a more distinctive minimum. As before, the corrections lower the temperature in the superfluid phase. In the normal phase the corrections do not really change the temperature anymore. For low temperature, i.e. low entropy we need to be cautious with the corrected results for low lattice depths which correspond to large values of J/U. For example we can spot a non-analyticity for $V_0 \approx 11.5E_R$, which is not connected to a phase transition. Further the general behaviour of the temperature for low V_0 is generally different from the other entropy values. This supports the conclusion that the behaviour here is unphysical and due to degeneracy effects. This also exemplarily justifies, why we have excluded other $S = 0.01$ figures from the discussion in this chapter.
In conclusion we have observed the behaviour we have expected from our analysis in the previous section. For non-integer particle number, the system simply cools off for increasing lattice depth. For integer particle number the system also cools off for increasing lattice depth until a phase transition occurs. After that the system heats up again, giving rise to a distinctive minimum at the phase transition.
In principle we can now predict the temperature of a Bose gas in an optical lattice when the initial entropy, that can for example be extracted from the theory of weakly interacting Bose gases, and the filling factor, i.e. the particle number, are

known. We have to keep in mind however that our higher order calculations will only make physical predictions when the lattice depth is large enough.

Chapter 7

Conclusion and Outlook

The goal of this thesis was to pursue a novel approach to the physics of the Bose-Hubbard model, in particular to the thermodynamics of the superfluid-Mott insulator transition. Up to now the approaches to the finite-temperature Bose-Hubbard model were mostly of purely numerical nature [27, 40, 44, 45] or purely analytical [55–61, 67, 68]. The analytical approaches further often restricted to mean-field theory. Analytical calculations that go beyond mean-field theory and investigate the finite-temperature case are still rather rare [67, 68].
In this thesis we pursued a novel "hybrid" approach to the problem. We utilized the decoupling of the mean-field Hamiltonian to numerically diagonalize it exactly and then analytically carried out a perturbative expansion around the mean-field Hamiltonian using the numerically known eigenenergies and eigenfunctions.
By comparing the critical J/U value at the tip of the $n = 1$ lobe in the fixed-U phase diagram for different dimensionalities and temperatures we could quantitatively show, that our second-order calculation already provides a significant improvement over the mean-field results and can be compared to other purely analytic beyond mean field calculations. While the mean-field prediction deviates by 17% from the correct value, the result from second-order corrections only deviates by 5%.
On top of that our calculation now also provides the possibility to calculate thermodynamic quantities in great parts of the phase diagram, which then constituted the main part of this thesis. We started in chapter 4 by analyzing the order parameter, the particle number and the entropy on horizontal as well as vertical lines through both the fixed-U and fixed-J phase diagrams at different fixed temperatures. This gave us some intuition for the thermodynamics of the Bose-Hubbard model in general and the superfluid-Mott insulator transition in particular. Further we were able to investigate the consequences of the beyond mean-field corrections.
In chapter 5 we then took a step closer to the experiment and considered lines of constant particle number again in both the fixed-U and fixed-J phase diagrams for different fixed temperatures. On these lines we then analyzed the order parameter and the entropy. In particular we provided a physical discussion of the behaviour of the entropy for different values of the other parameters.
In the last chapter 6 we then first investigated the temperature for constant entropy and particle number mostly in the fixed-U case but also sometimes referred to the fixed-J one. By this we gained some insights into how the temperature of a Bose gas behaves when adiabatically turning on an optical lattice. Further were able to compare $S(T)$ for two different sets of parameters with quantum Monte Carlo

data. Our results generally were in good agreement with the exact data, however for one set of parameters our results, both mean field and corrected, predicted a phase transition, that was not predicted by the exact data. This is connected to the small discrepancy in the phase boundary already mentioned above.
By considering a concrete lattice potential, we were then further able to actually investigate the temperature for varying lattice depth, bringing our calculations another step towards the situation of an experiment. These final results now show that we are able to predict the temperature of a Bose gas after turning on an optical lattice when the particle number and the entropy are known. This is valuable, since measuring the temperature of a strongly correlated system, like bosons in a deep optical lattice, is experimentally very challenging.
This analysis can be made more realistic by taking into account infinite range hopping. In appendix D it is shown how this can be done, there was however not enough time in the scope of this thesis to pursue this. Thus, this could be subject of further work, as the theoretical ground work has already been done in this thesis and it would make the results more realistic, in particular for low lattice depths.
In section 3.3 we have argued that our hybrid approach also comes with problems. Because we expand around the mean-field Hamiltonian, i.e. use the mean-field product states as basis for our perturbative treatment our expansion does not converge when the correct eigenstates are too different from the mean-field ones. This happens when the correct eigenstates are highly entangled, which happens in the case of (almost) degenerate one- or many-site spectra and in the deep superfluid phase in general. These problems render our corrected calculations unphysical.
Recently a group dealt with a similar problem [105, 106]. They investigated degeneracies in the spectrum of the part of the Hamiltonian that is diagonal in the occupation number representation. They solved the problem by employing a projector operator formalism with which they diagonalized the degenerate subspaces and hence got rid of the problems. However they used a Landau expansion, so that their results are still only valid in the vicinity of the phase boundary or in the Mott/normal phases. It might be subject of further work to apply a similar formalism to our case where the degeneracies occur in the mean-field spectrum. This would then allow us to calculate thermodynamic quantities in great parts of the phase diagram, as our hybrid approach does not rely on a Landau expansion.
Furthermore, throughout this thesis, we have always assumed a homogeneous lattice. In the experiment however the lattice potential is typically superimposed by some trapping potential. This additional potential can be taken into account by considering a site dependent effective chemical potential, which is called local density approximation. It could be subject of further work to include this into our calculations, which would make the predictions more realistic.
In chapter 4, we have argued that the corrections do not seem to change the critical exponent β, in particular they predict the transition at the tip to be in the mean-field universality class. It could be subject of further work to analyze this more carefully and also try to extract other critical exponents in order to investigate the consequences of the corrections on them. In Ref. [108] the critical exponents were calculated perturbatively using the part of the Hamiltonian that is diagonal in the occupation number representation as a basis. It would be interesting to see how the results for critical exponents extracted from our calculations compare to those from Ref. [108].

A further improvement that could be achieved in the future is of course go to higher order. In this thesis we have developed a diagrammatic formalism for calculating terms coming up in the perturbative expansion. This formalism could be generalized to higher orders and it should be possible to teach a computer the generalized rules to evaluate the higher order terms.
An interesting application of thermodynamic analysis conducted in this thesis, in particular the data for the temperature as a function of the lattice depth would be, to develop a cooling protocol for bosons in optical lattices, which would be of great interest for experiments.
In conclusion, in this thesis we have developed a beyond mean-field theory of the thermodynamics of the superfluid-Mott insulator transition of bosons in optical lattices. Although our calculations notably improve the mean-field result for the critical J/U value at the tip of the $n = 1$ lobe, and also show a great agreement with quantum Monte-Carlo data when comparing $S(T)$, our calculations still do not work everywhere in the phase diagram, due to degeneracies. Thus, there is still work to be done. In the future it would be interesting to either lift restrictions we have used for simplicity, or to investigate further questions, for which there was no time to pursue in the scope of this thesis.

Appendix A

Calculation of the Band Structure for a Cosine Lattice

In this appendix we will show that is is possible to analytically solve the eigenvalue problem of the one-particle Hamiltonian

$$\hat{H}^{(1)} = \frac{\hat{p}^2}{2m} + \hat{V}_{\text{lat}}(\hat{x}) \tag{A.1}$$

for a simple cosine-lattice potential in terms of known special functions, the so called Mathieu functions. With the calculated eigenenergies and eigenfunctions we can then for example calculate the parameters of the Bose-Hubbard model, J and U, in terms of the lattice depth, which is experimentally accessible.
The lattice potential is given by

$$V_{\text{lat}}(\boldsymbol{x}) = \frac{V_0}{2} \sum_{i=1}^{d} \cos(2k_{\text{L}} x_i), \tag{A.2}$$

where $k_{\text{L}} = 2\pi/\lambda_{\text{L}}$ is the wave vector of the lasers generating the optical lattice, λ_{L} is the corresponding wavelength, V_0 is the lattice depth and d is the dimensionality of the lattice. The lattice constant is given by $\lambda_{\text{L}}/2 = \pi/k_{\text{L}}$. Note that due to the trigonometric identity $\cos 2x = 1 - 2\sin^2 x$ this potential is equivalent to a sine squared lattice, which is also commonly seen as the standard form of a simple cubic optical lattice potential [70].
With the potential (A.2) the time independent Schrödinger equation in real space becomes, with $\hbar = 1$:

$$\left(-\frac{\nabla^2}{2m} + \frac{V_0}{2} \sum_{i=1}^{d} \cos(2k_{\text{L}} x_i) \right) \phi(\boldsymbol{x}) = E\phi(\boldsymbol{x}). \tag{A.3}$$

A separation ansatz $\phi(\boldsymbol{x}) = \prod_{i=1}^{d} \phi_i(x_i)$ yields

$$\left(-\frac{1}{2m} \frac{\mathrm{d}^2}{\mathrm{d}x_i^2} + \frac{V_0}{2} \cos(2k_{\text{L}} x_i) \right) \phi_i(\boldsymbol{x_i}) = E_i \phi_i(\boldsymbol{x_i}) \tag{A.4}$$

for each $i \in \{1, ..., d\}$. The E_i are the separation constants satisfying $\sum_{i=1}^{d} E_i = E$. It is clear that it suffices to look at only one of these equations. We will therefore drop the subscript i in the following. We now go over to dimensionless quantities.

To this end we introduce a natural energy scale, the recoil energy $E_\mathrm{R} = k_\mathrm{L}^2/2m$. We further define the dimensionless coordinate $z = k_\mathrm{L}x$, the dimensionless energy $\epsilon = E/E_\mathrm{R}$ and the dimensionless and scaled potential depth $v = V_0/4E_\mathrm{R}$. With this the Schrödinger equation goes over into the Mathieu equation [109]

$$\frac{\mathrm{d}^2}{\mathrm{d}z^2}\phi(z) + (\epsilon - 2v\,\cos(2z))\,\phi(z) = 0. \tag{A.5}$$

One linear independent set of solutions are the Mathieu functions of the first kind $\mathcal{C}$ and $\mathcal{S}$, also called Mathieu cosine and Mathieu sine [109]. They are complex valued functions depending both on the parameters ϵ and v as well as the variable z. $\mathcal{C}$ is an even function and $\mathcal{S}$ is an odd function of z. We can write a general solution as a linear combination of these two functions:

$$\phi(z) = \alpha\mathcal{C}(\epsilon, v, z) + \beta\mathcal{S}(\epsilon, v, z) \tag{A.6}$$

with $\alpha, \beta \in \mathbb{C}$. Due to Bloch's theorem we also know that ϕ has to fulfill

$$\phi(z) = e^{i\nu z}u_\nu(z) \tag{A.7}$$

for some ν with $\nu = k/k_\mathrm{L}$ and $u_\nu(z+\pi) = u_\nu(z)$, as the periodicity of the lattice is π in dimensionless coordinates. In the following we will label each such $\phi(z)$ with its corresponding ν. In the context of the Mathieu equation ν is also referred to as the characteristic exponent. From equation (A.7) it follows

$$\phi_\nu(z \pm \pi) = e^{\pm i\nu\pi}\phi_\nu(z). \tag{A.8}$$

If we now plug (A.6) into this and set $z = 0$ we get two equations:

$$\alpha\mathcal{C}(\epsilon, v, \pi) + \beta = \alpha e^{i\nu\pi}, \tag{A.9}$$

$$\alpha\mathcal{C}(\epsilon, v, \pi) - \beta = \alpha e^{-i\nu\pi}. \tag{A.10}$$

Here we used the symmetries of the Mathieu functions, in particular $\mathcal{S}(\epsilon, v, 0) = 0$ for all ϵ, v, and rescaled the functions such that $\mathcal{C}(\epsilon, v, 0) = \mathcal{S}(\epsilon, v, \pi) = 1$. If one of these two is zero so that we can not rescale in this way it is still possible to make a similar argument. If $\mathcal{S}(\epsilon, v, \pi)$ is zero for example we could simply shift by 2π instead of π in equation (A.8). We will thus without loss of generality assume that this rescaling works.
If we now add and subtract the equations (A.9) and (A.10) we get the two conditions

$$\mathcal{C}(\epsilon, v, \pi) = \cos(\nu\pi), \tag{A.11}$$

$$\beta = i\alpha\,\sin(\nu\pi). \tag{A.12}$$

In particular we found the eigenfunctions

$$\phi_\nu(z) = \mathcal{N}_\nu\left[\mathcal{C}(\epsilon, v, z) + i\,\sin(\nu\pi)\mathcal{S}(\epsilon, v, z)\right], \tag{A.13}$$

where $\mathcal{N}_\nu$ is some normalization constant that in general will depend on ν. Equation (A.11) has to be understood as an equation for ϵ with v and ν given. Thus, this equation determines the energy levels of the system. The solutions to this equation are functions $\epsilon(\nu)$ for fixed v which give the energy bands, because ν is the dimensionless lattice momentum and ϵ is the dimensionless energy.

In principle we could now solve equation (A.11) numerically to find $\epsilon(\nu)$ for a given v, i.e. find ϵ such that $\phi(z) = e^{i\nu z}u_\nu(z)$, with $u_\nu(z)$ π-periodic, is a solution of the Schrödinger equation (Mathieu equation) (A.5). However, the values of ϵ for given v and ν such that this is true are actually known numerically, they are for example predefined in Mathematica, and are called characteristic values $a_\nu(v)$ of the Mathieu equation. For positive integer ν there are two characteristic values $a_\nu(v)$ and $b_\nu(v)$. Some authors only refer to these as characteristic values and not to those with non-integer ν. We have seen that the characteristic values understood as a function of ν give the dispersion, i.e. the band structure. We can thus physically understand why there are two characteristic values at integer ν: integer $\nu = k/k_\mathrm{L}$ corresponds to k being on the boundary of a Brillouin zone, $\nu = 1$ for example corresponds to the boundary of the first. For $v \neq 0$ this is where the band gaps open up, so the two characteristic values refer to the upper edge of the lower and the lower edge of the upper of the two bands. For example $a_1(v)$ ($b_1(v)$) is the energy at the boundary of the first Brillouin zone in the second band (first band). Figure

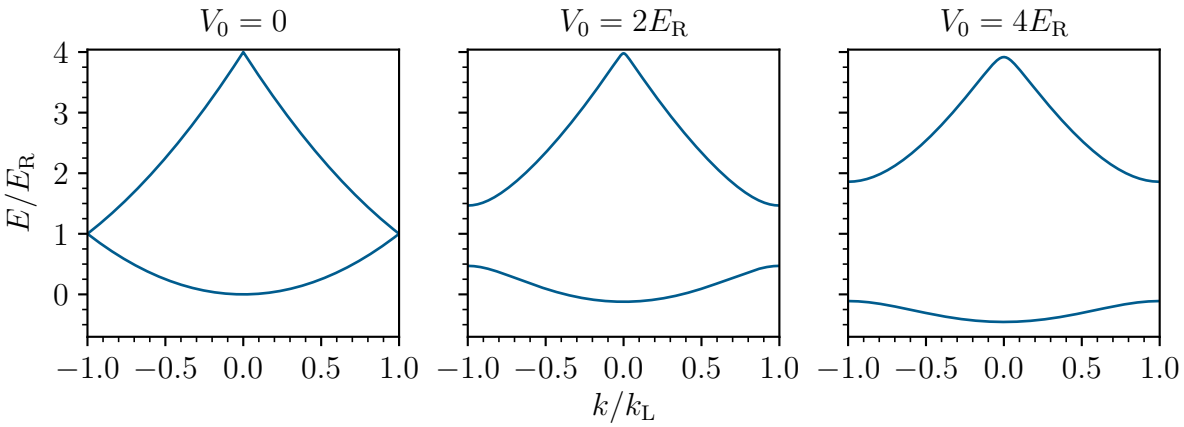

Figure A.1: The lowest bands of the one-dimensional cosine lattice for different lattice depths in the reduced zone scheme.

A.1 shows the two lowest bands for different potential depths $v = V_0/4E_\mathrm{R}$. The second band is simply given by $a_\nu(v)$ as a function of ν in the second Brillouin zone, i.e. for $\nu \in (-2,-1] \cup [1,2)$, and by $b_{\pm 2}(v)$ at the boundary of the second Brillouin zone, where $|\nu| = 2$. In order to get the reduced zone scheme we simply shifted these functions into the first Brillouin zone using the periodicity of the lattice momentum, i.e. identifying ν with $\nu + m$, $m \in \mathbb{Z}$. You can see that for $V_0 = 0$ the dispersion is simply the free dispersion. For increasing V_0 or v we then observe that band gaps open up and we get a band structure.
In summary, we have seen that we can find analytic expressions for the Bloch states and the band structure of the simple cosine lattice. In the lowest band the Bloch states in real space, i.e. the solutions of the dimensionless Schrödinger equation (A.4), are given by:

$$\phi_{\boldsymbol{\nu}}(\boldsymbol{z}) = \mathcal{N}_{\boldsymbol{\nu}} \prod_{i=1}^{d} \left[\mathcal{C}\left(c_{\nu_i}(v), v, z_i\right) + i \sin\left(\nu_i \pi\right) \mathcal{S}\left(c_{\nu_i}\left(v\right), v, z_i\right)\right] \tag{A.14}$$

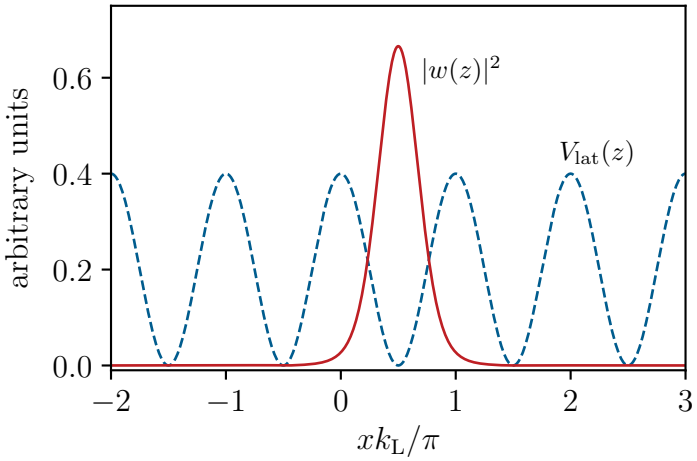

Figure A.2: Wannier function (red solid line) and the shifted lattice potential (blue dashed) in terms of the dimensionless coordinate $z = k_{\mathrm{L}}x$ in units of π.

for given v and $\boldsymbol{\nu} \in [-1, 1]^d$. Here, we defined

$$c_\nu(q) = \begin{cases} a_\nu(v) & \text{for } \nu \in (-1, 1) \\ b_\nu(v) & \text{for } |\nu| = 1 \end{cases} . \tag{A.15}$$

The corresponding energies are given by

$$E(\boldsymbol{\nu}) = \sum_{i=1}^{d} c_{\nu_i}(v), \tag{A.16}$$

for given v. With the Bloch functions we found we can now numerically calculate the Wannier functions (2.25). Figure A.2 shows the probability density of a particle in a Wannier state of the lowest band being at some dimensionless position z, together with the shifted one-dimensional lattice potential.
In section 6.2 we will use the results found in this appendix to calculate J/U in terms of the lattice depth V_0, in order to investigate the temperature as a function of V_0 for fixed entropy and particle number.

Appendix B

Calculation of the Second Order Post Mean-Field Correction for Finite Temperature

In this appendix we want to calculate the second order correction to the grand-canonical partition function and correspondingly to the grand-canonical potential for finite temperature as outlined in section 3.1. Our starting point for this is equation (3.11):

$$\mathcal{Z}_2 = \mathrm{Tr}\left\{ e^{-\beta \hat{H}_{\mathrm{MF}}} \int_0^\beta d\tau \int_0^\tau \mathrm{d}\tau_1 \; e^{\tau \hat{H}_{\mathrm{MF}}} (\hat{H}_{\mathrm{BH}} - \hat{H}_{\mathrm{MF}}) e^{-(\tau-\tau_1)\hat{H}_{\mathrm{MF}}} \right. \\ \left. \times (\hat{H}_{\mathrm{BH}} - \hat{H}_{\mathrm{MF}}) e^{-\tau_1 \hat{H}_{\mathrm{MF}}} \right\}, \tag{B.1}$$

with

$$\hat{H}_{\mathrm{BH}} - \hat{H}_{\mathrm{MF}} = -J \sum_{\langle i,j \rangle \in \Lambda^2} \hat{a}_i^\dagger \hat{a}_j + zJ \sum_{i \in \Lambda} \left(\psi^* \hat{a}_i + \psi \hat{a}_i^\dagger - |\psi|^2 \right). \tag{B.2}$$

When multiplying this out we get

$$\begin{aligned}
\mathcal{Z}_2 = {} & J^2 \sum_{\langle i,j \rangle \in \Lambda^2} \sum_{\langle k,l \rangle \in \Lambda^2} \mathcal{I}_{\hat{a}_i^\dagger \hat{a}_j, \hat{a}_k^\dagger \hat{a}_l} - zJ^2 \psi^* \sum_{\langle i,j \rangle \in \Lambda^2} \sum_{k \in \Lambda} \mathcal{I}_{\hat{a}_i^\dagger \hat{a}_j, \hat{a}_k} - zJ^2 \psi \sum_{\langle i,j \rangle \in \Lambda^2} \sum_{k \in \Lambda} \mathcal{I}_{\hat{a}_i^\dagger \hat{a}_j, \hat{a}_k^\dagger} \\
& - zJ^2 \psi^* \sum_{i \in \Lambda} \sum_{\langle k,l \rangle \in \Lambda^2} \mathcal{I}_{\hat{a}_i, \hat{a}_k^\dagger \hat{a}_l} - zJ^2 \psi \sum_{i \in \Lambda} \sum_{\langle k,l \rangle \in \Lambda^2} \mathcal{I}_{\hat{a}_i^\dagger, \hat{a}_k^\dagger \hat{a}_l} + z^2 J^2 (\psi^*)^2 \sum_{i \in \Lambda} \sum_{k \in \Lambda} \mathcal{I}_{\hat{a}_i, \hat{a}_k} \\
& + z^2 J^2 |\psi|^2 \sum_{i \in \Lambda} \sum_{k \in \Lambda} \mathcal{I}_{\hat{a}_i, \hat{a}_k^\dagger} + z^2 J^2 |\psi|^2 \sum_{i \in \Lambda} \sum_{k \in \Lambda} \mathcal{I}_{\hat{a}_i^\dagger, \hat{a}_k} + z^2 J^2 \psi^2 \sum_{i \in \Lambda} \sum_{k \in \Lambda} \mathcal{I}_{\hat{a}_i^\dagger, \hat{a}_k^\dagger} \\
& + zJ^2 |\psi|^2 \sum_{\langle i,j \rangle \in \Lambda^2} \sum_{k \in \Lambda} \mathcal{I}_{\hat{a}_i^\dagger \hat{a}_j, 1} - z^2 J^2 |\psi|^2 \psi^* \sum_{i \in \Lambda} \sum_{k \in \Lambda} \mathcal{I}_{\hat{a}_i, 1} - z^2 J^2 |\psi|^2 \psi \sum_{i \in \Lambda} \sum_{k \in \Lambda} \mathcal{I}_{\hat{a}_i^\dagger, 1} \\
& + zJ^2 |\psi|^2 \sum_{i \in \Lambda} \sum_{\langle k,l \rangle \in \Lambda^2} \mathcal{I}_{1, \hat{a}_k^\dagger \hat{a}_l} - z^2 J^2 |\psi|^2 \psi^* \sum_{i \in \Lambda} \sum_{k \in \Lambda} \mathcal{I}_{1, \hat{a}_k} - z^2 J^2 |\psi|^2 \psi \sum_{i \in \Lambda} \sum_{k \in \Lambda} \mathcal{I}_{1, \hat{a}_k^\dagger} \\
& + z^2 J^2 |\psi|^4 \sum_{i \in \Lambda} \sum_{k \in \Lambda} \mathcal{I}_{1,1},
\end{aligned} \tag{B.3}$$

with $\mathcal{I}_{\cdot,\cdot}$ as defined in equation (3.12). In section 3.1 we gave a recipe for calculating each of the $\mathcal{I}$s using a diagrammatic representation of the different cases for the involved operators acting on the same site or not. We will now use this recipe

to calculate each of these terms. To make this more clear we will sort the terms depending on the number of diagrams needed.
1 diagram: The simplest term is $\mathcal{I}_{1,1}$ with only the diagram containing no dots. The recipe thus gives

$$\mathcal{I}_{1,1} = \frac{1}{2}\beta^2 \mathcal{Z}_{\mathrm{MF}}. \tag{B.4}$$

For $\mathcal{I}_{\hat{a}_i,1}$ we only have the diagram containing one dot:

$i\bullet$

The recipe gives us

$$\mathcal{I}_{\hat{a}_i,1} = \frac{1}{2}\beta^2 \mathcal{Z}_{\mathrm{MF}}\phi. \tag{B.5}$$

Similarly:

$$\mathcal{I}_{\hat{a}_i^\dagger,1} = \frac{1}{2}\beta^2 \mathcal{Z}_{\mathrm{MF}}\phi^*, \tag{B.6}$$

$$\mathcal{I}_{1,\hat{a}_k} = \frac{1}{2}\beta^2 \mathcal{Z}_{\mathrm{MF}}\phi, \tag{B.7}$$

$$\mathcal{I}_{1,\hat{a}_k^\dagger} = \frac{1}{2}\beta^2 \mathcal{Z}_{\mathrm{MF}}\phi^*. \tag{B.8}$$

For $\mathcal{I}_{\hat{a}_i^\dagger \hat{a}_j,1}$ we only have the diagram with a double dot:

$i\bullet$
$j\bullet$

The recipe gives

$$\mathcal{I}_{\hat{a}_i^\dagger \hat{a}_j,1} = \frac{1}{2}\beta^2 \mathcal{Z}_{\mathrm{MF}}|\phi|^2. \tag{B.9}$$

Similarly:

$$\mathcal{I}_{1,\hat{a}_k^\dagger \hat{a}_l} = \frac{1}{2}\beta^2 \mathcal{Z}_{\mathrm{MF}}|\phi|^2. \tag{B.10}$$

2 diagrams: Terms that gives rise to two diagrams have the form $\mathcal{I}_{\hat{a}_i,\hat{a}_k}$. These terms give rise to two dots that can either be connected or not:

$i\bullet \qquad \bullet\, k \qquad\qquad i\bullet\!\!-\!\!-\!\!-\!\!-\!\!\bullet\, k$

The recipe gives

$$\mathcal{I}_{\hat{a}_i,\hat{a}_k} = (1-\delta_{ik})\frac{1}{2}\beta^2 \mathcal{Z}_{\mathrm{MF}}\phi^2 + \delta_{ik}\mathcal{Z}_{\mathrm{MF,S}}^{N_{\mathrm{S}}-1} S_{\hat{a},\hat{a}}. \tag{B.11}$$

Similarly

$$\mathcal{I}_{\hat{a}_i,\hat{a}_k^\dagger} = (1-\delta_{ik})\frac{1}{2}\beta^2 \mathcal{Z}_{\mathrm{MF}}|\phi|^2 + \delta_{ik}\mathcal{Z}_{\mathrm{MF,S}}^{N_{\mathrm{S}}-1} S_{\hat{a},\hat{a}^\dagger}, \tag{B.12}$$

$$\mathcal{I}_{\hat{a}_i^\dagger,\hat{a}_k} = (1-\delta_{ik})\frac{1}{2}\beta^2 \mathcal{Z}_{\mathrm{MF}}|\phi|^2 + \delta_{ik}\mathcal{Z}_{\mathrm{MF,S}}^{N_{\mathrm{S}}-1} S_{\hat{a}^\dagger,\hat{a}}, \tag{B.13}$$

$$\mathcal{I}_{\hat{a}_i^\dagger,\hat{a}_k^\dagger} = (1-\delta_{ik})\frac{1}{2}\beta^2 \mathcal{Z}_{\mathrm{MF}}(\phi^*)^2 + \delta_{ik}\mathcal{Z}_{\mathrm{MF,S}}^{N_{\mathrm{S}}-1} S_{\hat{a}^\dagger,\hat{a}^\dagger}. \tag{B.14}$$

3 diagrams: The type of term giving rise to three diagrams has the form $\mathcal{I}_{\hat{a}_i^\dagger \hat{a}_j,\hat{a}_k}$. We already calculated this term in detail in section 3.1. With that calculation and

similar ones we get

$$\mathcal{I}_{\hat{a}_i^\dagger \hat{a}_j, \hat{a}_k} = (1-\delta_{ik})(1-\delta_{jk})\frac{1}{2}\beta^2 \mathcal{Z}_{\mathrm{MF}} \phi^2 \phi^* + \delta_{ik} \mathcal{Z}_{\mathrm{MF,S}}^{N_\mathrm{S}-1} S_{\hat{a}^\dagger, \hat{a}} \phi + \delta_{jk} \mathcal{Z}_{\mathrm{MF,S}}^{N_\mathrm{S}-1} S_{\hat{a}, \hat{a}} \phi^*, \tag{B.15}$$

$$\mathcal{I}_{\hat{a}_i^\dagger \hat{a}_j, \hat{a}_k^\dagger} = (1-\delta_{ik})(1-\delta_{jk})\frac{1}{2}\beta^2 \mathcal{Z}_{\mathrm{MF}} \phi (\phi^*)^2 + \delta_{ik} \mathcal{Z}_{\mathrm{MF,S}}^{N_\mathrm{S}-1} S_{\hat{a}^\dagger, \hat{a}^\dagger} \phi + \delta_{jk} \mathcal{Z}_{\mathrm{MF,S}}^{N_\mathrm{S}-1} S_{\hat{a}, \hat{a}^\dagger} \phi^*, \tag{B.16}$$

$$\mathcal{I}_{\hat{a}_i, \hat{a}_k^\dagger \hat{a}_l} = (1-\delta_{ik})(1-\delta_{il})\frac{1}{2}\beta^2 \mathcal{Z}_{\mathrm{MF}} \phi^2 \phi^* + \delta_{ik} \mathcal{Z}_{\mathrm{MF,S}}^{N_\mathrm{S}-1} S_{\hat{a}, \hat{a}^\dagger} \phi + \delta_{il} \mathcal{Z}_{\mathrm{MF,S}}^{N_\mathrm{S}-1} S_{\hat{a}, \hat{a}} \phi^*, \tag{B.17}$$

$$\mathcal{I}_{\hat{a}_i^\dagger, \hat{a}_k^\dagger \hat{a}_l} = (1-\delta_{ik})(1-\delta_{il})\frac{1}{2}\beta^2 \mathcal{Z}_{\mathrm{MF}} \phi (\phi^*)^2 + \delta_{ik} \mathcal{Z}_{\mathrm{MF,S}}^{N_\mathrm{S}-1} S_{\hat{a}^\dagger, \hat{a}^\dagger} \phi + \delta_{il} \mathcal{Z}_{\mathrm{MF,S}}^{N_\mathrm{S}-1} S_{\hat{a}^\dagger, \hat{a}} \phi^*. \tag{B.18}$$

7 diagrams: There is only one term missing: $\mathcal{I}_{\hat{a}_i^\dagger \hat{a}_j, \hat{a}_k^\dagger \hat{a}_l}$. The diagrams it gives rise to consist of two double dots. In total there are seven diagrams emerging from this term:

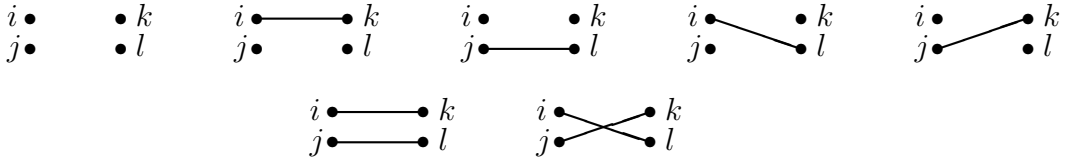

By applying the recipe we get

$$\begin{aligned}\mathcal{I}_{\hat{a}_i^\dagger \hat{a}_j, \hat{a}_k^\dagger \hat{a}_l} = {} & (1-\delta_{ik})(1-\delta_{il})(1-\delta_{jk})(1-\delta_{jl})\frac{1}{2}\beta^2 \mathcal{Z}_{\mathrm{MF}} |\phi|^4 \\ & + \delta_{ik}(1-\delta_{jl}) \mathcal{Z}_{\mathrm{MF,S}}^{N_\mathrm{S}-1} S_{\hat{a}^\dagger, \hat{a}^\dagger} \phi^2 + \delta_{jl}(1-\delta_{ik}) \mathcal{Z}_{\mathrm{MF,S}}^{N_\mathrm{S}-1} S_{\hat{a}, \hat{a}} (\phi^*)^2 \\ & + \delta_{il}(1-\delta_{jk}) \mathcal{Z}_{\mathrm{MF,S}}^{N_\mathrm{S}-1} S_{\hat{a}^\dagger, \hat{a}} |\phi|^2 + \delta_{jk}(1-\delta_{il}) \mathcal{Z}_{\mathrm{MF,S}}^{N_\mathrm{S}-1} S_{\hat{a}, \hat{a}^\dagger} |\phi|^2 \\ & + \delta_{ik}\delta_{jl} \mathcal{Z}_{\mathrm{MF,S}}^{N_\mathrm{S}-2} S_{\hat{a}^\dagger, \hat{a}^\dagger; \hat{a}, \hat{a}} + \delta_{il}\delta_{jk} \mathcal{Z}_{\mathrm{MF,S}}^{N_\mathrm{S}-2} S_{\hat{a}^\dagger, \hat{a}; \hat{a}, \hat{a}^\dagger}.\end{aligned} \tag{B.19}$$

We now have to plug in all of the found $\mathcal{I}$s and evaluate the sums in (B.3). Notice that the only site dependency of the $\mathcal{I}$s comes from the Kronecker deltas. Further we can realize that a lot of the sums appearing are actually the same because we can simply relabel the summation indices:

$$\begin{aligned}\sum_{\langle i,j\rangle \in \Lambda^2} \sum_{\langle k,l\rangle \in \Lambda^2} \delta_{ik}(1-\delta_{jl}) = \sum_{\langle i,j\rangle \in \Lambda^2} \sum_{\langle k,l\rangle \in \Lambda^2} \delta_{jl}(1-\delta_{ik}) = \sum_{\langle i,j\rangle \in \Lambda^2} \sum_{\langle k,l\rangle \in \Lambda^2} \delta_{il}(1-\delta_{jk}) \\ = \sum_{\langle i,j\rangle \in \Lambda^2} \sum_{\langle k,l\rangle \in \Lambda^2} \delta_{jk}(1-\delta_{il}),\end{aligned} \tag{B.20}$$

$$\sum_{\langle i,j\rangle \in \Lambda^2} \sum_{\langle k,l\rangle \in \Lambda^2} \delta_{ik}\delta_{jl} = \sum_{\langle i,j\rangle \in \Lambda^2} \sum_{\langle k,l\rangle \in \Lambda^2} \delta_{il}\delta_{jk}, \tag{B.21}$$

$$\sum_{\langle i,j\rangle \in \Lambda^2} \sum_{k \in \Lambda} (1-\delta_{ik})(1-\delta_{jk}) = \sum_{i \in \Lambda} \sum_{\langle k,l\rangle \in \Lambda^2} (1-\delta_{ik})(1-\delta_{il}), \tag{B.22}$$

$$\sum_{\langle i,j\rangle\in\Lambda^2}\sum_{k\in\Lambda}\delta_{ik}=\sum_{\langle i,j\rangle\in\Lambda^2}\sum_{k\in\Lambda}\delta_{jk}=\sum_{i\in\Lambda}\sum_{\langle k,l\rangle\in\Lambda^2}\delta_{ik}=\sum_{i\in\Lambda}\sum_{\langle k,l\rangle\in\Lambda^2}\delta_{il}, \tag{B.23}$$

$$\sum_{\langle i,j\rangle\in\Lambda^2}\sum_{k\in\Lambda}1=\sum_{i\in\Lambda}\sum_{\langle k,l\rangle\in\Lambda^2}1. \tag{B.24}$$

If we now factor out the sums that are the same we get, after dividing by J^2 for convenience:

$$\begin{aligned}
\frac{\mathcal{Z}_2}{J^2}=&\frac{1}{2}\beta^2\mathcal{Z}_{\mathrm{MF}}|\phi|^4\sum_{\langle i,j\rangle\in\Lambda^2}\sum_{\langle k,l\rangle\in\Lambda^2}(1-\delta_{ik})(1-\delta_{il})(1-\delta_{jk})(1-\delta_{jl})\\
&+\mathcal{Z}_{\mathrm{MF,S}}^{N_\mathrm{S}-1}\left(S_{\hat{a}^\dagger,\hat{a}^\dagger}\phi^2+S_{\hat{a},\hat{a}}(\phi^*)^2+S_{\hat{a}^\dagger,\hat{a}}|\phi|^2+S_{\hat{a},\hat{a}^\dagger}|\phi|^2\right)\\
&\quad\times\sum_{\langle i,j\rangle\in\Lambda^2}\sum_{\langle k,l\rangle\in\Lambda^2}\delta_{ik}(1-\delta_{jl})\\
&+\mathcal{Z}_{\mathrm{MF,S}}^{N_\mathrm{S}-2}\left(S_{\hat{a}^\dagger,\hat{a}^\dagger;\hat{a},\hat{a}}+S_{\hat{a}^\dagger,\hat{a};\hat{a},\hat{a}^\dagger}\right)\sum_{\langle i,j\rangle\in\Lambda^2}\sum_{\langle k,l\rangle\in\Lambda^2}\delta_{ik}\delta_{jl}\\
&-\frac{1}{2}\beta^2\mathcal{Z}_{\mathrm{MF}}z\left(\psi^*\phi^2\phi^*+\psi\phi(\phi^*)^2+\psi^*\phi^2\phi^*+\psi\phi(\phi^*)^2\right)\\
&\quad\times\sum_{\langle i,j\rangle\in\Lambda^2}\sum_{k\in\Lambda}(1-\delta_{ik})(1-\delta_{jk})\\
&-\mathcal{Z}_{\mathrm{MF,S}}^{N_\mathrm{S}-1}z\left(\psi^*\phi S_{\hat{a}^\dagger,\hat{a}}+\psi^*\phi^*S_{\hat{a},\hat{a}}+\psi\phi S_{\hat{a}^\dagger,\hat{a}^\dagger}+\psi\phi^*S_{\hat{a},\hat{a}^\dagger}+\psi^*\phi S_{\hat{a},\hat{a}^\dagger}\right.\\
&\qquad\left.+\psi^*\phi^*S_{\hat{a},\hat{a}}+\psi\phi S_{\hat{a}^\dagger,\hat{a}^\dagger}+\psi\phi^*S_{\hat{a}^\dagger,\hat{a}}\right)\sum_{\langle i,j\rangle\in\Lambda^2}\sum_{k\in\Lambda}\delta_{ik}\\
&+\frac{1}{2}\beta^2\mathcal{Z}_{\mathrm{MF}}z^2\left((\psi^*)^2\phi^2+|\psi|^2|\phi|^2+|\psi|^2|\phi|^2+\psi^2(\phi^*)^2\right)\sum_{i\in\Lambda}\sum_{k\in\Lambda}(1-\delta_{ik})\\
&+\mathcal{Z}_{\mathrm{MF,S}}^{N_\mathrm{S}-1}z^2\left((\psi^*)^2S_{\hat{a},\hat{a}}+|\psi|^2S_{\hat{a},\hat{a}^\dagger}+|\psi|^2S_{\hat{a}^\dagger,\hat{a}}+\psi^2S_{\hat{a}^\dagger,\hat{a}^\dagger}\right)\sum_{i\in\Lambda}\sum_{k\in\Lambda}\delta_{ik}\\
&+\frac{1}{2}\beta^2\mathcal{Z}_{\mathrm{MF}}z\left(|\psi|^2|\phi|^2+|\psi|^2|\phi|^2\right)\sum_{\langle i,j\rangle\in\Lambda^2}\sum_{k\in\Lambda}1\\
&-\frac{1}{2}\beta^2\mathcal{Z}_{\mathrm{MF}}z^2\left(|\psi|^2\psi^*\phi+|\psi|^2\psi\phi^*+|\psi|^2\psi^*\phi+|\psi|^2\psi\phi^*\right)\sum_{i\in\Lambda}\sum_{k\in\Lambda}1\\
&+\frac{1}{2}\beta^2\mathcal{Z}_{\mathrm{MF}}z^2|\psi|^4\sum_{i\in\Lambda}\sum_{k\in\Lambda}1.
\end{aligned} \tag{B.25}$$

Next, we evaluate the sums. To do this we will make use of the definition of the nearest neighbour sum

$$\sum_{\langle i,j\rangle\in\Lambda^2}\equiv\sum_{i\in\Lambda}\sum_{j\in\mathrm{nn}(i)}, \tag{B.26}$$

where $\mathrm{nn}(i)\subset\Lambda$ is the set of nearest neighbour sites of a site $i\in\Lambda$. The evaluation of the sums gives:

$$\sum_{i\in\Lambda}\sum_{k\in\Lambda}1=N_\mathrm{S}^2, \tag{B.27}$$

$$\sum_{\langle i,j\rangle\in\Lambda^2}\sum_{k\in\Lambda}1=\sum_{i\in\Lambda}\sum_{j\in\mathrm{nn}(i)}\sum_{k\in\Lambda}1=N_\mathrm{S}^2z, \tag{B.28}$$

$$\sum_{i\in\Lambda}\sum_{k\in\Lambda}\delta_{ik} = N_\mathrm{S}, \tag{B.29}$$

$$\sum_{i\in\Lambda}\sum_{k\in\Lambda}(1-\delta_{ik}) = \sum_{i\in\Lambda}(N_\mathrm{S}-1) = N_\mathrm{S}(N_\mathrm{S}-1), \tag{B.30}$$

$$\sum_{\langle i,j\rangle\in\Lambda^2}\sum_{k\in\Lambda}\delta_{ik} = \sum_{\langle i,j\rangle}1 = N_\mathrm{S}z, \tag{B.31}$$

$$\sum_{\langle i,j\rangle\in\Lambda^2}\sum_{k\in\Lambda}(1-\delta_{ik})(1-\delta_{jk}) = \sum_{\langle i,j\rangle\in\Lambda^2}(N_\mathrm{S}-2) = N_\mathrm{S}(N_\mathrm{S}-2)z, \tag{B.32}$$

$$\sum_{\langle i,j\rangle\in\Lambda^2}\sum_{\langle k,l\rangle\in\Lambda^2}\delta_{ik}\delta_{jl} = \sum_{\langle i,j\rangle\in\Lambda^2}1 = N_\mathrm{S}z, \tag{B.33}$$

$$\begin{aligned}\sum_{\langle i,j\rangle\in\Lambda^2}\sum_{\langle k,l\rangle\in\Lambda^2}\delta_{ik}(1-\delta_{jl}) &= \sum_{i\in\Lambda}\sum_{j\in\mathrm{nn}(i)}\sum_{l\in\mathrm{nn}(i)}(1-\delta_{jl}) = \sum_{i\in\Lambda}\sum_{j\in\mathrm{nn}(i)}(z-1)\\ &= N_\mathrm{S}z(z-1).\end{aligned} \tag{B.34}$$

To calculate the missing sum we multiply out the brackets and again notice that we can simplify by relabeling indices:

$$\begin{aligned}&\sum_{\langle i,j\rangle\in\Lambda^2}\sum_{\langle k,l\rangle\in\Lambda^2}(1-\delta_{ik})(1-\delta_{jl})(1-\delta_{jk})(1-\delta_{il})\\ &\quad= \sum_{\langle i,j\rangle\in\Lambda^2}\sum_{\langle k,l\rangle\in\Lambda^2}(1-\delta_{ik}-\delta_{il}+\underbrace{\delta_{ik}\delta_{il}}_{=0})(1-\delta_{jk}-\delta_{jl}+\underbrace{\delta_{jk}\delta_{jl}}_{=0})\\ &\quad= \sum_{\langle i,j\rangle\in\Lambda^2}\sum_{\langle k,l\rangle\in\Lambda^2}\big[1-(\delta_{jk}+\delta_{jl}+\delta_{ik}+\delta_{il})+\underbrace{\delta_{ik}\delta_{jk}}_{=0}+\delta_{ik}\delta_{jl}+\delta_{il}\delta_{jk}+\underbrace{\delta_{il}\delta_{jl}}_{=0}\big]\\ &\quad= \sum_{\langle i,j\rangle\in\Lambda^2}\sum_{\langle k,l\rangle\in\Lambda^2}(1-4\delta_{ik}+2\delta_{ik}\delta_{jl})\\ &\quad= N_\mathrm{S}^2z^2-4N_\mathrm{S}z^2+2N_\mathrm{S}z.\end{aligned} \tag{B.35}$$

Now we need to plug in the results for the sums and simplify the expression we get. We can distinguish the terms into three categories: the ones with a factor of $\frac{1}{2}\beta^2\mathcal{Z}_\mathrm{MF}$, coming from the disconnected terms, the ones with a factor of $\mathcal{Z}_\mathrm{MF,S}^{N_\mathrm{S}-1}$, coming from the diagrams with one connection, and the ones with a factor of $\mathcal{Z}_\mathrm{MF,S}^{N_\mathrm{S}-2}$, coming from the diagrams with two connections. As terms from different categories will never mix we can evaluate them independently.

(terms in $\mathcal{Z}_2/J^2$ coming from disconnected diagrams)

$$
\begin{aligned}
&= \frac{1}{2}\beta^2 \mathcal{Z}_{\mathrm{MF}} \left\{ |\phi|^4 \left(N_{\mathrm{S}}^2 z^2 - 4N_{\mathrm{S}} z^2 + 2N_{\mathrm{S}} z \right) - 2\left(|\phi|^2 \phi\psi^* + |\phi|^2 \phi^* \psi \right) N_{\mathrm{S}}(N_{\mathrm{S}} - 2) z^2 \right. \\
&\quad + \left((\psi^*)^2 \phi^2 + 2|\psi|^2 |\phi|^2 + \psi^2 (\phi^*)^2 \right) N_{\mathrm{S}}(N_{\mathrm{S}} - 1) z^2 + 2|\psi|^2 |\phi|^2 N_{\mathrm{S}}^2 z^2 \\
&\quad \left. -2(|\psi|^2 \psi^* \phi + |\psi|^2 \psi\phi^*) N_{\mathrm{S}}^2 z^2 + |\psi|^4 N_{\mathrm{S}}^2 z^2 \right\} \\
&= \frac{1}{2}\beta^2 \mathcal{Z}_{\mathrm{MF}} \left\{ N_{\mathrm{S}}^2 z^2 \left(|\phi|^4 - 2|\phi|^2 \phi\psi^* - 2|\phi|^2 \phi^* \psi + (\psi^*)^2 \phi^2 + 4|\psi|^2 |\phi|^2 + \psi^2 (\phi^*)^2 \right. \right. \\
&\qquad \left. -2|\psi|^2 \psi^* \phi - 2|\psi|^2 \psi\phi^* + |\psi|^4 \right) \\
&\quad + N_{\mathrm{S}} z^2 \left(-4|\phi|^4 + 4\left(|\phi|^2 \phi\psi^* + |\phi|^2 \phi^* \psi \right) - \left((\psi^*)^2 \phi^2 + 2|\psi|^2 |\phi|^2 + \psi^2 (\phi^*)^2 \right) \right) \\
&\quad \left. + 2N_{\mathrm{S}} z |\phi|^4 \right\} \\
&= \frac{1}{2}\beta^2 \mathcal{Z}_{\mathrm{MF}} \left\{ N_{\mathrm{S}}^2 z^2 |\phi - \psi|^4 - N_{\mathrm{S}} z^2 \left[(2\phi - \psi)\phi^* - \phi\psi^* \right]^2 + 2N_{\mathrm{S}} z |\phi|^4 \right\}, \qquad \text{(B.36)}
\end{aligned}
$$

(terms in $\mathcal{Z}_2/J^2$ coming from diagrams with one connection)

$$
\begin{aligned}
&= \mathcal{Z}_{\mathrm{MF,S}}^{N_{\mathrm{S}}-1} \left\{ \left(S_{\hat{a}^\dagger,\hat{a}^\dagger} \phi^2 + S_{\hat{a},\hat{a}} (\phi^*)^2 + S_{\hat{a}^\dagger,\hat{a}} |\phi|^2 + S_{\hat{a},\hat{a}^\dagger} |\phi|^2 \right) N_{\mathrm{S}} z(z-1) \right. \\
&\quad - \left(S_{\hat{a}^\dagger,\hat{a}} \psi^* \phi + S_{\hat{a},\hat{a}^\dagger} \psi\phi^* + S_{\hat{a},\hat{a}^\dagger} \psi^* \phi + S_{\hat{a}^\dagger,\hat{a}} \psi\phi^* + 2S_{\hat{a},\hat{a}} \psi^* \phi^* + 2S_{\hat{a}^\dagger,\hat{a}^\dagger} \psi\phi \right) N_{\mathrm{S}} z^2 \\
&\quad \left. + \left((\psi^*)^2 S_{\hat{a},\hat{a}} + |\psi|^2 S_{\hat{a},\hat{a}^\dagger} + |\psi|^2 S_{\hat{a}^\dagger,\hat{a}} + \psi^2 S_{\hat{a}^\dagger,\hat{a}^\dagger} \right) N_{\mathrm{S}} z^2 \right\} \\
&= \mathcal{Z}_{\mathrm{MF,S}}^{N_{\mathrm{S}}-1} \left\{ N_{\mathrm{S}} z^2 \left[S_{\hat{a},\hat{a}} \left((\phi^*)^2 - 2\psi^* \phi^* + (\psi^*)^2 \right) + S_{\hat{a},\hat{a}^\dagger} \left(|\phi|^2 - \psi\phi^* - \psi^* \phi + |\psi|^2 \right) \right. \right. \\
&\qquad \left. + S_{\hat{a}^\dagger,\hat{a}} \left(|\phi|^2 - \psi^* \phi - \psi\phi^* + |\psi|^2 \right) + S_{\hat{a}^\dagger,\hat{a}^\dagger} \left(\phi^2 + 2\psi\phi + \psi^2 \right) \right] \\
&\quad \left. - N_{\mathrm{S}} z \left(S_{\hat{a},\hat{a}} (\phi^*)^2 + S_{\hat{a},\hat{a}^\dagger} |\phi|^2 + S_{\hat{a}^\dagger,\hat{a}} |\phi|^2 + S_{\hat{a}^\dagger,\hat{a}^\dagger} \phi^2 \right) \right\} \\
&= \mathcal{Z}_{\mathrm{MF,S}}^{N_{\mathrm{S}}-1} \left\{ N_{\mathrm{S}} z^2 \left(S_{\hat{a},\hat{a}} (\phi^* - \psi^*)^2 + S_{\hat{a},\hat{a}^\dagger} |\phi - \psi|^2 + S_{\hat{a}^\dagger,\hat{a}} |\phi - \psi|^2 + S_{\hat{a}^\dagger,\hat{a}^\dagger} (\phi - \psi)^2 \right) \right. \\
&\quad \left. - N_{\mathrm{S}} z \left(S_{\hat{a},\hat{a}} (\phi^*)^2 + S_{\hat{a},\hat{a}^\dagger} |\phi|^2 + S_{\hat{a}^\dagger,\hat{a}} |\phi|^2 + S_{\hat{a}^\dagger,\hat{a}^\dagger} \phi^2 \right) \right\}, \qquad \text{(B.37)}
\end{aligned}
$$

(terms in $\mathcal{Z}_2/J^2$ coming from diagrams with two connections)

$$
= \mathcal{Z}_{\mathrm{MF,S}}^{N_{\mathrm{S}}-2} N_{\mathrm{S}} z \left(S_{\hat{a}^\dagger,\hat{a}^\dagger;\hat{a},\hat{a}} + S_{\hat{a}^\dagger,\hat{a};\hat{a},\hat{a}^\dagger} \right). \qquad \text{(B.38)}
$$

After multiplying with J^2, because we computed $\mathcal{Z}_2/J^2$, and adding the zeroth and first order which we found in section 3.1 we end up with the result for the grand-canonical potential given in equation (3.27):

$$
\begin{aligned}
\mathcal{Z}_{\leq 2} = \mathcal{Z}_{\mathrm{MF}} \Bigg\{ & 1 + \beta J N_{\mathrm{S}} z |\psi - \phi|^2 + \frac{1}{2}\beta^2 J^2 \left\{ 2N_{\mathrm{S}} z |\phi|^4 - N_{\mathrm{S}} z^2 \left[(2\phi - \psi)\phi^* - \phi\psi^* \right]^2 \right. \\
& \qquad \left. + N_{\mathrm{S}}^2 z^2 |\phi - \psi|^4 \right\} \\
& + \mathcal{Z}_{\mathrm{MF,S}}^{-1} J^2 \left\{ N_{\mathrm{S}} z^2 \left[S_{\hat{a},\hat{a}} (\phi^* - \psi^*)^2 + S_{\hat{a},\hat{a}^\dagger} |\phi - \psi|^2 + S_{\hat{a}^\dagger,\hat{a}} |\phi - \psi|^2 \right. \right. \\
& \qquad \left. + S_{\hat{a}^\dagger,\hat{a}^\dagger} (\phi - \psi)^2 \right] \\
& \qquad \left. - N_{\mathrm{S}} z \left[S_{\hat{a},\hat{a}} (\phi^*)^2 + S_{\hat{a},\hat{a}^\dagger} |\phi|^2 + S_{\hat{a}^\dagger,\hat{a}} |\phi|^2 + S_{\hat{a}^\dagger,\hat{a}^\dagger} \phi^2 \right] \right\} \\
& + \mathcal{Z}_{\mathrm{MF,S}}^{-2} J^2 N_{\mathrm{S}} z (S_{\hat{a}^\dagger,\hat{a};\hat{a},\hat{a}^\dagger} + S_{\hat{a}^\dagger,\hat{a}^\dagger;\hat{a},\hat{a}}) \Bigg\}. \qquad \text{(B.39)}
\end{aligned}
$$

Appendix C

Calculation of the Second Order Post Mean-Field Correction for Zero Temperature

In this appendix we want to calculate the second-order post mean-field correction to the ground-state energy, after including the $-\mu\hat{N}$ term in the Hamiltonian, for zero temperature using non-degenerate perturbation theory as outlined in section 3.4. To this end we will proceed completely analogous to the finite-temperature calculation in appendix B.
The second order correction to the ground state energy in non-degenerate perturbation theory is given by

$$E_{0,2} = \sum_{\vec{n}\in\mathbb{N}^{N_S}\setminus\{\vec{0}\}} \frac{|\langle\chi_{\vec{n}}|\hat{H}_{\mathrm{BH}} - \hat{H}_{\mathrm{MF}}|\chi_{\vec{0}}\rangle|^2}{\epsilon_{\vec{0}} - \epsilon_{\vec{n}}}, \tag{C.1}$$

with

$$\hat{H}_{\mathrm{BH}} - \hat{H}_{\mathrm{MF}} = -J\sum_{\langle i,j\rangle\in\Lambda^2} \hat{a}_i^\dagger\hat{a}_j + zJ\sum_{i\in\Lambda}\left(\psi^*\hat{a}_i + \psi\hat{a}_i^\dagger - |\psi|^2\right). \tag{C.2}$$

If we now multiply this out we get an expression completely analogous to the finite-temperature case:

$$\begin{aligned}
E_{0,2} = {} & J^2\sum_{\langle i,j\rangle\in\Lambda^2}\sum_{\langle k,l\rangle\in\Lambda^2}\mathcal{T}_{\hat{a}_i^\dagger\hat{a}_j,\hat{a}_k^\dagger\hat{a}_l} - zJ^2\psi^*\sum_{\langle i,j\rangle\in\Lambda^2}\sum_{k\in\Lambda}\mathcal{T}_{\hat{a}_i^\dagger\hat{a}_j,\hat{a}_k} - zJ^2\psi\sum_{\langle i,j\rangle\in\Lambda^2}\sum_{k\in\Lambda}\mathcal{T}_{\hat{a}_i^\dagger\hat{a}_j,\hat{a}_k^\dagger} \\
& - zJ^2\psi^*\sum_{i\in\Lambda}\sum_{\langle k,l\rangle\in\Lambda^2}\mathcal{T}_{\hat{a}_i,\hat{a}_k^\dagger\hat{a}_l} - zJ^2\psi\sum_{i\in\Lambda}\sum_{\langle k,l\rangle\in\Lambda^2}\mathcal{T}_{\hat{a}_i^\dagger,\hat{a}_k^\dagger\hat{a}_l} + z^2J^2(\psi^*)^2\sum_{i\in\Lambda}\sum_{k\in\Lambda}\mathcal{T}_{\hat{a}_i,\hat{a}_k} \\
& + z^2J^2|\psi|^2\sum_{i\in\Lambda}\sum_{k\in\Lambda}\mathcal{T}_{\hat{a}_i,\hat{a}_k^\dagger} + z^2J^2|\psi|^2\sum_{i\in\Lambda}\sum_{k\in\Lambda}\mathcal{T}_{\hat{a}_i^\dagger,\hat{a}_k} + z^2J^2\psi^2\sum_{i\in\Lambda}\sum_{k\in\Lambda}\mathcal{T}_{\hat{a}_i^\dagger,\hat{a}_k^\dagger} \\
& + zJ^2|\psi|^2\sum_{\langle i,j\rangle\in\Lambda^2}\sum_{k\in\Lambda}\mathcal{T}_{\hat{a}_i^\dagger\hat{a}_j,1} - z^2J^2|\psi|^2\psi^*\sum_{i\in\Lambda}\sum_{k\in\Lambda}\mathcal{T}_{\hat{a}_i,1} - z^2J^2|\psi|^2\psi\sum_{i\in\Lambda}\sum_{k\in\Lambda}\mathcal{T}_{\hat{a}_i^\dagger,1} \\
& + zJ^2|\psi|^2\sum_{i\in\Lambda}\sum_{\langle k,l\rangle\in\Lambda^2}\mathcal{T}_{1,\hat{a}_k^\dagger\hat{a}_l} - z^2J^2|\psi|^2\psi^*\sum_{i\in\Lambda}\sum_{k\in\Lambda}\mathcal{T}_{1,\hat{a}_k} - z^2J^2|\psi|^2\psi\sum_{i\in\Lambda}\sum_{k\in\Lambda}\mathcal{T}_{1,\hat{a}_k^\dagger} \\
& + z^2J^2|\psi|^4\sum_{i\in\Lambda}\sum_{k\in\Lambda}\mathcal{T}_{1,1},
\end{aligned} \tag{C.3}$$

with $\mathcal{T}_{\cdot,\cdot}$ as defined in equation (3.47). We can now again calculate each of these terms using the recipe from section 3.4. Because the diagrams are the same as in the finite-temperature case and only the translation from a diagram to the corresponding expression is different, we will not give the diagrams again as they were already shown in appendix B. Here we will simply give the result of the recipe for all $\mathcal{T}$. Note that the expressions will be simpler than in the finite-temperature case as the disconnected diagrams do not contribute. In particular, all $\mathcal{T}$s with the identity operator in at least one of their arguments are identically zero. The remaining $\mathcal{T}$s are given by:

$$\mathcal{T}_{\hat{a}_i,\hat{a}_k} = \delta_{ik} S^{(0)}_{\hat{a},\hat{a}}, \tag{C.4}$$

$$\mathcal{T}_{\hat{a}_i,\hat{a}_k^\dagger} = \delta_{ik} S^{(0)}_{\hat{a},\hat{a}^\dagger}, \tag{C.5}$$

$$\mathcal{T}_{\hat{a}_i^\dagger,\hat{a}_k} = \delta_{ik} S^{(0)}_{\hat{a}^\dagger,\hat{a}}, \tag{C.6}$$

$$\mathcal{T}_{\hat{a}_i^\dagger,\hat{a}_k^\dagger} = \delta_{ik} S^{(0)}_{\hat{a}^\dagger,\hat{a}^\dagger}, \tag{C.7}$$

$$\mathcal{T}_{\hat{a}_i^\dagger\hat{a}_j,\hat{a}_k} = \delta_{ik} S^{(0)}_{\hat{a}^\dagger,\hat{a}}\phi + \delta_{jk} S^{(0)}_{\hat{a},\hat{a}}\phi^*, \tag{C.8}$$

$$\mathcal{T}_{\hat{a}_i^\dagger\hat{a}_j,\hat{a}_k^\dagger} = \delta_{ik} S^{(0)}_{\hat{a}^\dagger,\hat{a}^\dagger}\phi + \delta_{jk} S^{(0)}_{\hat{a},\hat{a}^\dagger}\phi^*, \tag{C.9}$$

$$\mathcal{T}_{\hat{a}_i,\hat{a}_k^\dagger\hat{a}_l} = \delta_{ik} S^{(0)}_{\hat{a},\hat{a}^\dagger}\phi + \delta_{il} S^{(0)}_{\hat{a},\hat{a}}\phi^*, \tag{C.10}$$

$$\mathcal{T}_{\hat{a}_i^\dagger,\hat{a}_k^\dagger\hat{a}_l} = \delta_{ik} S^{(0)}_{\hat{a}^\dagger,\hat{a}^\dagger}\phi + \delta_{il} S^{(0)}_{\hat{a}^\dagger,\hat{a}}\phi^*, \tag{C.11}$$

$$\begin{aligned}\mathcal{T}_{\hat{a}_i^\dagger\hat{a}_j,\hat{a}_k^\dagger\hat{a}_l} = {} & \delta_{ik}(1-\delta_{jl}) S^{(0)}_{\hat{a}^\dagger,\hat{a}^\dagger}\phi^2 + \delta_{jl}(1-\delta_{ik}) S^{(0)}_{\hat{a},\hat{a}}(\phi^*)^2 \\ & + \delta_{il}(1-\delta_{jk}) S^{(0)}_{\hat{a}^\dagger,\hat{a}}|\phi|^2 + \delta_{jk}(1-\delta_{il}) S^{(0)}_{\hat{a},\hat{a}^\dagger}|\phi|^2 \\ & + \delta_{ik}\delta_{jl} S^{(0)}_{\hat{a}^\dagger,\hat{a}^\dagger;\hat{a},\hat{a}} + \delta_{il}\delta_{jk} S^{(0)}_{\hat{a}^\dagger,\hat{a};\hat{a}^\dagger,\hat{a}}.\end{aligned} \tag{C.12}$$

As in the finite-temperature calculation we now have to evaluate the sums. Again many of these sums are the same after relabeling indices so we can factor them out:

$$\begin{aligned}\frac{E_{0,2}}{J^2} = {} & \left(S^{(0)}_{\hat{a}^\dagger,\hat{a}^\dagger}\phi^2 + S^{(0)}_{\hat{a},\hat{a}}(\phi^*)^2 + S^{(0)}_{\hat{a}^\dagger,\hat{a}}|\phi|^2 + S^{(0)}_{\hat{a},\hat{a}^\dagger}|\phi|^2\right) \sum_{\langle i,j\rangle\in\Lambda^2} \sum_{\langle k,l\rangle\in\Lambda^2} \delta_{ik}(1-\delta_{jl}) \\ & + \left(S^{(0)}_{\hat{a}^\dagger,\hat{a}^\dagger;\hat{a},\hat{a}} + S^{(0)}_{\hat{a}^\dagger,\hat{a};\hat{a},\hat{a}^\dagger}\right) \sum_{\langle i,j\rangle\in\Lambda^2} \sum_{\langle k,l\rangle\in\Lambda^2} \delta_{ik}\delta_{jl} \\ & - z\left(S^{(0)}_{\hat{a}^\dagger,\hat{a}}\psi^*\phi + S^{(0)}_{\hat{a},\hat{a}}\psi^*\phi^* + S^{(0)}_{\hat{a}^\dagger,\hat{a}^\dagger}\psi\phi + S^{(0)}_{\hat{a},\hat{a}^\dagger}\psi\phi^* + S^{(0)}_{\hat{a},\hat{a}^\dagger}\psi^*\phi + S^{(0)}_{\hat{a},\hat{a}}\psi^*\phi^*\right. \\ & \qquad \left. + S^{(0)}_{\hat{a}^\dagger,\hat{a}^\dagger}\psi\phi + S^{(0)}_{\hat{a}^\dagger,\hat{a}}\psi\phi^*\right) \sum_{\langle i,j\rangle\in\Lambda^2} \sum_{k\in\Lambda} \delta_{ik} \\ & + z^2\left(S^{(0)}_{\hat{a},\hat{a}}(\psi^*)^2 + S^{(0)}_{\hat{a},\hat{a}^\dagger}|\psi|^2 + S^{(0)}_{\hat{a}^\dagger,\hat{a}}|\psi|^2 + S^{(0)}_{\hat{a}^\dagger,\hat{a}^\dagger}\psi^2\right) \sum_{i\in\Lambda} \sum_{k\in\Lambda} \delta_{ik}.\end{aligned} \tag{C.13}$$

We can now plug in the results for the sums found in appendix B, i.e. equations (B.29), (B.31), (B.33), (B.34), and simplify.

$$\begin{aligned}
\frac{E_{0,2}}{J^2} &= N_{\mathrm{S}} z^2 \Big[S^{(0)}_{\hat{a}^\dagger,\hat{a}^\dagger}\phi^2 + S^{(0)}_{\hat{a},\hat{a}}(\phi^*)^2 + S^{(0)}_{\hat{a}^\dagger,\hat{a}}|\phi|^2 + S^{(0)}_{\hat{a},\hat{a}^\dagger}|\phi|^2 \\
&\qquad - \Big(S^{(0)}_{\hat{a}^\dagger,\hat{a}}\psi^*\phi + 2S^{(0)}_{\hat{a},\hat{a}}\psi^*\phi^* + 2S^{(0)}_{\hat{a}^\dagger,\hat{a}^\dagger}\psi\phi + S^{(0)}_{\hat{a},\hat{a}^\dagger}\psi\phi^* + S^{(0)}_{\hat{a},\hat{a}^\dagger}\psi^*\phi + S^{(0)}_{\hat{a}^\dagger,\hat{a}}\psi\phi^* \Big) \\
&\qquad + S^{(0)}_{\hat{a},\hat{a}}(\psi^*)^2 + S^{(0)}_{\hat{a},\hat{a}^\dagger}|\psi|^2 + S^{(0)}_{\hat{a}^\dagger,\hat{a}}|\psi|^2 + S^{(0)}_{\hat{a}^\dagger,\hat{a}^\dagger}\psi^2 \Big] \\
&\quad + N_{\mathrm{S}} z \Big[S^{(0)}_{\hat{a}^\dagger,\hat{a}^\dagger;\hat{a},\hat{a}} + S^{(0)}_{\hat{a}^\dagger,\hat{a};\hat{a},\hat{a}^\dagger} - \Big(S^{(0)}_{\hat{a}^\dagger,\hat{a}^\dagger}\phi^2 + S^{(0)}_{\hat{a},\hat{a}}(\phi^*)^2 + S^{(0)}_{\hat{a}^\dagger,\hat{a}}|\phi|^2 + S^{(0)}_{\hat{a},\hat{a}^\dagger}|\phi|^2 \Big) \Big] \\
&= N_{\mathrm{S}} z^2 \Big[S^{(0)}_{\hat{a},\hat{a}} \left((\phi^*)^2 - 2\psi^*\phi^* + (\psi^*)^2 \right) + S^{(0)}_{\hat{a},\hat{a}^\dagger} \left(|\phi|^2 - \psi\phi^* - \psi^*\phi + |\psi|^2 \right) \\
&\qquad + S^{(0)}_{\hat{a}^\dagger,\hat{a}} \left(|\phi|^2 - \psi^*\phi - \psi\phi^* + |\psi|^2 \right) + S^{(0)}_{\hat{a}^\dagger,\hat{a}^\dagger} \left(\phi^2 - \psi\phi - \psi\phi + \psi^2 \right) \Big] \\
&\quad + N_{\mathrm{S}} z \left(\tilde{S}^{(0)}_{\hat{a}^\dagger,\hat{a}^\dagger;\hat{a},\hat{a}} + \tilde{S}^{(0)}_{\hat{a}^\dagger,\hat{a};\hat{a},\hat{a}^\dagger} \right) \\
&= N_{\mathrm{S}} z^2 \Big[S^{(0)}_{\hat{a},\hat{a}} \left(\phi^* - \psi^* \right)^2 + S^{(0)}_{\hat{a},\hat{a}^\dagger}|\phi - \psi|^2 + S^{(0)}_{\hat{a}^\dagger,\hat{a}}|\phi - \psi|^2 + S^{(0)}_{\hat{a}^\dagger,\hat{a}^\dagger} \left(\phi - \psi \right)^2 \Big] \\
&\quad + N_{\mathrm{S}} z \left(\tilde{S}^{(0)}_{\hat{a}^\dagger,\hat{a}^\dagger;\hat{a},\hat{a}} + \tilde{S}^{(0)}_{\hat{a}^\dagger,\hat{a};\hat{a},\hat{a}^\dagger} \right). \qquad \text{(C.14)}
\end{aligned}$$

After multiplying by J^2 and adding the zeroth and first orders found in section 3.4 we find the result (3.58) also given in that section:

$$\begin{aligned}
E_{0,\leq 2} &= \epsilon_{\vec{0}} - JN_{\mathrm{S}} z|\psi - \phi|^2 + J^2 N_{\mathrm{S}} z \left(\tilde{S}^{(0)}_{\hat{a}^\dagger,\hat{a};\hat{a},\hat{a}^\dagger} + \tilde{S}^{(0)}_{\hat{a}^\dagger,\hat{a}^\dagger;\hat{a},\hat{a}} \right) \\
&\quad + J^2 N_{\mathrm{S}} z^2 \Big\{ S^{(0)}_{\hat{a},\hat{a}}(\phi^* - \psi^*)^2 + S^{(0)}_{\hat{a},\hat{a}^\dagger}|\phi - \psi|^2 + S^{(0)}_{\hat{a}^\dagger,\hat{a}}|\phi - \psi|^2 \\
&\qquad + S^{(0)}_{\hat{a}^\dagger,\hat{a}^\dagger}(\phi - \psi)^2 \Big\}. \qquad \text{(C.15)}
\end{aligned}$$

Appendix D

Including Infinite-Range Hopping

In the derivation of the Bose-Hubbard model in section 2.3, we restricted to nearest-neighbour hopping, i.e. we only considered the possibility of a particle hopping from one site to a nearest-neighbour one. In reality however the wave functions of the particles might be delocalized over multiple lattice sites, such that there is a non-negligible possibility of the particles also hopping to lattice sites, which are further away. In this appendix we want to investigate how we can take into account infinite-range hopping, i.e. we want to consider the possibility of particles hopping from one site to an arbitrary other one. To this end we lift the restriction of summing only over nearest-neighbour pairs in the hopping term:

$$\sum_{\langle i,j\rangle\in\Lambda^2} J\hat{a}_i^\dagger\hat{a}_j \longrightarrow \sum_{(i,j)\in\Lambda^2\setminus\Delta(\Lambda)} J_{ij}\hat{a}_i^\dagger\hat{a}_j, \tag{D.1}$$

where $\Delta(\Lambda) = \{(i,i) \mid i \in \Lambda\} \subset \Lambda^2$ is the diagonal of the lattice. We still exclude the diagonal terms, i.e. the ones with $i = j$, because we absorbed them into the chemical potential. In the following we will restrict to lattice potentials of the form $V_{\text{lat}}(\boldsymbol{x}) = \sum_{i=1}^d V_{\text{lat}}^{(i)}(x_i)$ like the cosine lattice we investigated in appendix A. We already saw in section 2.3 that in this case J_{ij} only depends on the distance $\boldsymbol{x}_i - \boldsymbol{x}_j$:

$$J_{ij} = -\frac{1}{N_{\text{S}}}\sum_{\boldsymbol{k}\in 1.\text{BZ}} E(\boldsymbol{k})e^{i\boldsymbol{k}\cdot(\boldsymbol{x}_i-\boldsymbol{x}_j)}. \tag{D.2}$$

Note that the symmetry of J_{ij}, which is needed for the Hamiltonian to be Hermitian, implies that the dispersion $E(\boldsymbol{k})$ is an even function of $\boldsymbol{k}$.
We will now show that including infinite-range hopping actually does not have any effect on the mean-field results apart from changing the dependency of J on the dispersion. To see this we take a look at the approximation we made to get from the Bose-Hubbard Hamiltonian to the mean-field one. There we used for small fluctuations:

$$\hat{a}_i^\dagger\hat{a}_j \approx \langle\hat{a}_i^\dagger\rangle\hat{a}_j + \langle\hat{a}_j\rangle\hat{a}_i^\dagger - \langle\hat{a}_i^\dagger\rangle\langle\hat{a}_j\rangle. \tag{D.3}$$

If we now use this in the case of infinite-range hopping we get, after relabeling indices and using that J_{ij} is symmetric in i, j,

$$\sum_{(i,j)\in\Lambda^2\setminus\Delta(\Lambda)} J_{ij}\hat{a}_i^\dagger\hat{a}_j \approx \sum_{i\in\Lambda}\left(\sum_{j\in\Lambda\setminus\{i\}} J_{ij}\right)\left(\psi^*\hat{a}_i + \psi\hat{a}_i^\dagger - |\psi|^2\right). \tag{D.4}$$

With the definition $J_1 = \sum_{j\in\Lambda\setminus\{i\}} J_{ij}$ we thus recover the ordinary mean-field Hamiltonian by the substitution $J_1 \to zJ$. Note that J_1 does not depend on i as J_{ij} only depends on $\boldsymbol{x}_i - \boldsymbol{x}_j$. So we can without loss of generality take i such that $\boldsymbol{x}_i = \mathbf{0}$, which always exists as we can simply shift the coordinate system. Using this we can find a simple expression for J_1 depending only on the dispersion:

$$J_1 = \sum_{j\in\Lambda\setminus\{i\}} J_{ij} = -\frac{1}{N_\mathrm{S}} \sum_{j\in\Lambda\setminus\{i\}} \sum_{\boldsymbol{k}\in 1.\mathrm{BZ}} E(\boldsymbol{k}) e^{-i\boldsymbol{k}\cdot\boldsymbol{x}_j} \tag{D.5}$$

$$= -\frac{1}{N_\mathrm{S}} \sum_{j\in\Lambda} \sum_{\boldsymbol{k}\in 1.\mathrm{BZ}} E(\boldsymbol{k}) e^{-i\boldsymbol{k}\cdot\boldsymbol{x}_j} + \frac{1}{N_\mathrm{S}} \sum_{\boldsymbol{k}\in 1.\mathrm{BZ}} E(\boldsymbol{k}) \tag{D.6}$$

$$= \bar{E} - E(\mathbf{0}), \tag{D.7}$$

where we used the well-known relation

$$\sum_{j\in\Lambda} e^{-i\boldsymbol{k}\cdot\boldsymbol{x}_j} = N_\mathrm{S}\delta_{\boldsymbol{k},\mathbf{0}} \tag{D.8}$$

and defined the arithmetic mean

$$\bar{E} = \frac{1}{N_\mathrm{S}} \sum_{\boldsymbol{k}\in 1.\mathrm{BZ}} E(\boldsymbol{k}). \tag{D.9}$$

We will now investigate which influence infinite-range hopping has on the corrected results. Here we can not simply replace all zJs with J_1 because we also had to evaluate additional sums over hopping terms in calculating the corrections and we first need to investigate what happens to them. However it is clear that the only thing that changes in the steps we did in appendix B is the evaluation of the sums. More precisely only the sums including at least one nearest-neighbour sum, coming from a hopping term. We will now reevaluate these sums including infinite-range hopping. In the other terms we can simply substitute $zJ \to J_1$ as these terms come from the mean-field part of $\hat{H}_\mathrm{BH} - \hat{H}_\mathrm{MF}$, see equation (B.2). The reevaluated sums give:

$$\sum_{(i,j)\in\Lambda^2\setminus\Delta(\Lambda)} \sum_{k\in\Lambda} J_{ij} = \sum_{i\in\Lambda}\sum_{k\in\Lambda} \left(\sum_{j\in\Lambda\setminus\{i\}} J_{ij} \right) \equiv N_\mathrm{S}^2 J_1 \tag{D.10}$$

$$\sum_{(i,j)\in\Lambda^2\setminus\Delta(\Lambda)} \sum_{k\in\Lambda} \delta_{ik} J_{ij} = \sum_{i\in\Lambda} \left(\sum_{j\in\Lambda\setminus\{i\}} J_{ij} \right) \equiv N_\mathrm{S} J_1 \tag{D.11}$$

$$\sum_{(i,j)\in\Lambda^2\setminus\Delta(\Lambda)} \sum_{k\in\Lambda} (1-\delta_{ik})(1-\delta_{jk}) J_{ij} = (N_\mathrm{S}-2) \sum_{i\in\Lambda} \left(\sum_{j\in\Lambda\setminus\{i\}} J_{ij} \right)$$
$$\equiv N_\mathrm{S}(N_\mathrm{S}-2) J_1. \tag{D.12}$$

Note that because we left out prefactors here, each normal sum over lattice sites, i.e. not the ones over the pairs, comes with an additional factor of J_1 as it stems from the mean-field Hamiltonian. In order to include infinite-range hopping in those terms that have two nearest-neighbour sums and thus also two factors of J_{ij}, as there is no mean-field part involved, we need another definition, which gets clear from the

following sum:

$$\sum_{(i,j)\in\Lambda^2\setminus\Delta(\Lambda)}\sum_{(k,l)\in\Lambda^2\setminus\Delta(\Lambda)}\delta_{ik}\delta_{jl}J_{ij}J_{kl}=\sum_{i\in\Lambda}\left(\sum_{j\in\Lambda\setminus\{i\}}J_{ij}^2\right)\equiv N_\mathrm{S}J_2^2, \tag{D.13}$$

where we defined $J_2^2=\sum_{j\in\Lambda\setminus\{i\}}J_{ij}^2$, which again does not depend on i so that we can choose i with $\boldsymbol{x}_i=\mathbf{0}$ as above. Again we can find a simple expression for J_2^2 in terms of the dispersion:

$$\begin{aligned}J_2^2&=\sum_{j\in\Lambda\setminus\{i\}}J_{ij}^2=\frac{1}{N_\mathrm{S}^2}\sum_{j\in\Lambda\setminus\{i\}}\sum_{\boldsymbol{k}\in1.\mathrm{BZ}}\sum_{\boldsymbol{q}\in1.\mathrm{BZ}}E(\boldsymbol{k})E(\boldsymbol{q})e^{-i(\boldsymbol{k}+\boldsymbol{q})\cdot\boldsymbol{x}_j}\\&=\frac{1}{N_\mathrm{S}}\sum_{\boldsymbol{k}\in1.\mathrm{BZ}}E(\boldsymbol{k})E(-\boldsymbol{k})-\frac{1}{N_\mathrm{S}^2}\sum_{\boldsymbol{k}\in1.\mathrm{BZ}}E(\boldsymbol{k})\sum_{\boldsymbol{q}\in1.\mathrm{BZ}}E(\boldsymbol{q})\\&=\bar{E^2}-\bar{E}^2\equiv(\Delta E)^2,\end{aligned} \tag{D.14}$$

where we again used equation (D.8) and that the dispersion is even. Further we defined the variance $(\Delta E)^2=\bar{E^2}-\bar{E}^2$.
We now extend the remaining double nearest-neighbour sums to infinite-range hopping starting with the first one:

$$\begin{aligned}&\sum_{(i,j)\in\Lambda^2\setminus\Delta(\Lambda)}\sum_{(k,l)\in\Lambda^2\setminus\Delta(\Lambda)}\delta_{ik}(1-\delta_{jl})J_{ij}J_{kl}\\&\quad=\sum_{i\in\Lambda}\left(\sum_{j\in\Lambda\setminus\{i\}}J_{ij}\right)\left(\sum_{j\in\Lambda\setminus\{k\}}J_{ik}\right)-\sum_{(i,j)\in\Lambda^2\setminus\Delta(\Lambda)}\sum_{(k,l)\in\Lambda^2\setminus\Delta(\Lambda)}\delta_{ik}\delta_{jl}J_{ij}J_{kl}\\&\quad=N_\mathrm{S}(J_1^2-J_2^2)\end{aligned} \tag{D.15}$$

To extend the last sum to infinite-range hopping we again multiply out the Kronecker deltas, where we already leave out the terms that are identically zero, see equation (B.35). We then again simplify by relabeling the indices:

$$\begin{aligned}&\sum_{(i,j)\in\Lambda^2\setminus\Delta(\Lambda)}\sum_{(k,l)\in\Lambda^2\setminus\Delta(\Lambda)}(1-\delta_{ik})(1-\delta_{jl})(1-\delta_{jk})(1-\delta_{il})J_{ij}J_{kl}\\&\quad=\sum_{(i,j)\in\Lambda^2\setminus\Delta(\Lambda)}\sum_{(k,l)\in\Lambda^2\setminus\Delta(\Lambda)}\left[1-(\delta_{ik}+\delta_{jl}+\delta_{jk}+\delta_{il})+\delta_{ik}\delta_{jl}+\delta_{il}\delta_{jk}\right]J_{ij}J_{kl}\\&\quad=\sum_{(i,j)\in\Lambda^2\setminus\Delta(\Lambda)}\sum_{(k,l)\in\Lambda^2\setminus\Delta(\Lambda)}\left(1-4\delta_{ik}+2\delta_{ik}\delta_{jl}\right)J_{ij}J_{kl}\\&\quad=\sum_{i,k\in\Lambda}\left(\sum_{j\in\Lambda\setminus\{i\}}J_{ij}\right)\left(\sum_{l\in\Lambda\setminus\{k\}}J_{kl}\right)-4\sum_{i\in\Lambda}\left(\sum_{j\in\Lambda\setminus\{i\}}J_{ij}\right)\left(\sum_{l\in\Lambda\setminus\{i\}}J_{il}\right)\\&\qquad+2\sum_{(i,j)\in\Lambda^2\setminus\Delta(\Lambda)}\sum_{(k,l)\in\Lambda^2\setminus\Delta(\Lambda)}\delta_{ik}\delta_{jl}J_{ij}J_{kl}\\&\quad=N_\mathrm{S}^2J_1^2-4N_\mathrm{S}J_1^2+2N_\mathrm{S}J_2^2.\end{aligned} \tag{D.16}$$

In the last step we used equation (D.13). If we now compare the found sums to the sums calculated for nearest-neighbour hopping in appendix B, we can see that

we can get the former from the latter through the substitutions $z^2J^2 \to J_1^2$ and $zJ^2 \to J_2^2$. Note that when calculating the nearest-neighbour sums we left out the prefactors, thus we must attach a factor of z to each simple sum over the lattice, i.e. no nearest-neighbour sum, as it stems from the mean-field Hamiltonian. Further we must attach a factor of J^2 to each sum. With the two substitutions we just found, we can now immediately write down the grand-canonical partition function to second order including the effect of infinite-range hopping:

$$\begin{aligned}\mathcal{Z}_{\leq 2} = \mathcal{Z}_{\mathrm{MF}} \Big\{ & 1 + \beta J_1 N_{\mathrm{S}} |\psi - \phi|^2 + \frac{1}{2}\beta^2 \left\{ 2N_{\mathrm{S}} J_2^2 |\phi|^4 - N_{\mathrm{S}} J_1^2 \left[(2\phi - \psi)\phi^* - \phi\psi^* \right]^2 \right. \\ & \left. + N_{\mathrm{S}}^2 J_1^2 |\phi - \psi|^4 \right\} \\ & + \mathcal{Z}_{\mathrm{MF,S}}^{-1} \left\{ N_{\mathrm{S}} J_1^2 \left[S_{\hat{a},\hat{a}} (\phi^* - \psi^*)^2 + S_{\hat{a},\hat{a}^\dagger} |\phi - \psi|^2 + S_{\hat{a}^\dagger,\hat{a}} |\phi - \psi|^2 \right. \right. \\ & \left. + S_{\hat{a}^\dagger,\hat{a}^\dagger} (\phi - \psi)^2 \right] \\ & - N_{\mathrm{S}} J_2^2 \left[S_{\hat{a},\hat{a}} (\phi^*)^2 + S_{\hat{a},\hat{a}^\dagger} |\phi|^2 + S_{\hat{a}^\dagger,\hat{a}} |\phi|^2 + S_{\hat{a}^\dagger,\hat{a}^\dagger} \phi^2 \right] \Big\} \\ & + \mathcal{Z}_{\mathrm{MF,S}}^{-2} J_2^2 N_{\mathrm{S}} (S_{\hat{a}^\dagger,\hat{a};\hat{a},\hat{a}^\dagger} + S_{\hat{a}^\dagger,\hat{a}^\dagger;\hat{a},\hat{a}}) \Big\} . \end{aligned} \tag{D.17}$$

As the only term that gets cancelled when going from the grand-canonical partition function to the grand-canonical potential is the non-extensive term which has a factor of J_1^2 just like the first order term squared, these terms still cancel and thus we can also extend the grand-canonical potential to infinite-range hopping by the simple substitutions found above:

$$\begin{aligned}\Phi_{\leq 2} = \Phi_{\mathrm{MF}} & - J_1 N_{\mathrm{S}} |\psi - \phi|^2 - \frac{1}{2}\beta \left\{ 2N_{\mathrm{S}} J_2^2 |\phi|^4 - N_{\mathrm{S}} J_1^2 [(2\phi - \psi)\phi^* - \phi\psi^*]^2 \right\} \\ & - \frac{1}{\beta} \mathcal{Z}_{\mathrm{MF,S}}^{-1} \left\{ N_{\mathrm{S}} J_1^2 \left[S_{\hat{a},\hat{a}} (\phi^* - \psi^*)^2 + S_{\hat{a},\hat{a}^\dagger} |\phi - \psi|^2 + S_{\hat{a}^\dagger,\hat{a}} |\phi - \psi|^2 \right. \right. \\ & \left. + S_{\hat{a}^\dagger,\hat{a}^\dagger} (\phi - \psi)^2 \right] \\ & - N_{\mathrm{S}} J_2^2 [S_{\hat{a},\hat{a}} (\phi^*)^2 + S_{\hat{a},\hat{a}^\dagger} |\phi|^2 + S_{\hat{a}^\dagger,\hat{a}} |\phi|^2 + S_{\hat{a}^\dagger,\hat{a}^\dagger} \phi^2] \Big\} \\ & - \frac{1}{\beta} \mathcal{Z}_{\mathrm{MF,S}}^{-2} J_2^2 N_{\mathrm{S}} (S_{\hat{a}^\dagger,\hat{a};\hat{a},\hat{a}^\dagger} + S_{\hat{a}^\dagger,\hat{a}^\dagger;\hat{a},\hat{a}}). \end{aligned} \tag{D.18}$$

The arguments from above still hold in the zero temperature case so we can also easily extend that result to infinite-range hopping:

$$\begin{aligned} E_{0,\leq 2} = \epsilon_{\vec{0}} & - J_1 N_{\mathrm{S}} |\psi - \phi|^2 + J_2^2 N_{\mathrm{S}} \left(\tilde{S}^{(0)}_{\hat{a}^\dagger,\hat{a};\hat{a},\hat{a}^\dagger} + \tilde{S}^{(0)}_{\hat{a}^\dagger,\hat{a}^\dagger;\hat{a},\hat{a}} \right) \\ & + J_1^2 N_{\mathrm{S}} \left\{ S^{(0)}_{\hat{a},\hat{a}} (\phi^* - \psi^*)^2 + S^{(0)}_{\hat{a},\hat{a}^\dagger} |\phi - \psi|^2 + S^{(0)}_{\hat{a}^\dagger,\hat{a}} |\phi - \psi|^2 \right. \\ & \left. + S^{(0)}_{\hat{a}^\dagger,\hat{a}^\dagger} (\phi - \psi)^2 \right\} . \end{aligned} \tag{D.19}$$

In conclusion, we saw that in order to account for infinite-range hopping in the corrected results we need to distinguish between two different Js. They are of course not independent as they both depend on the dispersion. For a given dispersion however we could now calculate J_1 and J_2, and of course also U, in terms of experimental parameters like the lattice depth, see appendix A for example, and thus easily take into account infinite-range hopping, which makes the theory more realistic.

References

[1] Chu, S. The manipulation of neutral particles. *Rev. Mod. Phys.* **70,** 685 (1998).

[2] Cohen-Tannoudji, C. Manipulating atoms with photons. *Rev. Mod. Phys.* **70,** 707 (1998).

[3] Phillips, W. Laser cooling and trapping of neutral atoms. *Rev. Mod. Phys.* **70,** 721 (1998).

[4] Anderson, M., Ensher, J., Matthews, M., Wieman, C. & Cornell, E. Observation of Bose-Einstein Condensation in a Dilute Atomic Vapor. *Science* **269,** 198 (1995).

[5] Davis, K. *et al.* Bose-Einstein Condensation in a Gas of Sodium Atoms. *Phys. Rev. Lett* **75,** 3969 (1995).

[6] Grimm, R., Weidemüller, M. & Ovchinnikov, Y. Optical Dipole Traps for Neutral Atoms. *Adv. Atom. Mol. Opt. Phy.* **42,** 95 (2000).

[7] Greiner, M., Mandel, O., Esslinger, T., Hänsch, T. & Bloch, I. Quantum phase transition from a superfluid to a Mott insulator in a gas of ultracold atoms. *Nature* **415,** 39 (2002).

[8] Lewenstein, M., Sanpera, A. & Ahufinger, V. *Ultracold Atoms in Optical Lattices: Simulating Quantum Many-Body Systems* 1st ed. (Oxford University Press, 2012).

[9] Bell, J. & Aspect, A. *Speakable and Unspeakable in Quantum Mechanics: Collected Papers on Quantum Philosophy* 2nd ed. (Cambridge University Press, 2004).

[10] Jotzu, G. *et al.* Experimental realization of the topological Haldane model with ultracold fermions. *Nature* **515,** 237 (2014).

[11] Aidelsburger, M. *et al.* Measuring the Chern number of Hofstadter bands with ultracold bosonic atoms. *Nature Phys.* **11,** 162 (2015).

[12] Lohse, M., Schweizer, C., Zilberberg, O., Aidelsburger, M. & Bloch, I. A Thouless quantum pump with ultracold bosonic atoms in an optical superlattice. *Nature Phys.* **12,** 350 (2016).

[13] Nakajima, S. *et al.* Topological Thouless pumping of ultracold fermions. *Nature Phys.* **12,** 296 (2016).

[14] Lewenstein, M. *et al.* Ultracold atomic gases in optical lattices: Mimicking condensed matter physics and beyond. *Adv. Phys.* **56,** 243 (2007).

[15] Jaksch, D. & Zoller, P. The cold atom Hubbard toolbox. *Ann. Phys. (New York)* **315,** 52 (2005).

[16] Feynman, R. Simulating Physics with Computers. *Int. J. Theor. Phys.* **21,** 467 (1982).

[17] Ladd, T. *et al.* Quantum computers. *Nature* **464,** 45 (2010).

[18] Bloch, I., Dalibard, J. & Nascimbène, S. Quantum simulations with ultracold quantum gases. *Nature Phys.* **8,** 267 (2012).

[19] Rodríguez, M., Clark, S. & Jaksch, D. Generation of twin Fock states via transition from a two-component Mott insulator to a superfluid. *Phys. Rev. A* **75,** 011601 (2007).

[20] Lewis-Swan, R. *Ultracold Atoms for Foundational Tests of Quantum Mechanics* 1st ed. (Springer International Publishing, 2016).

[21] Zohar, E., Cirac, J. & Reznik, B. Quantum simulations of lattice gauge theories using ultracold atoms in optical lattices. *Rep. Prog. Phys.* **79,** 014401 (2016).

[22] Bentsen, G., Hashizume, T., Buyskikh, A., Davis, E. & Daley, A. Treelike Interactions and Fast Scrambling with Cold Atoms. *Phys. Rev. Lett.* **123,** 130601 (2019).

[23] Jaksch, D., H.-J., B., Cirac, J., Gardiner, C. & Zoller, P. Entanglement of Atoms via Cold Controlled Collisions. *Phys. Rev. Lett.* **82,** 1975 (1999).

[24] Mandel, O. *et al.* Controlled collisions for multi-particle entanglement of optically trapped atoms. *Nature* **425,** 937 (2003).

[25] Wieman, C., Pritchard, D. & Wineland, D. Atom cooling, trapping, and quantum manipulation. *Rev. Mod. Phys.* **71,** S253 (1999).

[26] Jaksch, D., Bruder, C., Cirac, J., Gardiner, C. & Zoller, P. Cold Bosonic Atoms in Optical Lattices. *Phys. Rev. Lett.* **81,** 3108 (1998).

[27] Capogrosso-Sansonse, B., Prokof'ev, N. & Svistunov, B. Phase diagram and thermodynamics of the three-dimensional Bose-Hubbard model. *Phys. Rev. B* **75,** 134302 (2007).

[28] Andersen, J. Theory of the weakly interacting Bose gas. *Rev. Mod. Phys.* **76,** 599 (2004).

[29] De Boer, J. & Verwey, E. Semi-conductors with partially and with completely filled 3d-lattice bands. *Proc. Phys. Soc.* **49,** 59 (1937).

[30] Mott, N. & Peierls, R. Discussion of the paper by de Boer and Verwey. *Proc. Phys. Soc.* **49,** 72 (1937).

[31] Mott, N. The Basis of the Electron Theory of Metals, withSpecial Reference to the Transition Metals. *Proc. Phys. Soc. A* **62,** 416 (1949).

[32] Hubbard, J. Electron correlations in narrow energy bands. *Proc. R. Soc. London, Ser. A* **276,** 238 (1963).

[33] Fisher, M., Weichmann, P., Grinstein, G. & Fisher, D. Boson localization and the superfluid-insulator transistion. *Phys. Rev. B* **40,** 546 (1989).

[34] Batrouni, G., Scalettar, R. & Zimanyi, G. Quantum Critical Phenomena in One-Dimensional Bose Systems. *Phys. Rev. Lett* **65,** 1765 (1990).

[35] Scalettar, R., Batrouni, G. & Zimanyi, G. Localization in Interacting, Disordered, Bose Systems. *Phys. Rev. Lett.* **66,** 3144 (1991).

[36] Niyaz, P., Scalettar, R., Fong, C. & Batrouni, G. Ground-state phase diagram of an interacting Bose model with near-neighbor repulsion. *Phys. Rev. B* **44,** 7143 (1991).

[37] Krauth, W. & Trivedi, N. Mott and Superfluid Transitions in a Strongly Interacting Lattice Boson system. *Europhys. Lett.* **14,** 627 (1991).

[38] Krauth, W., Trivedi, N. & Ceperley, D. Superfluid-Insulator Transition in Disordered Boson Systems. *Phys. Rev. Lett.* **67,** 2307 (1991).

[39] Batrouni, G. *et al.* Mott Domains of Bosons Confined on Optical Lattices. *Phys. Rev. Lett.* **89,** 117203 (2002).

[40] Capogrosso-Sansone, B., Söyler, S., Prokof'ev, N. & Svistunov, B. Monte Carlo study of the two-dimensional Bose-Hubbard model. *Phys. Rev. A* **77,** 015602 (2008).

[41] Kühner, T. & Monien, H. Phases of the one-dimensional Bose-Hubbard model. *Phys. Rev. B* **58,** R14741 (1998).

[42] Rapsch, S., Schollwöck, U. & Zwerger, W. Density matrix renormalization group for disordered bosonsin one dimension. *Europhys. Lett.* **46,** 559 (1999).

[43] Kollath, C., Schollwöck, U., von Delft, J. & Zwerger, W. Spatial correlations of trapped one-dimensional bosons in an optical lattice. *Phys. Rev. A* **69,** 031601 (2004).

[44] Kollath, C., Läuchli, A. & Altman, E. Quench Dynamics and Nonequilibrium Phase Diagram of the Bose-Hubbard Model. *Phys. Rev. Lett* **98,** 180601 (2007).

[45] Byczuk, K. & Vollhardt, D. Correlated bosons on a lattice: Dynamical mean-field theory for Bose-Einsteincondensed and normal phases. *Phys. Rev. B* **77,** 235106 (2008).

[46] Freericks, J. & Monien, H. Strong-coupling expansions for the pure and disordered Bose-Hubbard model. *Phys. Rev. B* **53,** 2691 (1996).

[47] Dos Santos, F. & Pelster, A. Quantum phase diagram of bosons in optical lattices. *Phys. Rev. A* **79,** 013614 (2009).

[48] Krauth, W., Caffarel, M. & Bouchaud, J.-P. Gutzwiller wave function for a model of strongly interacting bosons. *Phys. Rev. B* **45,** 3137 (1992).

[49] Sheshadri, K., Krishnamurthy, H., Pandit, R. & Ramakrishnan, T. Superfluid and Insulating Phases in an Interacting-Boson Model: Mean-Field Theory and the RPA. *Europhys. Lett.* **22,** 257 (1993).

[50] Van Otterlo, A. *et al.* Quantum phase transitions of interacting bosons in the supersolid phase. *Phys. Rev. B* **52,** 16176 (1995).

[51] Van Oosten, D., van der Straten, P. & Stoof, H. Quantum phases in an optical lattice. *Phys. Rev. A* **63,** 053601 (2001).

[52] Singh, K. & Rokhsar, D. Real-space renormalization study of disordered interacting bosons. *Phys. Rev. B* **46,** 3002 (1992).

[53] Elstner, N. & Monien, H. Dynamics and thermodynamics of the Bose-Hubbard model. *Phys. Rev. B* **59,** 12184 (1999).

[54] Freericks, J., Krishnamurthy, H., Kato, Y., Kawashima, N. & Trivedi, N. Strong-coupling expansion for the momentum distribution of the Bose-Hubbard modelwith benchmarking against exact numerical results. *Phys. Rev. A* **79,** 053631 (2009).

[55] Kampf, A. & Zimanyi, G. Superconductor-insulator phase transition in the boson Hubbard model. *Phys. Rev. B* **47,** 279 (1993).

[56] Dickerscheid, D., van Oosten, D., Denteneer, P. & Stoof, H. Ultracold atoms in optical lattices. *Phys. Rev. A* **68,** 043623 (2003).

[57] Buonsante, P. & Vezzani, A. Phase diagram for ultracold bosons in optical lattices and superlattices. *Phys. Rev. A* **70,** 033608 (2004).

[58] Kleinert, H., Schmidt, S. & Pelster, A. Reentrant Phenomenon in the Quantum Phase Transitionsof a Gas of Bosons Trapped in an Optical Lattice. *Phys. Rev. Lett.* **93,** 160402 (2004).

[59] Konabe, S., Nikuni, T. & Nakamura, M. Laser probing of the single.particle energy gap of a Bose gas in an optical lattice in the Mott-insulator phase. *Phys. Rev. A* **73,** 033621 (2006).

[60] Krutitsky, K., Pelster, A. & Graham, R. Mean-field phase diagram of disordered bosons in a lattice at nonzero temperature. *New. J. Phys.* **8,** 187 (2006).

[61] Stasyuk, I. & Mysakovych, T. Phase diagrams of the Bose-Hubbard model at finite temperature. *Condens. Matter Phys.* **12,** 539 (2009).

[62] Schroll, C., Marquardt, F. & Bruder, C. Perturbative corrections to the Gutzwiller mean-field solution of the Mott-Hubbard model. *Phys. Rev. A* **70,** 053609 (2004).

[63] Teichmann, N., Hinrichs, D. & Holthaus, M. Bose-Hubbard phase diagram with arbitrary integer filling. *Phys. Rev. B* **79,** 100503 (2009).

[64] Eckardt, A. Process-chain approach to high-order perturbation calculus for quantum lattice models. *Phys. Rev. B* **79,** 195131 (2009).

[65] Teichmann, N., Hinrichs, D. & Holthaus, M. Process-chain approach to the Bose-Hubbard model: Ground-state properties and phase diagram. *Phys. Rev. B* **79,** 224515 (2009).

[66] Wang, T., Zhang, X.-F., Hou, C.-F., Eggert, S. & Pelster, A. High-order symbolic strong-coupling expansion for the Bose-Hubbard model. *Phys. Rev. B* **98,** 245107 (2018).

[67] Bradlyn, B., dos Santos, F. & Pelster, A. Effective action approach for quantum phase transitions in bosonic lattices. *Phys. Rev. A* **79,** 013615 (2009).

[68] Ohliger, M. & Pelster, A. Green's Function Approach to the Bose-Hubbard Model. *WJCMP* **3,** 125 (2013).

[69] Foot, C. Atomic Physics (2005).

[70] Bloch, I. Ultracold quantum gases in optical lattices. *Nature Phys.* **1,** 23 (2005).

[71] Verkerk, P., Lounis, B., Salomon, C. & Cohen-Tannoudji, C. Dynamics and Spatial Order of Cold Cesium Atoms in a Periodic Optical Potential. *Phys. Rev. Lett.* **68,** 3861 (1992).

[72] Jessen, P. *et al.* Observation of Quantized Motion of Rb Atoms in an Optical Field. *Phys. Rev. Lett.* **69,** 49 (1992).

[73] Stöferle, T., Moritz, H., Schori, C., Köhl, M. & Esslinger, T. Transition from a Strongly Interacting 1D Superfluid to a Mott Insulator. *Phys. Rev. Lett.* **92,** 130403 (2004).

[74] Paredes, B. *et al.* Tonks–Girardeau gas of ultracold atoms in an optical lattice. *Nature* **429,** 277 (2004).

[75] Hemmerich, A. & Hänsch, T. Two-Dimensional Atomic Crystal Bound by Light. *Phys. Rev. Lett.* **70,** 410 (1993).

[76] Hemmerich, A., Zimmermann, C. & Hänsch, T. Sub-kHz Rayleigh Resonance in a Cubic Atomic Crystal. *Europhys. Lett.* **22,** 89 (1993).

[77] Weidemüller, M., Hemmerich, A., Görlitz, A., Esslinger, T. & Hänsch, T. Bragg Diffraction in an Atomic Lattice Bound by Light. *Phys. Rev. Lett.* **75,** 4583 (1995).

[78] Grynberg, G., Lounis, B., Verkerk, P., J.-Y., C. & Salomon, C. Quantized Motion of Cold Cesium Atoms in Two- and Three-Dimensional Optical Potentials. *Phys. Rev. Lett.* **70,** 2249 (1993).

[79] Soltan-Panahi, P. *et al.* Multi-component quantum gases in spin-dependent hexagonal lattices. *Nature Phys.* **7,** 434 (2011).

[80] Becker, C. *et al.* Ultracold quantum gases in triangular optical lattices. *New J. Phys.* **12,** 065025 (2010).

[81] Santos, L. *et al.* Atomic Quantum Gases in Kagomé Lattices. *Phys. Rev. Lett.* **93,** 030601 (2004).

[82] Amico, L., Osterloh, A. & Cataliotti, F. Quantum Many Particle Systems in Ring-Shaped Optical Lattices. *Phys. Rev. Lett.* **95,** 063201 (2005).

[83] Papoular, D., Shlyapnikov, G. & Dalibard, J. Microwave-induced Fano-Feshbach resonances. *Phys. Rev. A* **81,** 041603 (2010).

[84] Theis, M. *et al.* Tuning the Scattering Length with an Optically Induced Feshbach Resonance. *Phys. Rev. Lett.* **93,** 123001 (2004).

[85] Lahaye, T., Menotti, C., Santos, L., Lewenstein, M. & Pfau, T. The physics of dipolar bosonic quantum gases. *Rep. Prog. Phys.* **72,** 126401 (2009).

[86] Pachos, J. & Rico, E. Effective three-body interactions in triangular optical lattices. *Phys. Rev. Lett.* **70,** 053620 (2004).

[87] Jaksch, D. & Zoller, P. Creation of effective magnetic fields in optical lattices: the Hofstadter butterfly for cold neutral atoms. *New J. Phys.* **5,** 56 (2003).

[88] Maschler, C. & Ritsch, H. Cold Atom Dynamics in a Quantum Optical Lattice Potential. *Phys. Rev. Lett.* **95,** 260401 (2005).

[89] Würtz, P., Langen, T., Gericke, T., Koglbauer, A. & Ott, H. Experimental Demonstration of Single-Site Addressability in a Two-Dimensional Optical Lattice. *Phys. Rev. Lett.* **103,** 080404 (2009).

[90] Ott, H. Single atom detection in ultracold quantum gases:a review of current progress. *Rep. Prog. Phys.* **79,** 054401 (2016).

[91] Sachdev, S. *Quantum Phase Transitions* 2nd ed. (Cambridge University Press, 2011).

[92] Greiner, M., Mandel, O., Hänsch, T. & Bloch, I. Collapse and revival of the matterwave field of a Bose–Einstein condensate. *Nature* **419,** 51 (2002).

[93] Bloch, I. Quantum gases in optical lattices. *Phys. World* **17,** 25 (2004).

[94] Conway, J. *A Course in Functional Analysis* 2nd ed. (Springer, 1990).

[95] Feynman, R. *Statistical Mechanics - A Set of Lectures* 2nd ed. (Westview Press, 1998).

[96] Bargmann, V. Remarks on a Hilbert space of analytic functions. *Proc. Natl. Acad. Sci. U.S.A.* **48,** 199 (1962).

[97] Beardon, A. *Algebra and Geometry* 1st ed. (Cambridge University Press, 2005).

[98] Shankar, R. *Principles of Quantum Mechanics* 2nd ed. (Springer, 1994).

[99] Bloch, I., Dalibard, J. & Zwerger, W. Many-body physics with ultracold gases. *Rev. Mod. Phys.* **80,** 885 (2008).

[100] Leggett, A. Bose-Einstein condensation in the alkali gases: Some fundamental concepts. *Rev. Mod. Phys.* **73,** 307 (2001).

[101] Wannier, G. The Structure of Electronic Excitation Levels in Insulating Crystals. *Phys. Rev.* **52,** 191 (1937).

[102] Pathria, R. & Beale, P. *Statistical Mechanics* 3rd ed. (Elsevier, 2011).

[103] Hoffmann, A. *Bosonen im optischen Gitter [Bosons in optical lattices]* diploma thesis (Freie Universität Berlin, 2007).

[104] Burkill, J. *A First Course in Mathematical Analysis* 1st ed. (Cambridge University Press, 1962).

[105] Kübler, M., Sant'Ana, F., dos Santos, F. & Pelster, A. Improving mean-field theory for bosons in optical lattices via degenerate perturbation theory. *Phys. Rev. A* **99,** 063603 (2019).

[106] Sant'Ana, F., Pelster, A. & dos Santos, F. Finite-temperature degenerate perturbation theory for bosons in optical lattices. *Phys. Rev. A* **100,** 043609 (2019).

[107] Egorov, M. *et al.* Measurement of s-wave scattering lengths in a two-component Bose-Einstein condensate. *Phys. Rev. A* **87,** 053614 (2013).

[108] Hinrichs, D., Pelster, A. & Holthaus, M. Perturbative calculation of critical exponents for the Bose–Hubbard model. *Appl. Phys. B* **113,** 57 (2013).

[109] Abramowitz, M. & Stegun, I. *Handbook of Mathematical Functions With Formulas, Graphs, and Mathematical Tables* ninth Dover printing, tenth GPO printing (Dover Publications, Inc., 1964).

Selbstständigkeitserklärung

Hiermit erkläre ich, dass ich diese Arbeit selbstständig verfasst und keine anderen als die angegebenen Quellen und Hilfsmittel verwendet, sowie Zitate kenntlich gemacht habe.

Kaiserslautern, den 14.07.2021

_____

Sven Stawinski